NATIONAL AERONAUTICS AND SPACE ADMINISTRATION

SCATTERING OF WAVES FROM A ROUGH LAYER

by

William D. Boles

CRES Technical Report 118-19
December 1969
The Remote Sensing Laboratory

Supported by NASA Manned Spacecraft Center Contract NAS 9-7175, the National Science Foundation Grants GK 1153 and GK 11381, the U.S. Army Topographic Laboratory Contract DAAK02-68-C-0089.

MANNED SPACECRAFT CENTER
HOUSTON, TEXAS

CRES
CENTER FOR RESEARCH, INC. · ENGINEERING SCIENCE DIVISION
THE UNIVERSITY OF KANSAS · LAWRENCE, KANSAS · 66044

SCATTERING OF WAVES FROM A ROUGH LAYER

by

William D. Boles

CRES Technical Report 118-19

September 1969

The Remote Sensing Laboratory

Supported by NASA Manned Spacecraft Center Contract NAS 9-7175, the National Science Foundation Grants GK 1153 and GK 11381, the U.S. Army Topographic Laboratory Contract DAAK02-68-C-0089.

TABLE OF CONTENTS

LIST OF FIGURES

ACKNOWLEDGEMENT

The first acknowledgement goes to my advisor, Dr. R. K. Moore, who not only suggested the topic but also found time in his busy schedule for much consultation on the details of the entire work.

The financial support of the NASA Manned Spacecraft Center under Contract NAS 9-7175, the National Science Foundation under grants GK 1153 and GK 11381, the U.S. Army Topographic Laboratory under Contract DAAK02-68-C 0089 and the Computation Center at the University of Kansas is gratefully acknowledged.

Appreciation is expressed to Dr. A. K. Fung without whose assistance the theoretical portions of this work could not have been completed.

Sincere gratitude is expressed for the help of many personnel of the Remote Sensing Laboratory, especially my office partners, Mr. Chan and Mr. Zachs, for their aid and understanding during this project. By no means forgotten, either, are the hours spent by Mrs. Summerfeld in typing the manuscript.

A special "thank you" is due my wife, Judi, and the children for the patience and encouragement they have shown.

ABSTRACT

In the past several years there has been much interest in the scattering of waves from rough surfaces. Many theories have been developed to describe the scattering phenomenon, but these generally consider only the return from a single surface and assume there is no return from below the surface. This assumption is generally violated in nature, which prompted an investigation of the effect of a layer on the backscatter signal.

This work is a study of acoustic wave scattering from a layer. The applications of the acoustic results to electromagnetic scatter are considered and the limitations are pointed out.

A theory is developed, using the method of physical optics, for the backscattering of acoustic waves from a semi-transparent layer having either the front or the rear face randomly rough and the other interface plane. It was found that, if the roughness is of the order of the incident wavelength or greater, the power returned from the two faces could be determined independently and added together to obtain the total power return from a layer.

An extensive experiment was conducted using layers with identical roughness and varying thicknesses to compare with the theory developed. Each layer was investigated under four conditions: (1) rough front and perfectly reflecting smooth rear, (2) rough front and smooth rear with both reflection coefficients of the same order of magnitude, (3) smooth front and perfectly reflecting rough rear, and (4) smooth front and rough rear with both reflection coefficients nearly the same. For each case the reflection coefficient of the front face was -24.6 dB. Selected experimental results were compared with the theoretical scattering cross section and found to be in agreement. Comparisons between layers of the same configuration and different thicknesses point out the increased effect of the rear face as the round-trip attenuation is decreased.

The results of the experiment show that a single-frequency system cannot detect the presence of a layer unless the returns from the two interfaces can be resolved in range.

CHAPTER I

INTRODUCTION

1.1 Motivation and Purpose

The problem of scattering of electromagnetic and acoustic waves from rough surfaces occurs in remote sensing by radar or sonar systems and propagation of waves over rough surfaces. The prediction and estimation of such scattered signals returned from various terrains is important in designing radar mapping systems and radio altimeters. Radar systems in orbit about the earth can yield valuable information about vegetation, cultural objects, and geology. For ground-to-ground microwave communication systems the terrain between the terminals may cause scattering of waves.

Presently available scattering theories are generally based on either of the following assumptions: (1) the surface is a perfect reflector, (2) in case the rough surface is not a perfect reflector it is homogeneous and semi-infinite such that no contribution is received from below the surface. While these are very "nice" mathematically they are quite often violated in real life. A somewhat more general approach is to consider a lossy layer covering such a surface. Examples of this are: a vegetation layer covering the earth, snow covered terrain, soil over rock, dust layer on moon or planets, and a sediment layer over a solid ocean floor. Experimental evidence of such layers can be found in the data presented in papers by Peake (1959) and Taylor (1959). In such cases, it seems reasonable to assume the scattering surface to be a rough layer covering an imperfectly reflecting surface. Such a layer will usually be somewhat lossy.

Preliminary investigation of backscatter from a layer has been conducted by the U.S. Army Engineer Waterways Experiment Station (Lundien, 1965) using pulsed radars at P, C, X, and Ka bands. They used large laboratory soil samples mounted above flat metal plates;

the moisture content, density and thickness of the layer were varied. The layer was flat on both sides and had a maximum thickness of two feet. As to be expected from such a configuration, the total return shows interference effects between the front and rear faces for those layers thin enough to have appreciable return from the rear.

An analysis has also been made for electromagnetic wave scatter from a layer with one interface plane and the other rough (Krishen, 1968) but only a smooth, perfectly conducting rear face was considered. This work also considered acoustic wave scattering with one smooth face and one one-dimensionally rough face. An attempt made to obtain experimental data for comparison was restricted to the case of a rough front only. The data obtained were biased, however, by the use of small flat facets which had a slope distribution that peaked away from normal incidence.

Four layer models were chosen for this investigation:

(1) a two-dimensionally randomly rough interface in front and a perfectly reflecting smooth interface in the rear,

(2) a two-dimensionally randomly rough interface in front and an imperfectly reflecting smooth interface in the rear,

(3) a smooth face in front and a perfectly reflecting two-dimensionally randomly rough interface in back,

(4) a smooth face in front and an imperfectly reflecting two-dimensionally randomly rough interface in back.

The scattering from these layers was investigated analytically using the Kirchhoff-Huygens method and experimentally using ultrasonic waves in water. The layers all had slight attenuation per unit thickness. The results appear in the form of average scattered power densities or average differential scattering cross sections. The assumptions used for the analysis are discussed in Chapter II.

The experimental phase of the study used acoustic modeling with carefully controlled parameters. The data available to date on layered rough surfaces is meager with surface and subsurface parameters poorly documented. Natural surfaces were usually used and measurement is very difficult for the scale of roughness important to the

scattering process. The layer used in this experiment is characterized by measured thickness and measured statistical description of the rough surface.

1.2 Discussion of the Kirchhoff Method

The Kirchhoff method has been used here since the roughness is comparable to the incident wavelength. The field scattered by the rough interface is formulated according to Huygens' Principle and is given by the Helmholtz integral. This integral expresses the field scattered by the rough interface in terms of the total field and its normal derivatives, or their equivalents, on the surface (Silver, 1941). The values of these two quantities are determined by the tangent plane approximation. The criterion for the validity of this approximation is (Brekhovskikh, 1952)

$$4\pi\rho\cos\theta \gg \lambda \qquad (1.1)$$

when the point is not an inflection point. In this inequality ρ is the smaller of the two principle radii of curvature at the point, θ is the local incident angle and λ the incident wavelength. In case the point is an inflection point, the condition is

$$24\pi^2\cos\theta \gg \frac{d}{dx}\left(\frac{1}{\rho}\right)^2 \qquad (1.2)$$

where x is the coordinate measured along the mean level of the rough surface. These requirements restrict this method to locally flat surfaces with small curvatures (gently undulating). Consequently this method cannot be applied in the low frequency limit.

1.3 Summary of Chapter Development

In Chapter II an acoustic wave scattering theory is developed for a layer with either the front or the back having two-dimensional roughness. The assumptions made in the derivation are listed. General two-dimensional rough-surface scatter is analyzed with a reflection coefficient other than ± 1 considered. This theory is then applied to

the simplest of the layers considered, the smooth front and the rough back. An expression for the average acoustic power backscattered from such a layer is determined. Next the more difficult case of the rough front interface is investigated and an expression is developed for the average backscatter power from this layer.

The experimental procedures and equipment are covered in Chapter III. The first section describes in some detail the method of measuring the average differential scattering cross section and the normalization procedure used in the experiment. A description of the acoustic simulation system appears next. This acoustic system was used to determine the average backscattered power of 1 MHz acoustic waves in water ($\lambda = 1.5$ mm) from the layer models used. The target was large enough that sufficient independent samples were obtained to reduce the averaging error to less than 2 dB. The rest of Chapter III describes the acoustic parameters of the material used for the layer and the statistical parameters of the rough interface.

Chapter IV presents the experimental data and a discussion of the results obtained. The total average power was obtained for all the layers considered and for the thicker layers it was also possible to obtain the backscattered power from the two interfaces separately. Several comparisons are made between the results obtained for layers of the same configuration but differing thickness to illustrate the effect of the layer thickness. The effect of the thicker layers is not very pronounced, since the signal from the rear face is attenuated. As the layer thickness is decreased the effect becomes greater until, for the thinnest, it is not obvious from the return which configuration is being observed. Following the experimental results is a discussion of the limitations of the investigation and their effects on the data. The most serious limitation is that the smooth surface was not in the far field region of the rough surface but any effect of this deviation was not noticed in the results. The conclusion reached is that the presence of a layer cannot be detected by a single-frequency radar or sonar system unless the the range resolution is less than the layer thickness.

Chapter V contains suggestions for future investigation of the nature of scattering from layered media.

Background information concerning acoustic waves in solids and the effect on reflection from a solid interface is in Appendices A and B while a detailed description of the measurements of the acoustic parameters is contained in Appendix C.

1.4 The Acoustic-Electromagnetic Analogy

The analogy between acoustic waves in water and electromagnetic waves in air becomes apparent when the differential equations of each case are examined. These "telegraphers equations" appear as (1.3) and (1.4). For waves traveling in the plus z-direction they are (Moore, 1960)

Electromagnetic	Acoustic	
$\frac{\partial E_x}{\partial z} = -\mu \frac{\partial H_y}{\partial t}$	$\frac{\partial p}{\partial z} = -\rho_v \frac{\partial u_z}{\partial t}$	(1.3)
$\frac{\partial H_y}{\partial z} = \epsilon \frac{\partial E_x}{\partial t}$	$\frac{\partial u_z}{\partial z} = -K \frac{\partial p}{\partial t}$	(1.4)

where H is the magnetic field
E is the electric field
μ is the permeability of the medium
ϵ is the permittivity of the medium
p is the acoustic pressure
U_z is the particle velocity in the z-direction
ρ_v is the mass density per unit volume
K is the compressibility of the medium

Combining the two equations in each case as usual yields wave equations of the form

Electromagnetic	Acoustic	
$\frac{\partial^2 E_x}{\partial z^2} = \frac{1}{c_{em}^2} \frac{\partial^2 E_x}{\partial t^2}$	$\frac{\partial^2 p}{\partial z^2} = \frac{1}{c_a^2} \frac{\partial^2 p}{\partial t^2}$	(1.5)
$\frac{\partial^2 H_y}{\partial z^2} = \frac{1}{c_{em}^2} \frac{\partial^2 H_y}{\partial t^2}$	$\frac{\partial^2 u_z}{\partial z^2} = \frac{1}{c_a^2} \frac{\partial^2 u_z}{\partial t^2}$	(1.6)

where c_{em} is the velocity of the electromagnetic wave

c_a is the velocity of the acoustic wave in water.

Thus it is seen that identical equations are valid for the two conditions and, as would be expected, the solutions are identical.

The boundary conditions are

Electromagnetic	Acoustic	
$E_{t1} = E_{t2}$	$p_1 = p_2$	(1.7)
$H_{t1} = H_{t2}$	$u_{n1} = u_{n2}$	(1.8)

where n refers to the normal components and t refers to the tangential components; 1 and 2 refer to the media on opposite sides of the interface. The electromagnetic portions of (1.7) and (1.8) show the continuity of the tangential components of E and H across the boundary. The acoustic condition states that, in an ideal fluid, the pressure on both sides of the boundary must be equal and the normal component of the velocity must be continuous across the boundary.

Only the scalar form of the electromagnetic wave equation has been considered since an acoustic wave in a fluid is a scalar. The restrictions imposed by this limitation have been considered in detail by Edison (1960) and Parkins (1965) but basically the analogy holds when the vector nature of the electromagnetic wave can be neglected

and the scalar radar equation is used, and for angles of incidence that are not too large.

CHAPTER II

ACOUSTIC WAVE SCATTERING FROM A LAYER

2.1 Introduction

The theory of reflection from a one-dimensionally rough layer (Krishen and Koepsel, 1968) is here extended to include the scattering from a layer with two-dimensional roughness on one face and to allow for transmission losses through the layer. The model considered for the layer has one smooth and one random, two-dimensionally rough, interface. The model is investigated with first the smooth interface and then with the rough one illuminated. The following assumptions are made in the derivation of the equations .

(1) The radius of curvature of the roughness is much greater than the wavelength of the incident radiation

(2) The illumination is a plane wave

(3) The layer thickness is such that the smooth interface is in the reradiation far field region of the rough one

(4) The observation point is in the far field region of the upper interface

(5) Shadowing effects on the rough surface are neglected

(6) Multiple scattering by the rough interface is neglected

(7) The reflection coefficient is independent of the local incident angle over the range of angles of interest.

2.2 General Two-Dimensionally Rough Solution

For a non-perfectly conducting, two-dimensionally rough surface state with equation (3.2.1) (Beckmann and Spizzichino, pg. 26)

$$P = \frac{1}{4XY\cos\theta_1} \int_{-X}^{X}\int_{-Y}^{Y} (a\xi_x' + c\xi_y' - b)\, e^{i\vec{v}\cdot\vec{r}}\, dx\, dy \qquad (2.1)$$

where

$$\vec{V} = k\left[(\sin\theta_1 - \sin\theta_2\cos\theta_3)\hat{x} - (\sin\theta_2\sin\theta_3)\hat{y} - (\cos\theta_1 + \cos\theta_2)\hat{z}\right] \quad (2.2)$$

$$a = (1-R)\sin\theta_1 + (1+R)\sin\theta_2\cos\theta_3 \quad (2.3)$$

$$b = (1+R)\cos\theta_2 - (1-R)\cos\theta_1 \quad (2.4)$$

$$c = (1+R)\sin\theta_2\sin\theta_3 \quad (2.5)$$

$$\xi'_x = \frac{\partial \xi}{\partial x}$$

$$\xi'_y = \frac{\partial \xi}{\partial y}$$

$\xi = \xi(x,y)$ is the surface height function
R is the reflection coefficient of the surface
r is the radius vector $x\hat{x} + y\hat{y} + z\hat{z}$
and the angles are defined in Figure 2.1.

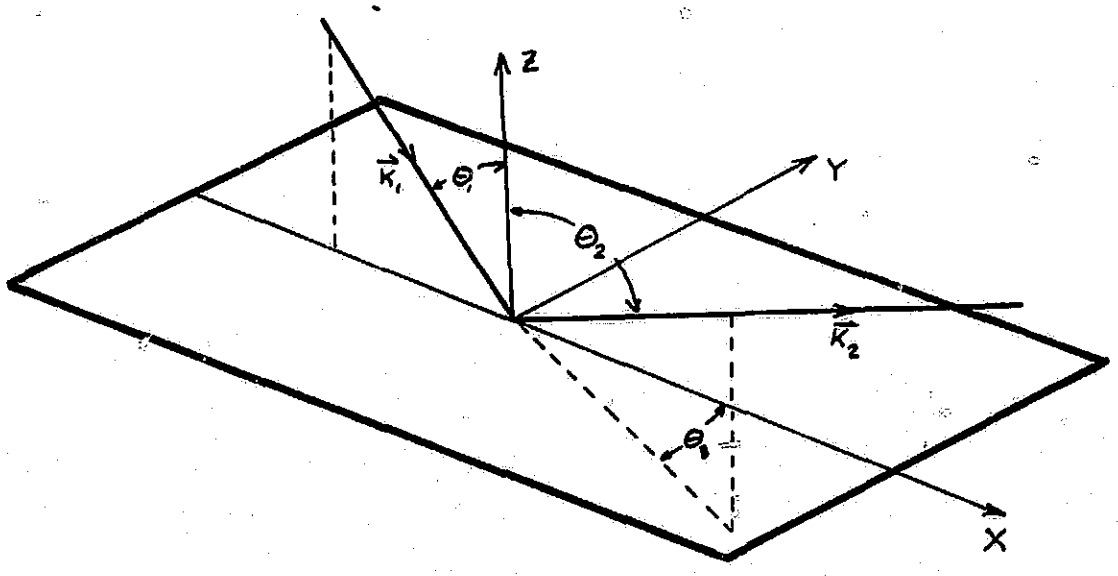

Figure 2-1. Scattering Geometry Defining θ_1, θ_2, and θ_3

If a, b, and c are constant over the illuminated area, i.e. if the reflection coefficient does not vary over the range of the local incident angle, (2.1) may be integrated by parts to give

$$p = \frac{1}{4XY\cos\theta_1}\left[b + \frac{aV_x + cV_y}{V_2}\right] \int_{-X}^{X}\int_{-Y}^{Y} e^{i\vec{v}\cdot\vec{r}}\, dx\, dy$$

$$- \frac{ic}{V_2}\int_{-X}^{X} e^{i\vec{v}\cdot\vec{r}}\Big|_{-Y}^{Y} dx - \frac{ia}{V_2}\int_{-Y}^{Y} e^{i\vec{v}\cdot\vec{r}}\Big|_{-X}^{X} dy \qquad (2.6)$$

It can be shown that if the illuminated area is much greater than the exploring wavelength the only significant contribution comes from the first term so (2.6) reduces to

$$p_2 = \frac{F_3}{A}\int_A\int e^{i\vec{v}\cdot\vec{r}}\, dx\, dy \qquad (2.7)$$

where

$$F_3(\theta_1, \theta_2, \theta_3) = \left(b + \frac{aV_x + cV_y}{V_2}\right)\frac{1}{\cos\theta_1}$$

$$= \frac{R}{\cos\theta_1}\left[\frac{1 + \cos\theta_1\cos\theta_2 - \sin\theta_1\sin\theta_2\cos\theta_3}{\cos\theta_1 + \cos\theta_2}\right] \qquad (2.8)$$

A = 4XY is the area projected onto the xy plane

From (2.7) we can compute the average power using the Poynting vector

$$\langle P_2 \rangle = \frac{1}{2Z}\langle p_2 p_2^* \rangle \qquad (2.9)$$

where Z is the acoustic impedance at the point and the brackets represent the ensemble average of the terms enclosed. The quantity pp^* is

$$pp^* = \frac{F_3^2}{A^2}\int_{-X}^{X}\int_{-X}^{X}\int_{-Y}^{Y}\int_{-Y}^{Y} e^{iV_x(x_1 - x_2) + iV_y(y_1 - y_2)}\, e^{iV_z(\zeta(x_1,y_1) - \zeta(x_2,y_2))}\, dx_1\, dx_2\, dy_1\, dy_2 \qquad (2.10)$$

Defining $\xi_1 \equiv \xi(x_1, y_1)$, $\xi_2 \equiv \xi(x_2, y_2)$ and averaging gives

$$\langle p p^* \rangle = \frac{F_3^2}{A^2} \int_{-Y}^{X} \int_{-X}^{Y} \int_{-Y}^{Y} e^{i v_x (x_1 - x_2) + i v_y (y_1 - y_2)} \langle e^{i v_z (\xi_1 - \xi_2)} \rangle \, dx_1 \, dx_2 \, dy_1 \, dy_2 \tag{2.11}$$

Now define the distance between (x_1, y_1) and (x_2, y_2) as τ and write (2.11) in polar coordinates

$$\langle p p^* \rangle = \frac{F_3^2}{A^2} \int_{\tau} \int_{\phi=0}^{2\pi} e^{i v_x \tau \cos\phi + i v_y \sin\phi} \langle e^{i v_z (\xi_1 - \xi_2)} \rangle \, \tau \, d\tau \, d\phi \tag{2.12}$$

Performing the integration over ϕ gives

$$\langle p p^* \rangle = \frac{2\pi F_3^2}{A^2} \int_{\tau} J_0 (\tau \sqrt{v_x^2 + v_y^2}) \langle e^{i v_z (\xi_1 - \xi_2)} \rangle \, \tau \, d\tau \tag{2.13}$$

To be considered now is the average of $\exp(i v_z (\xi_1 - \xi_2))$ which is given by

$$\langle e^{i v_z (\xi_1 - \xi_2)} \rangle = \int_{-\infty}^{\infty} \int_{-\infty}^{\infty} e^{i v_z (\xi_1 - \xi_2)} P(\xi_1, \xi_2) \, d\xi_1 \, d\xi_2 \tag{2.14}$$

where $P(\xi_1, \xi_2)$ is the joint probability distribution of the random variables ξ_1 and ξ_2. Equation (2.14) defines the joint characteristic function $\chi(v_z, -v_z)$ (Davenport and Root, pg. 52) so (2.13) can be written as

$$\langle p p^* \rangle = \frac{2\pi F_3^2}{A^2} \int_{\tau} J_0 (\tau \sqrt{v_x^2 + v_y^2}) \chi(v_z, -v_z) \, \tau \, d\tau \tag{2.15}$$

It is now necessary to assume a specific roughness distribution to perform the integration. The most important and probably the most typical is the normal distribution. The variance can be chosen to

represent any degree of roughness and the correlation distance represents the density of irregularities.

Let ζ be normally distributed with zero mean and standard deviation σ, in particular let ζ's distribution be given by

$$W(z) = \frac{1}{\sigma\sqrt{2\pi}} e^{-\frac{z^2}{2\sigma^2}} \tag{2.16}$$

Note that this does not say anything about the density of the irregularities. This information is conveyed by the correlation function, which gives the correlation between the random values assumed by ζ at two points (x_1, y_2) and (x_2, y_2) separated by a distance τ. One autocorrelation function that can be handled analytically is

$$C(\tau) = e^{-\frac{\tau^2}{L^2}} \tag{2.17}$$

where L is the "correlation distance" for which $C(\tau)$ drops to the value e^{-1}.

The two-dimensional normal distribution of two random variables ζ_1 and ζ_2 with zero mean values, variances σ^2 and correlated by a correlation function C, is

$$W(z_1, z_2) = \frac{1}{2\pi\sigma^2\sqrt{1-C^2}} \exp\left[\frac{-z_1^2 + 2C z_1 z_2 - z_2^2}{2\sigma^2(1-C^2)}\right]. \tag{2.18}$$

The characteristic function of this distribution is given by

$$\chi(v_2, -v_2) = \exp\left[-v_2^2\sigma^2(1-C)\right]. \tag{2.19}$$

Substituting (2.17) into (2.19) and expanding in an exponential series gives

$$\chi(v_2, -v_2) = e^{-v_2^2\sigma^2} \sum_{m=0}^{\infty} \frac{v_2^{2m}\sigma^{2m}}{m!} e^{-\frac{m\tau^2}{L^2}}. \tag{2.20}$$

For ease of notation let

$$v_2^2\sigma^2 = q$$

or

$$\sqrt{g} = 2\pi \frac{\sigma}{\lambda} (\cos\theta_1 + \cos\theta_2) \tag{2.21}$$

and

$$v_{xy} = \sqrt{v_x^2 + v_y^2}. \tag{2.22}$$

Substituting (2.20) into (2.15) yields

$$\langle \rho\rho^* \rangle = \frac{2\pi F_3^2}{A^2} \int_{\tau=0}^{\infty} J_0(\tau v_{xy}) \left[e^{-g} \sum_{m=0}^{\infty} \frac{a^m}{m!} e^{-\frac{m\tau^2}{L^2}} \right] \tau \, d\tau. \tag{2.23}$$

Here the limit of integration has been extended to ∞ which is permissible since for a rough surface the only significant contribution comes from the region near $\tau = 0$. This can also be expressed as

$$\langle \rho\rho^* \rangle = \frac{L^2 \pi F_3^2}{A^2} e^{-g} \sum_{m=0}^{\infty} \frac{g^m}{m!} \int_0^{\infty} e^{-\frac{m\tau^2}{L^2}} J_0(\tau v_{xy}) \tau \, d\tau \tag{2.24}$$

by interchanging summation and integration which can be done since the convergence of (2.23) is uniform. From the theory of Bessel functions

$$\int_0^{\infty} J_0(vr) e^{-mr^2} r \, dr = \frac{1}{2m} e^{-\frac{v^2}{4m}} \quad (Re(m) > 0). \tag{2.25}$$

Applying (2.25) to (2.25) gives

$$\langle \rho\rho^* \rangle = \frac{L^2 \pi F_3^2}{A^2} e^{-g} \sum_{m=1}^{\infty} \frac{g^m}{m!m} e^{-\frac{L^2 v_{xy}^2}{4m}}. \tag{2.26}$$

The series converges more rapidly than the exponential series but when g is large it is too slow to be practical for computation. To enable us to obtain a reasonable solution consider three cases: (A) $g << 1$, (B) $g \approx 1$, and (C) $g >> 1$.

(A) This corresponds to a slightly rough surface. For this case only the first term of the series needs to be considered to give

$$\langle \rho\rho^* \rangle = \frac{L^2 \pi F_3^2 g}{A^2} e^{-g - \frac{L^2 v_{xy}^2}{4}} \qquad g << 1. \tag{2.27}$$

(B) This corresponds to a moderately rough surface with the RMS roughness comparable to the incident wavelength. In this case (2.26) can be used with a reasonable number of terms.

(C) This is a very rough surface. For this case saddle-point integration must be used. Going back to (2.15) and substituting in (2.19) and (2.21) we get

$$\langle p p^* \rangle = \frac{2\pi F_3^2}{A^2} \int_0^\infty J_0(v_{xy}\tau)\, e^{-g(1-c)}\, \tau\, d\tau \qquad (2.28)$$

or using (2.17)

$$\langle p p^* \rangle = \frac{2\pi F_3^2}{A^2} \int_0^\infty J_0(v_{xy}\tau)\, e^{-g\left[1-e^{-\frac{\tau^2}{L^2}}\right]}\, \tau\, d\tau. \qquad (2.29)$$

Using only the first two terms of the expansion of $\exp(\tau^2/L^2) \approx 1 + \frac{\tau^2}{L^2}$ this becomes

$$\langle p p^* \rangle = \frac{2\pi F_3^2}{A^2} \int_0^\infty J_0(v_{xy}\tau)\, e^{-\frac{g\tau^2}{L^2}}\, \tau\, d\tau. \qquad (2.30)$$

Using (2.25) again we get

$$\langle p p^* \rangle = \frac{\pi L^2 F_3^2}{A^2 g}\, e^{\frac{-v_{xy}^2 L^2}{4g}} \qquad (2.31)$$

or replacing g this becomes

$$\langle p p^* \rangle = \frac{\pi L^2 F_3^2}{A^2 v_2^2 \sigma^2}\, e^{-\frac{v_{xy}^2 L^2}{4 v_2^2 \sigma^2}} \qquad g >> 1. \qquad (2.32)$$

Thus the average scattered acoustic power can be determined for any set of Θ_1, Θ_2, Θ_3.

2.3 Layer with Smooth front Face and Two-Dimensionally Rough Back Interface

This is the simpler of the two cases since the effect of the layer can be broken up into a specular signal from the smooth front and a scattered signal from the rough back appropriately modified by refraction and attenuation. For backscatter the front will not contribute except near vertical incidence where it should be the dominant term. For non-vertical incidence the main contribution will come from the roughness, as modified by the refraction through the front face.

The incident wave on the rough surface must be modified to take into account the changed incident angle and the signal loss through attenuation. This is done by considering the system shown in Figure 2.2. Note that Θ_1 and ϕ_1 are related by Snell's law such that

$$\phi_1 = \sin^{-1}\left[\frac{v}{v}\sin\Theta_1\right] = \sin^{-1}\left[\frac{1}{n}\sin\Theta_1\right]. \qquad (2.33)$$

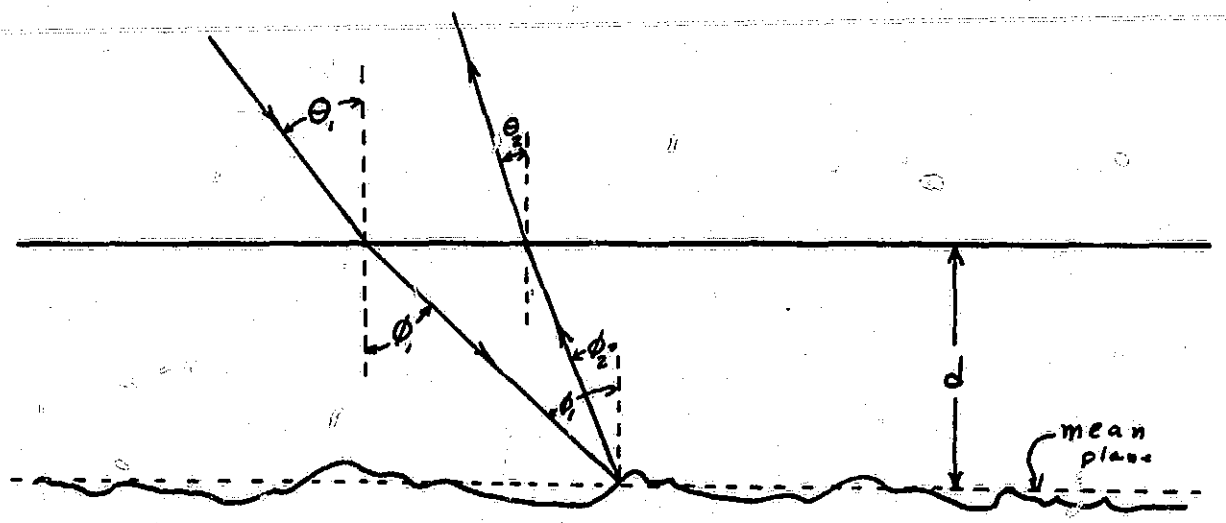

Figure 2.2 Layer with Smooth Front and Rough Rear

For the attenuation effect consider a plane wave of unit amplitude incident on the top surface. Just below the surface the wave will have the amplitude T, i,e., the incident amplitude multiplied by the transmission coefficient. On the rough surface this will then become

$$= T e^{-\alpha d \sec \phi_1} \qquad (2.34)$$

The wave scattered back to the smooth surface is given by (2.7) as

$$p_3 = \frac{F_3}{A} T e^{-\alpha d(\sec\phi_1 + \sec\phi_2)} \iint_A e^{i\vec{v}\cdot\vec{r}}\, dx\, dy \tag{2.35}$$

where ϕ_3 has been considered to be zero. Above the layer we have again by Snell's law

$$\theta_2 = \sin^{-1}(n \sin\phi_2) \tag{2.36}$$

and

$$p_3' = \frac{F_3}{A} T T' e^{-\alpha d(\sec\phi_1 + \sec\phi_2)} \iint_A e^{i\vec{v}\cdot\vec{r}}\, dx\, dy. \tag{2.37}$$

Now if we restrict the discussion to the case of backscatter which means

$$\theta_1 = -\theta_2\ ,\ \theta_3 = 0 \tag{2.38}$$

this becomes

$$p_3' = \frac{F_3}{A} T T' e^{2\alpha d \sec\phi_1} \iint_A e^{i\vec{v}\cdot\vec{r}}\, dx\, dy. \tag{2.39}$$

Finding the average backscatter power by the same method as the preceding section yields

$$\langle p p^* \rangle = \frac{\pi F_3^2}{A^2} T^2 T'^2 L^2 e^{-g - 4\alpha d \sec\phi_1} \sum_{m=0}^{\infty} \frac{g^m}{m\,m!} e^{-\frac{L^2 v_y^2}{4m}} \tag{2.40}$$

where $F_3 = \dfrac{R}{\cos^2\theta_1}$

R is the reflection coefficient of the bottom interface

T is the transmission coefficient from medium 1 to 2

T' is the transmission coefficient from medium 2 to 1

$g = v_2^2 \sigma^2 = 4k^2 \cos^2\phi_1 \sigma^2$

$\phi_1 = \sin^{-1}(n^{-1} \sin\theta_1)$

$v_{xy} = 2k \sin\phi_1$

d = thickness of the layer.

Rewriting this gives us

$$\langle pp^* \rangle = \pi \left[\frac{LRTT'}{A \cos\theta_1} e^{-2k^2 \cos^2\phi_1 \sigma^2} e^{-2\alpha d \sec\phi_1} \right]^2 X$$

$$\sum_{m=0}^{\infty} \frac{(4k^2 \cos^2\phi_1 \sigma^2)^m}{m\, m!} e^{-\frac{L^2 k^2 \sin^2\phi}{m}} \qquad (2.41)$$

which describes the return backscattered from the rear of the layer as seen from in front of the layer.

2.4 Layer with Two-Dimensionally Rough Front and Plane Rear Face

This case is much more complex since the rough surface is seen twice by the waves returned from the rear of the layer.

The backscattered power from the rough front is given by (2.26) as before with the appropriate choice of parameters and

$$F_3 = \frac{R}{\cos^2\theta_1}. \qquad (2.42)$$

To find the field scattered into the layer as a function of direction it is necessary to go back to equation (3.1.18a) (Beckmann and Spizzichino, pg. 22) and modify it to allow for the transmission. This is written as:

$$E(Q_2) = \frac{i e^{ik_2 R_o}}{R_o} \int_S (T\vec{v} - \vec{p}) \cdot \vec{n}\, e^{i\vec{v}\cdot\vec{r}}\, dS \qquad (2.43)$$

where $\vec{v} = \vec{k}_1 - \vec{k}_2$

$\vec{p} = \vec{k}_1 + \vec{k}_2$

n is the local normal to the surface

r is the radius vector = $x\hat{x} + y\hat{y} + \zeta(x,y)\,\hat{z}$

and the geometry of the system is shown in Figure 2.3.

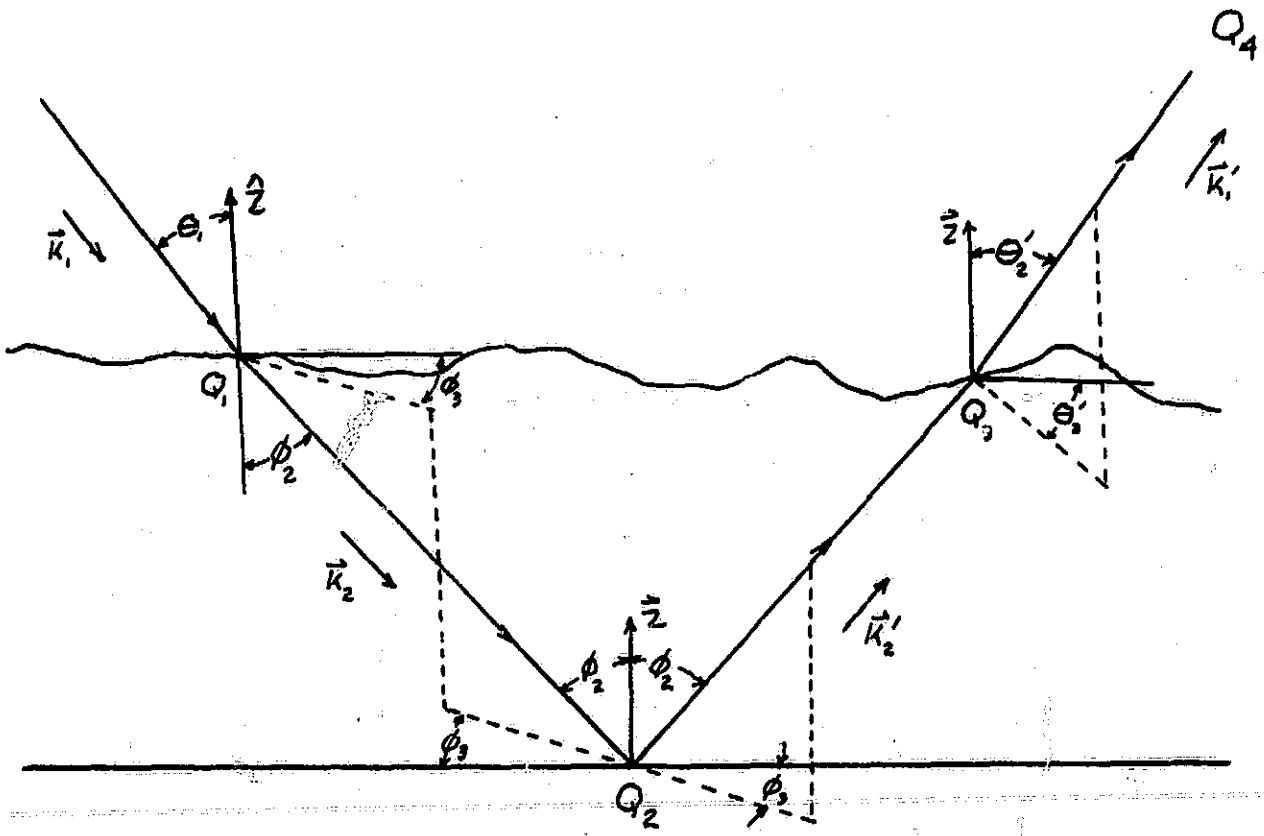

Figure 2.3 Geometry of the Rough Front Case

Writing the k vectors in terms of the xyz coordinate system gives

$$\vec{k}_1 = k_1(\sin\Theta_1\,\hat{x} - \cos\Theta_1\,\hat{z}) \tag{2.44}$$

$$\vec{k}_2 = k_2(\sin\phi_2\cos\phi_3\,\hat{x} + \sin\phi_2\sin\phi_3\hat{y} - \cos\phi_2\,\hat{z}) \tag{2.45}$$

$$\vec{k}_2' = k_2(\sin\phi_2\cos\phi_3\hat{x} + \sin\phi_2\sin\phi_3\hat{y} + \cos\phi_2\,\hat{z}) \tag{2.46}$$

$$\vec{k}_1' = k_1(\sin\Theta_2'\cos\Theta_3'\,\hat{x} + \sin\Theta_2'\sin\Theta_3'\,\hat{y} + \cos\Theta_2'\,\hat{z}) \tag{2.47}$$

where $k_1 = \omega/v_1$ and $k_2 = \omega/v_2$.

Using these

$$\vec{v} = (k_1\sin\Theta_1 - k_2\sin\phi_2\cos\phi_3)\,\hat{x} - k_2\sin\phi_2\sin\phi_3\hat{y}$$

$$+ (k_2\cos\phi_2 - k_1\cos\Theta_1)\hat{z} \tag{2.48}$$

$$\vec{p} = (k_1 \sin\Theta_1 + k_2 \sin\phi_2 \cos\phi_3)\hat{x} + k_2 \sin\phi_2 \sin\phi_3 \hat{y}$$

$$- (k_2 \cos\phi_2 + k_1 \cos\Theta_1)\hat{z}. \qquad (2.49)$$

Now consider the factor n dS and define the local slope of the surface in the x-direction as β , and in the y-direction as γ . This definition gives

$$\vec{n} = \sin\beta \cos\gamma\, \hat{x} + \sin\gamma \cos\beta\, \hat{y} + \cos\gamma \cos\beta\, \hat{z}$$

$$= \cos\gamma \cos\beta\, (\tan\beta \hat{x} + \tan\gamma \hat{y} + \hat{z}) \qquad (2.50)$$

and $$dS = \sec\beta \sec\gamma\, dxdy \qquad (2.51)$$

such that

$$\vec{n}\, dS = (\tan\beta \hat{x} + \tan\gamma\, \hat{y} + \hat{z})\, dxdy$$

$$= \left(\frac{\partial f}{\partial x}\, \hat{x} + \frac{\partial f}{\partial y}\, \hat{y} + \hat{z}\right) dxdy \qquad (2.52)$$

which is the projection of dS onto the xy-plane. The term $(T\vec{v} - \vec{p})$ reduces to

$$T\vec{v} - \vec{p} = [(T-1)k_1 \sin\Theta_1 - (T+1)k_2 \sin\phi_2 \cos\phi_3]\hat{x} - (T+1)k_2 \sin\phi_2 \sin\phi_3 \hat{y}$$

$$+ [(T+1)k_2 \cos\phi_2 - (T-1)k_1 \cos\Theta_1]\hat{z}$$

$$= a\hat{x} + b\hat{y} + c\hat{z}. \qquad (2.53)$$

Thus (2.43) can be written as

$$E(Q_2) = \frac{i e^{ik_2 R_o}}{4\pi R_o} \int_S [a f_x' + b f_y' + c]\, e^{i\vec{v}\cdot\vec{r}}\, dx\, dy. \qquad (2.54)$$

If T is a constant over the range of incident angles encountered during any one set of conditions this can be integrated by parts as was done for (2.1) to give

$$E(Q_2) = \frac{i e^{ik_2 R_o}}{4\pi R_o}\left[c + \frac{a v_x + b v_y}{v_2}\right]\int_{-X}^{X}\int_{-Y}^{Y} e^{i\vec{v}\cdot\vec{r}}\, dx\, dy + \text{edge effect} \tag{2.55}$$

where the edge effect term is similar to that encountered before and is negligable if the illuminated area is large enough. Solving for the bracketed term in front of the integral gives

$$c + \frac{a v_x + b v_y}{v_2} = \frac{k_2^2 - k_1^2 + T(k_2^2 + k_1^2) + 2T k_1 k_2 (\cos\phi_2 \cos\theta_1 + \sin\theta_1 \sin\phi_2 \cos\phi_3)}{k_2 \cos\phi_2 - k_1 \cos\theta_1}$$

$$\equiv F_4. \tag{2.56}$$

Thus the field on the rough surface at point Q_3 due to the scattering around Q_1 is given by

$$E(Q_3) = \frac{i e^{i 2 k_2 R_o}}{4\pi 2 R_o} R F_4 \int_{-X}^{X}\int_{-Y}^{Y} e^{i\vec{v}\cdot\vec{r}}\, dx\, dy \tag{2.57}$$

where $R_o = d \sec\phi_2$.

Using this as the incident field in the Helmholtz integral again to find the field scattered to Q_4 yields

$$E(Q_4) = \frac{e^{i 2(k_2 d \sec\phi_2 + k_1 R_o')}}{2 d \sec\phi_2 + R_o'} F_4 F_4' R \int_{X}^{Y}\int_{X'}^{Y'}\int_{X}^{Y}\int_{X'}^{Y'} e^{i\vec{v}\cdot\vec{r}}\, e^{i\vec{v}'\cdot\vec{r}'}\, dx\, dy\, dx'\, dy' \tag{2.58}$$

where $$F_4' = \frac{(T'-1)k_2^2 + (T'+1)k_1^2 - 2T' k_1 k_2 [\cos\theta_2' \cos\phi_2 - \sin\phi_2 \sin\theta_2' \cos(\phi_3 + \theta_3')]}{k_2 \cos\phi_2 - k_1 \cos\theta_2'}$$

T' is the transmission coefficient from medium 1 to medium 2.

To find the average power at Q_4 we proceed as before to get

$$\langle E E^* \rangle = \frac{F_4 F_4' R}{2d \sec\phi_2 + R_0} \iiiint\limits_{x\bar{x}y\bar{y}x'\bar{x}'y'\bar{y}'} e^{i[v_x(x-\bar{x}) + v_y(y-\bar{y}) + v_x'(x'-\bar{x}') + v_y'(y'-\bar{y}')]} \times$$

$$\langle e^{i[v_2(\xi_1-\xi_2) + v_2'(\xi_1'-\xi_2')]} \rangle \, dx\, d\bar{x}\, dy\, d\bar{y}\, dx'\, d\bar{x}'\, dy'\, d\bar{y}'. \tag{2.59}$$

Making the change of variables

$$x - \bar{x} = \tau \cos\phi$$

$$y - \bar{y} = \tau \sin\phi$$

$$x' - \bar{x}' = \tau' \cos\phi'$$

$$y' - \bar{y}' = \tau' \sin\phi'$$

gives

$$\langle E E^* \rangle = \frac{F_4 F_4' R}{2d \sec\phi_2 + R_0} \int_\tau \int_\phi \int_{\tau'} \int_{\phi'} e^{i\tau(v_x \cos\phi + v_y \sin\phi) + i\tau'(v_x' \cos\phi' + v_y' \sin\phi')} \times$$

$$\langle e^{i[v_2(\xi_1-\xi_2) + v_2'(\xi_1'-\xi_2')]} \rangle \, \tau\, \tau'\, d\tau\, d\tau'\, d\phi\, d\phi'. \tag{2.60}$$

Now note that τ is independent of τ' and ϕ of ϕ' so this becomes

$$\langle E E^* \rangle = K \int_\tau \int_{\tau'} J_0(\tau v_{xy}) J_0(\tau' v_{xy}') \langle e^{i[v_2(\xi_1-\xi_2) + v_2'(\xi_1'-\xi_2')]} \rangle \, \tau\, \tau'\, d\tau\, d\tau' \tag{2.61}$$

where $V_{xy} = \sqrt{V_x^2 + V_y^2}$

$$V'_{xy} = \sqrt{V_x'^2 + V_y'^2}.$$

Let us now examine the term $\langle e^{i[V_z(\zeta_1 - \zeta_2) + V_z'(\zeta_1' - \zeta_2')} \rangle$ in more detail. This can be written as

$$\langle e^{iV_z\zeta_1} e^{-iV_z\zeta_2} e^{iV_z'\zeta_1'} e^{-iV_z'\zeta_2'} \rangle \tag{2.62}$$

where ζ_1, ζ_2, ζ_1', and ζ_2' are random variables with a Gaussian distribution function of the form

$$W(z) = \frac{1}{\sigma\sqrt{2\pi}} e^{-\frac{Z^2}{2\sigma^2}} \tag{2.63}$$

where Z is the surface height.

Equation (2.62) is of the form (Fung 1967)

$$\langle Z_1 Z_2 Z_3 Z_4 \rangle = \langle Z_1 Z_2 \rangle \langle Z_3 Z_4 \rangle + \langle Z_1 Z_3 \rangle \langle Z_2 Z_4 \rangle + \langle Z_1 Z_4 \rangle \langle Z_2 Z_3 \rangle \tag{2.64}$$

where each of the double averages can be written as

$$\langle e^{i(aS - bS')} \rangle = e^{-\frac{\sigma^2}{2}(a^2 + b^2 - 2ab\rho_{ss'})} \tag{2.65}$$

with $\rho_{ss'}$ being the correlation function between S and S'. Expanding the averages in detail gives

$$\langle Z_1 Z_2 \rangle = \langle e^{i(v_2 \xi_1 - v_2 \xi_2)} \rangle = e^{-\sigma^2 v_2^2 (1 - \rho_{12})} \tag{2.66a}$$

$$\langle Z_3 Z_4 \rangle = \langle e^{i(v_2' \xi_1' - v_2' \xi_2')} \rangle = e^{-\sigma^2 v_2^2 (1 - \rho_{34})} \tag{2.66b}$$

$$\langle Z_1 Z_3 \rangle = \langle e^{i(v_2 \xi_1 + v_2' \xi_1')} \rangle = e^{-\frac{\sigma^2}{2}(v_2^2 + v_2'^2 - 2 v_2 v_2' \rho_{13})} \tag{2.66c}$$

$$\langle Z_2 Z_4 \rangle = \langle e^{i(-v_2 \xi_2 - v_2' \xi_2')} \rangle = e^{-\frac{\sigma^2}{2}(v_2^2 + v_2'^2 - 2 v_2 v_2' \rho_{24})} \tag{2.66d}$$

$$\langle Z_1 Z_4 \rangle = \langle e^{i(v_2 \xi_1 - v_2' \xi_2')} \rangle = e^{-\frac{\sigma^2}{2}(v_2^2 + v_2'^2 + 2 v_2 v_2' \rho_{14})} \tag{2.66e}$$

$$\langle Z_2 Z_3 \rangle = \langle e^{i(-v_2 \xi_2 + v_2' \xi_1')} \rangle = e^{-\frac{\sigma^2}{2}(v_2^2 + v_2'^2 + 2 v_2 v_2' \rho_{23})} \tag{2.66f}$$

These are then placed back into (2.61) to yield

$$\begin{aligned}\langle E E^* \rangle = K & \int_\tau J_0(\tau v_{xy}) e^{-\sigma^2 v_2^2 (1-\rho_{12})} \tau \, d\tau \; \times \\ & \times \int_{\tau'} J_0(\tau' v_{xy}') e^{-\sigma^2 v_2'^2 (1-\rho_{34})} \tau' \, d\tau' \\ & + K \int_\tau \int_{\tau'} J_0(\tau v_{xy}) J_0(\tau' v_{xy}') e^{-\sigma^2 [v_2^2 + v_2'^2 - v_2 v_2' (\rho_{13} + \rho_{24})]} \tau \tau' \, d\tau \, d\tau' \\ & + K \int_\tau \int_{\tau'} J_0(\tau v_{xy}) J_0(\tau' v_{xy}') e^{-\sigma^2 [v_2^2 + v_2'^2 + v_2 v_2' (\rho_{14} + \rho_{23})]} \tau \tau' \, d\tau \, d\tau'\end{aligned} \tag{2.67}$$

where $$v_z = k_2 \cos\phi_2 - k_1 \cos\theta_1$$

$$v_z' = k_2 \cos\phi_2 - k_1 \cos\theta_2'$$

and

$$v_z^2 = k_2^2 \cos^2\phi_2 - 2k_1k_2 \cos\phi_2 \cos\theta_1 + k_1^2 \cos^2\theta_1$$

$$v_z'^2 = k_2^2 \cos^2\phi_2 - 2k_1k_2 \cos\phi_2 \cos\theta_2' + k_1^2 \cos^2\theta_2'.$$

To find the significance of the correlation functions in (2.67) refer back to the geometry in Figure (2.3) and note that the unprimed variables refer to the region about Q_1 and the primed variables refer to the region about Q_3. In particular, ρ_{12} and ρ_{34} are the surface height auto-correlation function about Q_1 and Q_2 respectively while the rest are the correlation of the surface heights between Q_1 and Q_2. This means that for ϕ_2 near zero (near vertical incidence) the last two terms will contribute to the scattered power but that for larger incident angles the largest contribution will be from the first part of (2.67). The first part of (2.67) can be integrated as before, (2.13), to give

$$\langle EE^* \rangle = KRF_1F_1'L^4 e^{-2q} \sum_{m=1}^{\infty}\sum_{n=1}^{\infty} \frac{q^{mn}}{m!n!} \frac{e^{-\frac{L^2v_{xy}^2}{4m}} e^{-\frac{L^2v_{xy}'^2}{4n}}}{mn}. \tag{2.68}$$

This then gives the first order scattered power from the layer for large angles of incidence. To better define this note that

$$\overline{Q_2Q_3} = 2\,d\tan\phi_2.$$

For the integrals of the last two terms to be small this distance should be of the order of several times the correlation distance of the surface heights.

2.5 Total Scattered Power from a Layer

The total scattered power from a layer of either configuration considered in this chapter can be determined by simply adding the power scattered from the front face to that scattered from the rear face of the layer. This is possible in the mean because the scattered signal has random phase.

CHAPTER III

EXPERIMENTAL PROCEDURES

3.1 Technique of Measurement

Re-radiation of acoustic waves from a rough surface is described by the differential scattering cross section of the surface. This quantity is defined by the radar or sonar equation:

$$\langle P(\theta) \rangle = \iint_S \left[\frac{P_t G_t(\psi_t)}{4\pi r_t^2}\right]\left[\frac{\lambda^2 G_r(\psi_r)}{4\pi r_r^2}\right]\left[\sigma_o\right] dA \qquad (3.1)$$

where $\langle P(\theta) \rangle$ is the average of the received power obtained over an ensemble of surfaces

P_t is the transmitted power

is the angle from the antenna boresight axis

$G_t(\psi_t)$ is the gain function of the transmitter antenna which is here assumed to be a function of ψ_t only

$G_r(\psi_r)$ is the gain function of the receiving antenna, here also assumed to be circularly symmetric

λ is the wavelength of the incident radiation

S is the mean surface illuminated

σ_o is the differential scattering cross section.

The integral of (3.1) can be interpreted as follows: the first factor is the incident power density, the second factor is the solid angle subtended by the receiving aperture, and the last factor is the scattering cross section. The incident power density is that of a spherical wave front at the surface, modified by the gain function of the transmitting transducer. The scattering cross section was defined in Chapter II

on the basis of a plane incident wave front, primarily for mathematical simplicity. So long as the correlation distance of the surface heights is small enough, the spherical wave front can be considered to be locally plane with negligible error.

Measurement of the differential scattering cross section can be made by using a transmitting or receiving transducer (or both) with a narrow beam width. This allows the approximation to be made that the scattering cross section is constant over the illuminated area and reduces the effect of the antenna pattern on the σ_o vs. θ curve. For the measurement considered here there is no time variation of the incident radiation over the illuminated area and the steady state is assumed to exist. This is shown in (3.1) by treating P_t as a constant and is referred to as "beam width limitation."

With these restrictions (3.1) becomes

$$\langle P(\theta)\rangle = \sigma_o(\theta) \iint_S \frac{P_t G_t(\psi_t) G_r(\psi_r) \lambda^2}{(4\pi r^2)^2} dA. \tag{3.2}$$

It is convenient to normalize this average scattered power with respect to the power received upon direct specular reflection from a perfect reflector, the smooth air-water interface, when illuminated with P_t. This power is

$$P_c = \frac{P_t G_t(0) G_r(0) \lambda^2}{(8\pi r_c^2)^2} \tag{3.3}$$

where r_c is the distance between the transducers and the surface and $G_t(0)$ and $G_r(0)$ are the boresight gains of the antennas. Dividing (3.2) by (3.3) gives

$$\langle P_n(\theta)\rangle \equiv \frac{\langle P(\theta)\rangle}{P_c}$$

$$= \frac{2\sigma_o r_c^4}{r^4} \iint_S g_t(\psi_t) g_r(\psi_r) dA \tag{3.4}$$

where $g_t(\psi_t)$ and $g_r(\psi_r)$ are the normalized antenna gain functions with the value of unity for $\psi_r = \psi_t = 0$ and falling off on either side. The integration accounts for the effect of the antenna patterns on the scattered signals.

The determination of σ_o for the set of angles is then a measurement of the average, normalized power and an evaluation of the aperture effect for these angles. The antenna pattern functions are given by (Morse, 1948)

$$g(\psi) = \frac{2 J_1(ka \sin\psi)}{ka \sin\psi} \qquad (3.5)$$

where J_1 is the Bessel function of order one

k is the wavenumber

a is the radius of the active face

ψ is the angle from the boresight axis.

The transducer used as the transmitter has an active face radius of 8.15 millimeters which means at 1 MHz, ka = 34 (λ = 1.5 mm) while the receiver disk corresponds to ka = 16. These gain functions are then substituted into (3.4) and the integral is evaluated to obtain the aperture effect. The integration was done by Parkins (1965) using numerical methods with the result shown in Figure 3.1.

The illuminated area must be large enough to permit the surface to have a sufficient number of variations to define the random process. Clark (1963) has shown that the dimensions of the illumination should be at least 10 times the correlation distance of the surface generating process. For antennas with 6^o half-power beamwidth such as used here, this requires the range to be greater than 11 times the correlation distance, L.

Also important is the number of independent samples used to obtain the average power. Moore (1969) states that the samples can be considered independent if the value of the correlation between them is less than $1/\pi^2$. The time corresponding to this decorrelation is

$$T_i = 0.65/\Delta f_d \qquad (3.6)$$

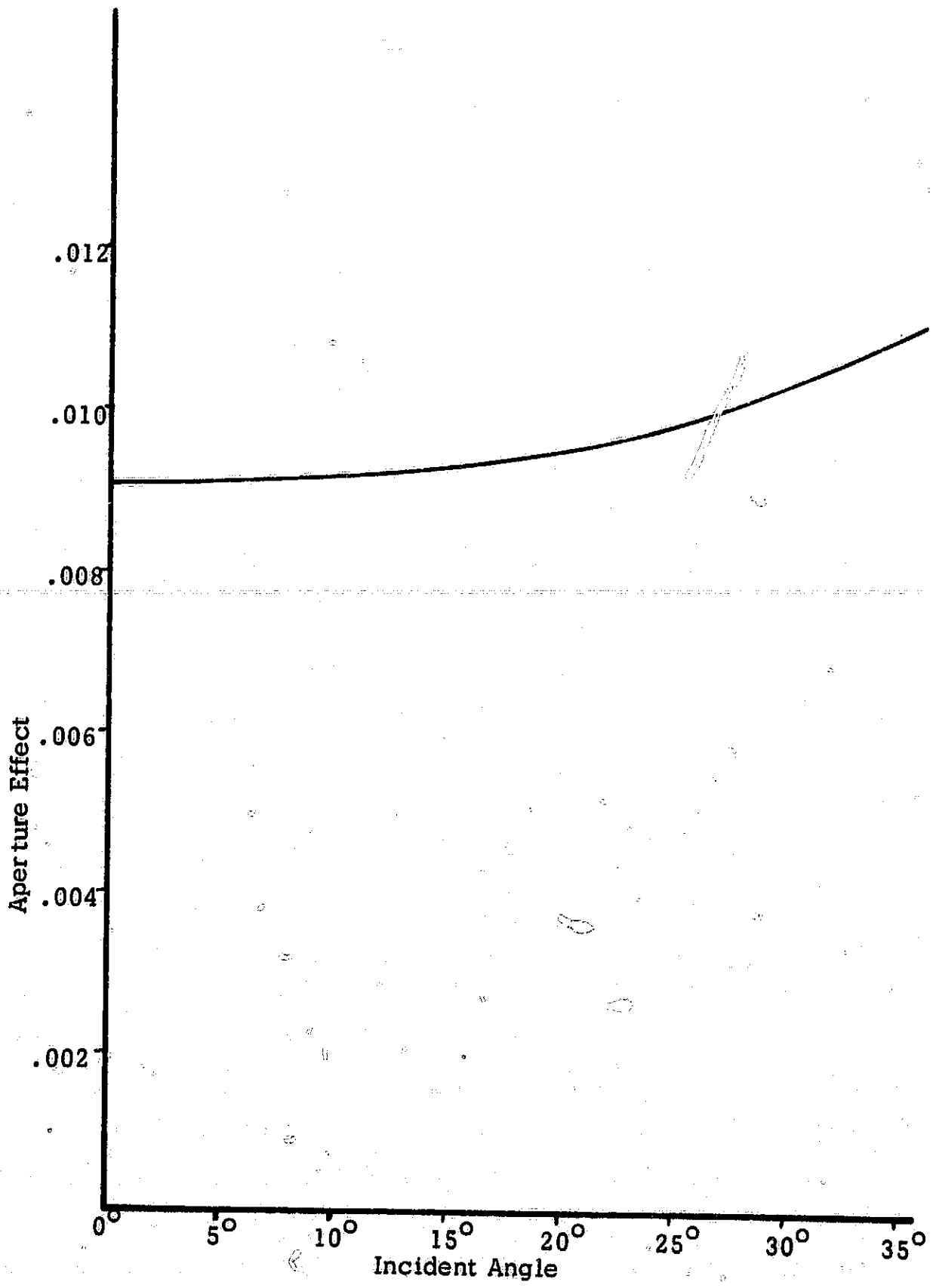

Figure 3-1. Aperture Effect Curve

where

$$\Delta f_d = \frac{2V}{\lambda}\left(\sin\theta_{max} - \sin\theta_{min}\right). \tag{3.7}$$

The worst case for this condition is at vertical incidence where, with 6° antenna beamwidth, 10 mm/sec velocity, and λ of 1.5 mm

$$\Delta f_d = \frac{20}{1.5}(.104) = 1.39 \text{ Hz}, \tag{3.8}$$

This means

$$T_i = .65/1.39 = .467 \text{ sec}, \tag{3.9}$$

Since the averaging time is 20 seconds the number of independent samples is

$$n_i = 20/.467 = 42.5 \tag{3.10}$$

which gives an averaging error of slightly less than 2 dB.

3.2 Description of the Equipment

Determination of σ_o requires the measurement of the average received power over an ensemble of surfaces. Knowing the antenna gain functions for the transducers allows the aperture effect to be evaluated. These measurements were performed using the acoustic simulation facility of the Remote Sensing Laboratory of the Center for Research, Inc. at the University of Kansas. This facility consists of a pair of large water-filled tanks, a mechanical system to provide the aiming of the transducers and scanning the surface, and an electronic system to generate, receive, and process the ultrasonic signals. An overall view of the area is shown in Figure 3.2

The transducer aiming system is shown with the transducers mounted in Figure 3.3. The angle from the vertical can be changed from outside the tank to allow easy determination of the average power vs. angle. Figure 3.4 is a close-up of the transducer assembly showing the size of the unit and the active areas of the two transducers (the

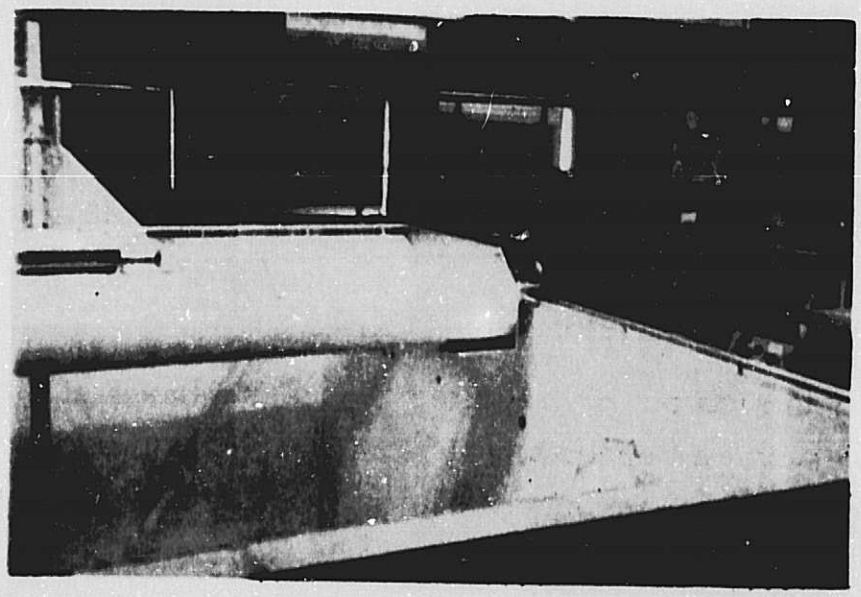

Figure 3.2. Overall View of the Acoustic Facility

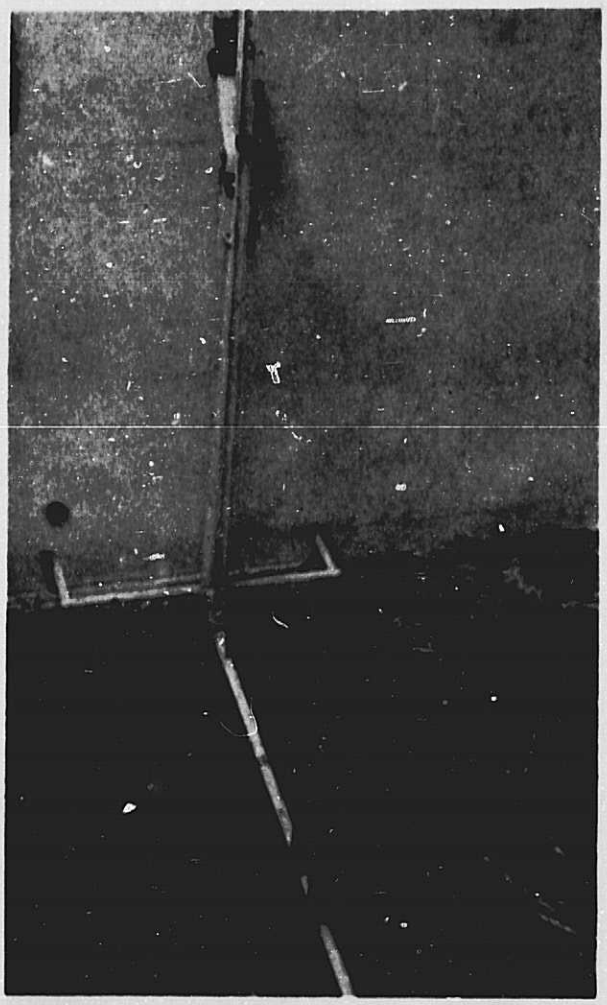

Figure 3.3. Transducer Aiming Mechanism

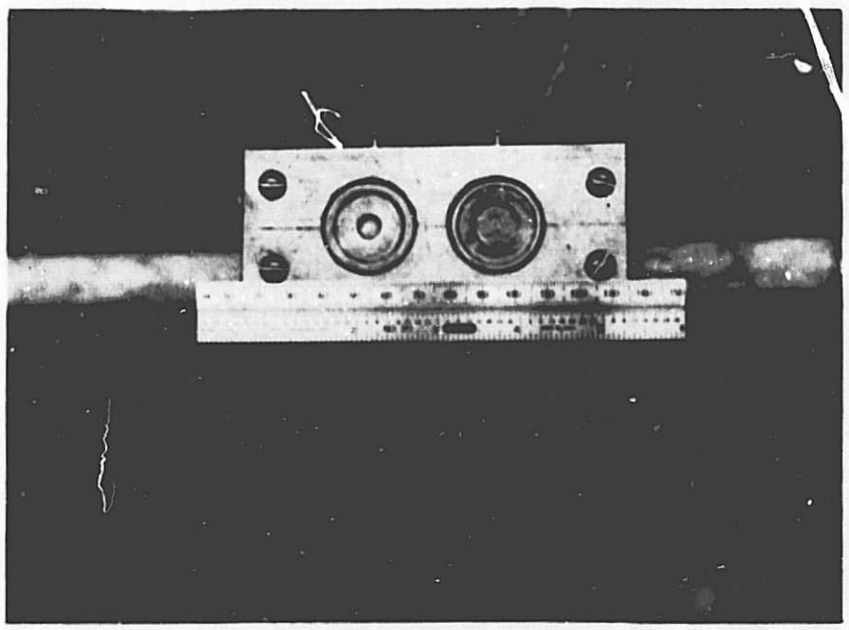

Figure 3.4. Close-up of Transducer Mount Showing Transducers Mounted

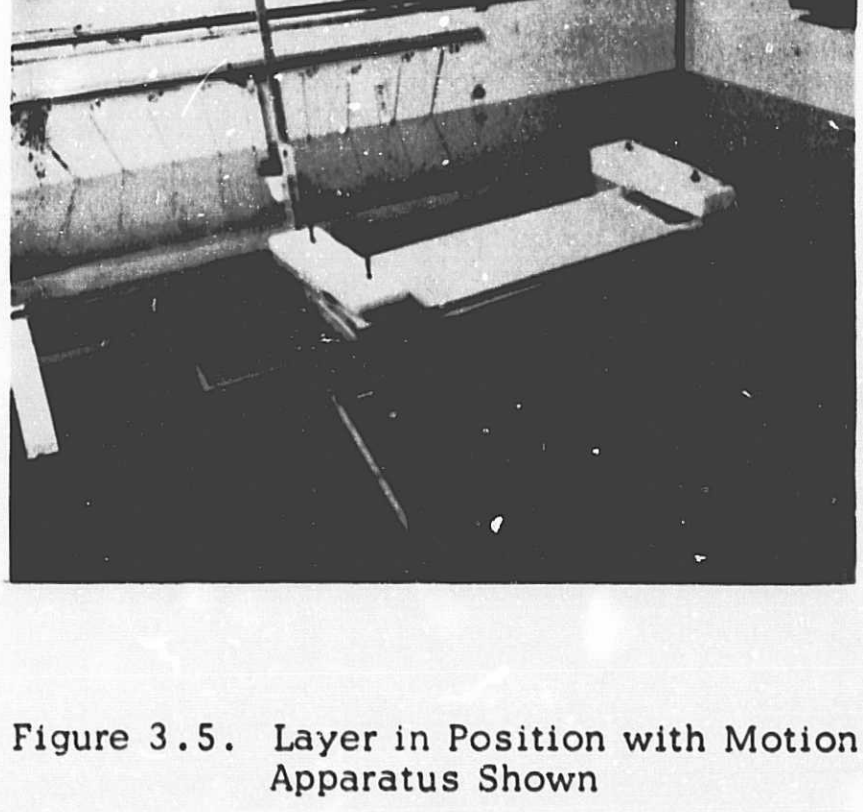

Figure 3.5. Layer in Position with Motion Apparatus Shown

center disks). The larger transducer is used as the transmitter to restrict the illuminated area since it has the narrower beam width, while the smaller is used as the receiving unit.

The method used to scan the surface of the layer is shown in Figure 3.5. The target is shown submerged slightly below the surface of the water with the transducers below it. The styrofoam blocks on the ends of the target are used to support the layer parallel to the surface and as a means of connecting the lines used to tow the assembly across the illuminated area. The motor and gear box seen on the edge of the tank at the upper right of the picture provide the motive force to pull the target to the right while a counterweight moves it to the left when the motor is reversed. A shunt D.C. motor is used, with field and armature voltages adjustable to vary the speed of the scan. For each incident angle of the acoustic wave the speed was adjusted to allow 20 seconds of averaging to cover the length of the layer.

The electronic system is shown photographically in Figure 3.6 and in block diagram form in Figure 3.7. This system is composed of four sub-systems: timing, transmitting, receiving, and data processing.

The timing sub-system is actually two separate units. The first part is the pulse generator which synchronizes the entire system, establishes the pulse repetition frequency, PRF, and the transmitted pulse width. A PRF of 60 Hertz, synchronized to the power line, was used for this experiment in order to avoid errors due to the large amount of power line hash in the locality. The pulse width was chosen to provide a steady-state (beamwidth limited) portion of the signal from the layer at the maximum depression angle. Although it was not essential for this experiment the pulse generator is coherently gated by the radio-frequency oscillator of the transmitter to reduce the leading edge transients of the tone burst. The pulse generator is shown in block diagram form in Figure 3.8. The second part of the timing sub-system is the delayed sweep portion of a Tektronix 535A oscilloscope which was used to select the sample point of the received signal for the processor. The screen of the oscilloscope is brightened during the sample gate to allow the operator to select the desired time delay.

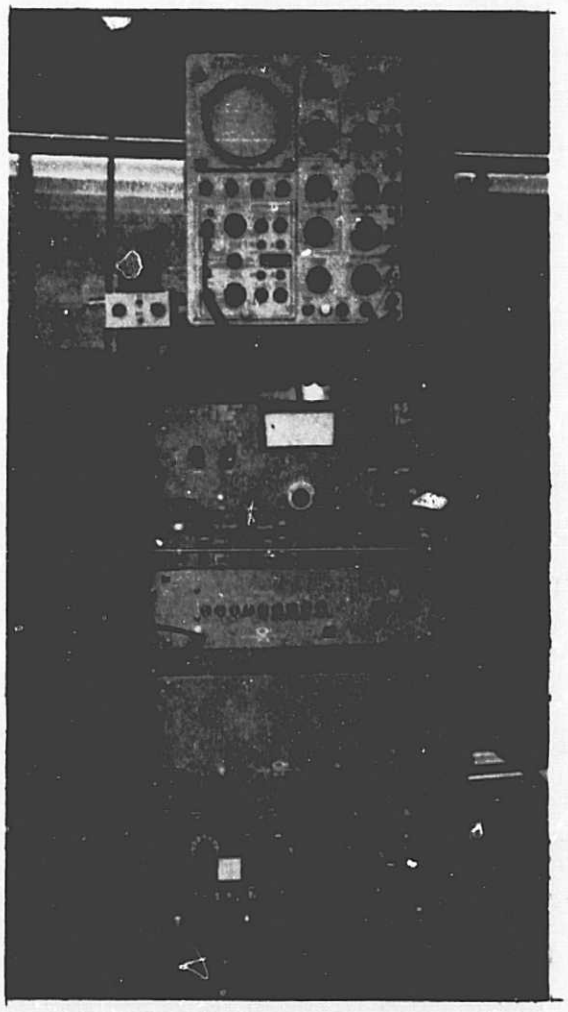

Figure 3.6. Photograph of the Electronic System

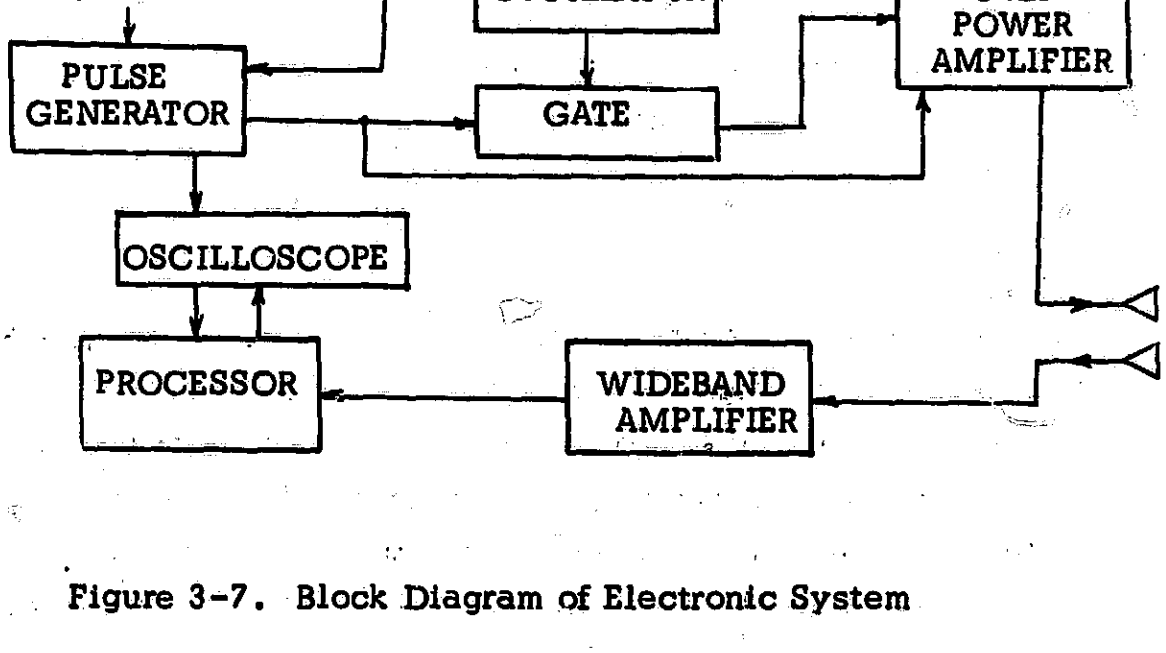

Figure 3-7. Block Diagram of Electronic System

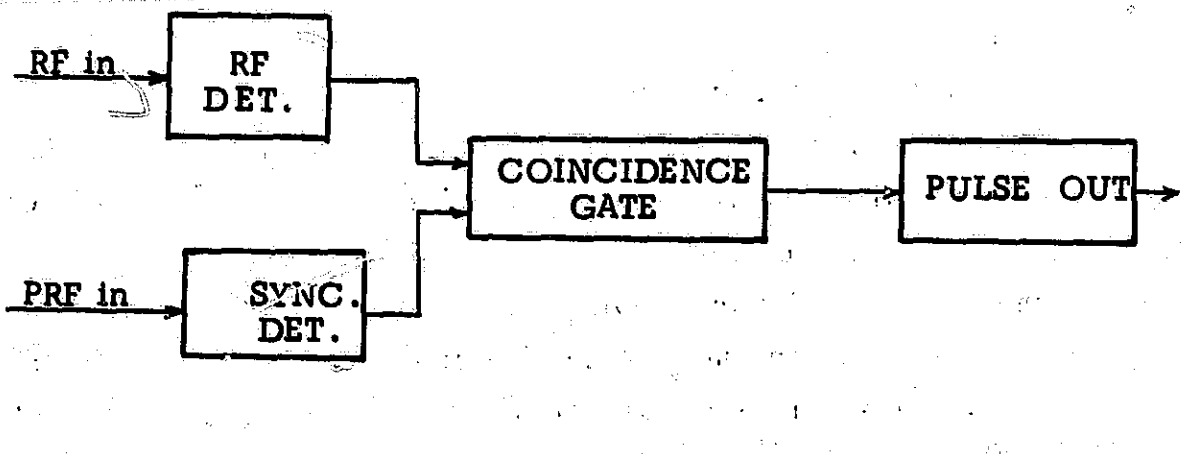

Figure 3-8. Block diagram of Pulse Generator

The transmitting sub-system contains an oscillator which operated continuously, an isolating buffer stage, a pulse modulating gate, and a commercial wideband, linear power amplifier (Coffman Industries, Inc. PA 51). These are all standard circuits and will not be further described here. The output of this sub-system is a radio-frequency tone burst of 60 volts peak-to-peak with length determined by the pulse generator.

The receiving sub-system is shown in more detail in Figure 3.9. The first amplifier has a high input impedance to avoid loading the transducer and a 50 ohm output to match the step-attenuator following it. The main amplifier is a commercial unit (Coffman Industries, Inc., PA-10) with a maximum gain of 40 dB. This amplifier is easily over-driven and care must be used to avoid saturation and distortion of the waveform. A very high impedance load is needed to avoid loading of the output stage. The final amplifier provides this high impedance load and boosts the signal with a voltage gain of 10 to reduce the error due to detector offset.

In the data processing system a peak detector rectifies the fading RF signals, using the base-emitter junction of a transistor to provide a light load on the final amplifier of the receiver. The offset voltage introduced by the detector junction is partially cancelled by using a common-base, direct coupled amplifier between the detector and the sample-hold unit. The sample-hold unit is an Intronics model FS 101 gated by the +A gate from the Tektronics 535A oscilloscope. The output of the sample-hold unit is a series of DC levels -- each one the value of the detected signal at the end of the sample gate. This output is then squared using an Analog Devices model 420A wideband multiplier to give a series of voltage levels proportional to the power of the received signal. These are averaged for a known time interval by an operational amplifier connected as an integrator. At the end of the averaging period the integrator is switched to "hold" automatically and the voltage attained is displayed as representing the average power. The block diagram of this sub-system is shown in Figure 3.10. The processor evaluates

$$\langle P \rangle = \frac{1}{T} \int_{\bullet}^{T} v^2 dt \qquad (3.11)$$

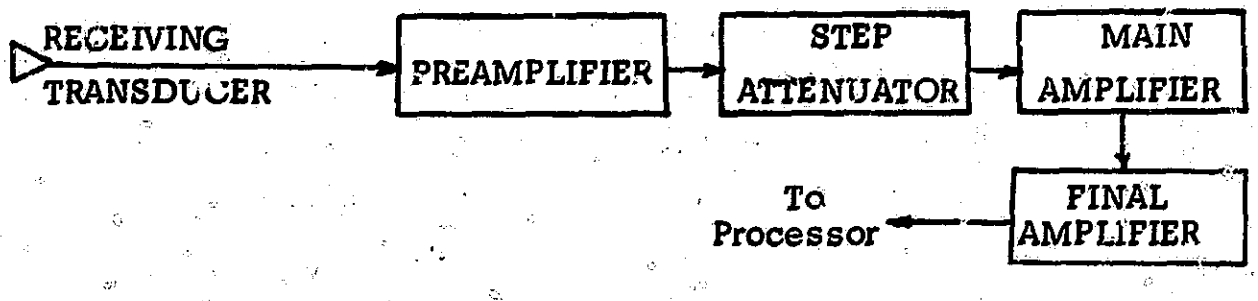

Figure 3-9. Receiving Wideband Amplifier System

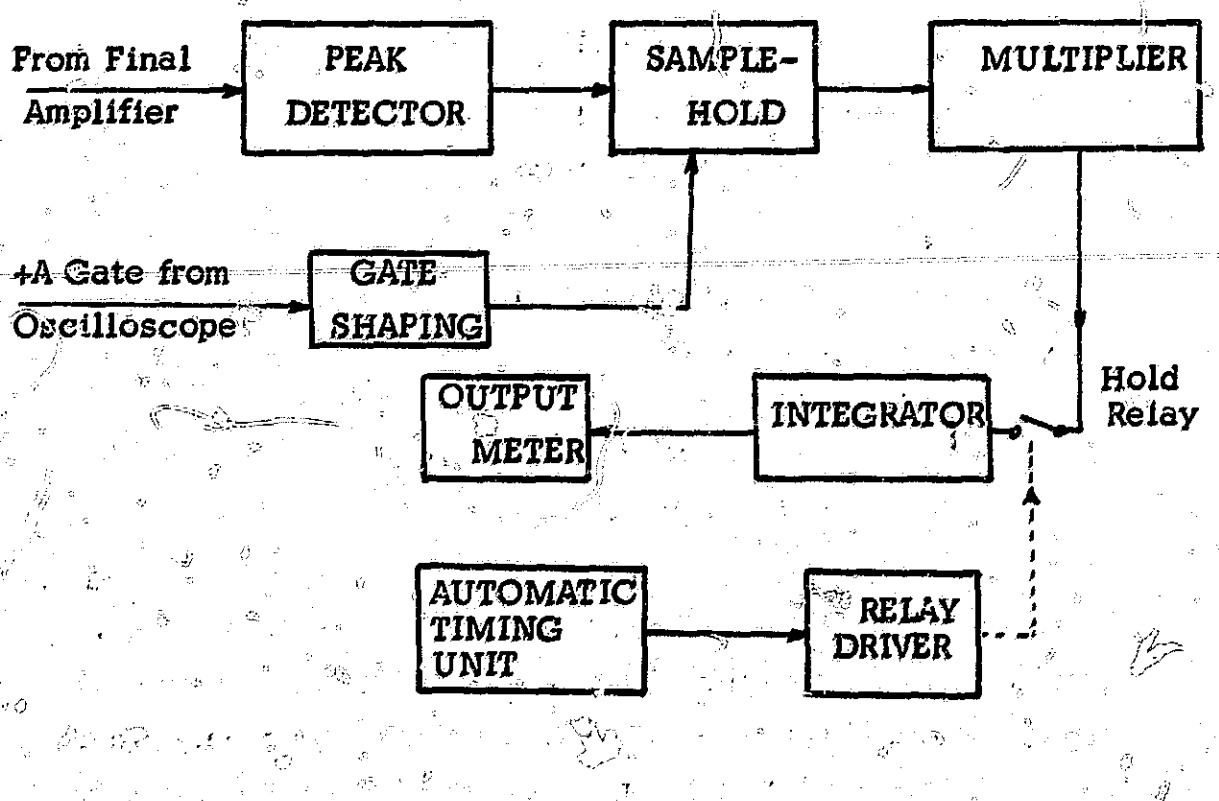

Figure 3-10. Data Procession System

with T held constant at 20 seconds. This calculation of the average power was done on a relative basis as the system was normalized with respect to a calibration power level. This was the power received by the system upon specular reflection from the calm water surface with a given transmitted power and a total path length of 1.5 meters. The experimentally recorded power was then normalized as described in (3.4) to eliminate the transducer gains and the transmitter power level from the calculation of σ_o. After each set of data the calibration procedure was repeated to assure that there had been no gain changes during the run.

3.3 Properties of the Layer Material

Finding a suitable material from which to form a layer occupied considerable time and effort. The properties desired were:

(a) reflection coefficient near 0.5
(b) low attenuation for longitudinal waves
(c) high attenuation for shear waves
(d) able to be formed into the desired shape
(e) not be adversely affected by submergence in water
(f) homogeneous in nature.

Several materials were tried with none satisfying all the criteria, but a soft wax was found which appears to be very close to the desired. The major difference with the specifications is that the reflection coefficient between the wax and water is quite low. While this reduces the level of the return, it is still sufficient to perform the desired experiment. One other minor problem is that the wax tends to absorb water after a period of time and change characteristics slightly. This can be avoided by making all the desired tests within about three days during which time no change can be detected.

3.1.1 Testing the Material

Preliminary work with the wax consisted of finding a suitable mold material to allow the nondestructive removal of the finished target. It was discovered early in the testing that the mold should be flexible

to allow it to be peeled off and "break" the vacuum formed by the close fit. A castable room temperature vulcanizing rubber proved to be satisfactory. To reduce the need for a mold release agent a silicon rubber was used as the mold proper with a backing of lower cost DPR #242 rubber to provide the needed support.

The first acoustic test was made on a slab of wax 37 mm thick with both surfaces parallel and smooth. This slab was floated on the surface of the water and the acoustic transducers were aimed at it from below at normal incidence. This was considered as a very rough test to check the reflection coefficient, attenuation and velocity of propagation for the longitudinal waves of the wax to determine if it warranted further testing. These results were

$$R \approx 0.04$$
$$\alpha_l \approx 0.42/\text{cm}$$
$$v_l \approx 2050 \text{ m/sec}$$

where R is the reflection coefficient

α_l is the attenuation constant

v_l is the velocity of propagation.

These results coupled with the expectation of high attenuation of the shear wave due to viscosity made it a good candidate for further testing.

The next test was to determine v_l and α_l more accurately. To do this a rod of wax was cast with a length of 130 mm and diameter of 50 mm, enough that the bulk longitudinal velocity was the velocity of propagation. With transmitting and receiving transducers mounted on opposite ends of this rod the time delay and the received amplitude were observed. The same transducers were then placed in contact with each other to obtain the effect of the wax. The procedure yielded:

$$v_l = 1870 \text{ m/sec}$$
$$\alpha_l = 0.45 \text{ /cm}$$

which are of the same order of magnitude as the preliminary results.

The shear wave properties remained to be defined after testing this rod. To determine the velocity of shear propagation, v_s, a prism was constructed of the wax. This prism was then submerged in the water and illuminated at an angle to excite a shear wave in the wax. This shear wave propagated through the wax and emerged as a longitudinal wave in the water at an angle determined by the ratio of the velocities. Measuring the angle yields this ratio by the prism equation (Born and Wolff). Another feature of this method is that v_ℓ was also determined at the same time. This conceptually simple experiment was not very successful because a smooth-surfaced prism large enough to occupy all the area illuminated by the transducer was not feasible with the limited molding facilities available. The results, however, were such that a reasonable estimate of v_ℓ and v_s could be made. These were

$$v_\ell = 2010 \text{ m/sec}$$

$$v_s = 900 \text{ m/sec},$$

The results obtained for the longitudinal wave were higher than found by the preceding methods but it was expected that the ratio v_s/v_ℓ would be fairly accurate. The main error in the experiment appeared to be the curvature of the sides of the prism which would tend to have the same effect for both waves. Further investigation using a larger, more accurate prism was not undertaken since an easier method of determining the velocities was found.

This method, which was proposed by Hughes (Hughes, et al., 1949) required that a specimen of the material be formed into a circular cylinder with longitudinal drive and detection to measure the velocity of propagation of both the longitudinal and shear waves. Two such cylinders were prepared with the critical dimensions different to provide a check of the results that should be free of any spurious resonance effects. The velocities obtained by this method were

	Cylinder #1	Cylinder #2
v_l	1800 m/s	1790 m/s
v_s	500 m/s	552 m/s

where the agreement between the two cylinders is much better than the expected error of measurement. No claim is made to this high accuracy but it does tend to add confidence to the method and the results obtained.

This left only the attenuation constant for the shear wave α_s to be determined. In order to avoid the inaccuracies that could arise from not knowing the mode conversion efficiencies accurately it was decided to use a differential method of measurement. To accomplish this two different thicknesses of material were illuminated at an angle of 66° from normal, beyond the critical angle for total reflection of the longitudinal wave which is 56.5°. This should leave only a shear wave to propagate through the slab and be detected. Due to the non-ideal antenna pattern of the transducer a small amount of signal was observed which had traversed the material as a longitudinal wave, but it was sufficiently small that it did not saturate the receiving system to interfere with the measurement of the shear wave. The resulting difference between the strengths of the shear waves received was assumed to be due to the absorption by the material since all other conditions were identical. By this method the shear attenuation constant was found to be 2.75 neper/cm.

3.3.2 Results of Tests

Summing up the results of the various tests gives:

v_l	1800 m/s
v_s	550 m/s
ρ_o	9.37×10^2 kg/m^3
μ_m	2.83×10^8 n/m^2
λ_m	2.46×10^9 n/m^2
σ_m	.447

ν	.449
k_m	2.65×10^9 n/m^2
E	8.21 n/m^2
α_l	.462 n/cm
α_s	2.75 n/cm

Here it is to be noted that only the velocities, attenuation constants and the density were determined experimentally. The other quantities of interest were determined as shown in Appendix C using the equations developed in Appendix A.

The results of the tests indicate that, while the wax is not an ideal material from which to form an acoustic layer, it does exhibit most of the desirable properties; hence, it was chosen as the material to use.

3.3.3 Reflection and Transmission Coefficients vs. Angle

Using the equations derived in Appendix B and the properties of the material given above the reflection and transmission coefficients for the cases of water-wax and wax-water interfaces were calculated. Figures 3.11, 3.12, and 3.13 show the results for propagation from the water onto the wax while figures 3.14, 3.15, and 3.16 are for the other case of a wave incident from within the wax.

3.4 Description of the Rough Surface Used

The characteristics of the scatter of waves from rough surfaces is, in general, determined by the properties of two random processes. These are the variation of surface heights and the variation of the material parameters. For most natural or artificial surfaces these processes are of such complexity that they can only be approximated in description. This problem is compounded by the lack of statistical independence between the processes and their non-stationarity in space and/or time.

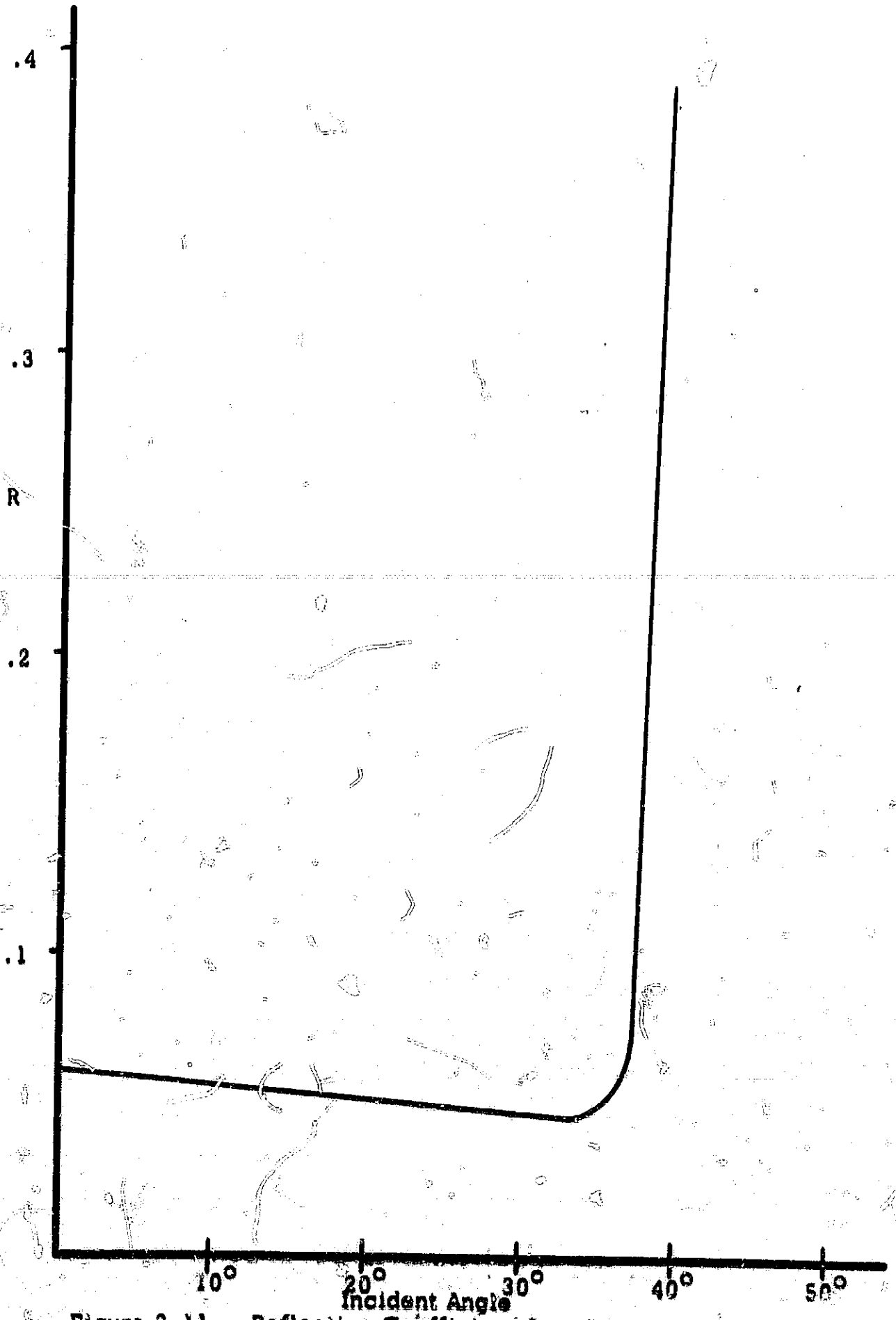

Figure 3-11. Reflection Coefficient from Water to Wax

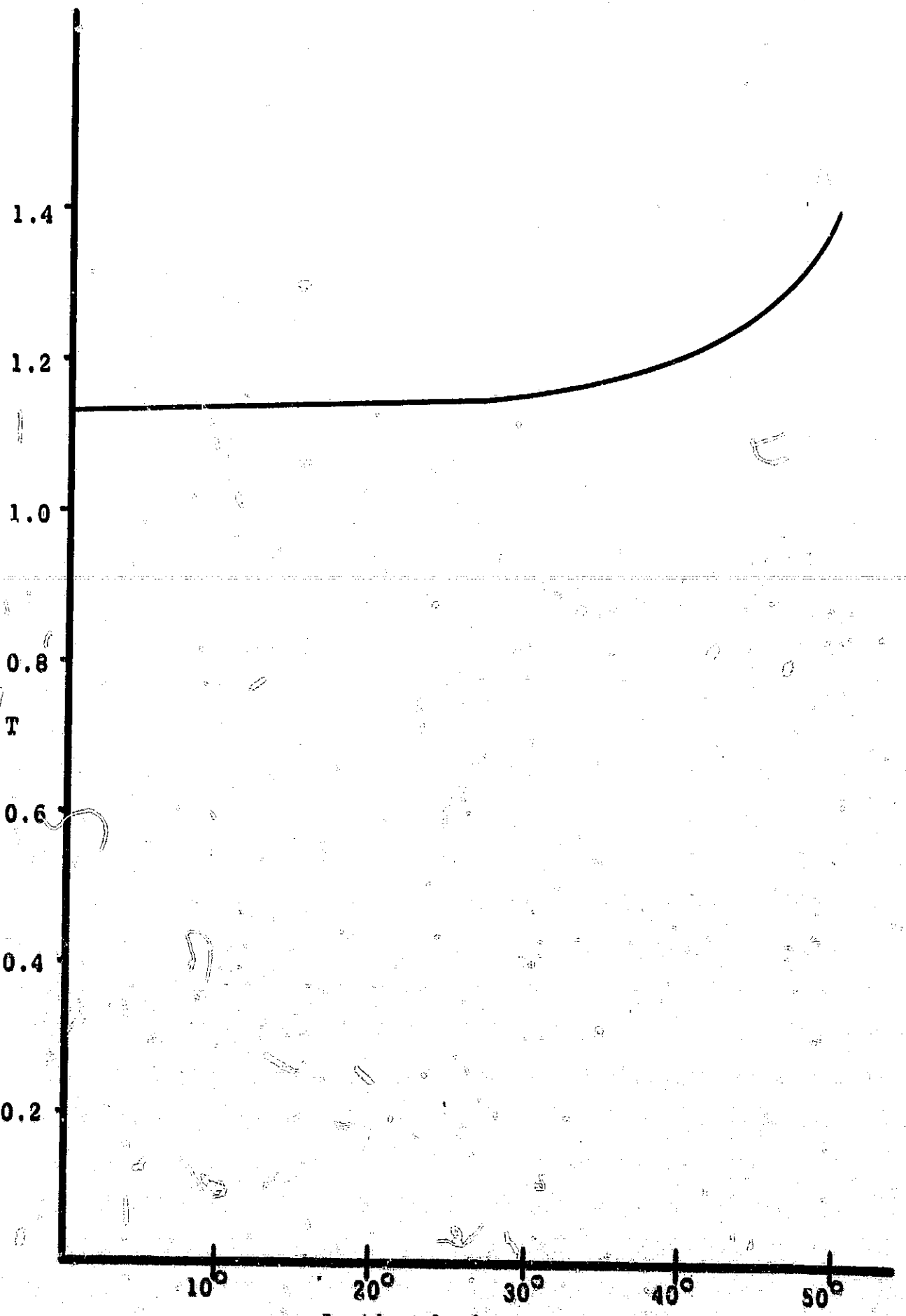

Figure 3-12. Transmission Coefficient from Water to Wax

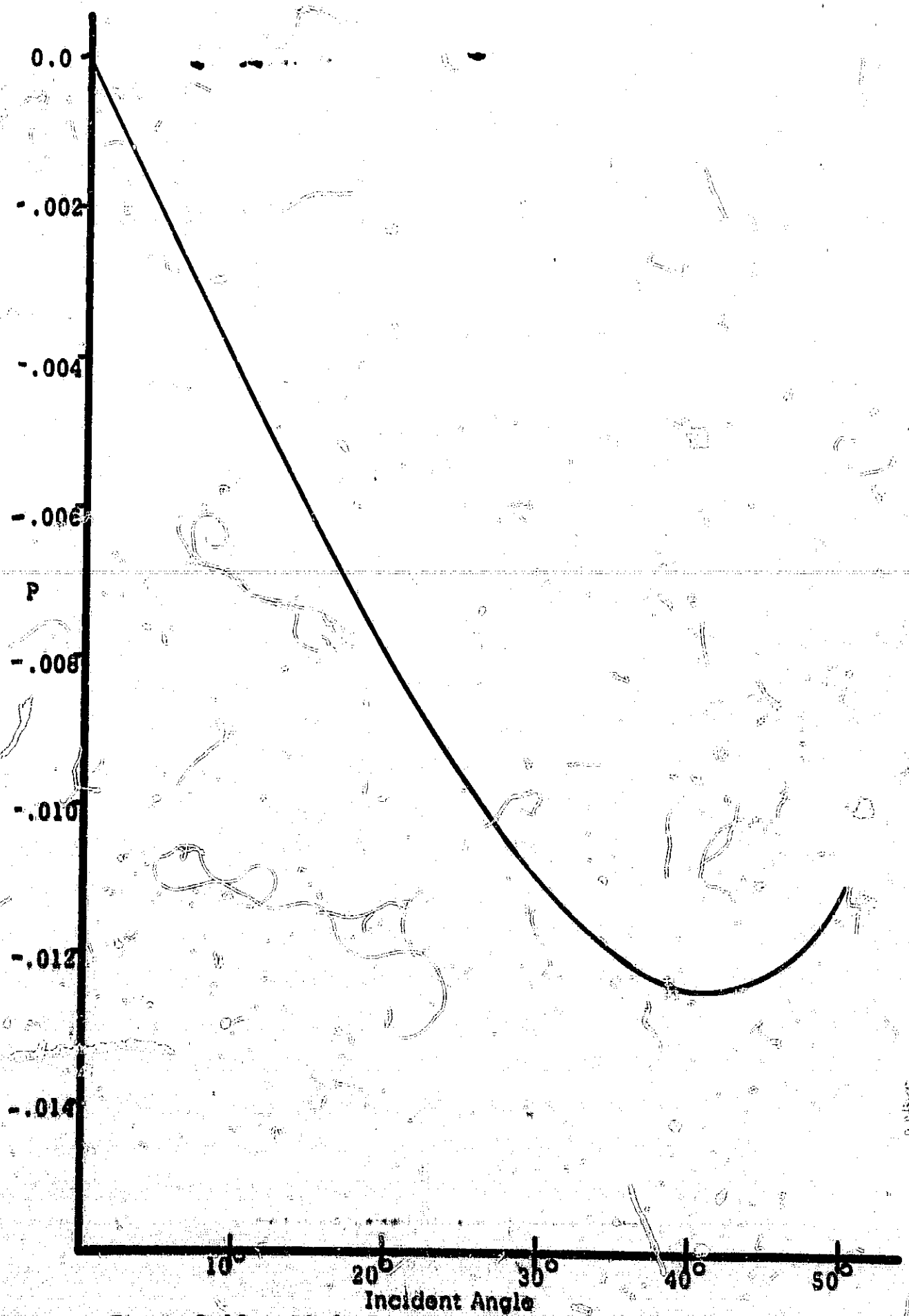

Figure 3-13. Mode Conversion from Water to Wax

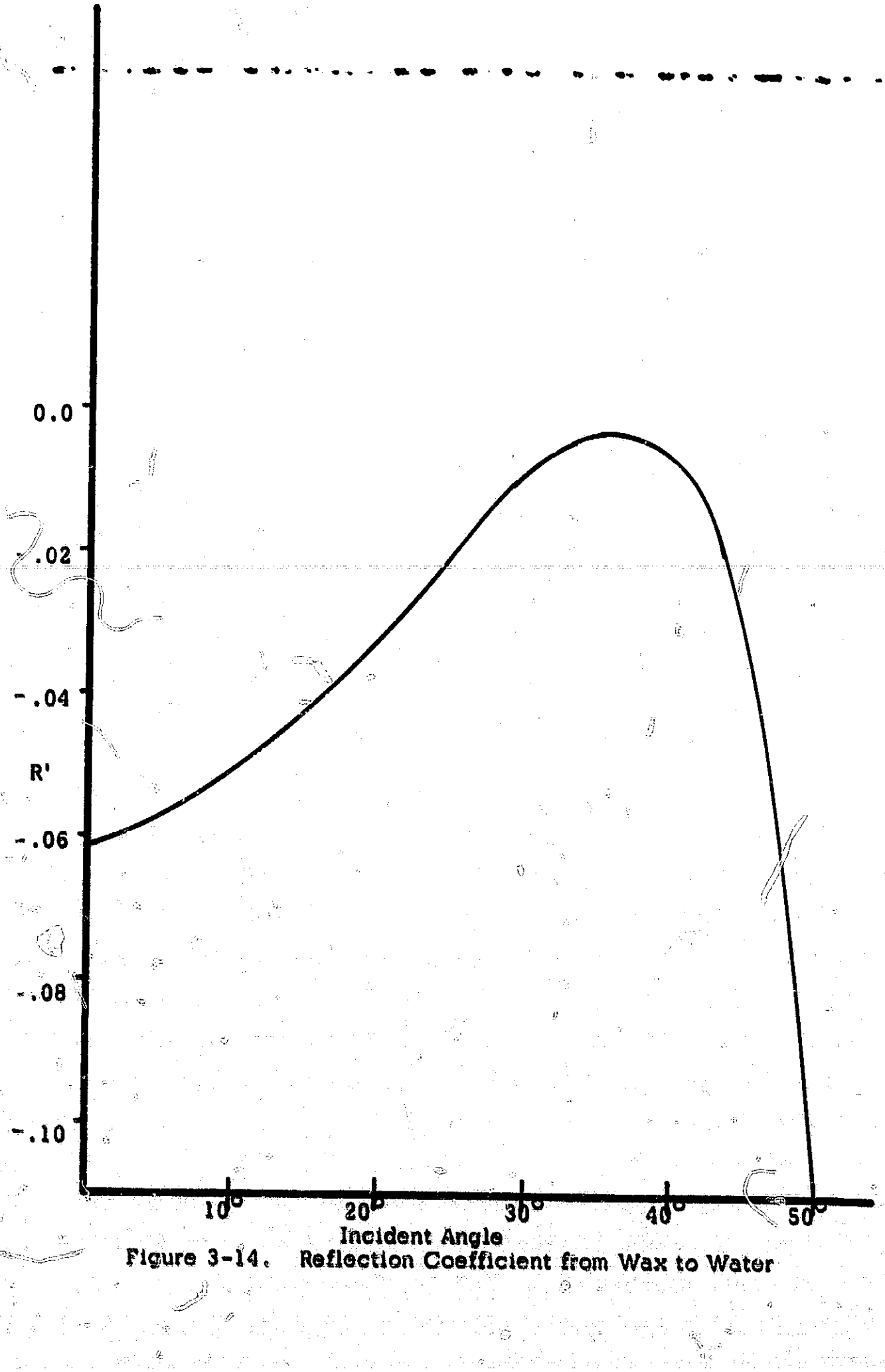

Figure 3-14. Reflection Coefficient from Wax to Water

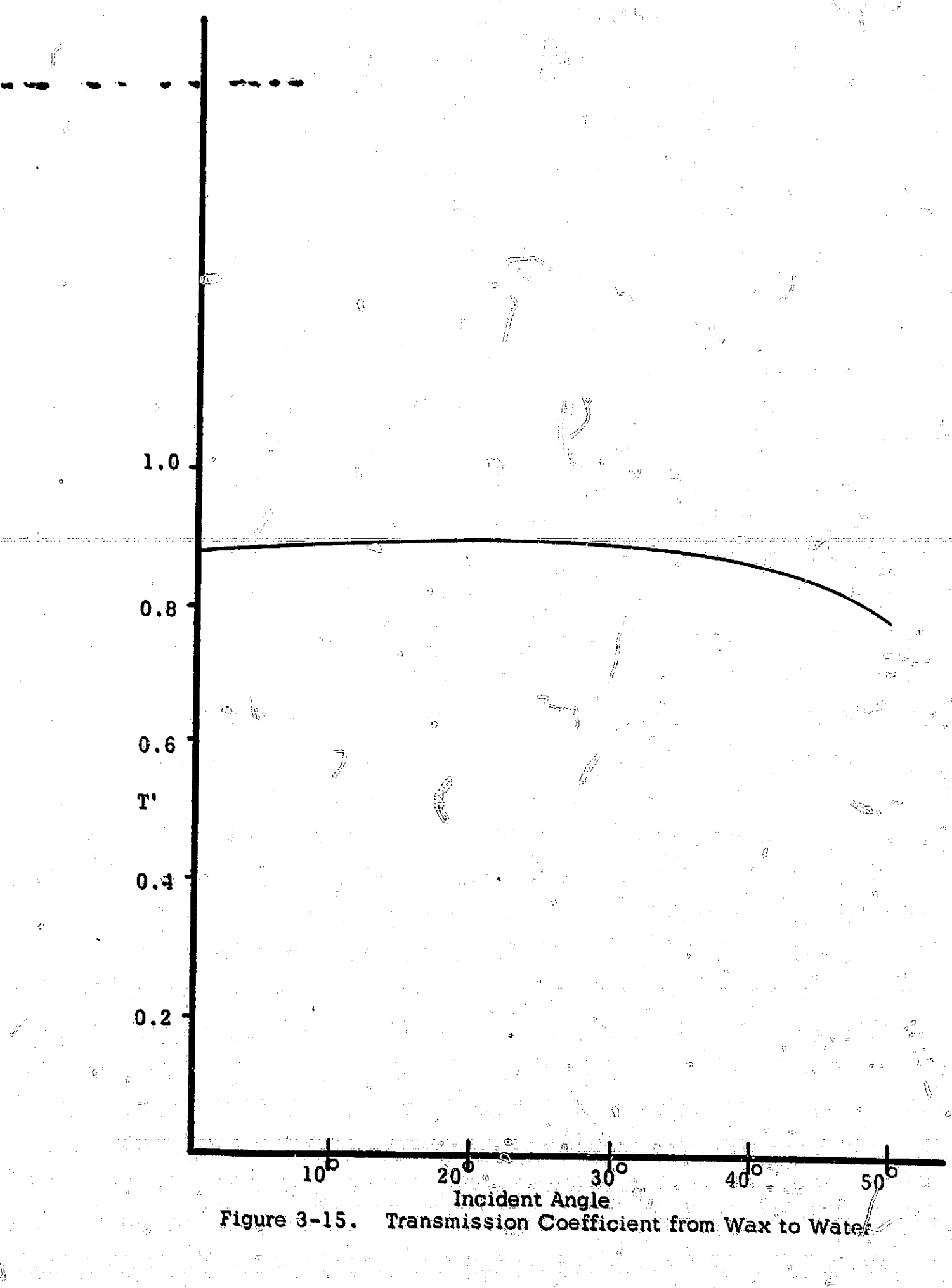

Figure 3-15. Transmission Coefficient from Wax to Water

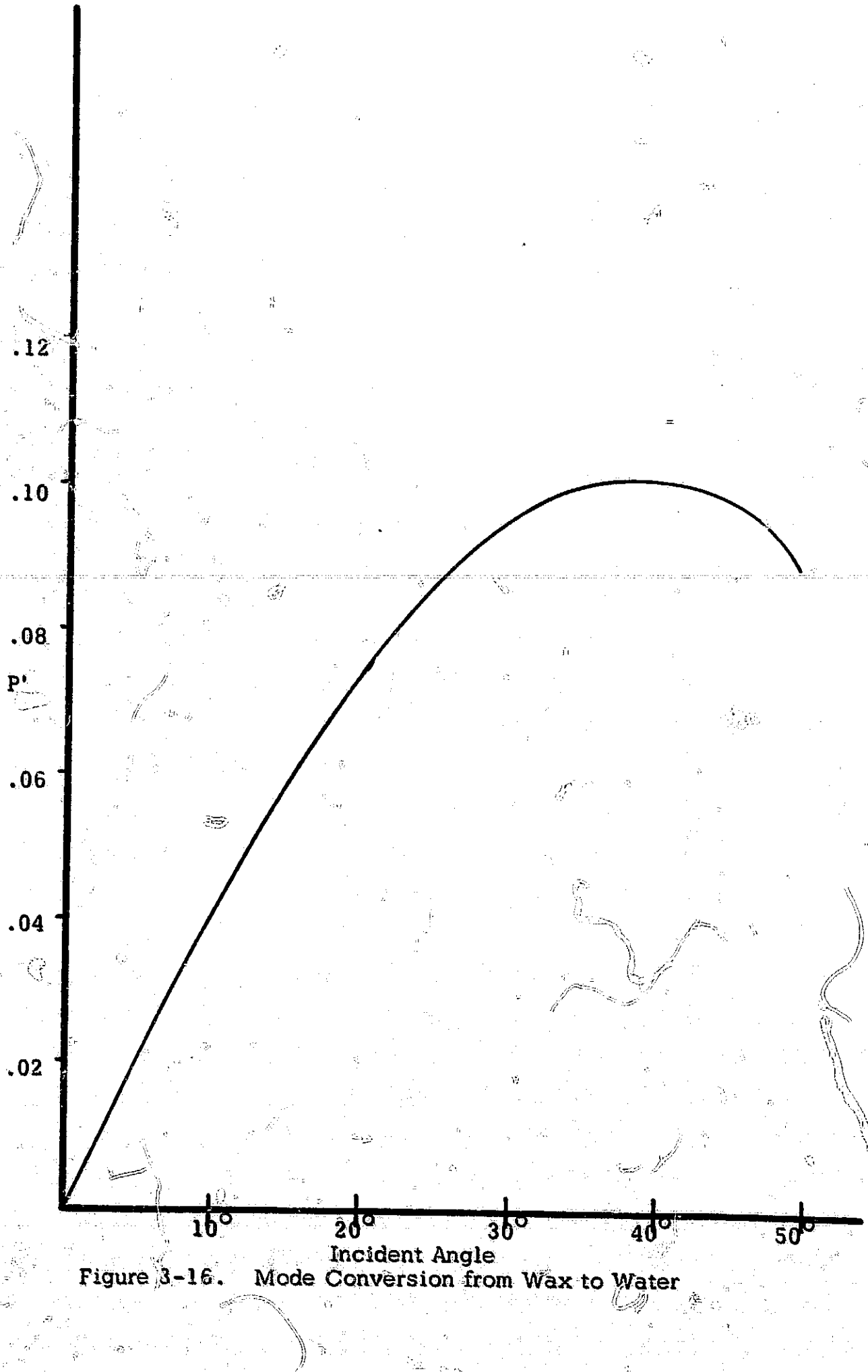

Figure 3-16. Mode Conversion from Wax to Water

In order to reduce these problems to a model that can be treated analytically, we will deal only with the surface height portion of the general case and further restrict it to be a stationary, isotropic process. Such a process can be described by its probability distribution function of height and the autocorrelation function of the heights as a function of separation on the surface. Estimates of these functions were computed from a series of sampled height measurements taken along profiles of the mold used to produce the rough surface. These measurements were made using the profilometer described by Parkins (1965). The probability distribution function, autocorrelation function, and the standard deviation of heights, σ, were computed from these profiles. Three of such profiles were made across separated portions of the mold to allow the stationarity of the process to be checked by comparing the sample estimates from different portions of the surface.

The estimate of the correlation function was calculated using the statistical estimator

$$F(l\Delta x) = \frac{\frac{1}{N-l}\sum_{i=1}^{N-l} h_i h_{i+l}}{\frac{1}{N}\sum_{i=1}^{N} h_i^2} \qquad (3.12)$$

where h_i is the i^{th} height in the series of N points

l is the lag number

Δx is the sampling interval

and the sample has a mean value of zero. The denominator of (3.12) is the sample variance, $\overline{\sigma}^2$, or the square of the sample standard deviation. The maximum lag used in the calculation of F was N/10 as recommended by Blackman and Tukey (1958) and N was made sufficiently large to adequately define F. According to the sampling theorem (Bendat, 1958) the sampling interval must not exceed half the period of the highest frequency component present in the profile. For the surface used the value of $\Delta x = 0.75$ mm amply satisfied this criterion. The sample autocorrelation functions computed (using the facilities of the Computation Center of the University of Kansas) are shown in Figure 3.17.

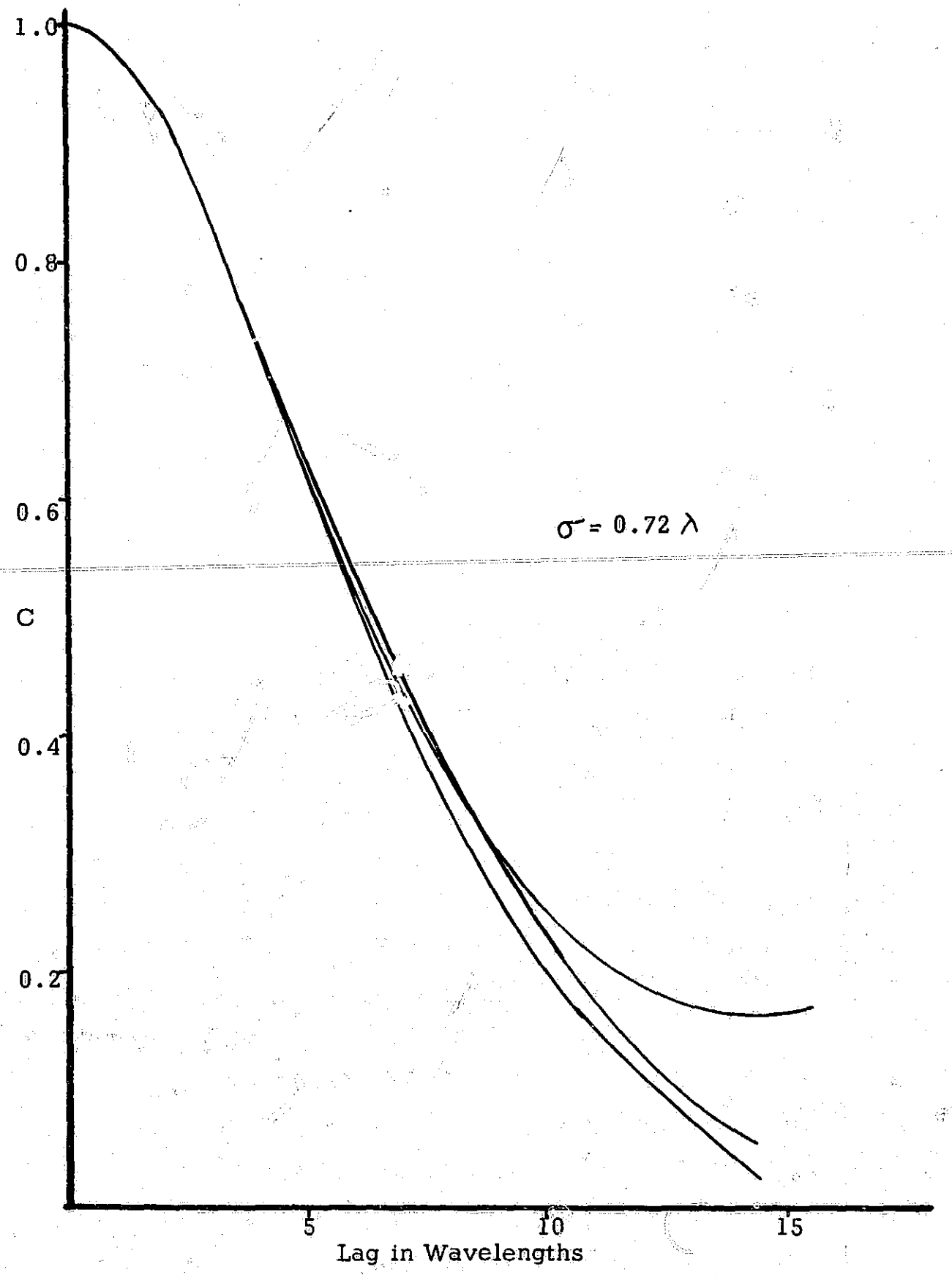

Figure 3-17. Surface Autocorrelation Function and Standard Deviation

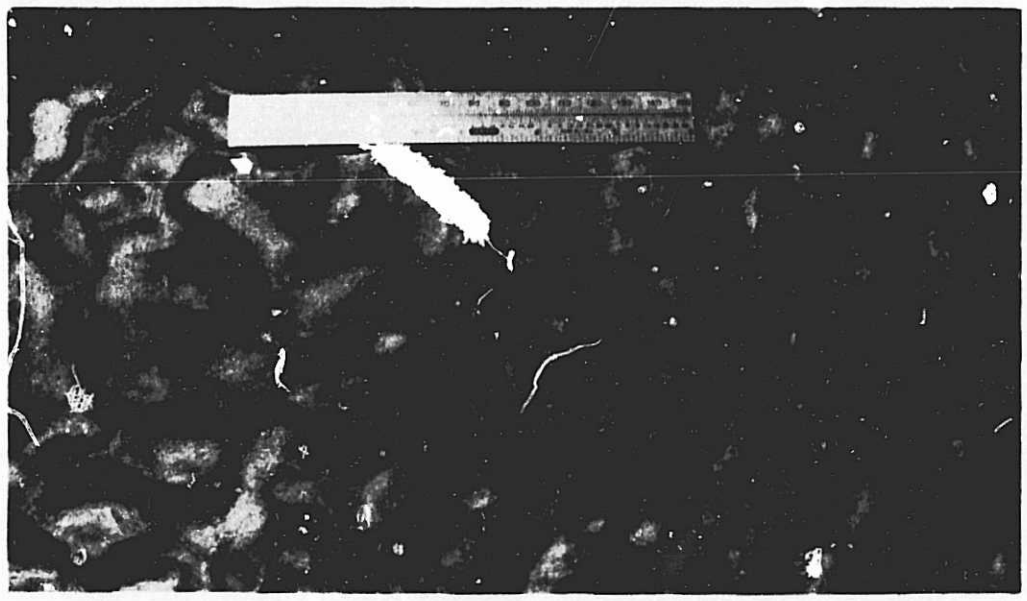

Figure 3.18. Photograph of the Mold Used to Produce the Rough Side of the Layers

The probability distribution function was determined to have a Gaussian nature as expected. The behavior of the sample autocorrelation functions shows that the process is quite stationary and smoothly undulating as indicated by the close curves and the smooth fall off from the origin. It was found that the sample autocorrelation functions are closely fit by the Gaussian function

$$F = \exp\left[-\left(\frac{X}{11.6}\right)^2\right]. \qquad (3.13)$$

CHAPTER IV

EXPERIMENTAL INVESTIGATION OF LAYER SCATTER

An experiment to determine the effect of a layer on the scattered return was conducted using the acoustic simulator described in Section 3.2. The layer was constructed of the wax with one side being rough (see statistical description in section 3.4) and the other one smooth.

4.1 Validity of Assumptions Made

The surface was constructed to fit the assumptions of Chapter II as closely as possible. Assumption 2, plane wave illumination, depends on the antenna pattern and the range to the surface and was closely fit with the transducers used but not exactly. As shown in Figures 3.11 - 3.16 the reflection and transmission coefficients of the wax-water interface change slowly enough with angle to be considered constant over the range of local incident angles encountered (assumption 7). Assumption 3, the two interfaces being in the far field region of each other, is violated. To investigate this further a definition of the far field region is in order. In the far field region the inequality

$$R > \frac{2\ell^2}{\lambda}$$

where R is the distance from the surface to the observation point

ℓ is the length of the scattering area and

λ is the incident wavelength,

must hold. Barrick (1965) has shown that this condition can be replaced by

$$R > \frac{2L^2}{\lambda}$$

where L is the surface correlation distance for a Gaussian correlated surface. This condition means the layer thickness must be

$$d \geq R$$

for the far field assumption to be valid. For the surface used in the experiment (L = 11.6 mm) this becomes

$$d \geq \frac{2(11.6)^2}{1.5} = \frac{2(135)}{1.5} = 18.0 \text{ cm}$$

This thickness was such that no return could be obtained from the rear face.

4.2 Theoretical Average Scattering Cross Section

The theory developed in Chapter II points out that the average power from the two interfaces can be determined separately and added together to obtain the total average power from a layer.

The expected return from the smooth surface is that of a specular reflector with the proper reflection coefficient. This is a convolution of a delta function, the specular reflection of a plane wave, and the antenna pattern. The effective antenna power gain was obtained experimentally by recording the received power from the smooth water-air interface as a function of incident angle. This was then normalized to unit area using the aperture effect to obtain the result given in Figure 4.1.

The signal from the rough interface is described in terms of the variation of average scattering cross section with incident angle. Equation (2.26) was solved using the measured parameters of the surface roughness to obtain the curve presented in Figure 4.2. This, when scaled as above, describes the contribution of the front face for the rough first case directly. For the smooth first case this must be modified to take into account refraction at the smooth interface as was done for Figure 4.3.

These curves can be combined by adding together, with the appropriate scaling for attenuation, reflection and transmission coefficients, to obtain the total average scattering cross section of the layer.

4.3 Experimental Results

The four configurations of the layer mentioned in Chapter I were examined in detail as a function of layer thickness and attenuation.

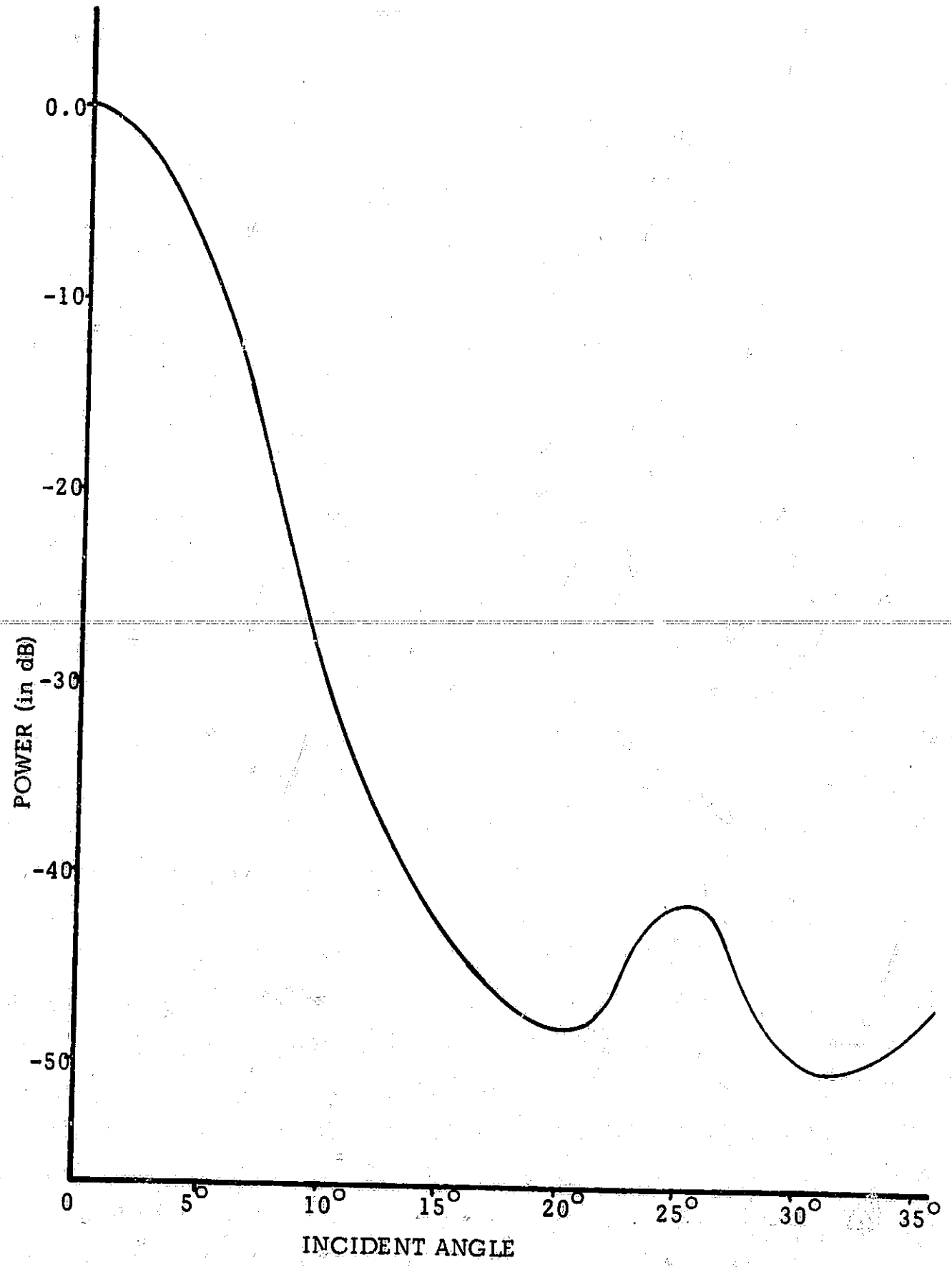

Figure 4-1. Antenna Power Gain as a Function of Angle

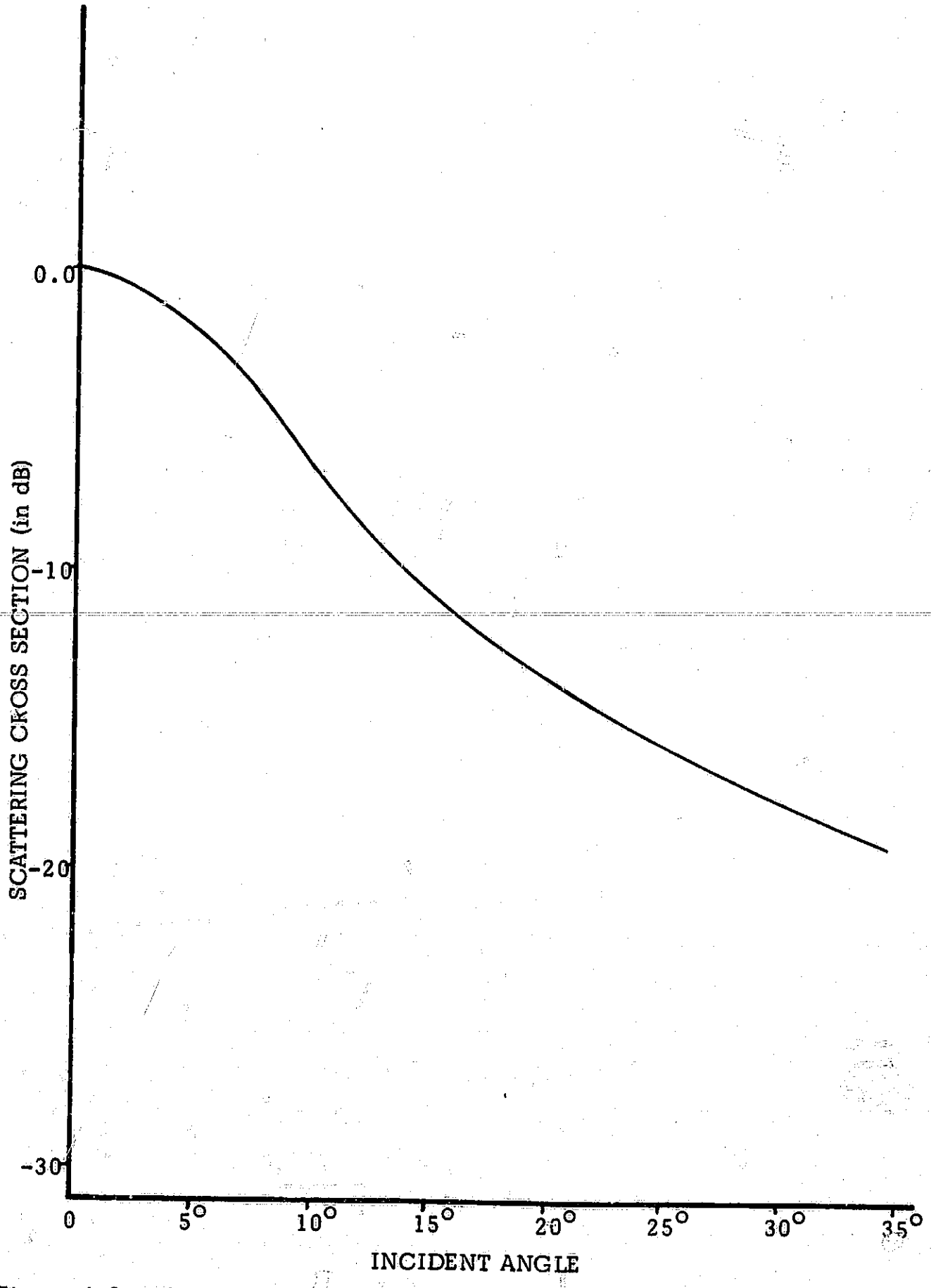

Figure 4-2. Theoretical Scattering Cross Section of the Rough Surface Used

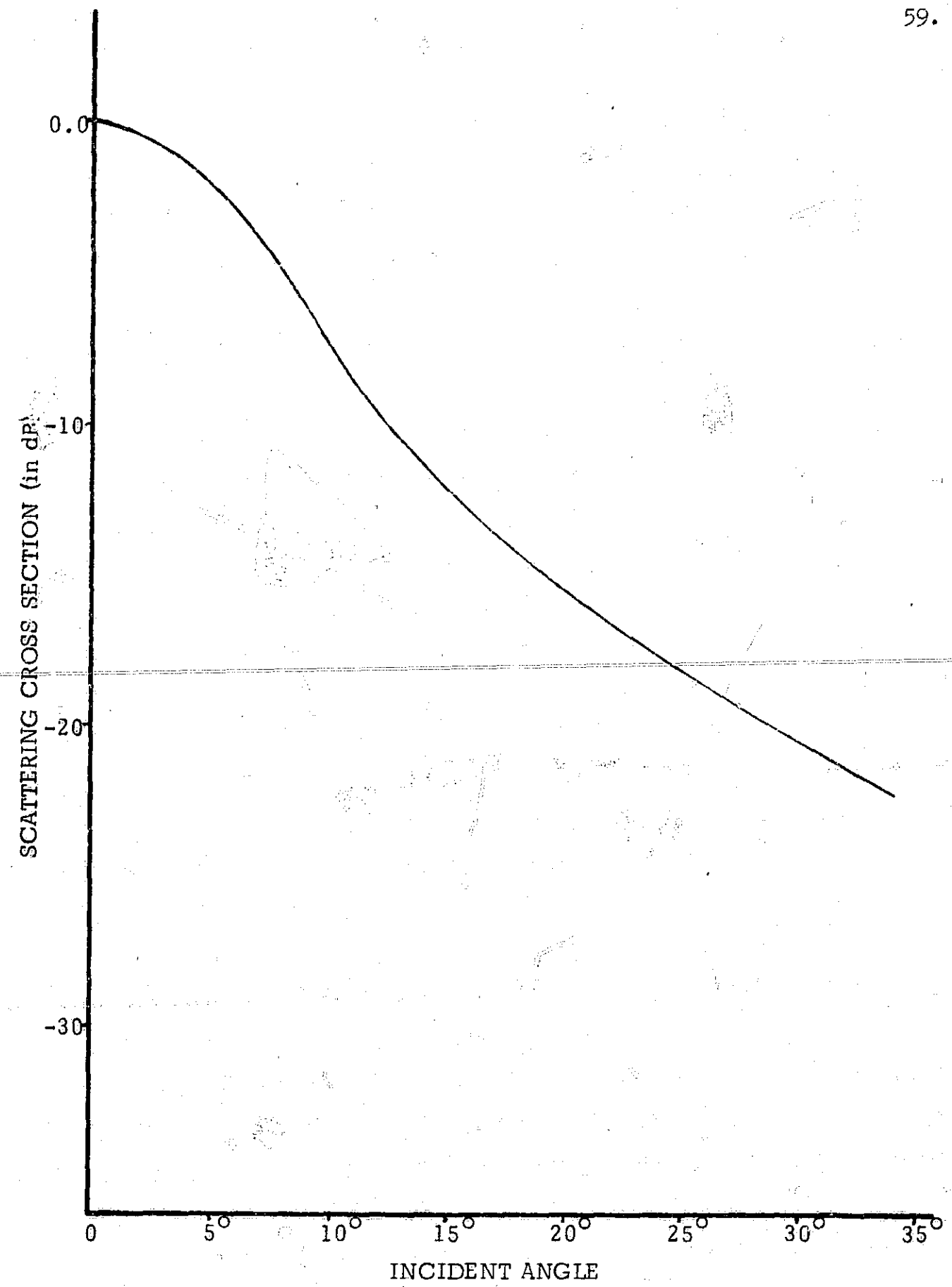

Figure 4-3. Theoretical Scattering Cross Section of the Rough Surface as Modified to Account for Diffraction Through the Smooth Front.

All the layers were prepared from the same mold in order to have identical roughness as the thickness was varied. The results of individual layers are presented first then a comparison of three thicknesses is offered for each configuration. Following these is a comparison of results from various configurations.

4.3.1 Rough Front Face and Perfectly Reflecting Smooth Second Face

For this configuration the Fresnel reflection coefficient for the front face is 5.9×10^{-2} at normal incidence and for the rear face is unity for all angles. These were obtained by floating the wax on the surface of the water such that the first interface was water-wax and the second was wax-air. The layer thickness used for this condition ranged from 11 cm to 1 cm. The thickest layer, Figure 4.4, did not exhibit any layer effect due to the large amount of total attenuation of the signal from the rear face. As the thickness of the layer was reduced the specular term from the smooth rear face becomes more pronounced until for the 1 cm layer, Figure 4.14, it was the dominant return. The complete set of curves for this configuration is presented in Figures 4.4 through 4.14. Figure 4.15 is a composite of the total average scattering cross section of the 11, 4.5, and 1 cm thick layers to point out the transition with thickness. It is noted that the effect of the rear face is evident only near vertical incidence implying that the average power represented by (2.68) is negligible compared to the rest of the terms.

4.3.2 Rough Front Face with Imperfectly Reflecting Smooth Rear

As above the Fresnel reflection coefficient of the front face was 5.9×10^{-2} but now the rear face was 5.7×10^{-2}. This was accomplished by weighting the wax to sink it below the surface to have water-wax then wax-water interfaces. The target was supported parallel to the surface of the water by styrofoam blocks. The thickest layer to exhibit a layer effect in this configuration was 3.5 cm. Figure 4.16 shows this as a very slight peaking of the curve near vertical incidence. The rest of the layers, Figures 4.17 through 4.21, exhibit more of this effect but never to the same extent as the case with a perfectly reflecting

rear face. The 1 cm layer for this configuration is quite similar to the 3 cm layer with a perfectly reflecting, smooth rear face. Other than the reduction of the magnitude of the return from the rear face the scattering cross section curves are similar to those obtained for the perfectly reflecting case. A composite curve of the total scattering cross section for the layers of thicknesses of 3.5, 2.5, and 1 cm is given in Figure 4.22. With both sides having nearly the same, low reflection coefficient it is noted that the effect of the layer is slight even for a thin layer.

4.3.3 Smooth Front Face and Perfectly Reflecting Rough Rear Face

The layers used for this configuration varied from 11 cm to 1 cm as before. The normal incidence reflection coefficient for the front face was 5.9×10^{-2} and for the rear face it was unity for all angles. No layer effect was noted for the thickest layer, Figure 4.23 and the σ_o vs. θ curve is very similar to that obtained from the water-air interface. There is evidence of small scale roughness on the basically flat surface as the drop off from vertical incidence is not quite so rapid as the antenna power curve. As the layer thickness was reduced the effect of the back-surface roughness becan to appear -- first as a further lifting of the curves for the large incident angles and finally, for a thickness of 4.5 cm (Figure 4.27), even at normal incidence. For the layers thinner than 2 cm, Figure 4.31, the return from the front face is completely masked by the effect of the highly reflecting rear face. This transition is quite evident in Figure 4.34 which compares the σ_o vs. θ curves for the 11, 4.5, and 1 cm layers.

4.3.4 Smooth Front Face and Imperfectly Reflecting Rough Rear Face

Here the layer was again submerged to give a normal incidence reflection coefficient of 5.7×10^{-2} from the rough rear face. A return from the rear face was first noted for the 4.5 cm thick layer where it had no effect near the vertical but became important for incident angles greater than 15° (Figure 4.35). This pattern continued as the thickness was reduced until for the 2 cm layer (Figure 4.39) some effect is noted at vertical incidence. Further reduction of the thickness continued

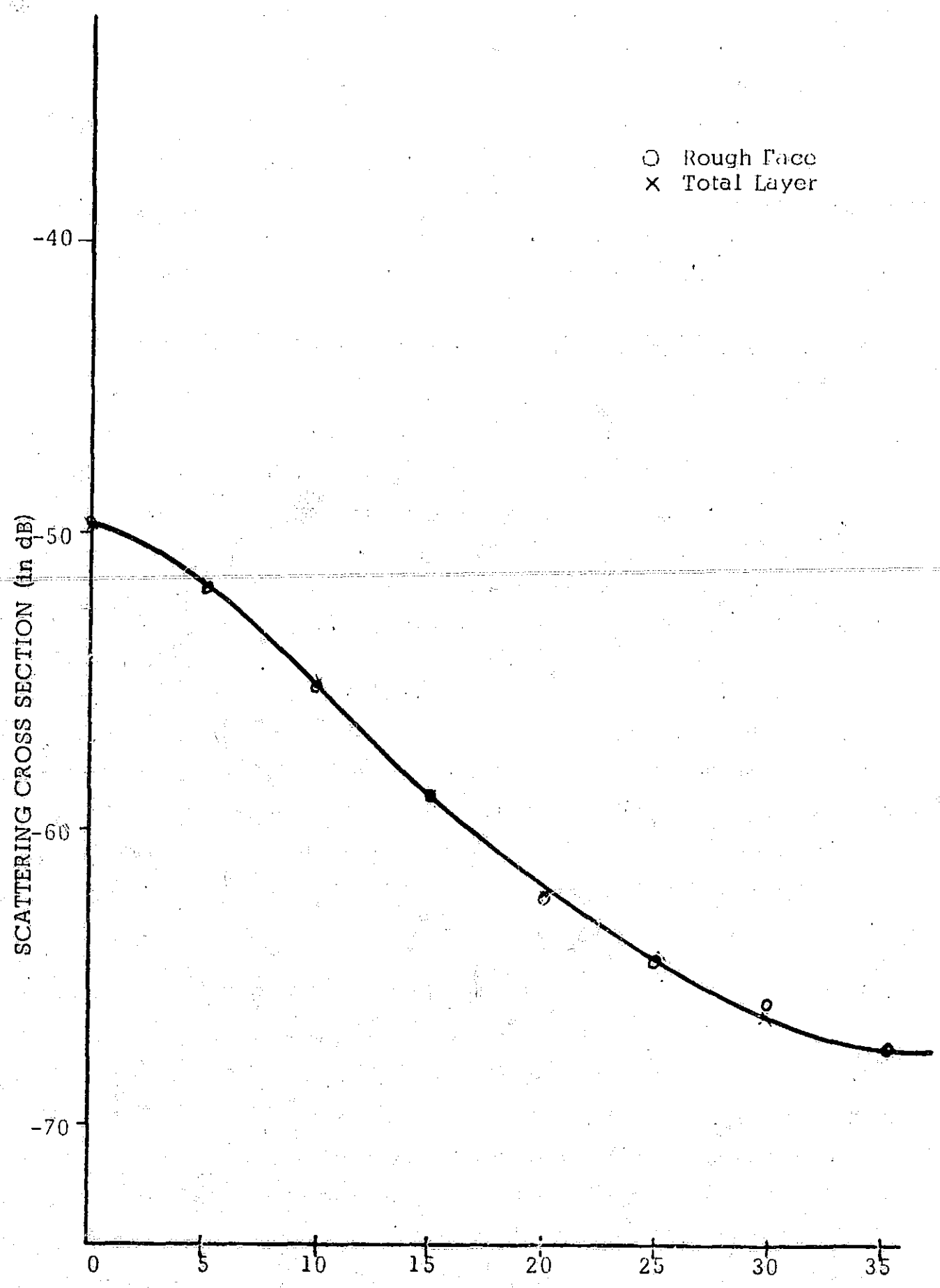

Figure 4-4. Scattering Cross Section of Layer with Front Rough , R=.059, and Rear Smooth, R=1.0, for Round-Trip Attenuation of 88 dB.

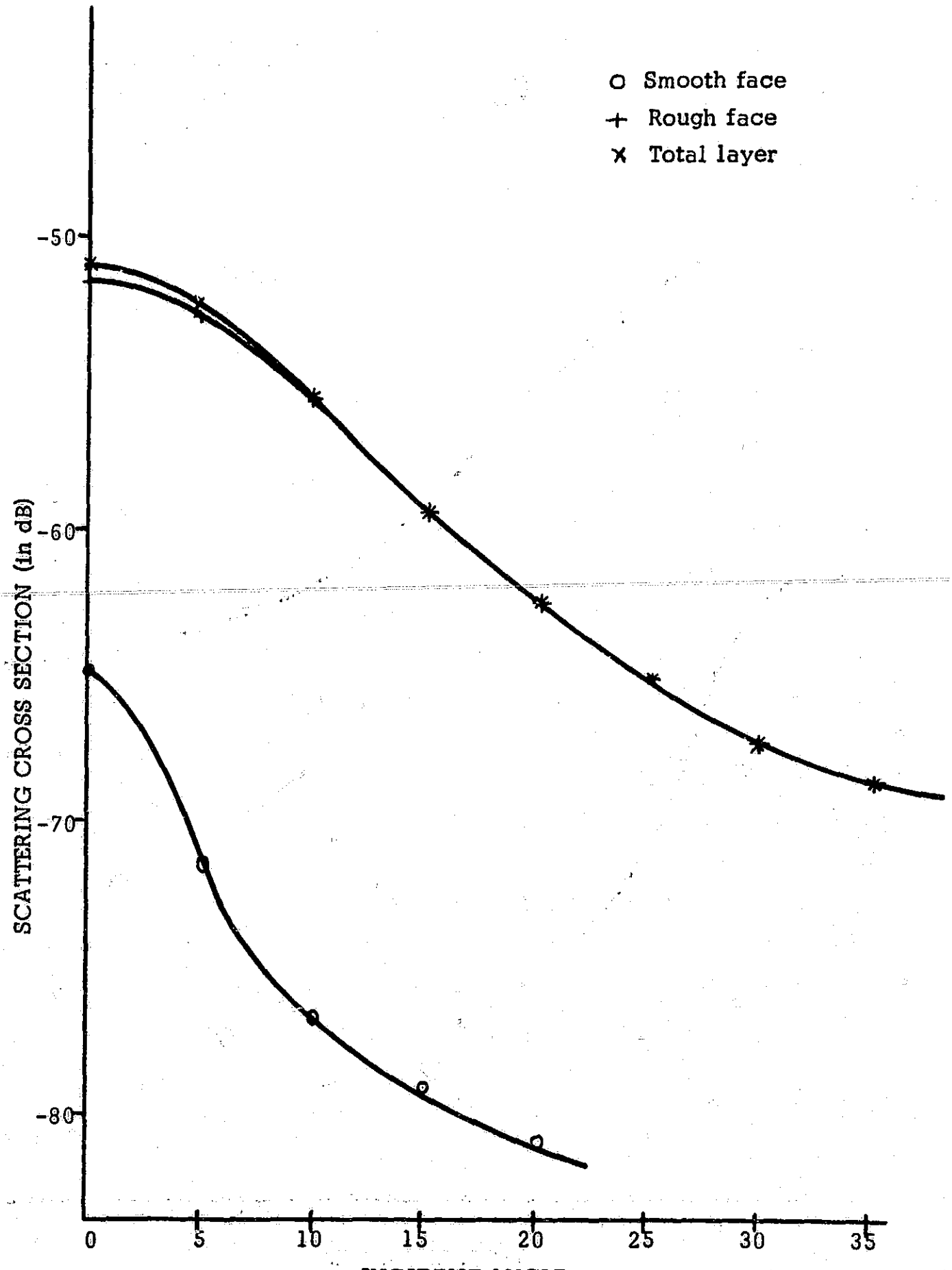

Figure 4-5. Scattering Cross Section of Layer with Rough Front, R =.059, and Smooth Rear, R=1.0, for Round-Trip Attenuation of 72dB.

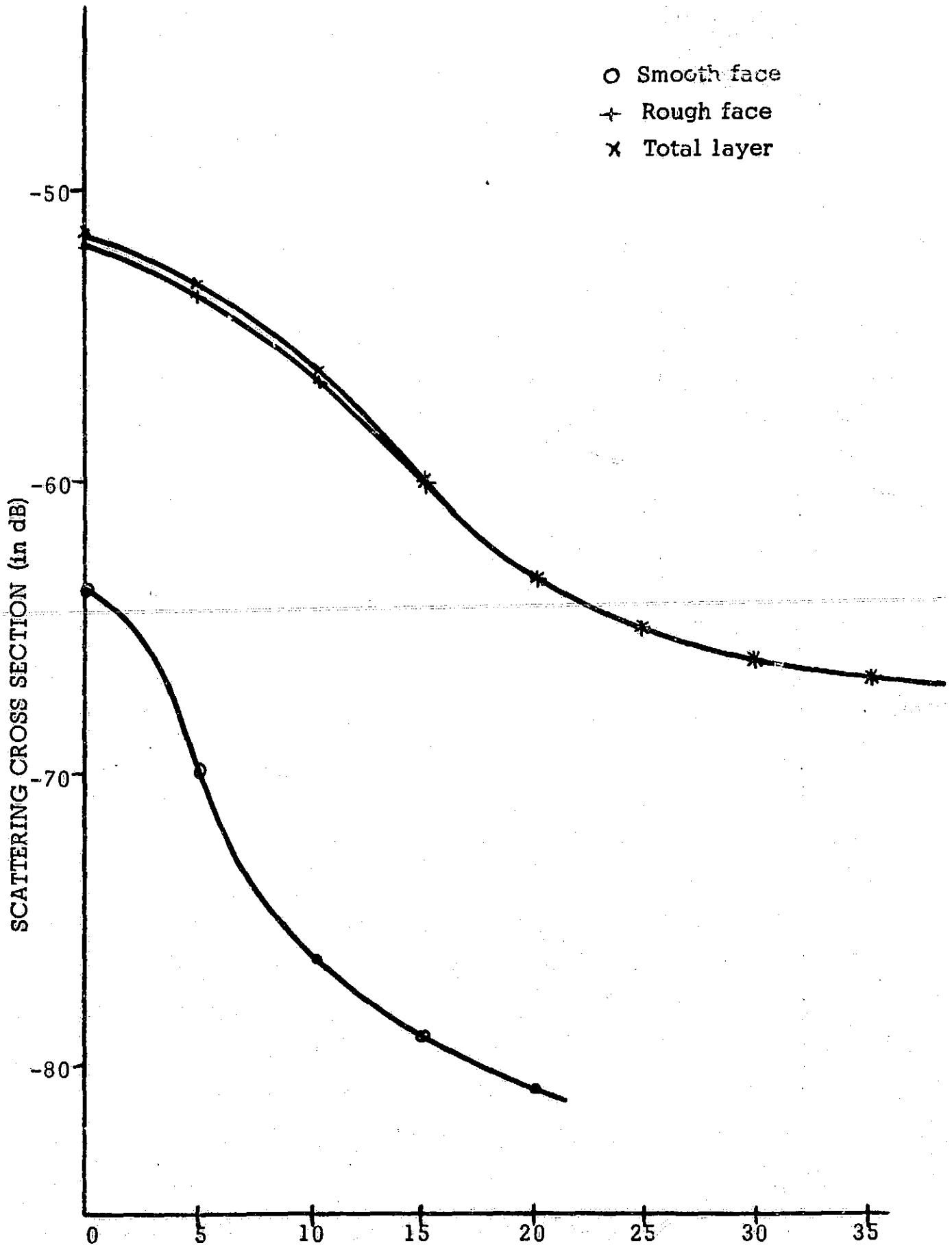

Figure 4-6. Scattering Cross Section of Layer with Rough Front, R=.059, and Smooth Rear, R=1.0, for Round-Trip Attenuation of 56 dB.

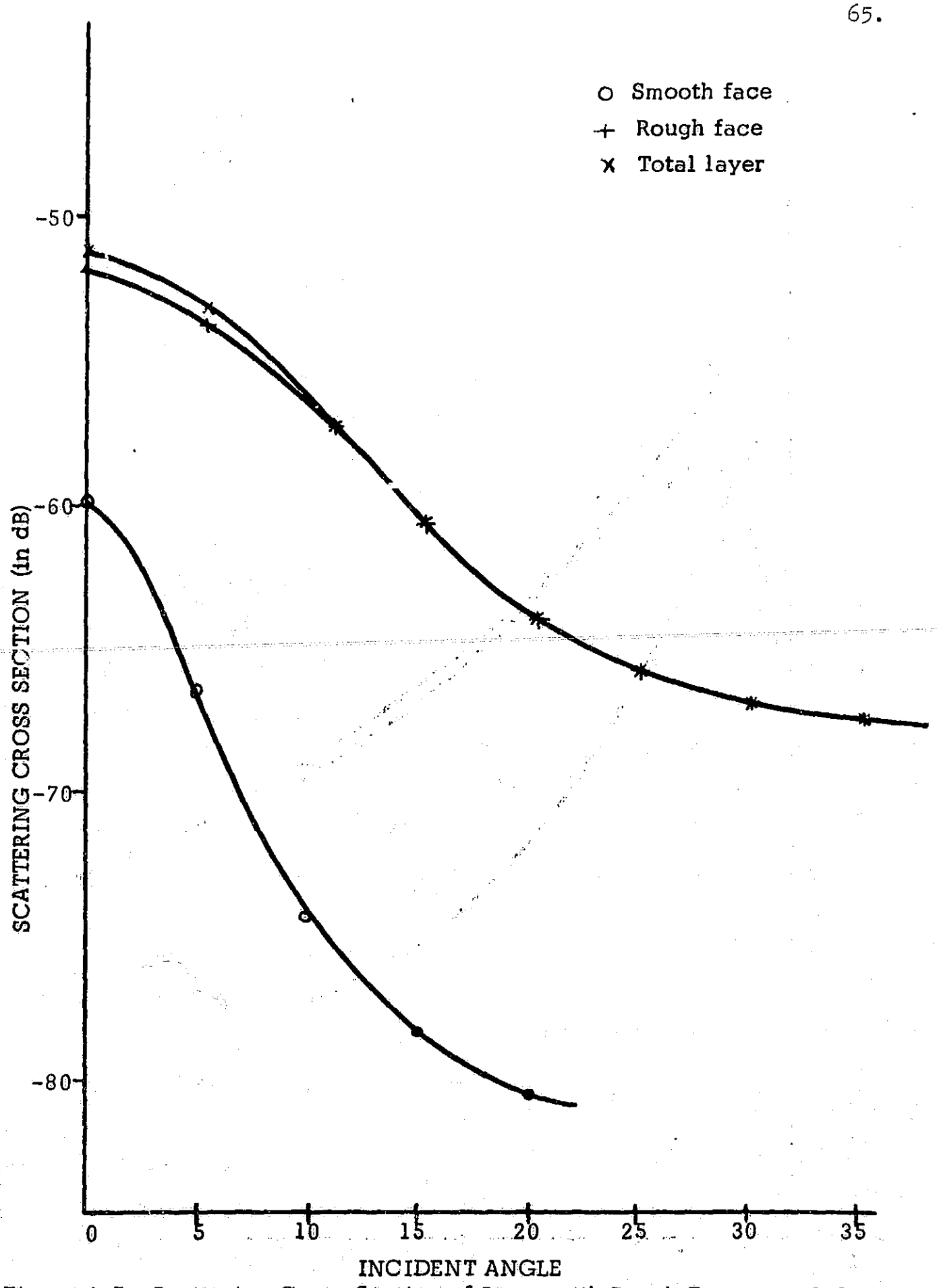

Figure 4-7. Scattering Cross Section of Layer with Rough Front, R=.059, and Smooth Rear, R=1.0, for Round-Trip Attenuation of 44 dB.

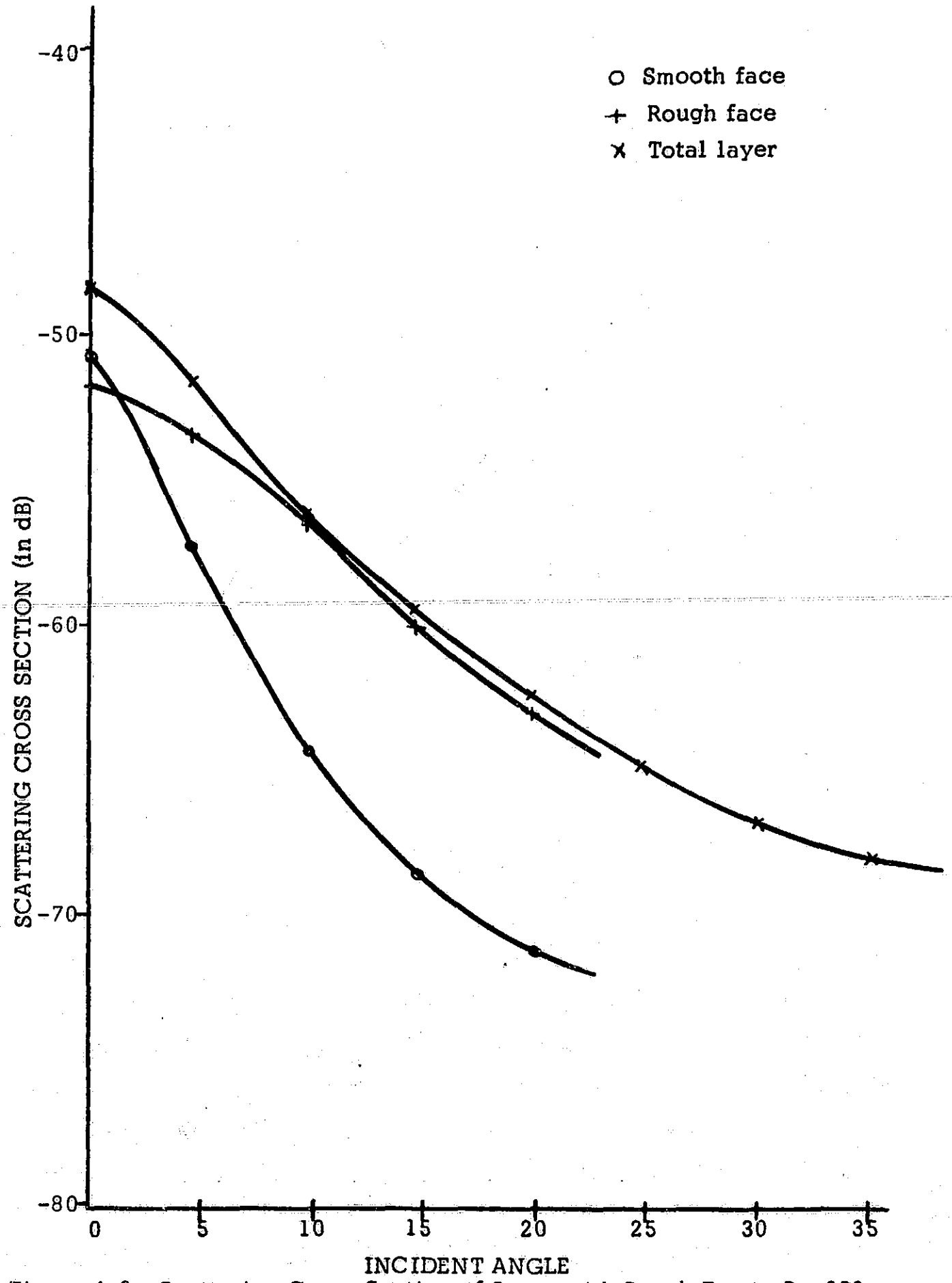

Figure 4-8. Scattering Cross Section of Layer with Rough Front, R=.059, and Smooth Rear, R=1.0, for Round-Trip Attenuation of 36 dB.

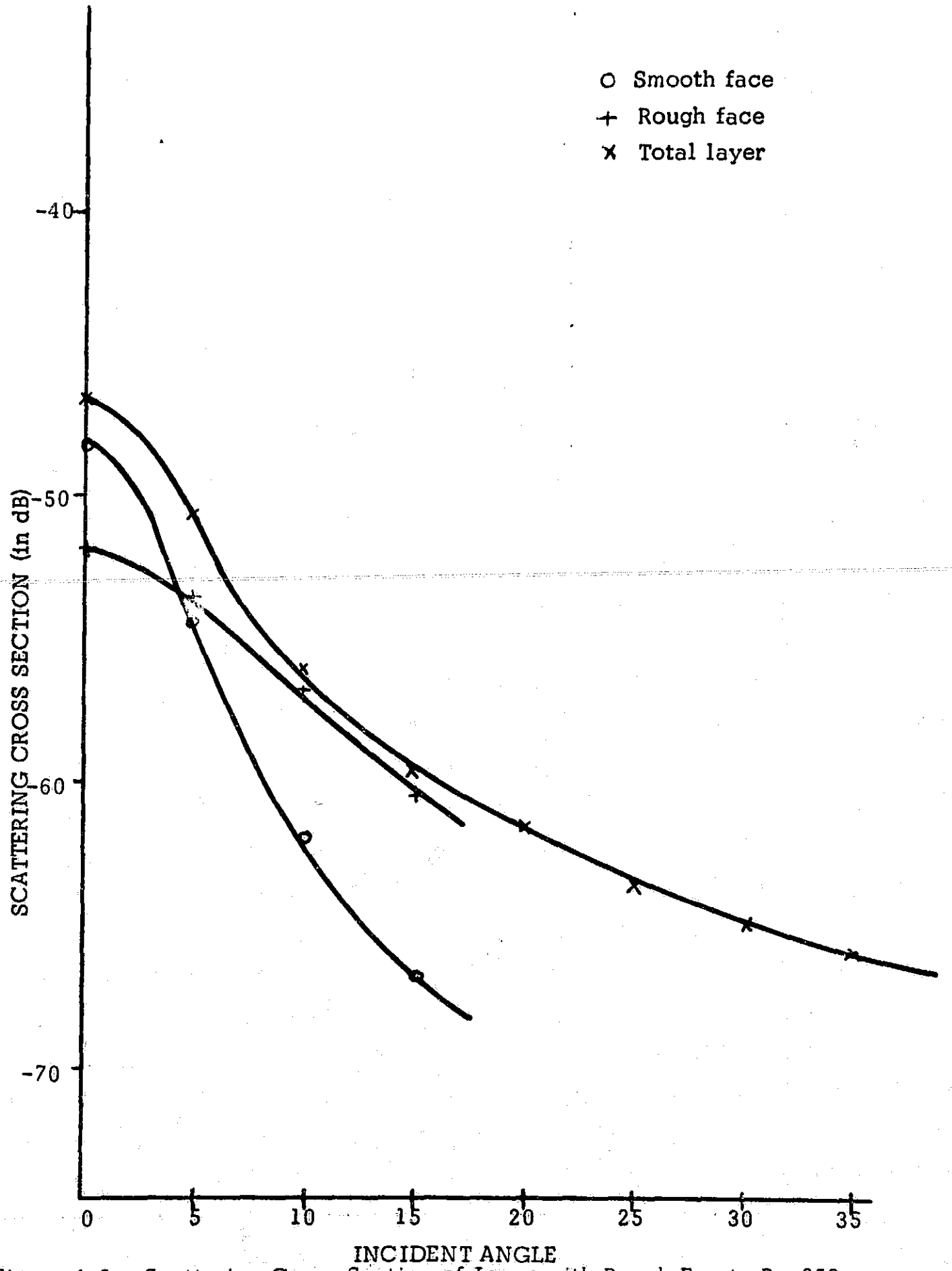

Figure 4-9. Scattering Cross Section of Layer with Rough Front, R=.059, and Smooth Rear, R=1.0, for Round-Trip Attenuation of 30 dB.

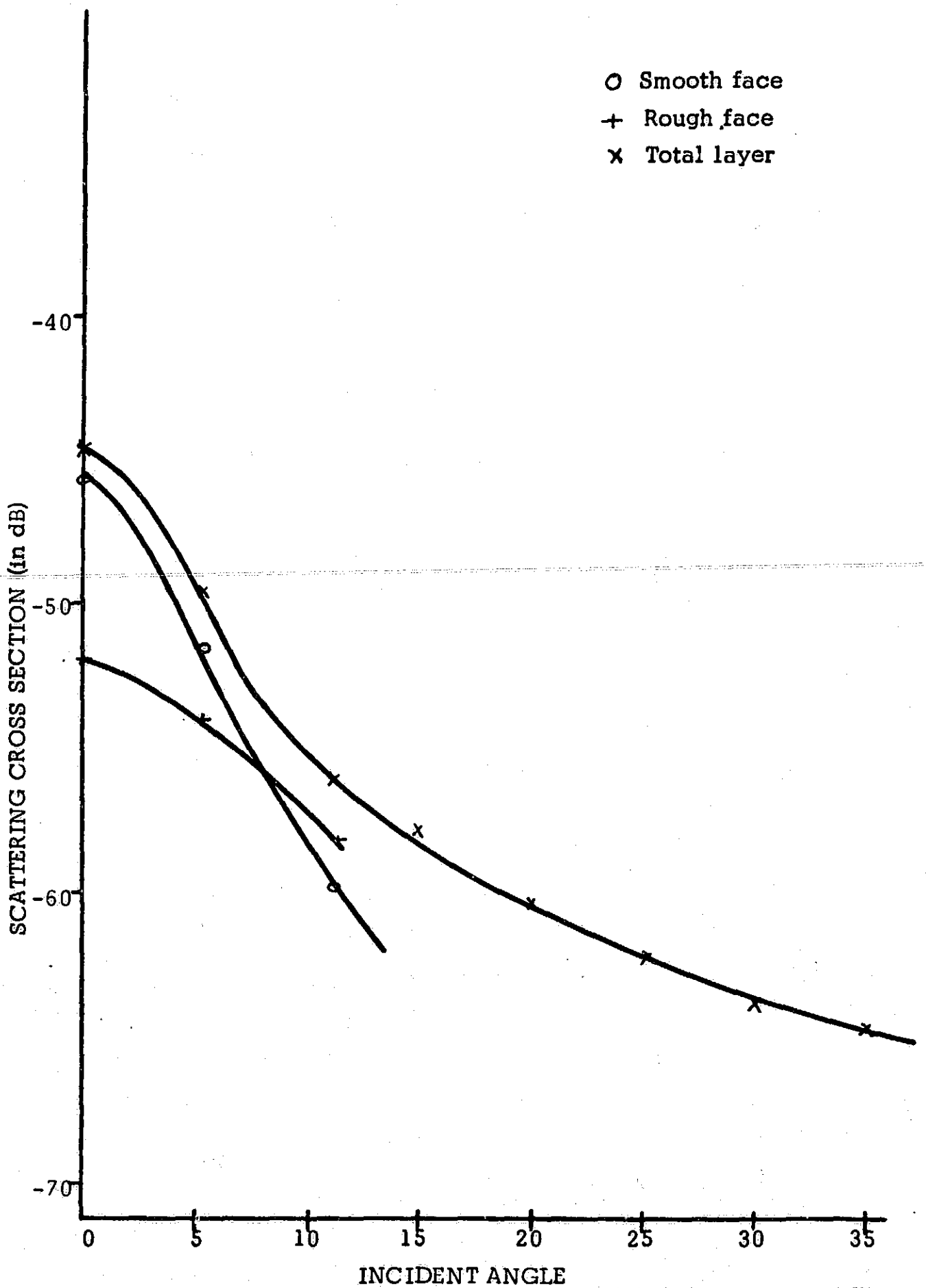

Figure 4-10. Scattering Cross Section of Layer with Rough Front, R=.059, and Smooth Rear, R=1.0, for Round-Trip Attenuation of 24 dB.

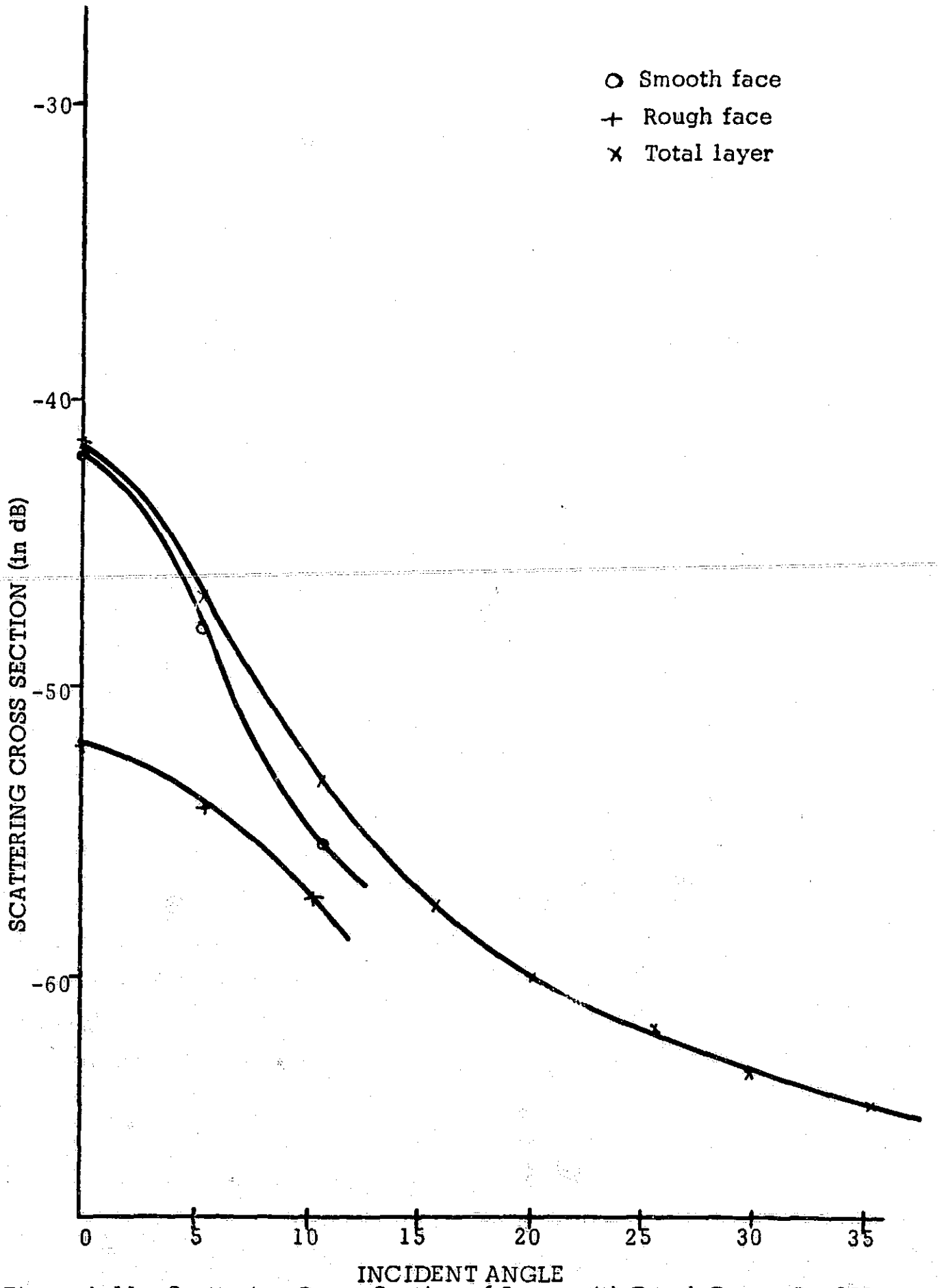

Figure 4-11. Scattering Cross Section of Layer with Rough Front, R=.059, and Smooth Rear, R=1.0, for Round-Trip Attenuation of 20 dB.

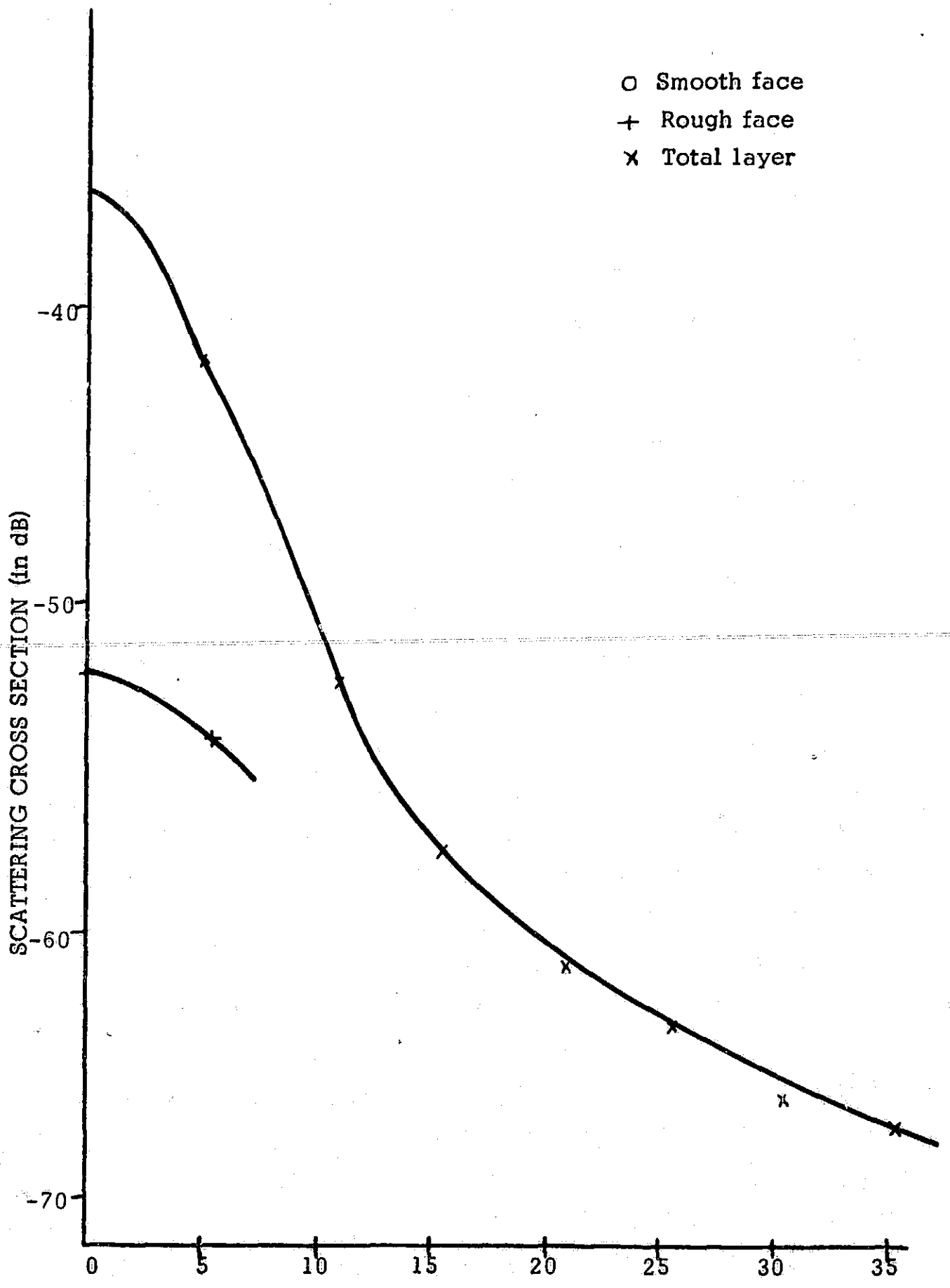

Figure 4-12. Scattering Cross Section of Layer with Rough Front, R=.059, and Smooth Rear, R=1.0, for Round-Trip Attenuation of 16dB.

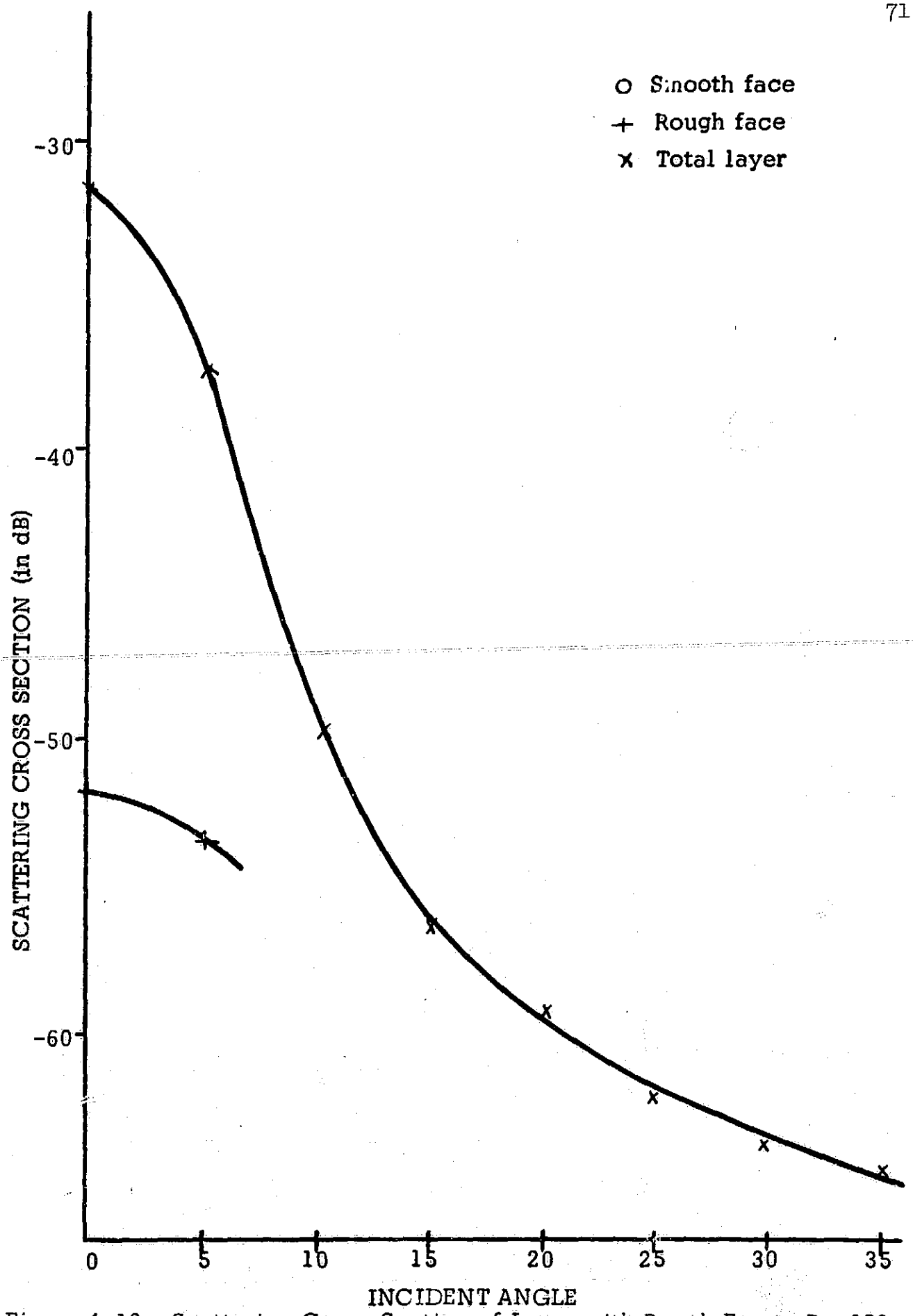

Figure 4-13. Scattering Cross Section of Layer with Rough Front, R=.059, and Smooth Rear, R=1.0, for Round-Trip Attenuation of 12dB.

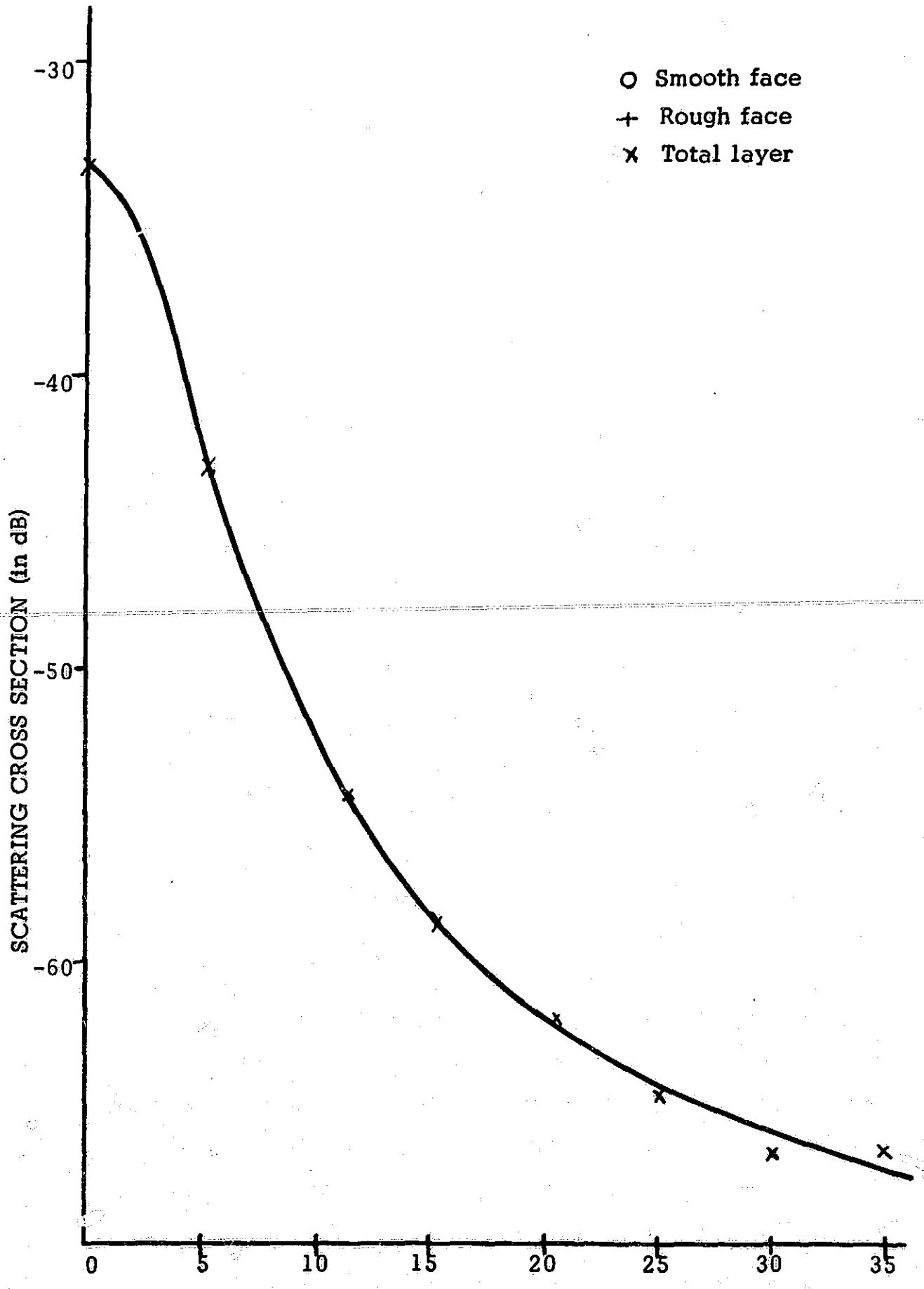

Figure 4-14. Scattering Cross Section of Layer with Rough Front, R=.059, and Smooth Rear, R=1.0, for Round-Trip Attenuation of 8 dB.

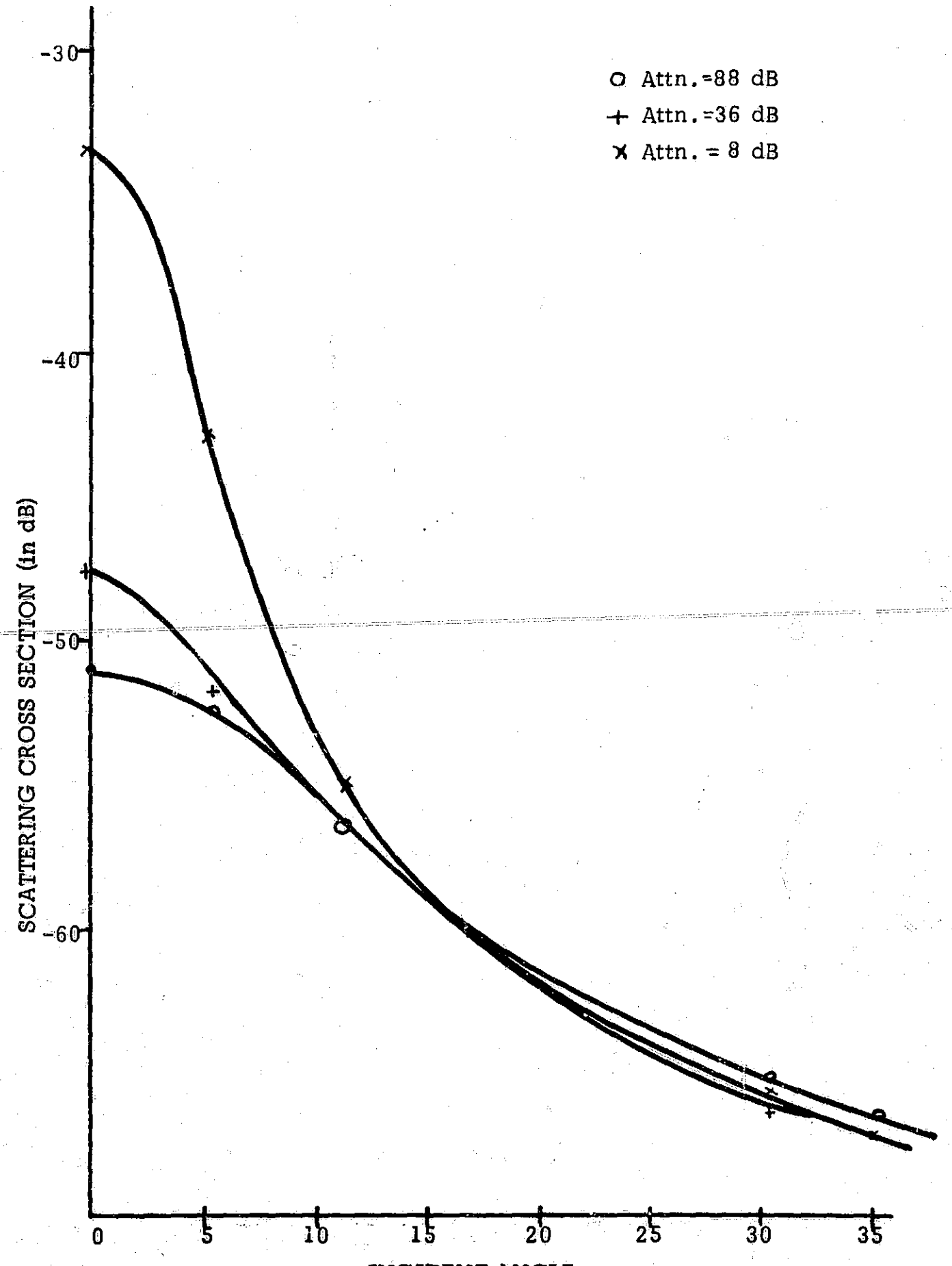

Figure 4-15. Scattering Cross Section of Layers with Rough Front, R=.059, and Smooth Rear, R=1.0, as a Function of Attenuation.

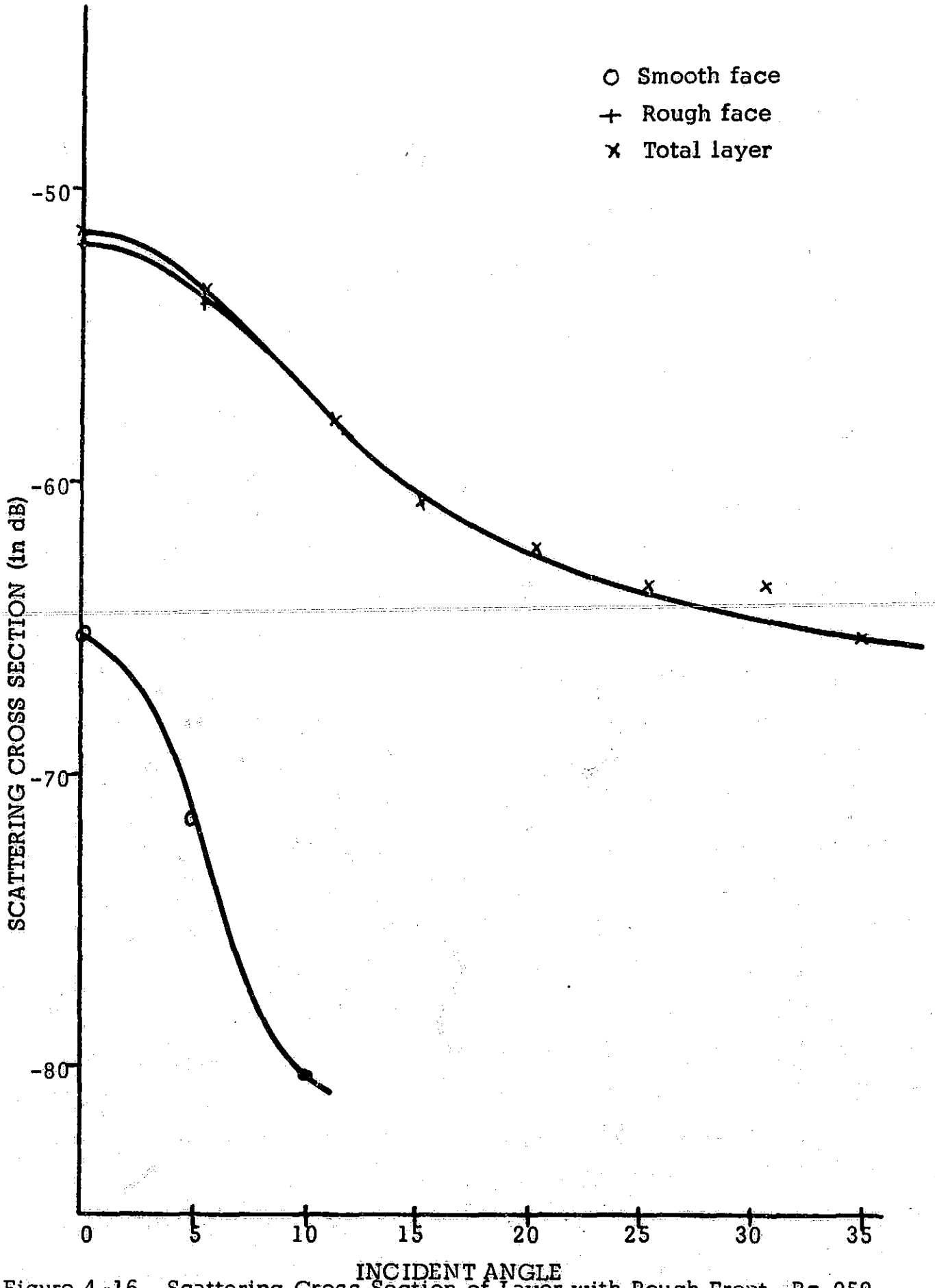

Figure 4-16. Scattering Cross Section of Layer with Rough Front, R=.059, and Smooth Rear, R=.057, for Round-Trip Attenuation of 30 dB.

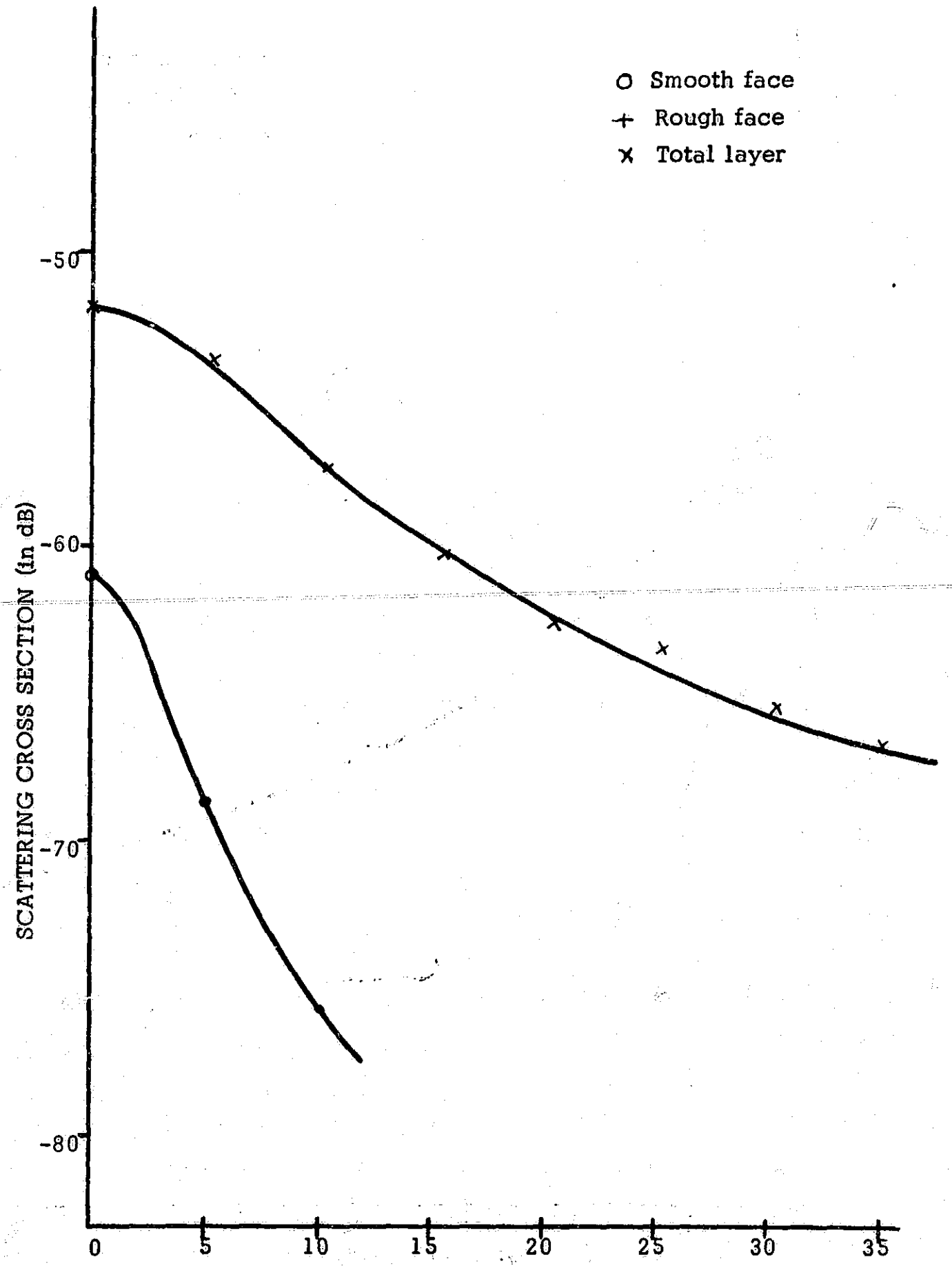

Figure 4-17. Scattering Cross Section of Layer with Rough Front, R=.059, and Smooth Rear, R=.057, for Round-Trip Attenuation of 24 dB.

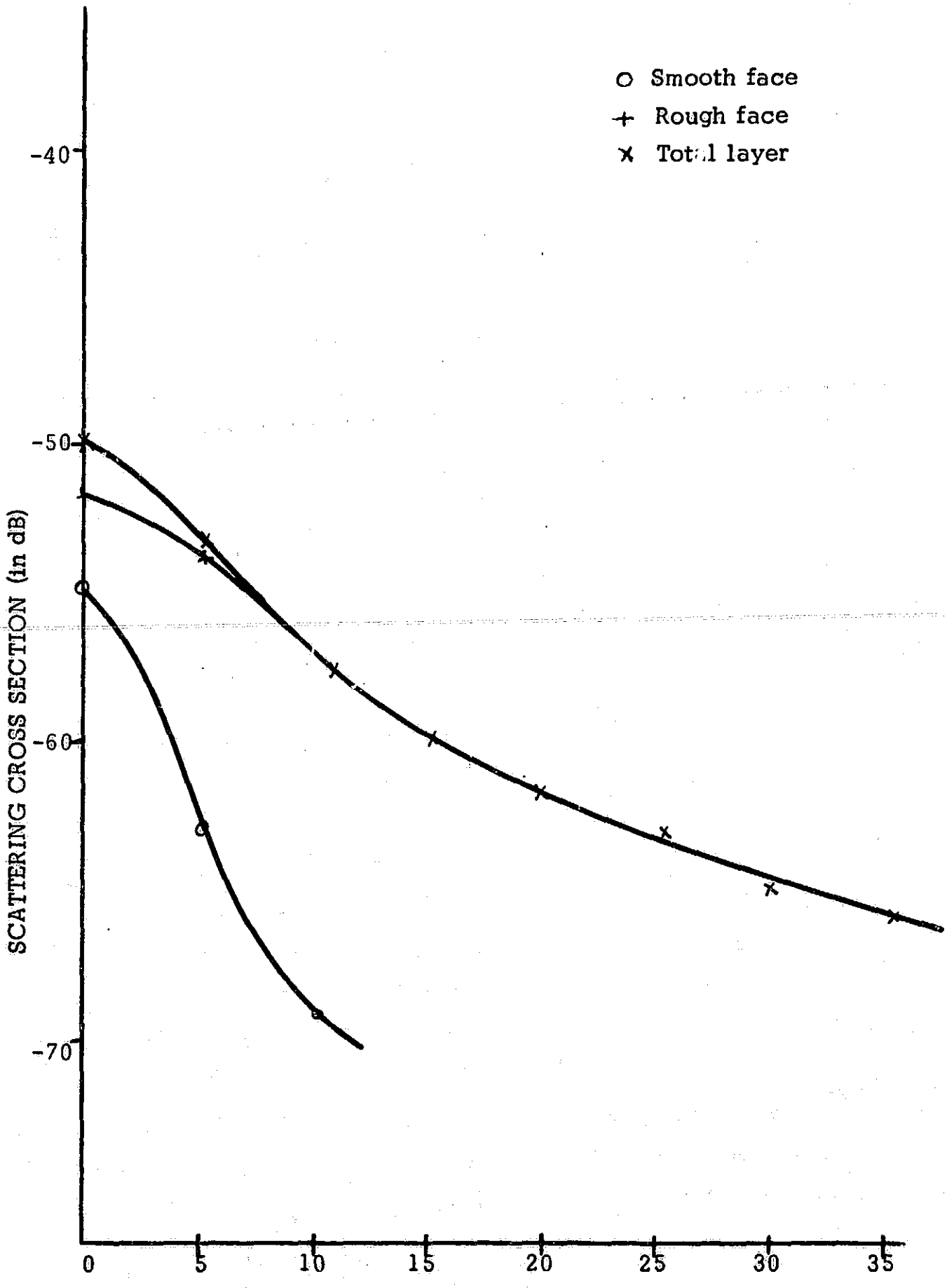

Figure 4-18. Scattering Cross Section of Layer with Rough Front, R=.059, and Smooth Rear, R=.057, for Round-Trip Attenuation of 20 dB.

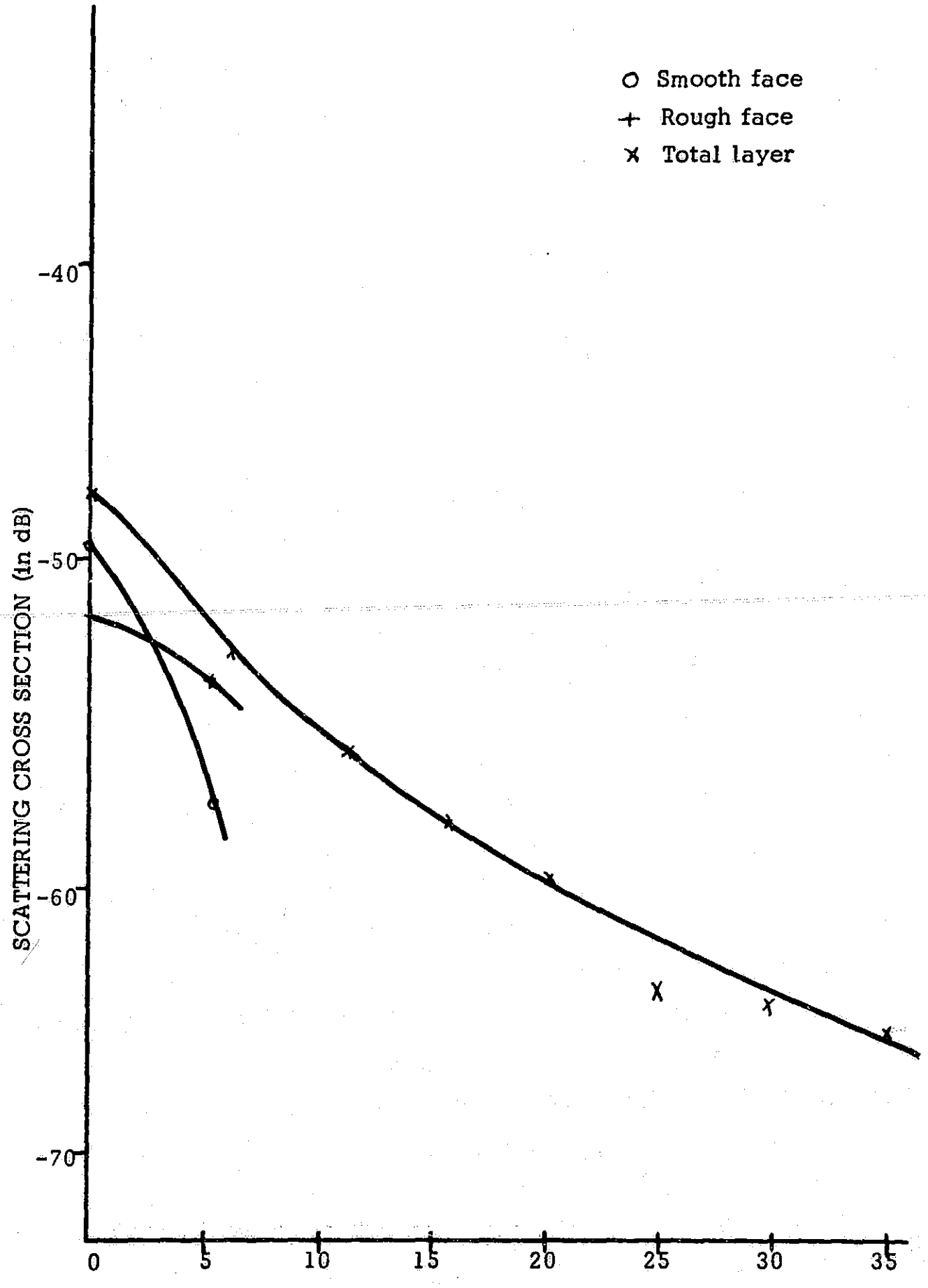

Figure 4-19. Scattering Cross Section of Layer with Rough Front, R=.059, and Smooth Rear, R=.057, for Round-Trip Attenuation of 16dB.

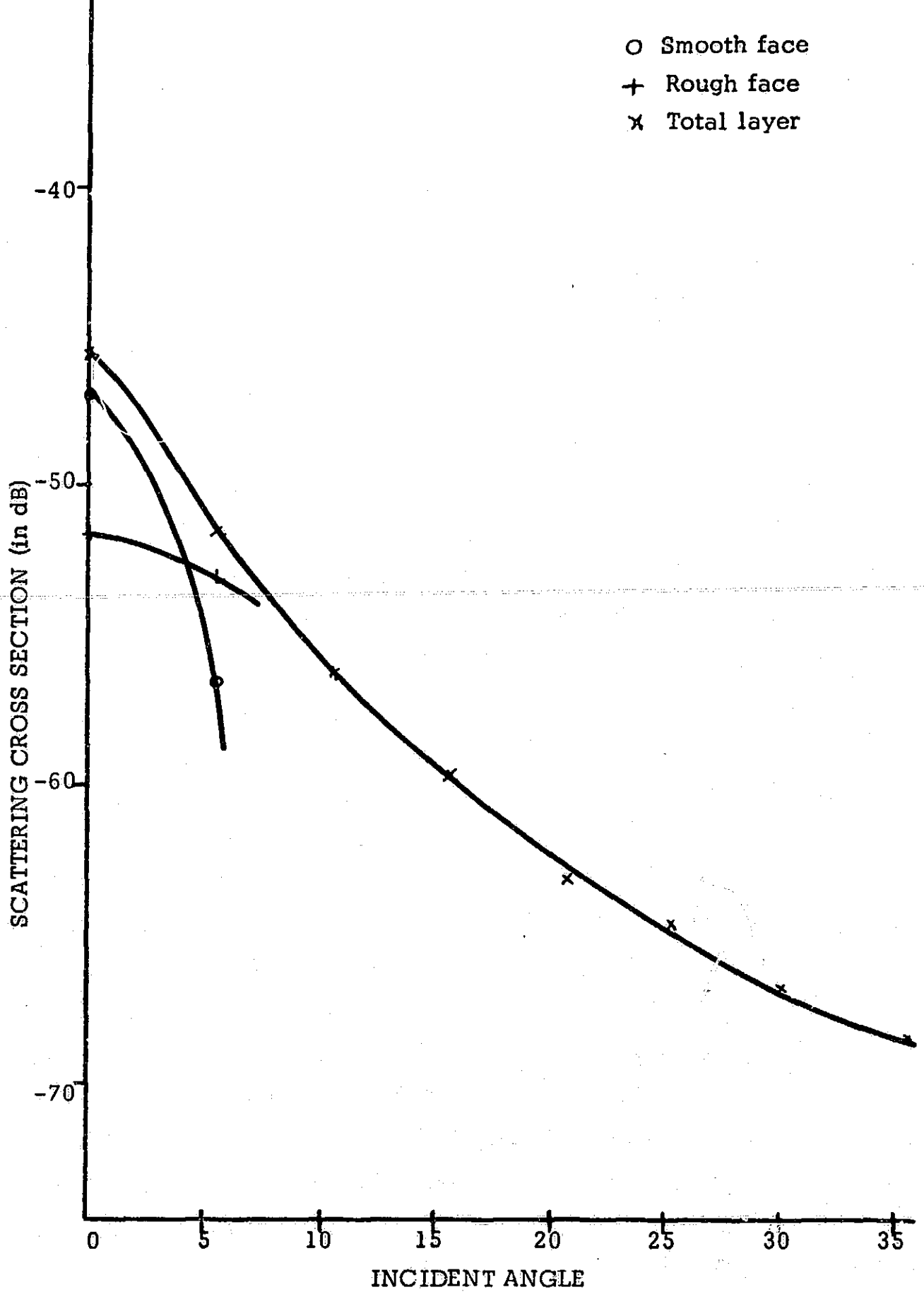

Figure 4-20. Scattering Cross Section of Layer with Rough Front, R=.059, and Smooth Rear, R=.057, for Round-Trip Attenuation of 12dB.

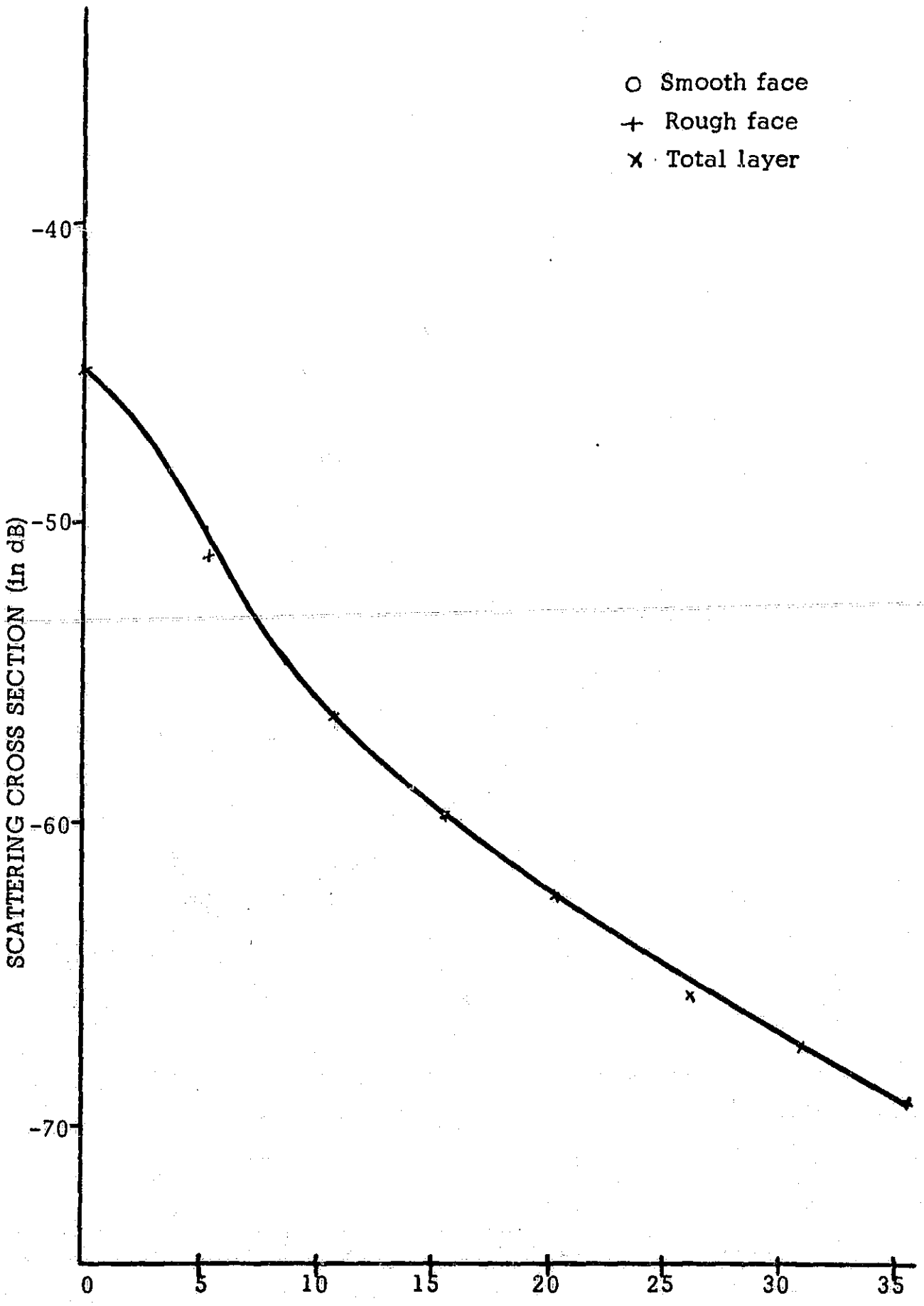

Figure 4-21. Scattering Cross Section of Layer with Rough Front, R=.059, and Smooth Rear, R=.057, for Round-Trip Attenuation of 8 dB.

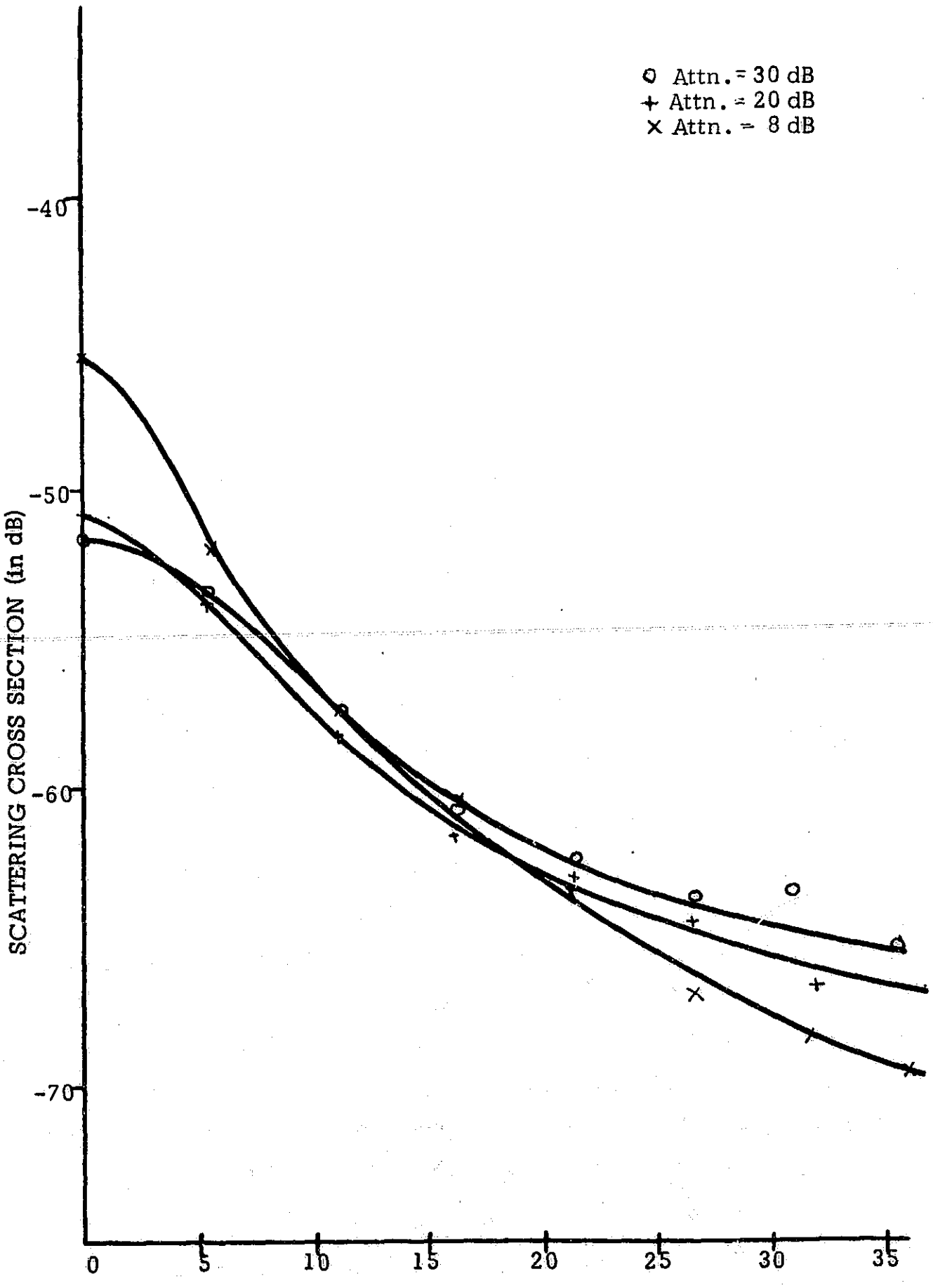

Figure 4-22. Scattering Cross Section of Layers with Rough Front, R=.059, and Smooth Rear, R=.057, as a Function of Attenuation.

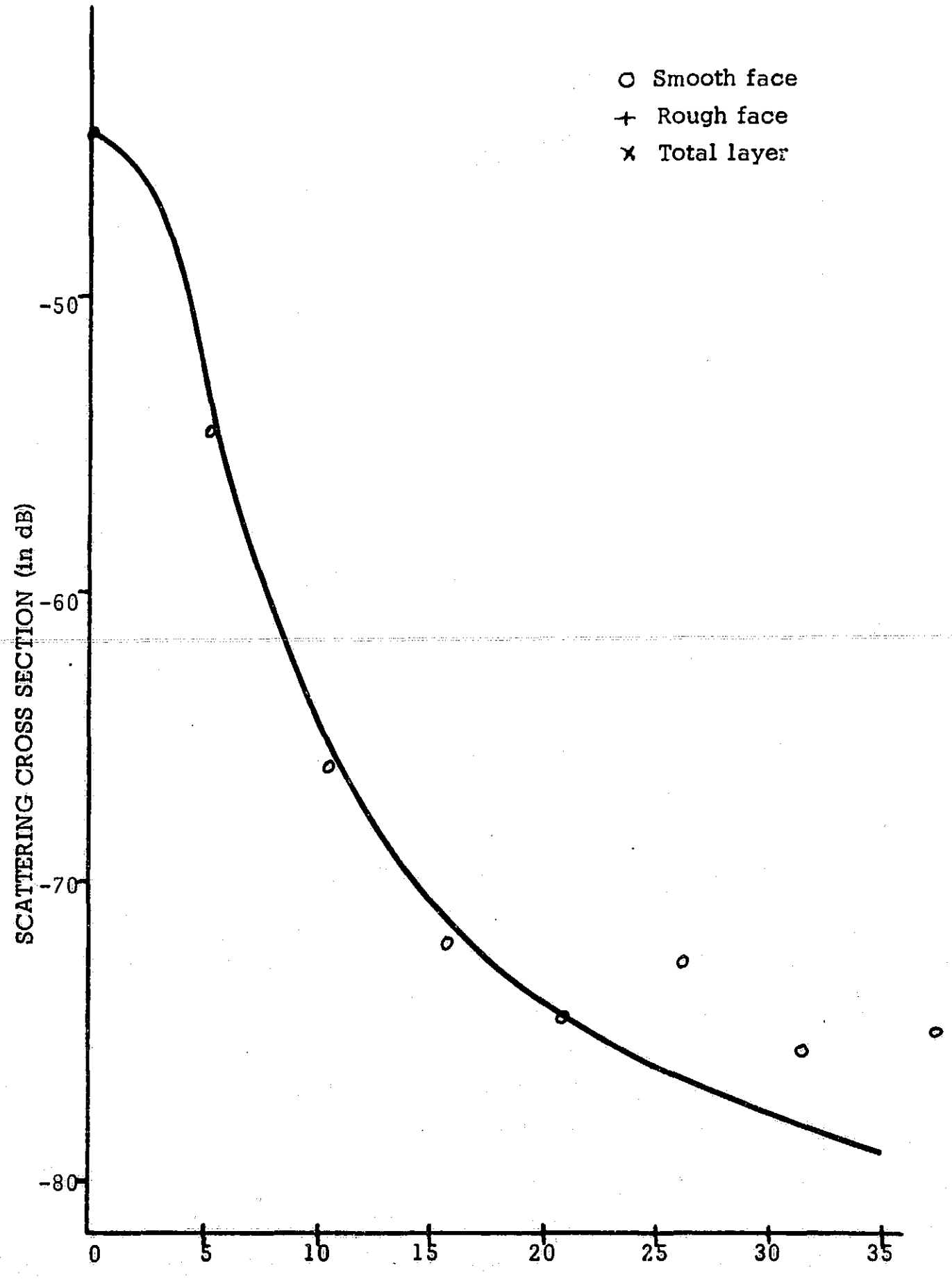

Figure 4-23. Scattering Cross Section of Layer with Smooth Front, R=.059, and Rough Rear, R=1.0, for Round-Trip Attenuation of 88 dB.

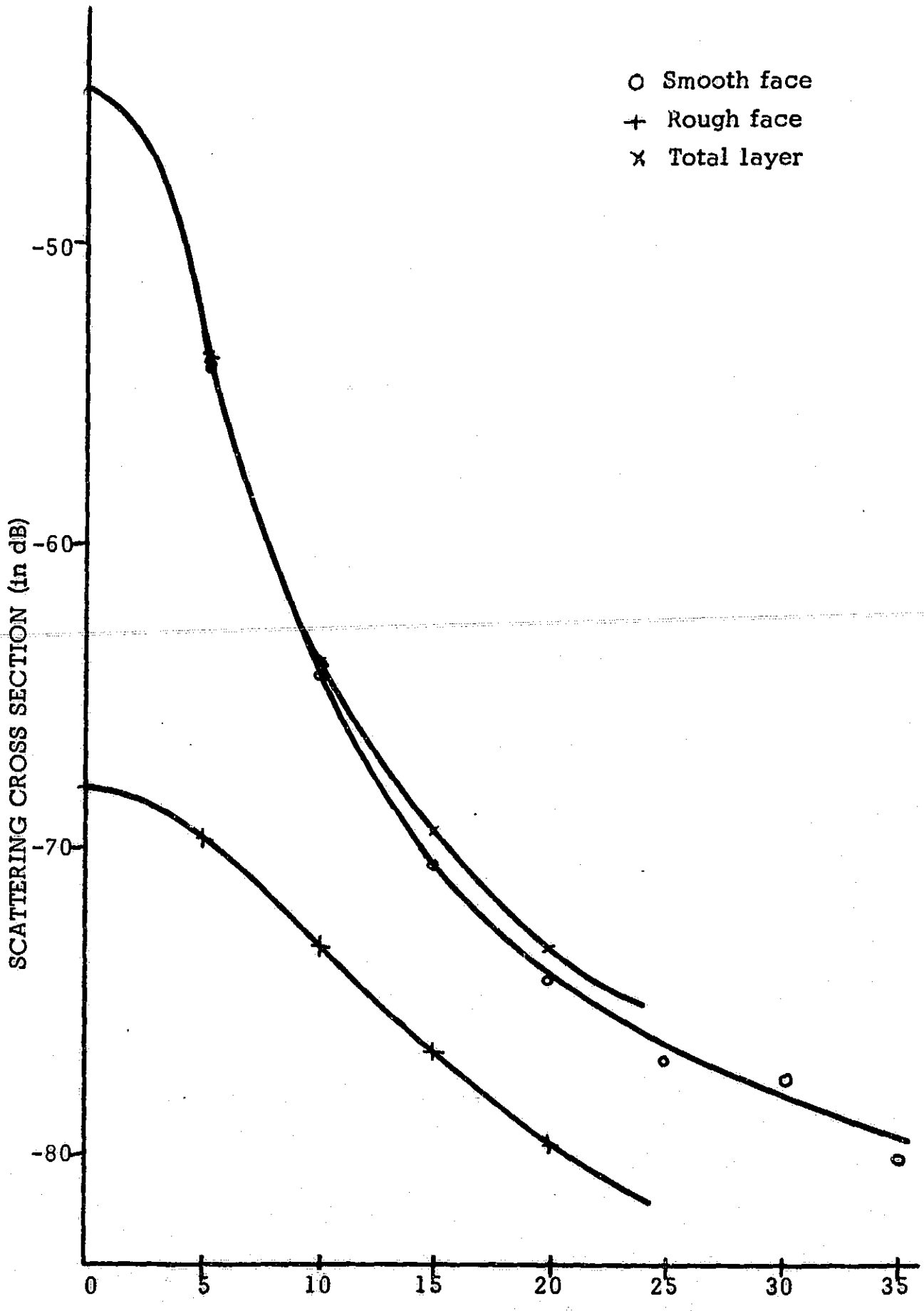

Figure 4-24. Scattering Cross Section of Layer with Smooth Front, R=.059, and Rough Rear, R=1.0, for Round-Trip Attenuation of 72 dB.

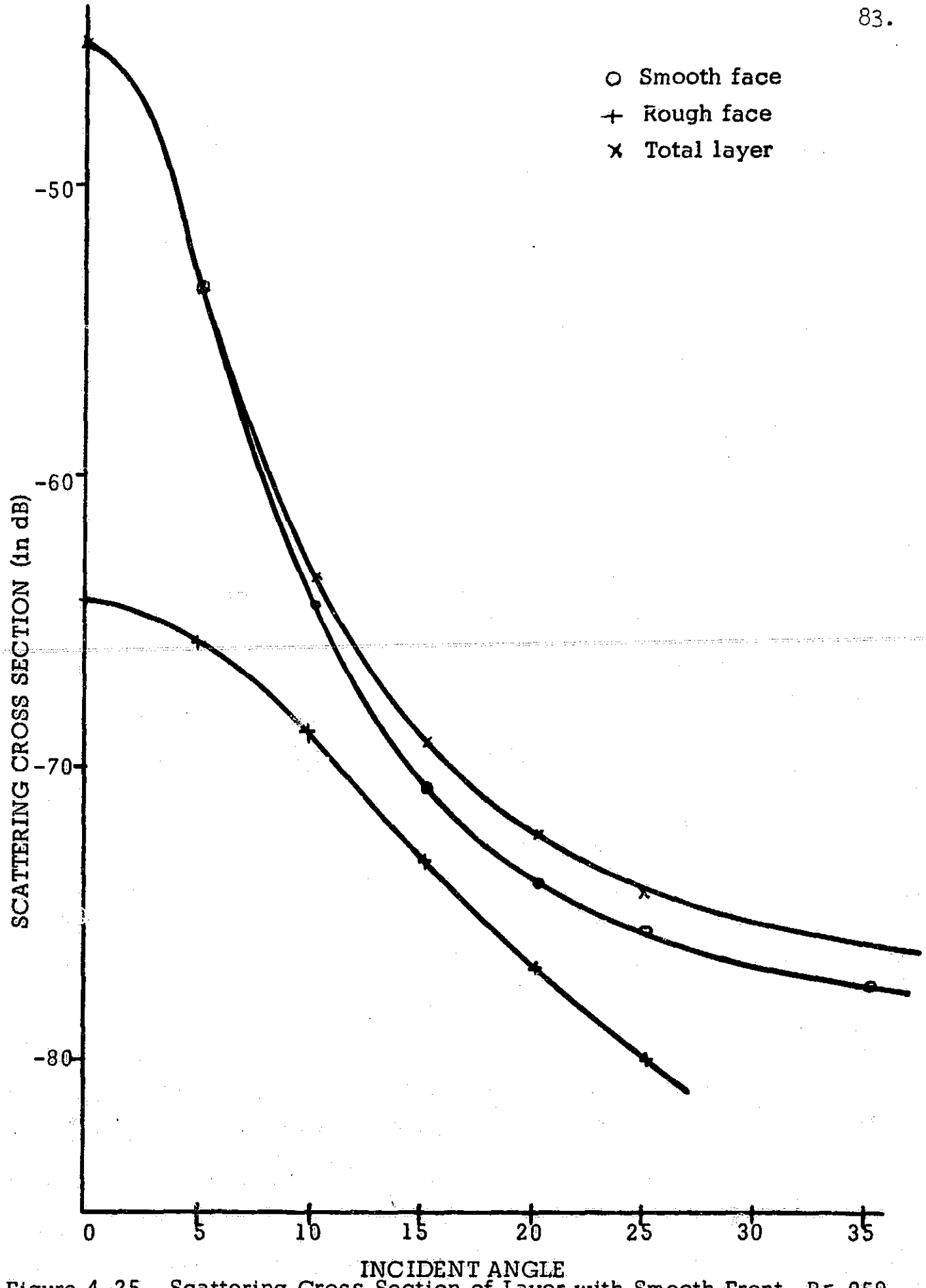

Figure 4-25. Scattering Cross Section of Layer with Smooth Front, R=.059, and Rough Rear, R=1.0, for Round-Trip Attenuation of 56 dB.

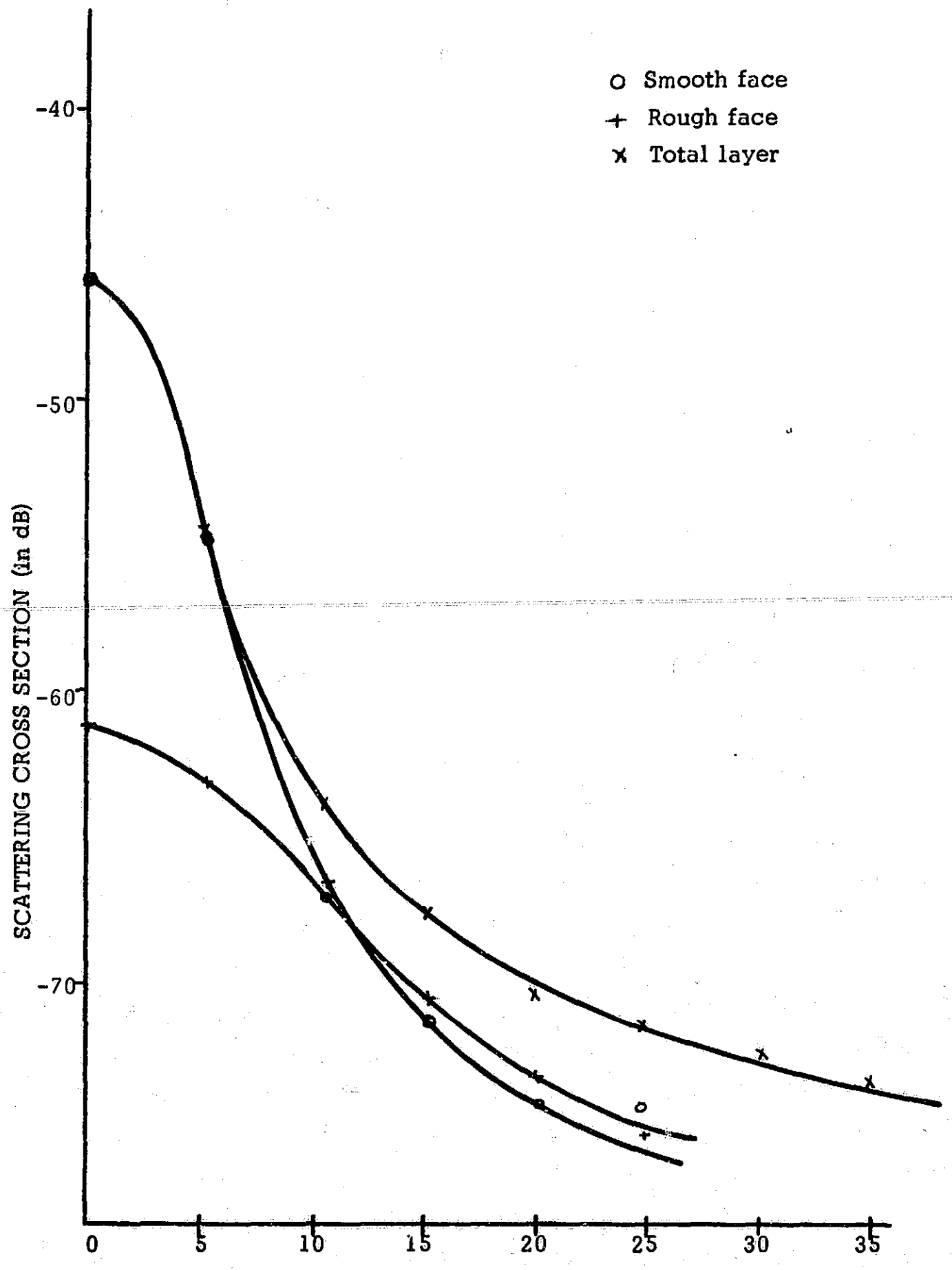

Figure 4-26. Scattering Cross Section of Layer with Smooth Front, R=.059, and Rough Rear, R=1.0, for Round-Trip Attenuation of 44 dB.

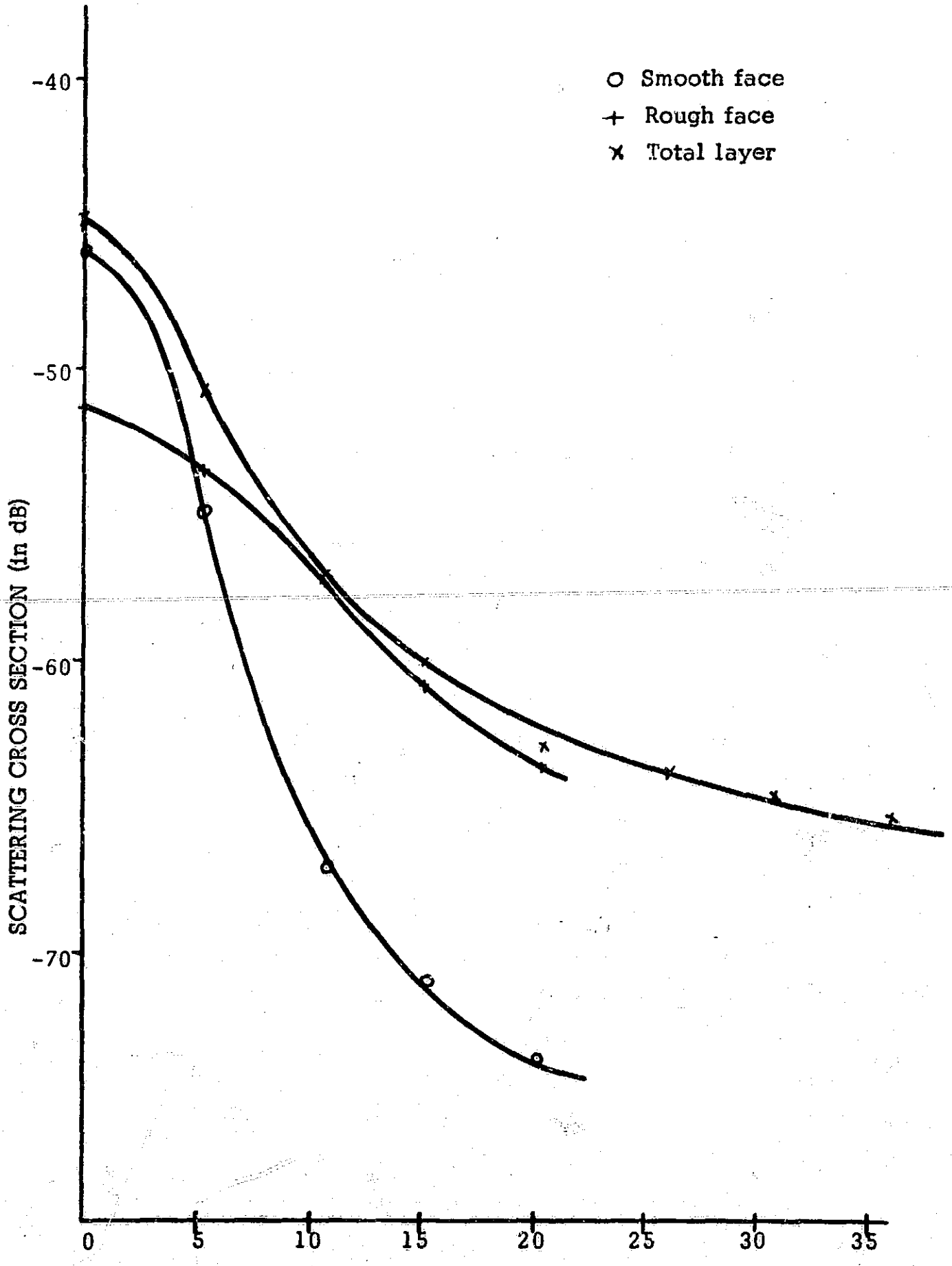

Figure 4-27. Scattering Cross Section of Layer with Smooth Front, R=.059, and Rough Rear, R=1.0, for Round-Trip Attenuation of 36 dB.

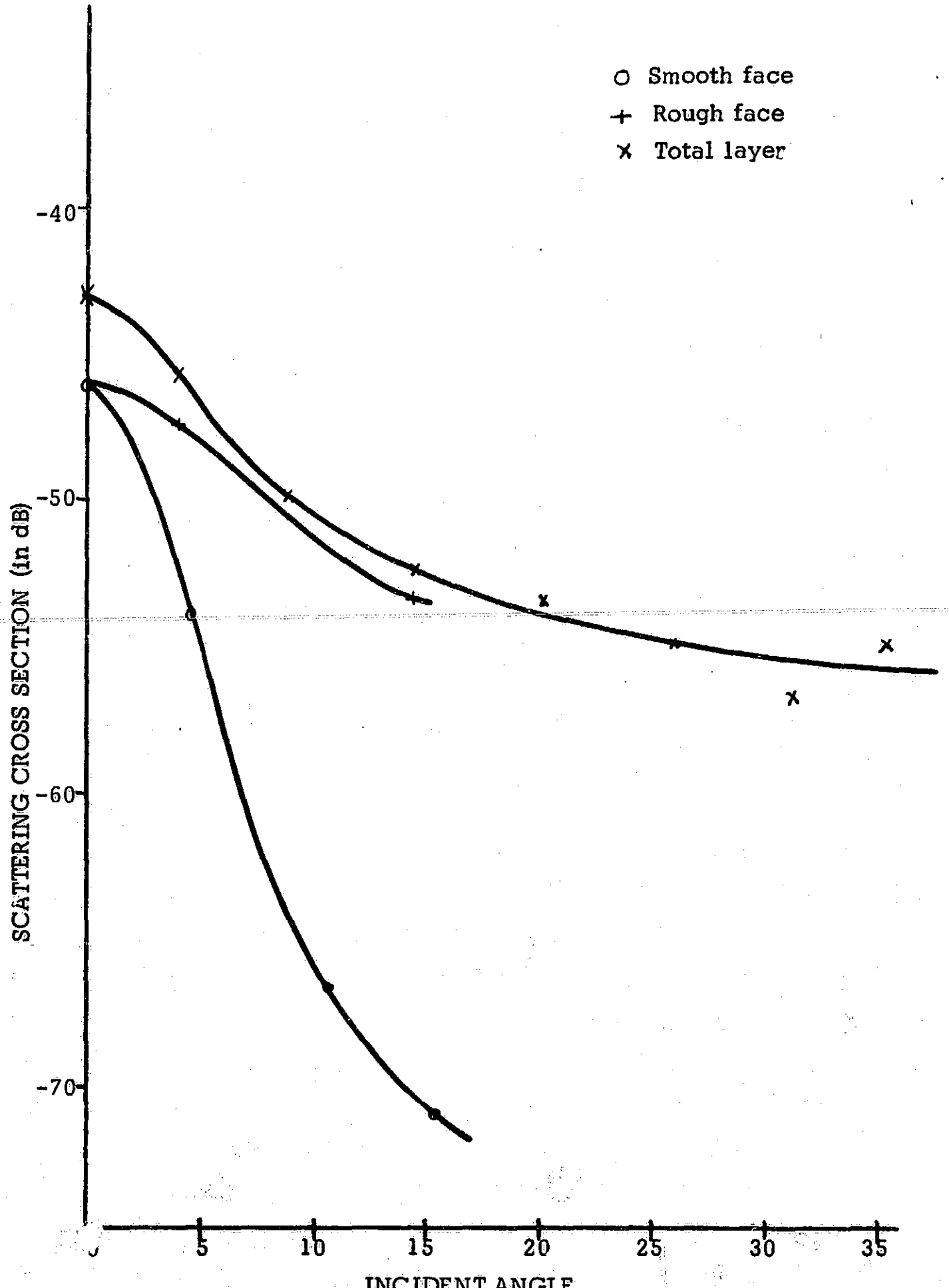

Figure 4-28. Scattering Cross Section of Layer with Smooth Front, R=.059, and Rough Rear, R=1.0, for Round-Trip Attenuation of 30 dB.

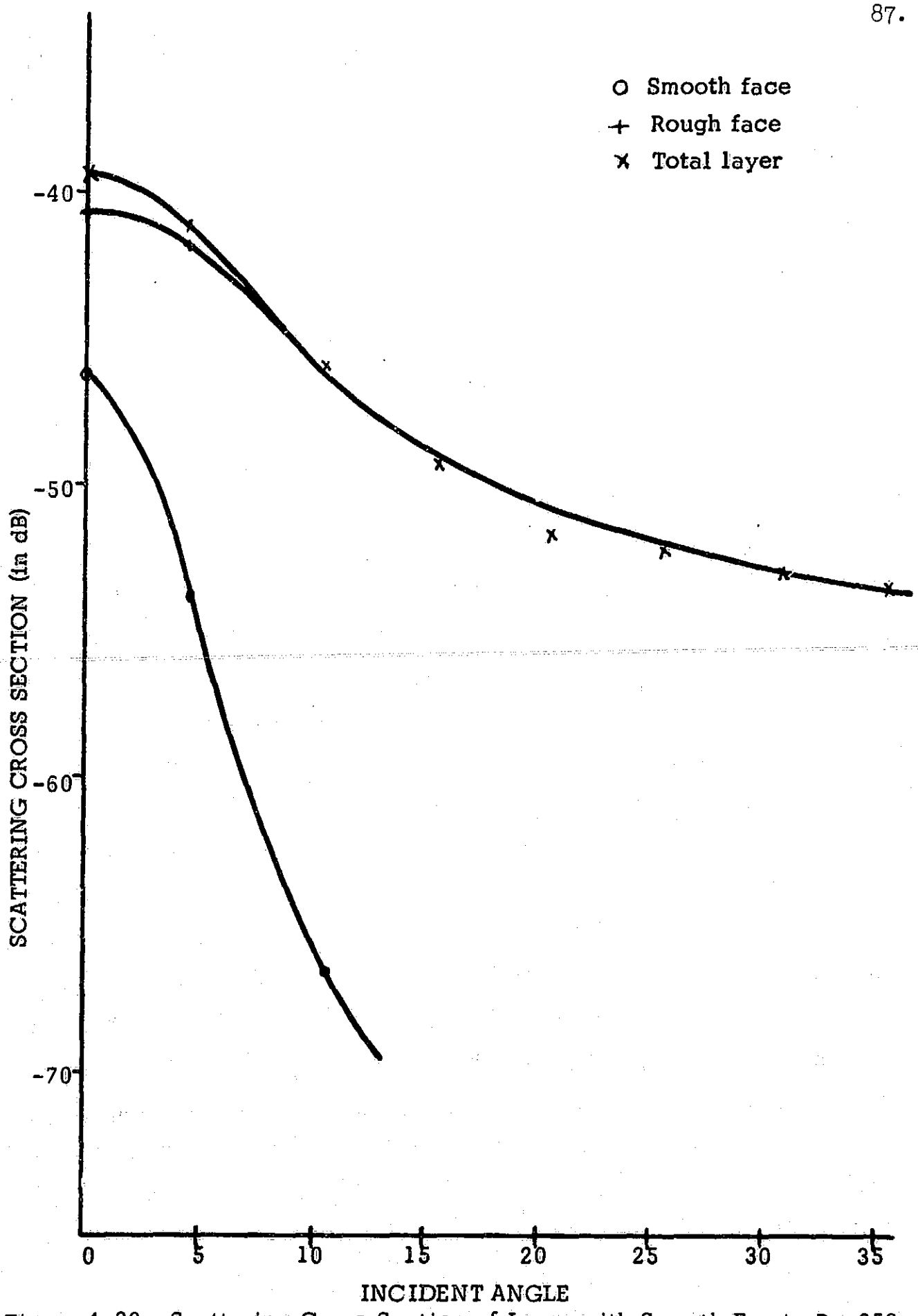

Figure 4-29. Scattering Cross Section of Layer with Smooth Front, R=.059, and Rough Rear, R=1.0, for Round-Trip Attenuation of 24 dB.

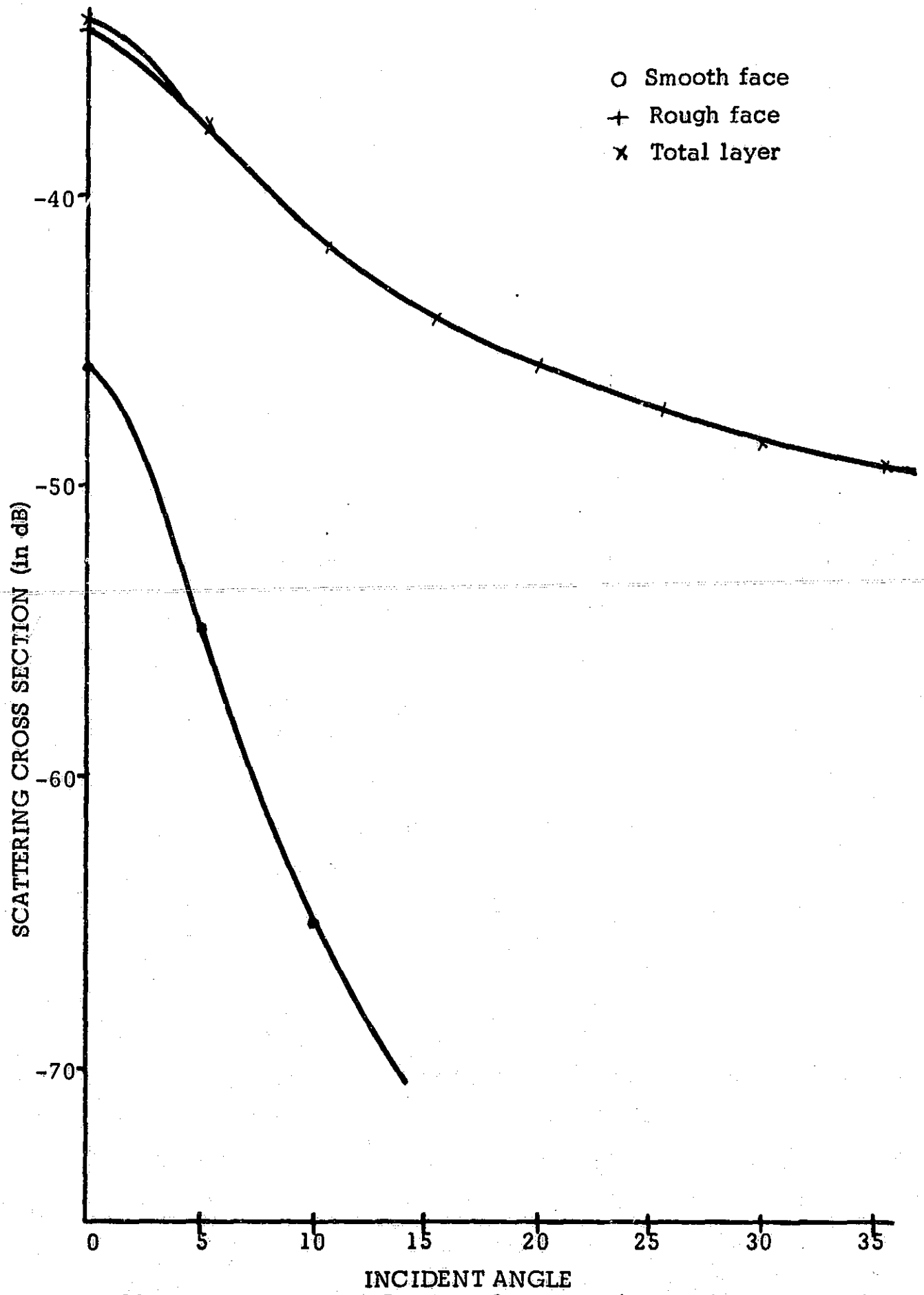

Figure 4-30. Scattering Cross Section of Layer with Smooth Front, R=.059, and Rough Rear, R=1.0, for Round-Trip Attenuation of 20 dB.

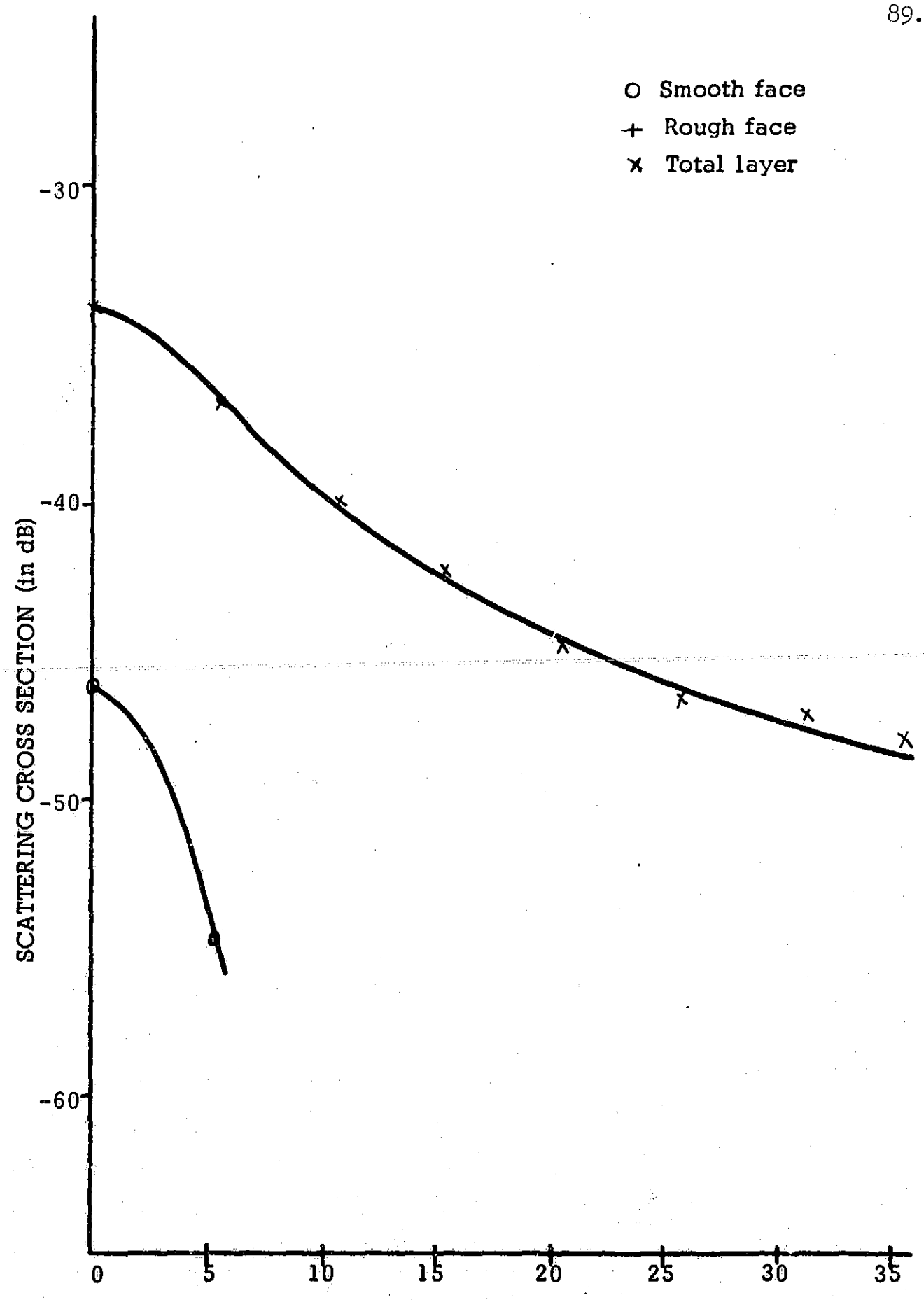

Figure 4-31. Scattering Cross Section of Layer with Smooth Front, R=.059, and Rough Rear, R=1.0, for Round-Trip Attenuation of 16dB.

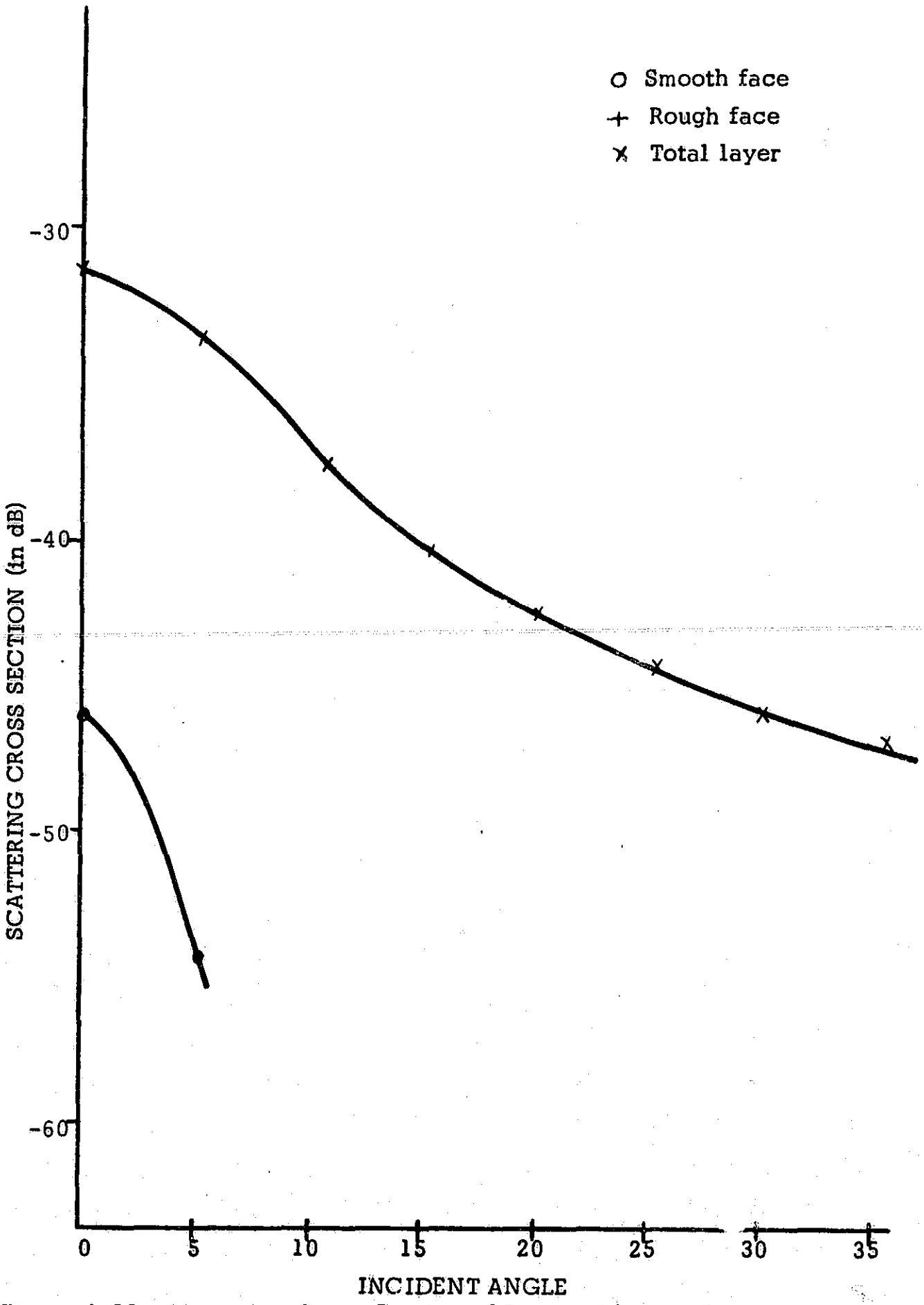

Figure 4-32. Scattering Cross Section of Layer with Smooth Front, R=.059, and Rough Rear, R=1.0, for Round-Trip Attenuation of 12dB.

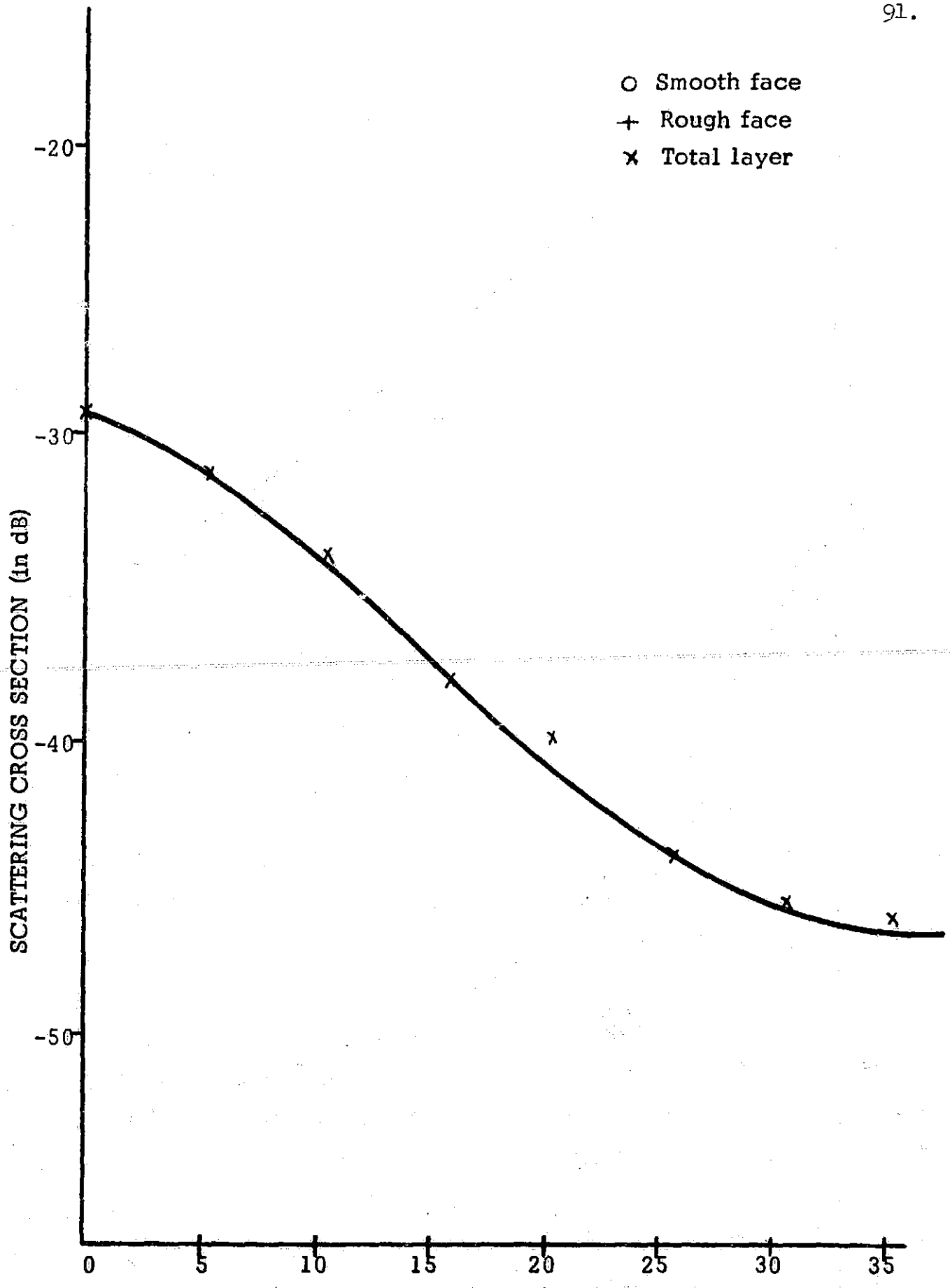

Figure 4-33. Scattering Cross Section of Layer with Smooth Front, R=.059, and Rough Rear, R=1.0, for Round-Trip Attenuation of 8 dB.

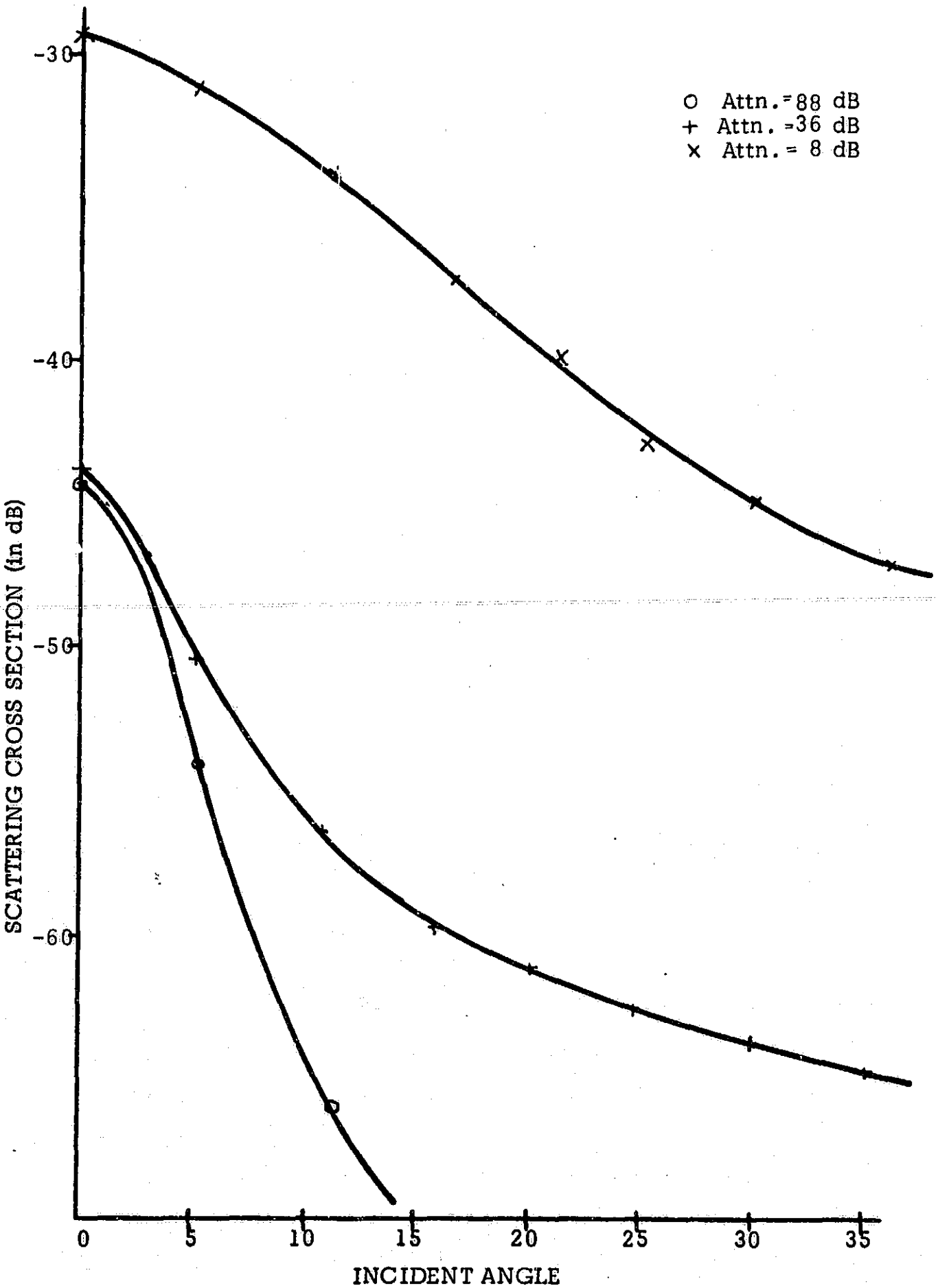

Figure 4-34. Scattering Cross Section of Layers with Smooth Front, R=.059, and Rough Rear, R=1.0, as a Function of Attenuation.

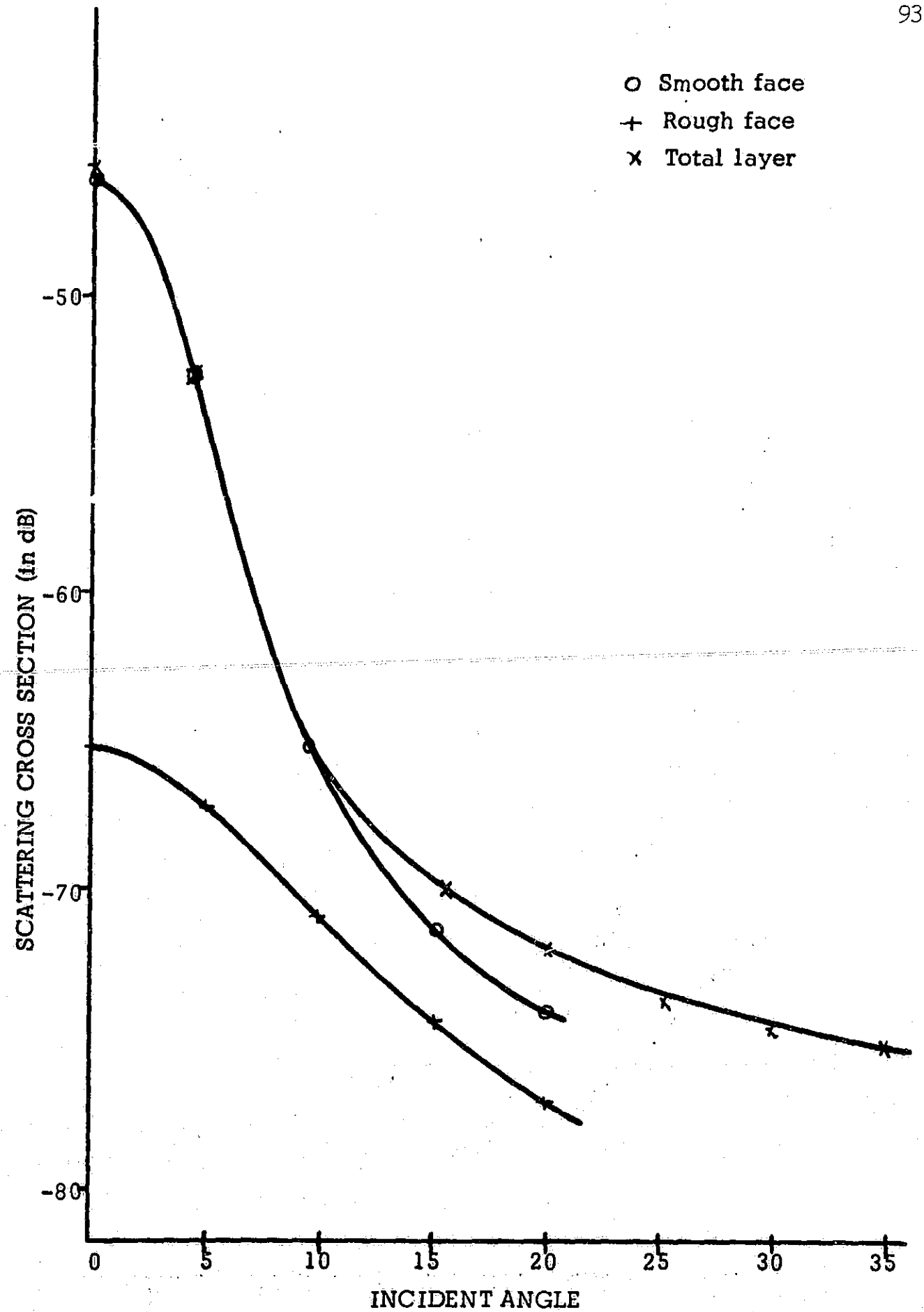

Figure 4-35. Scattering Cross Section of Layer with Smooth Front, R=.059, and Rough Rear, R=.057, for Round-Trip Attenuation of 36 dB.

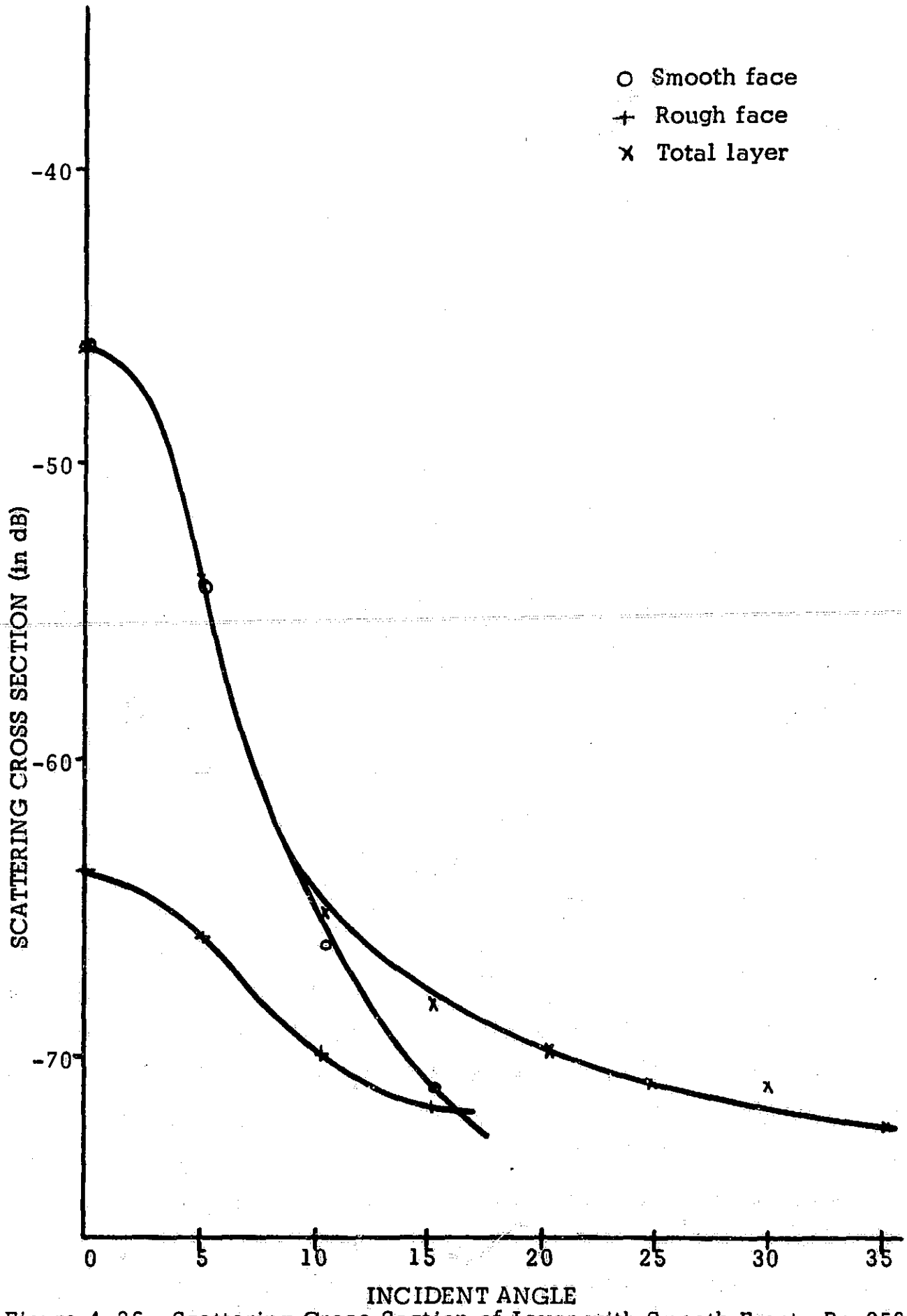

Figure 4-36. Scattering Cross Section of Layer with Smooth Front, R=.059, and Rough Rear, R=.057, for Round-Trip Attenuation of 30 dB.

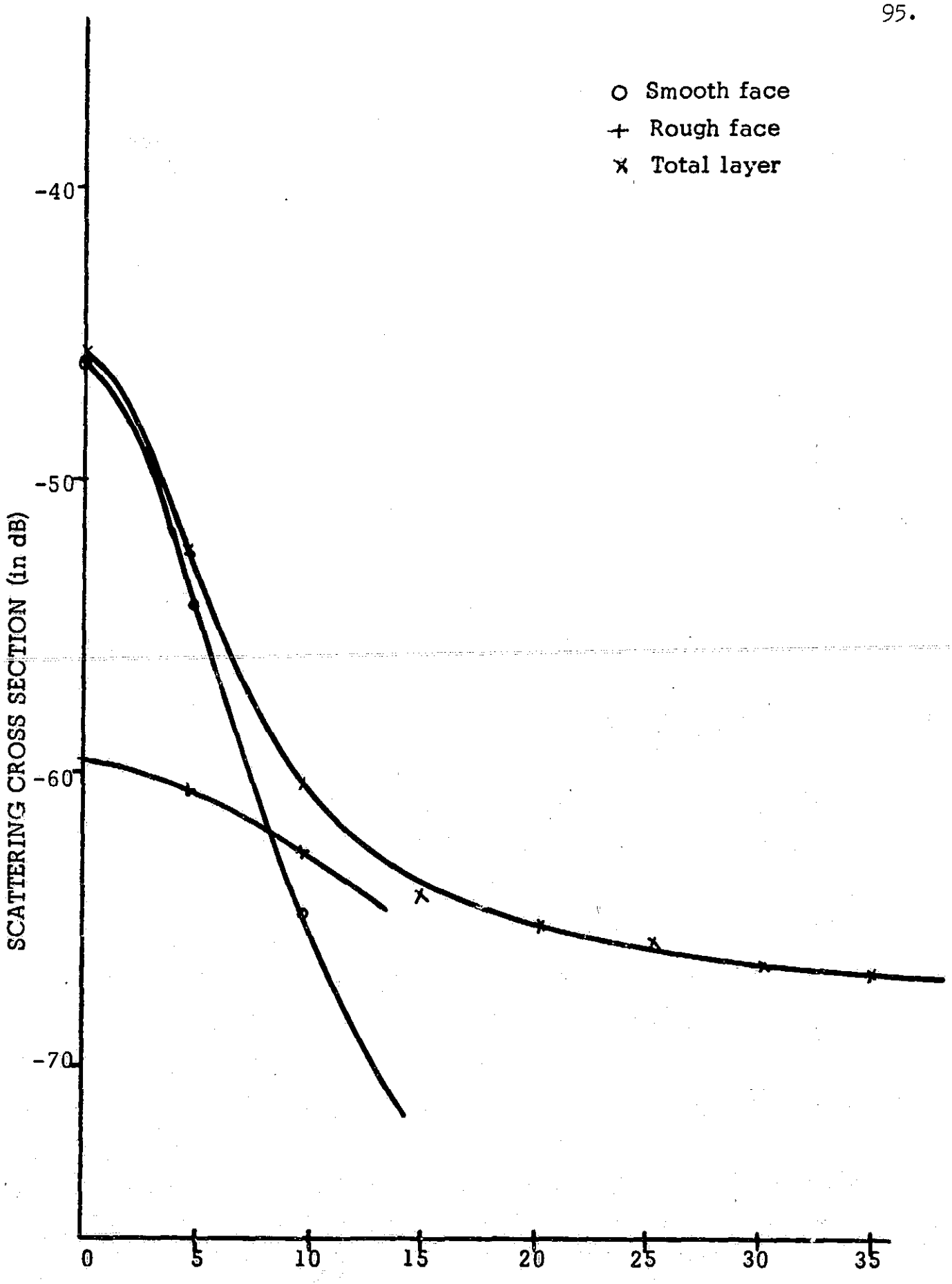

Figure 4-37. Scattering Cross Section of Layer with Smooth Front, R=.059, and Rough Rear, R=.057, for Round-Trip Attenuation of 24 dB.

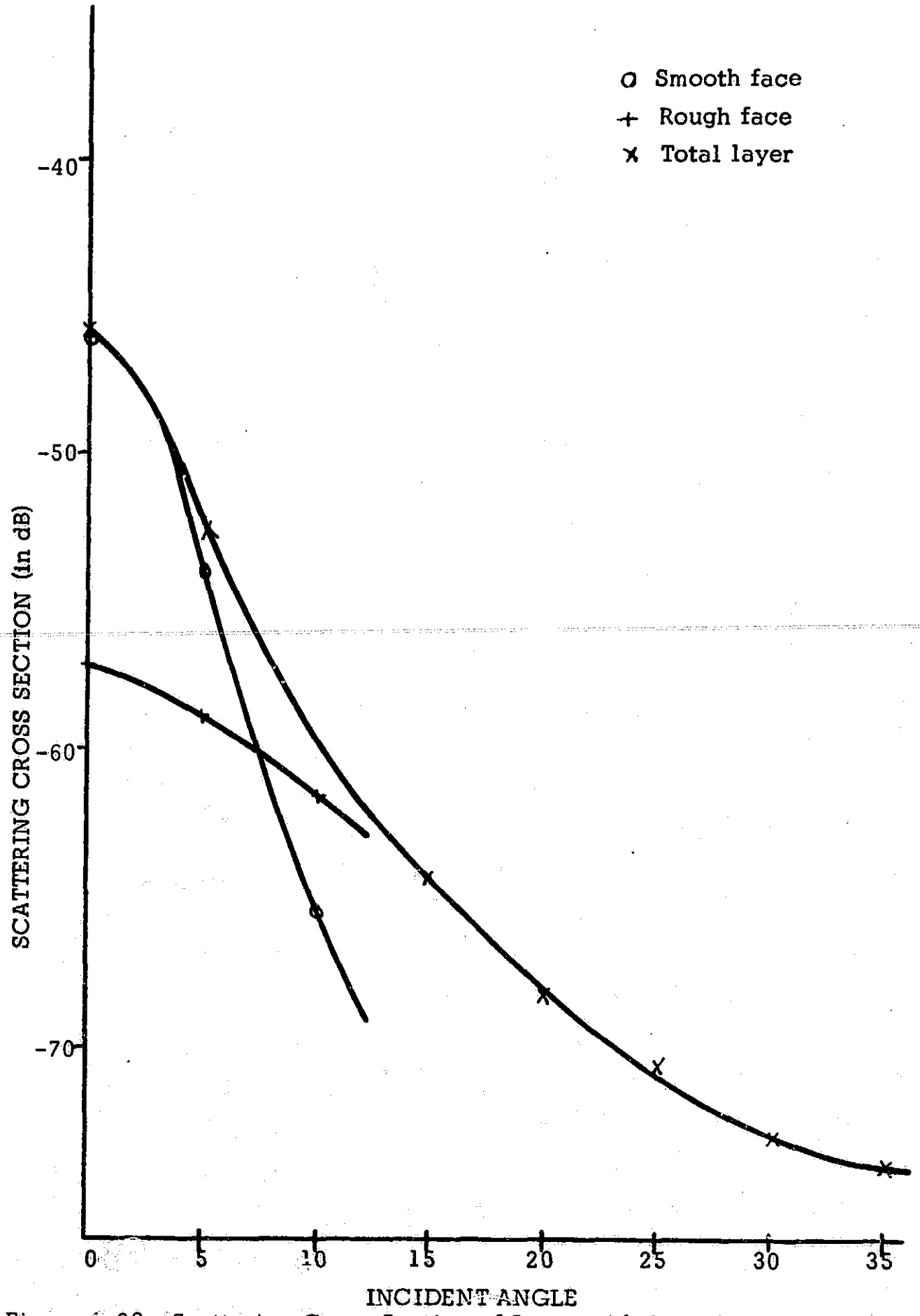

Figure 4-38. Scattering Cross Section of Layer with Smooth Front, R=.059, and Rough Rear, R=.057, for Round-Trip Attenuation of 20 dB.

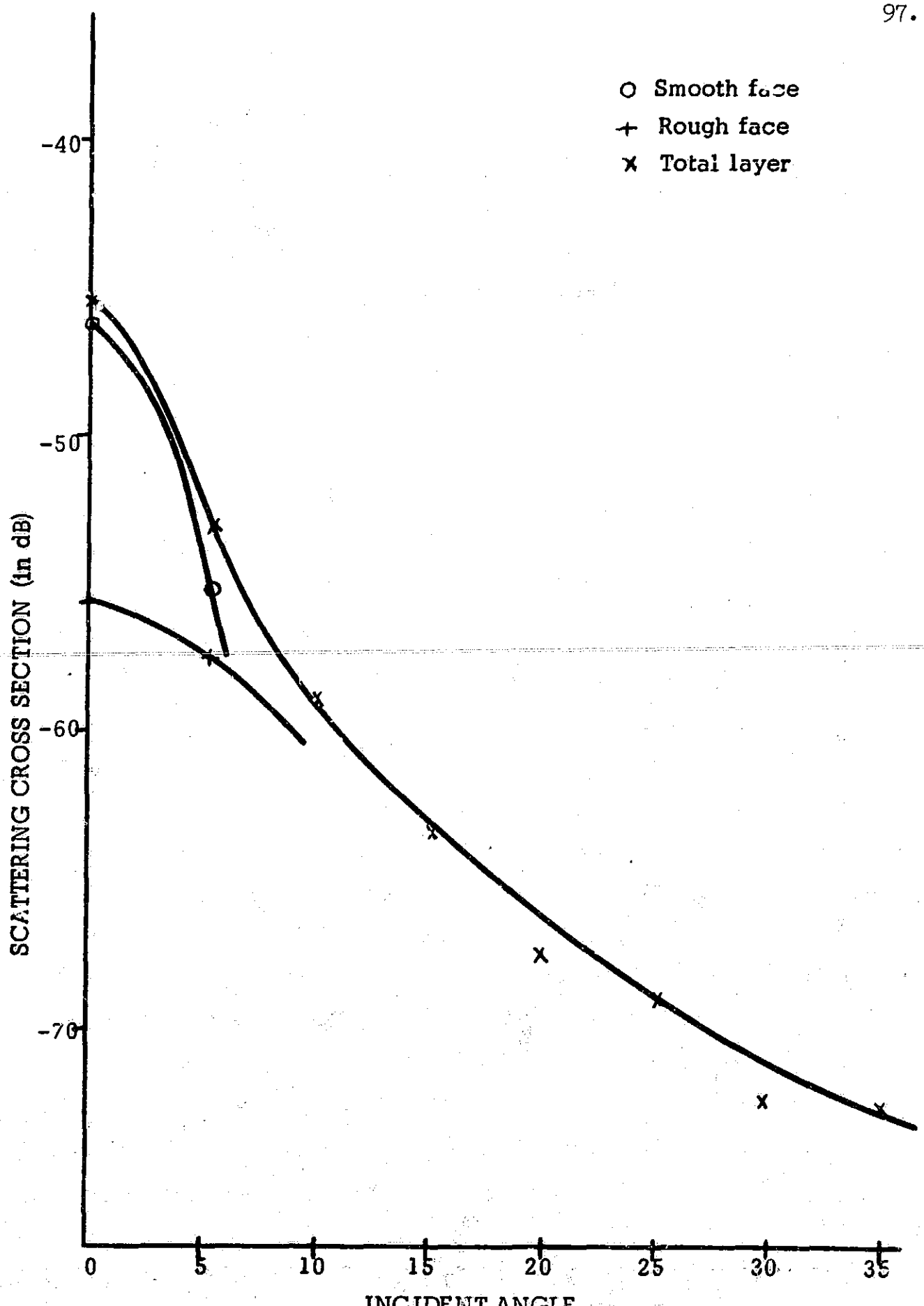

Figure 4-39. Scattering Cross Section of Layer with Smooth Front, R=.059, and Rough Rear, R=.057, for Round-Trip Attenuation of 16dB.

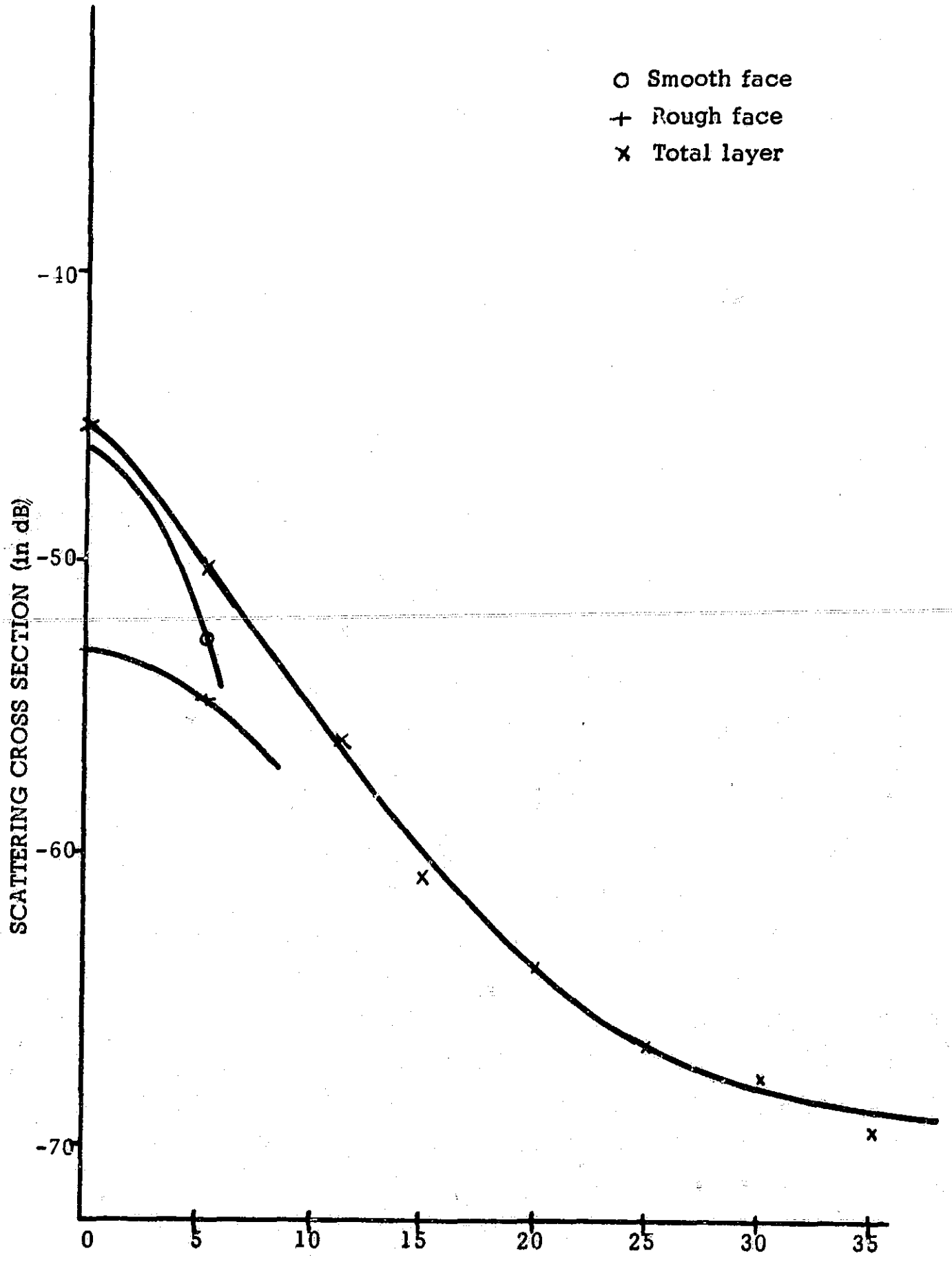

Figure 4-40. Scattering Cross Section of Layer with Smooth Front, R=.059, and Rough Rear, R=.057, for Round-Trip Attenuation of 12dB.

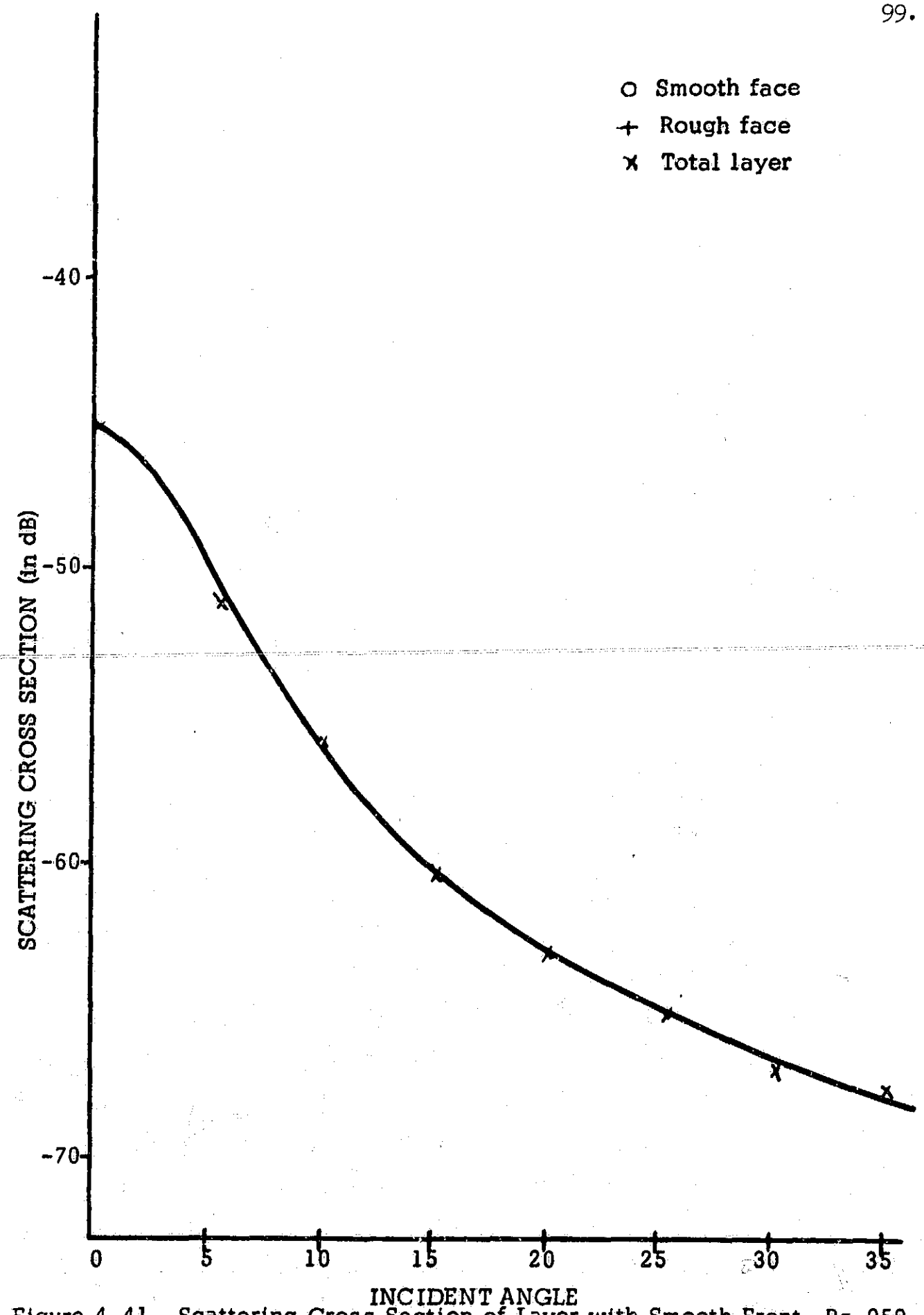

Figure 4-41. Scattering Cross Section of Layer with Smooth Front, R=.059, and Rough Rear, R=.057, for Round-Trip Attenuation of 8 dB.

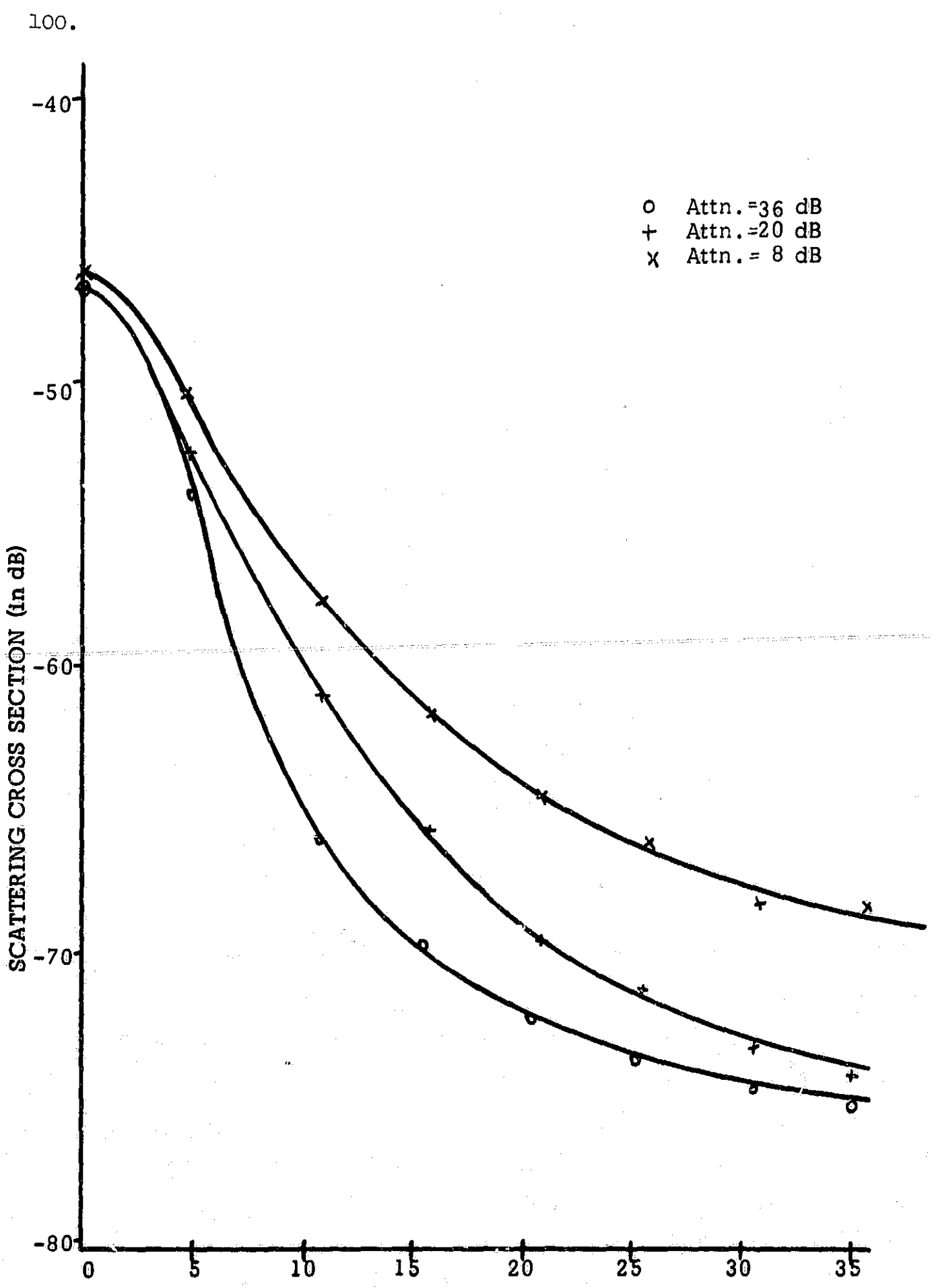

Figure 4-42. Scattering Cross Section of Layers with Smooth Front, R=.059, and Rough Rear, R=.057, as a Function of Attenuation.

the trend toward a return resembling a rough surface with a peak near the vertical. Figure 4.42 shows this trend as the layer thickness is changed.

4.4 Comparison of Experimental and Theoretical Results

Since this is primarily an experimental investigation no detailed comparison of the experiment and the theory will be attempted. The simpler cases can be compared directly with the three theoretical curves, Figures 4.1 through 4.3, however.

4.4.1 Scattering Cross Section of the Smooth Face Compared to the Antenna Power Gain

For the thickest layer with a smooth front face the return from the rough rear was attenuated enough that it had no observable effect on the return. This case was used to examine the scattering cross section of the smooth side of the layer by superimposing Figure 4.23 and Figure 4.1, the antenna power gain curve, in Figure 4.43. The experimental curve fits the antenna curve very closely from vertical down to 6^{o}. For larger incident angles the return from the smooth side of the layer is much more than expected, indicating the presence of small scale roughness on the supposedly plane surface. Visual observation of the flat side of the layer revealed just such an effect in the form of a slight "alligatoring" of the surface.

4.4.2 Scattering Cross Section of the Rough Face Compared to the Theory

Again the thickest layer did not have any return from the rear face when the rough side was illuminated first so it was used. Figure 4.44 is a plot of the theoretical scattering cross section with the experimentally determined points shown for comparison. There is a deviation of 2 dB at vertical incidence but the rest of the curve is fit quite closely.

4.4.3 Scattering Cross Section of the Rough Face in the Rear Compared to the Theory

The thinnest layer with the rough perfectly reflecting rear face was used for the experimental data since the expected effect of the

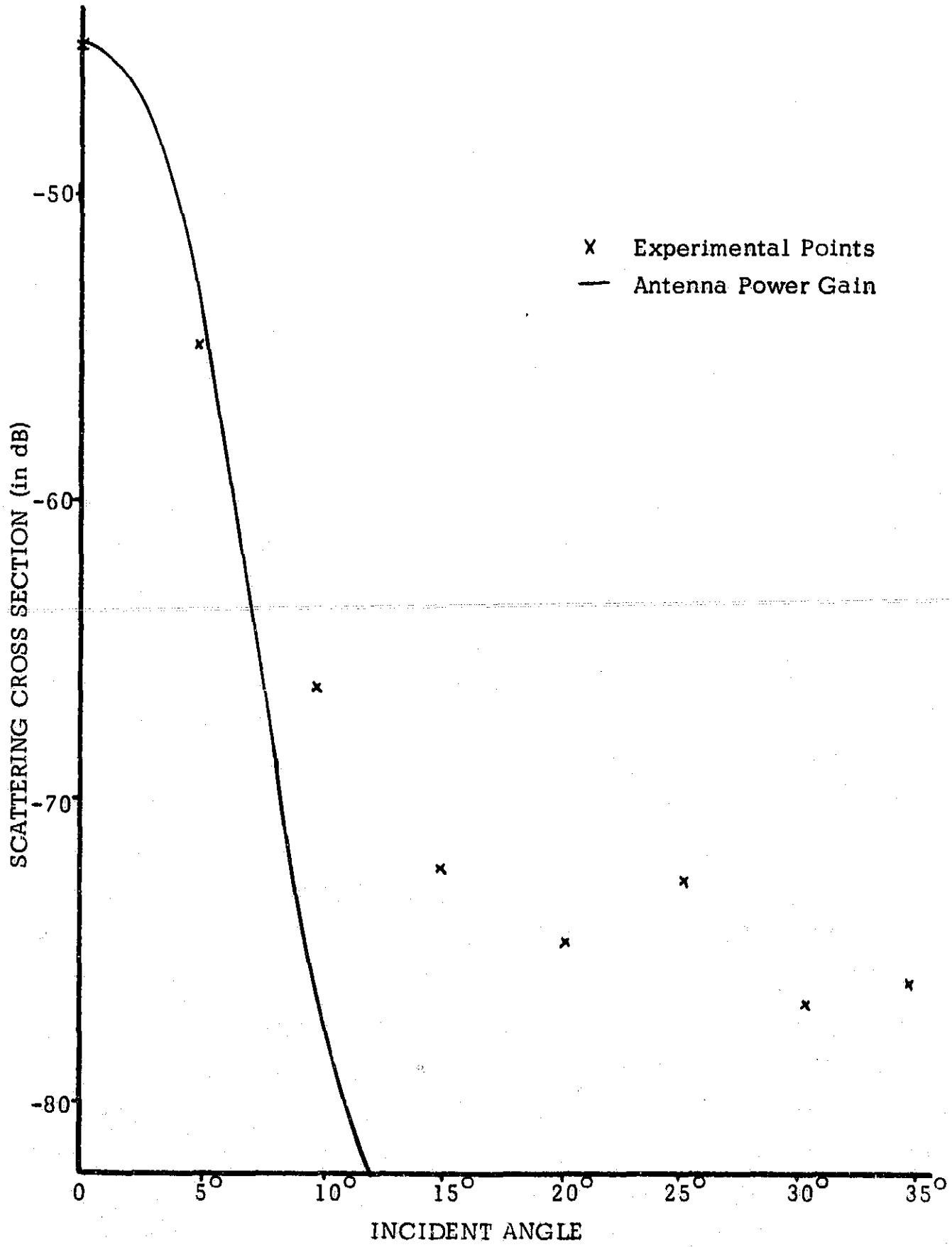

Figure 4-43. Comparison of the Scattering Cross Section of the Smooth Side and the Antenna Power Gain Function.

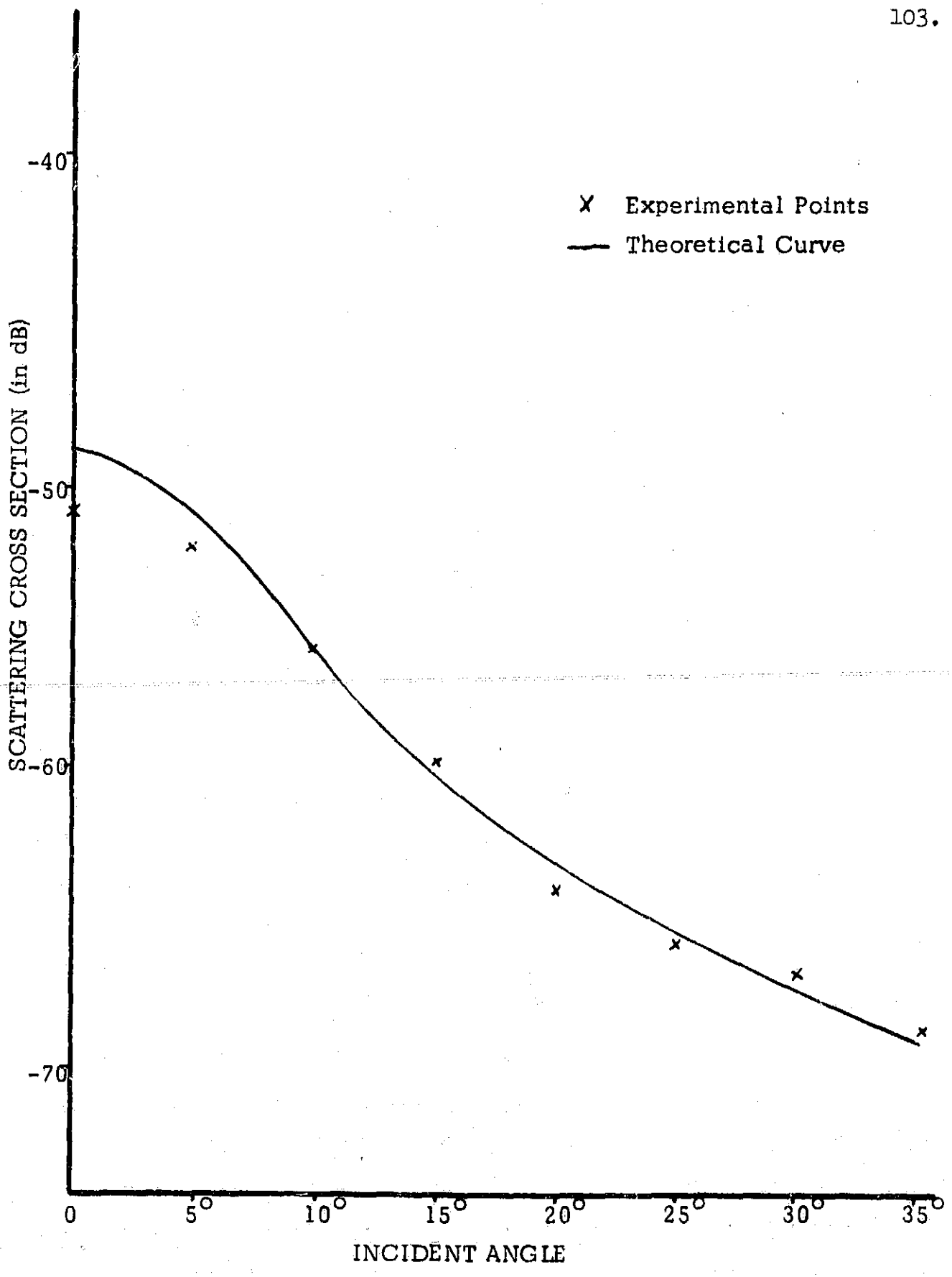

Figure 4-44. Comparison of Experimental and Theoretical Scattering Cross Sections of the Rough Surface Used.

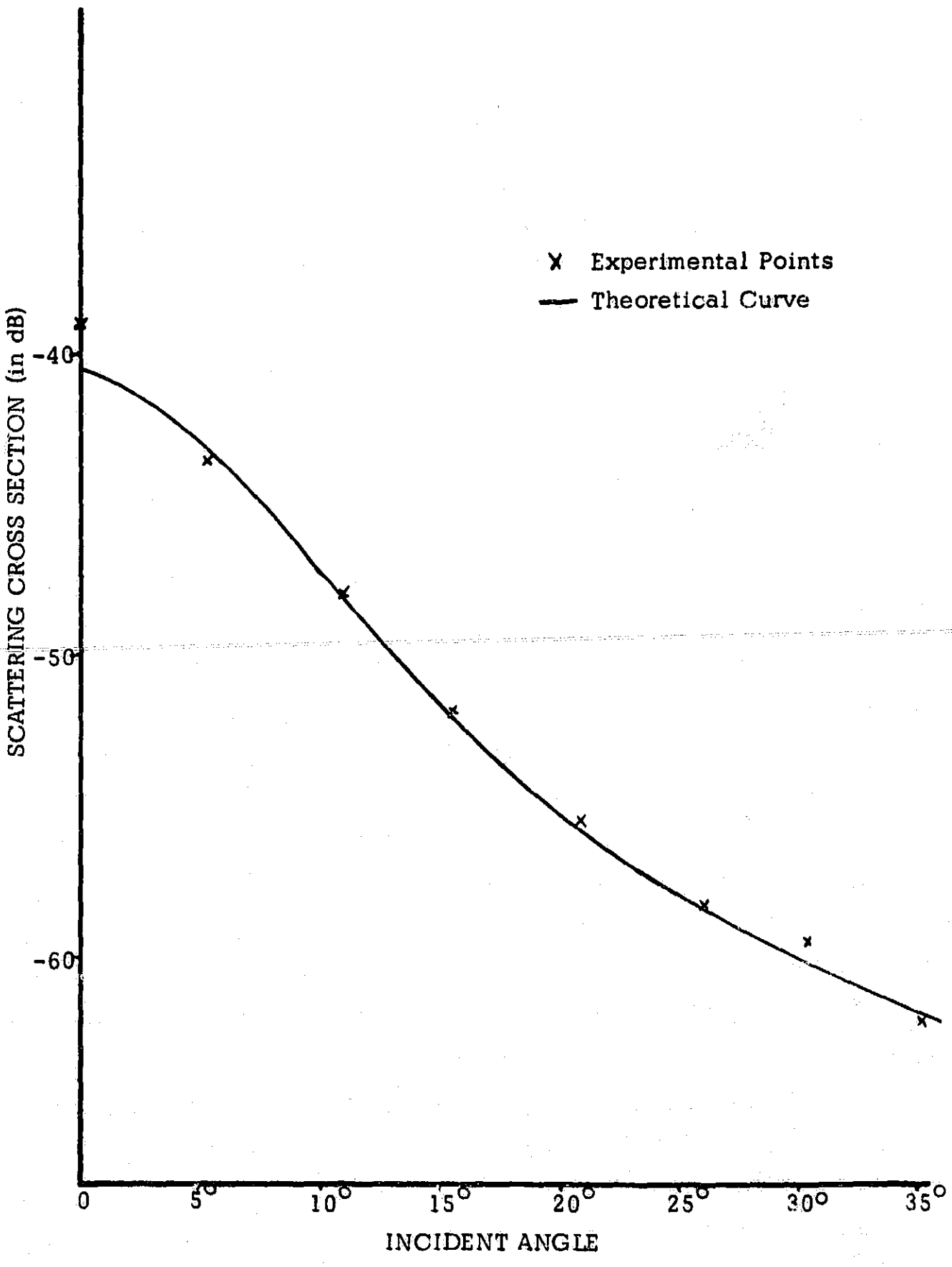

Figure 4-45. Comparison of Experimental and Theoretical Scattering Cross Sections for the Rough Face in the Rear.

smooth front is 16 dB below the return from the rear at vertical incidence and even lower as the angle is increased. As seen in Figure 4.45, the experimental points are very near that predicted by the theory, except for vertical incidence, as expected due to the effect of the smooth front.

4.5 Summary of the Experiment and Conclusions

The experimental layer model used had one smooth face and the other two-dimensionally rough. Both rough front and smooth front cases were considered with the front face having a reflection coefficient of 0.059 for all configurations. The rear face was either perfectly reflecting or had a reflection coefficient of 0.057. For each case the layer thickness was varied from that for which no return was received from the rear to the thinnest that could be produced. The summary of each configuration as a function of round-trip attenuation in the layer, layer thickness, is given in Figure 4.46. For each case it is noted that the effect of the rear face is small for the layers with high total attenuation but becomes increasinbly important as the layer attenuation is reduced.

Also of interest is the effect of the configurations with the same attenuation within the layer. This is shown in Figure 4.47 where four sets of curves are presented with the attenuation fixed for each set. The most important observation here is that the layer effect is greater when the reflection coefficient of the rear face is high than when it is low. Also noted is that, when the layer attenuation is low and the reflection coefficient of each face is of the same order of magnitude, the return is basically the same no matter which face is illuminated first (see curves 2 and 4 of Figure 4.47a).

Another comparison to be made is one in which the layer attenuation and the reflection coefficient of the rear face are such that the return from the rear is expected to be the same for two cases. For the rear reflection coefficient of 0.057 (-24.8 dB) and 8 dB layer attenuation the total effective attenuation is 32.8 dB. This could be compared to the case of a perfectly reflecting rear face with 32.8 dB attenuation in the layer. No such layer was examined with the closest being one in which the layer attenuation was 30 dB, which should still be a good

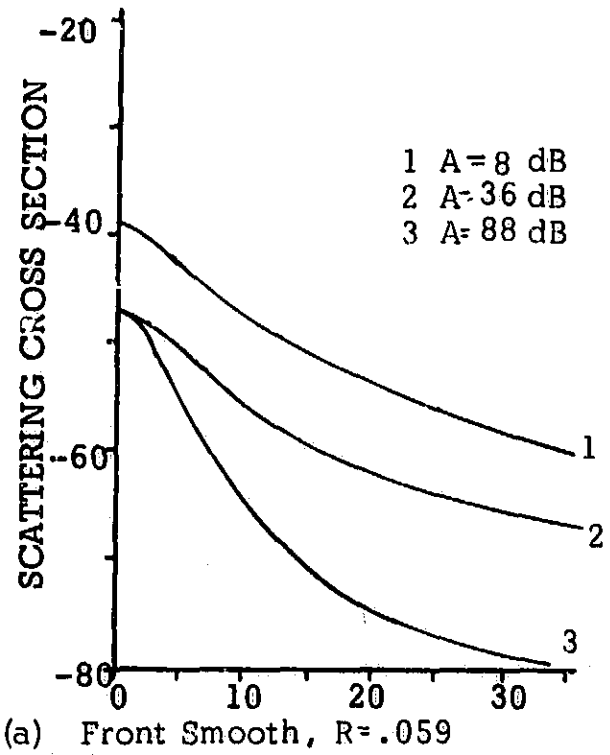

(a) Front Smooth, R=.059
Rear Rough, R=1.0

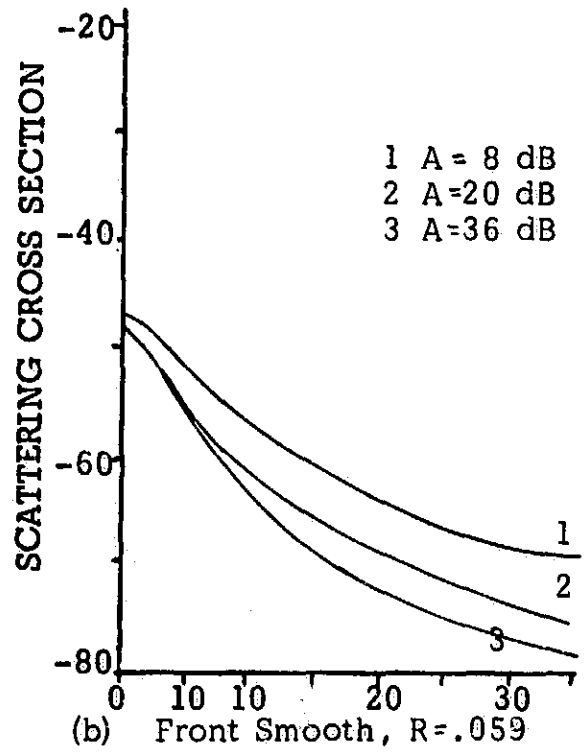

(b) Front Smooth, R=.059
Rear Rough, R=.057

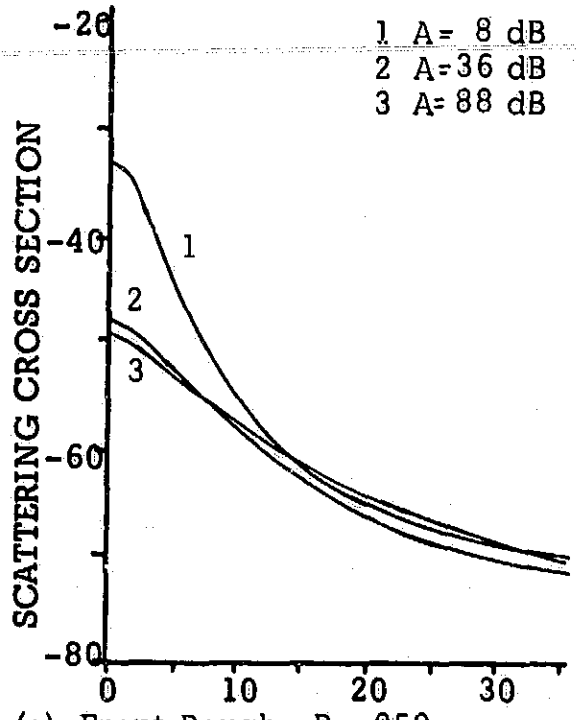

(c) Front Rough, R=.059
Rear Smooth, R=1.0

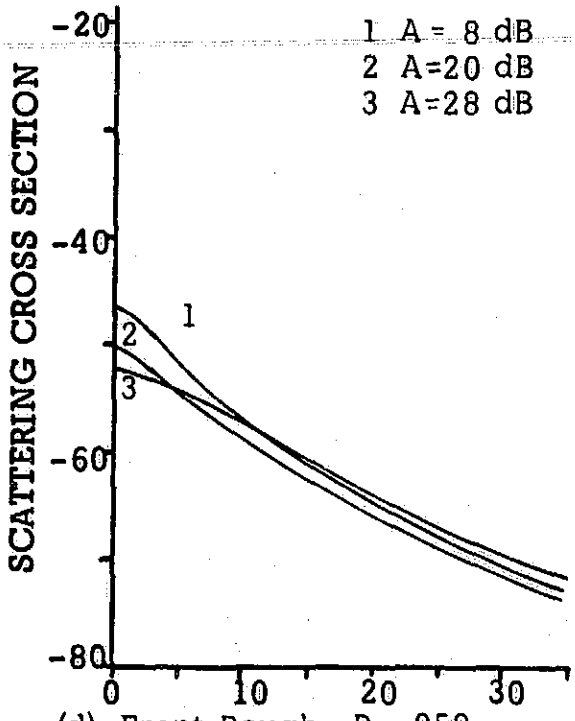

(d) Front Rough, R=.059
Rear Smooth, R=.057

Figure 4-46: Effect of Varying Round-Trip Attenuation, A, in the Layer for the Configurations Examined.

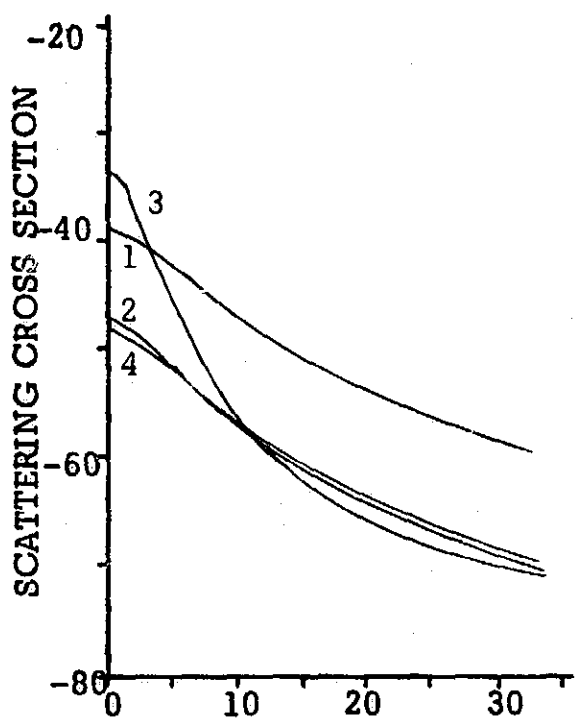

(a) Attenuation = 8 dB

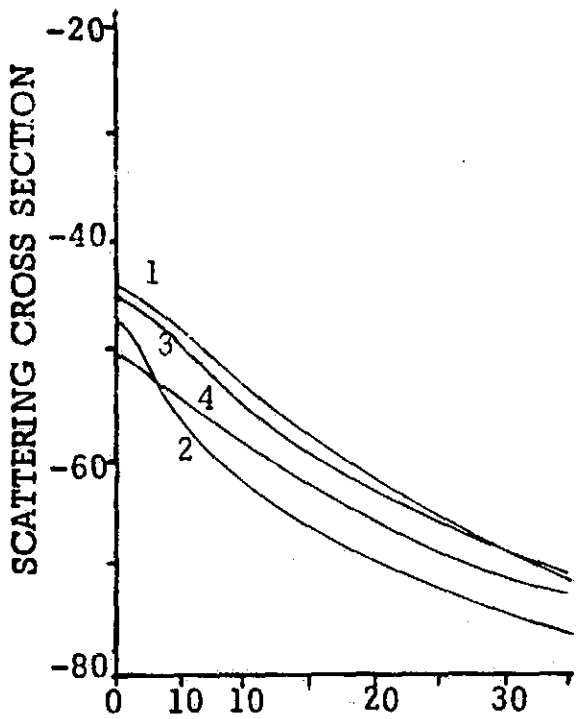

(b) Attenuation =20 dB

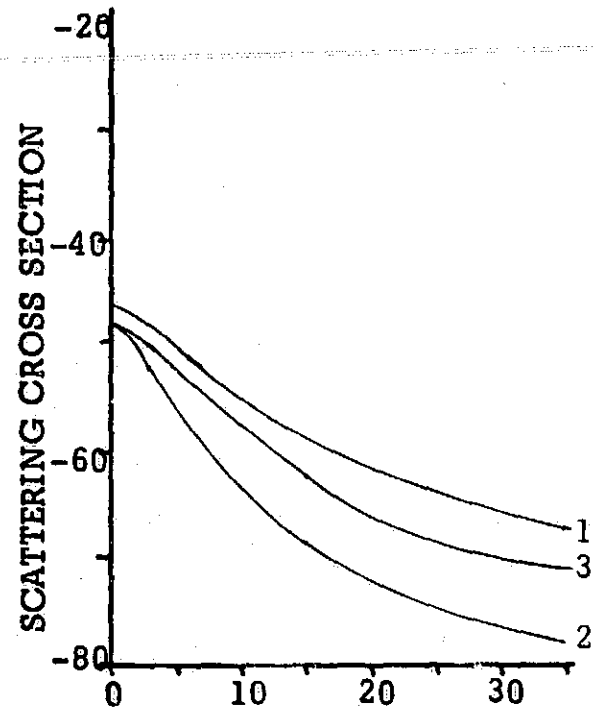

(c) Attenuation =36 dB

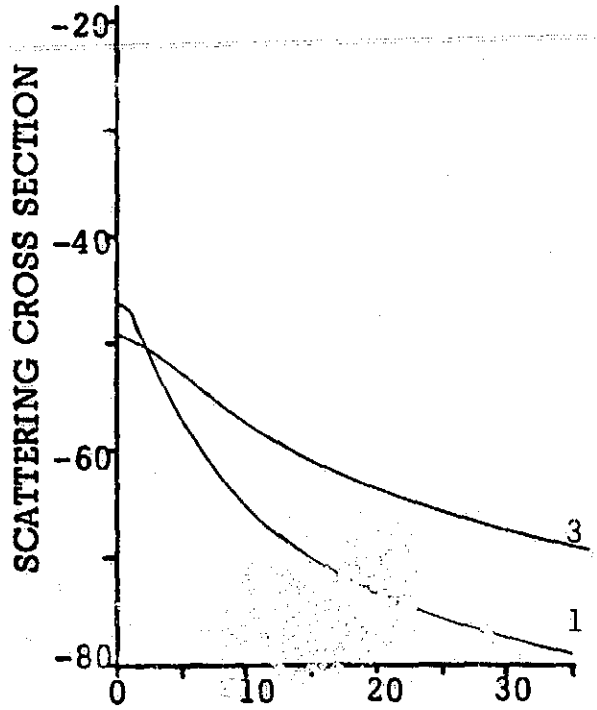

(d) Attenuation =88 dB

1 Front Smooth R=.059
Rear Rough R = 1.0

2 Front Smooth R=.059
Rear Rough R=.057

3 Front Rough R=.059
Rear Smooth R=1.0

4 Front Rough R=.059
Rear Smooth R=.057

Figure 4-47. Comparison of the Four Configurations with Fixed Attenuation in the Layer.

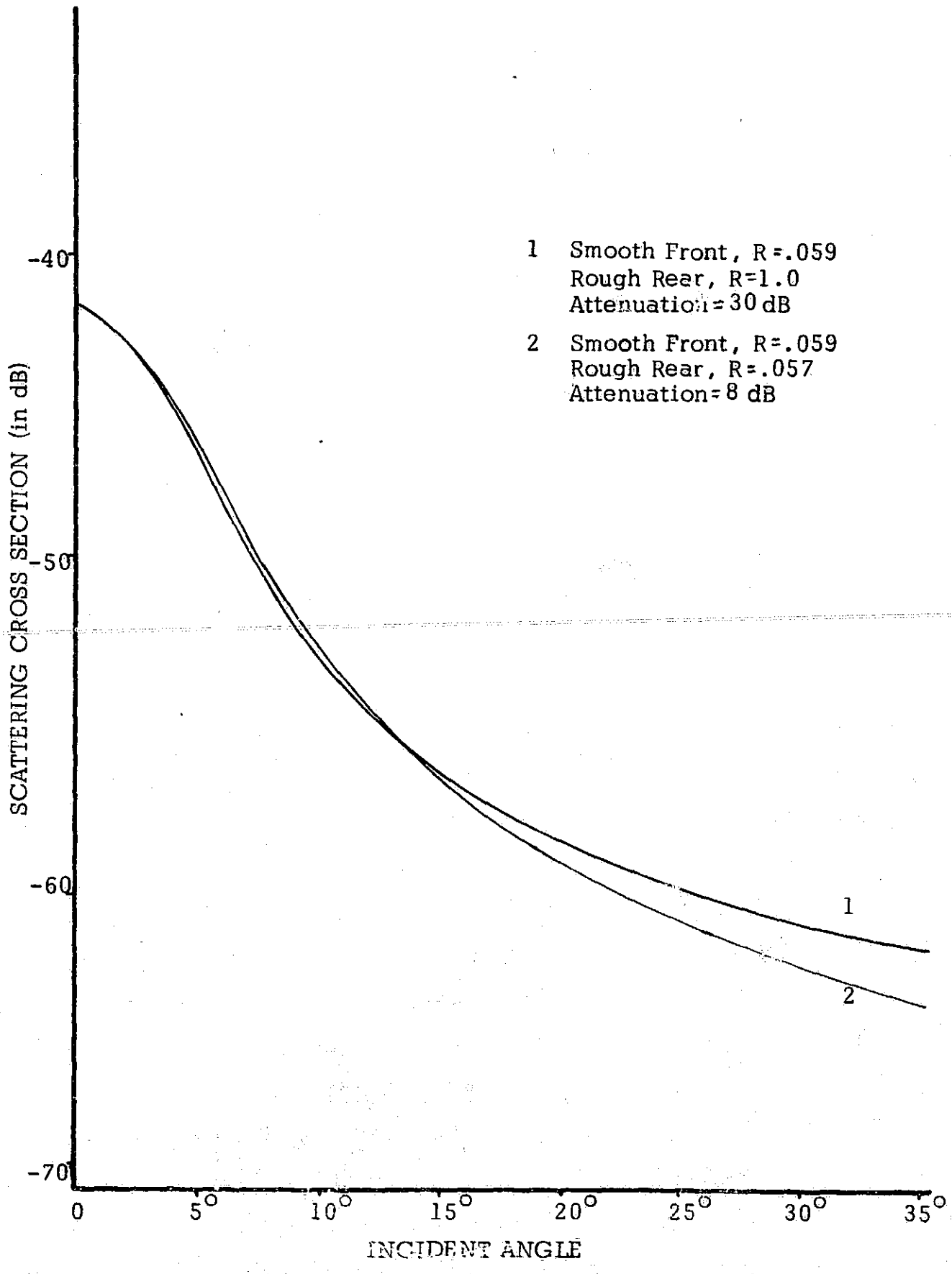

Figure 4-48. Comparison of Two Layers with Smooth Front Face and the Same Expected Effect of the Rough Rear Face.

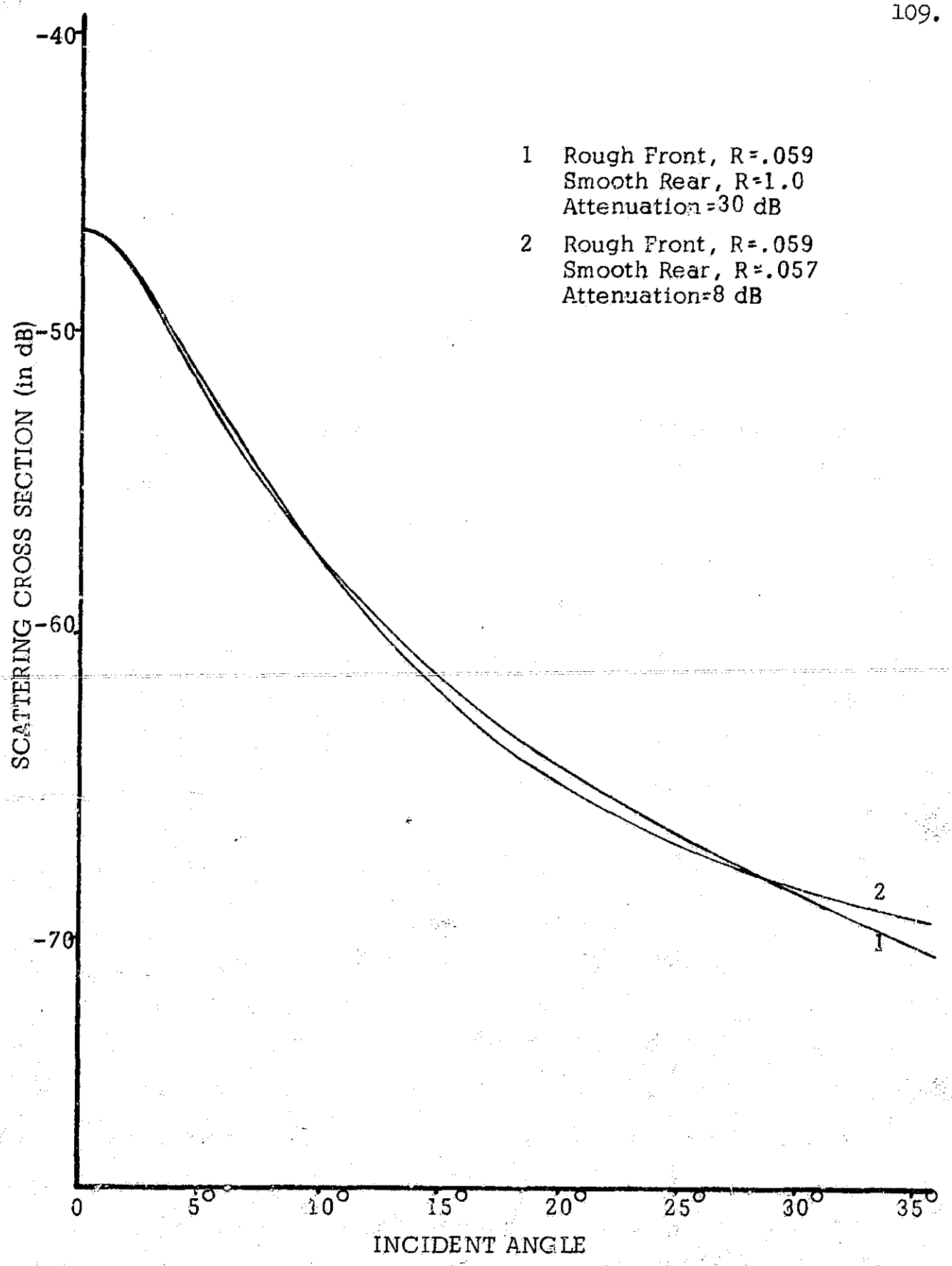

Figure 4-49. Comparison of Two Layers with Rough Front Face and the Same Expected Effect of the Smooth Rear Face.

comparison. When these two thicknesses are compared for the layer with the smooth side first, Figure 4.48, it is seen that there is very little difference in the curves except for incident angles beyond 15^{o} where they start to separate. Even for the extreme of 35^{o} incident angle the difference is only 2.5 dB which is within the total error possible in the measurements.

The effects, if any, of the violation of the assumption that the smooth face is in the far field region of the rough face should be more noticeable when the rough face is illuminated first. Making the same comparison as above except illuminating the rough face first, Figure 4.49, fails to show any change in the shape of the curves. Thus, for the roughness and materials used in this experiment, there appears to be no effect due changing the layer thickness except that due to the attenuation within the layer.

The most important goal of this investigation was to determine if the presence of a layer could be detected by backscatter investigation of an unknown surface. The conclusion is that it cannot be done with a single frequency system unless the range resolution is fine enough to allow the separation of the return from the two faces. This can be done using a system with a very narrow antenna pattern at vertical incidence and a range resolution smaller than the layer thickness.

The implications of this conclusion are quite important. It casts doubt on the validity of the curve fitting procedures used to predict the roughness of terrain, both terrestrial and celestial, from radar backscatter measurements. The majority of these measurements are made with no knowledge of the presence or absence of a layer. Referring to Figures 4.46 and 4.47 one can see that even for the same surface conditions the return can be greatly affected by a layer. However, if addional information is available, the presence and nature of a layer may be remotely sensed. For example, comparing returns from the same terrain in winter and summer could yield the depth and moisture content of a snow blanket.

CHAPTER V

RECOMMENDATIONS FOR FUTURE INVESTIGATIONS

This work was undertaken to provide a starting point for the study of a general rough layer. As such it was restricted to a single frequency investigation of a particular layer situation. A logical extension would be to repeat the same experiment for different frequencies to see if the presence of a layer can be detected in this manner. After this the layer material and roughness parameters should be varied systematically to determine their effect.

Extending the theory to include a layer with both surfaces rough is feasible even though it will generate complicated multiple integrals which may not be possible to evaluate analytically. The experimental investigation of a layer with two rough surfaces should be conducted also.

The effect of inhomogeneities within the layer may be of equal, or even greater, importance for practical cases; hence, it should be investigated thoroughly.

Polarization effects may be quite important. For example, the Brewster angle for front and back faces (present only for "vertical" polarization) may be different and cause serious changes in the shape of the curves. Ultrasonic simulation, of course, cannot show these phenomena, so electromagnetic experiments are called for.

BIBLIOGRAPHY

PRECEDING PAGE BLANK NOT FILMED.

BIBLIOGRAPHY

Aksenov, V. I., "On the Scattering of Electromagnetic Waves from Sinusoidal and Trochoidal Surfaces of Finite Conductivity," Radio Engineering and Electronic Physics, vol. 3, 1958, p. 459.

Aksenov, V. I., "Experimental Investigation of the Scattering of Electromagnetic Waves by Periodically Rough Surfaces," Radio Engineering and Electronic Physics, vol. 5, 1960, pp. 782-795.

Aksenov, V. I., "Application of the Kirchhoff Approximation to the Problem of the Scattering from Periodically Rough Surfaces of Finite Conductivity," Radio Engineering and Electronic Physics, vol. 6, 1961, pp. 307-314.

Ament, W. S., "Toward a Theory of Reflection by a Rough Surface," Proc. IRE, vol. 41, 1953, pp. 142-146.

Ament, W. S., "Forward and Backscattering by Certain Rough Surfaces," Trans. IRE AP-4, 1956, pp. 369-373.

Ament, W. S., "Reciprocity and Scattering by Certain Rough Surfaces," Trans. IRE AP-8, 1960, pp. 167-174.

Ayiku, M.N.B. and R. K. Moore, "Acoustic Simulation of Knife Edge Diffraction," Spring Meeting International Scientific Radio Union, 1965.

Barrick, D. E., "Normalization of Bistatic Radar Return," The Ohio State University Antenna Laboratory Report No. 1388-13, 1964.

Barrick, D. E., "A More Exact Theory of Backscattering from Statistically Rough Surfaces," Report 1388-18. Antenna Laboratory, The Ohio State University Research Foundation, 1965.

Barrick, D. E. and W. H. Peake, "Scattering from Surfaces with Different Roughness Scales: Analysis and Interpretation," Report No. BAT-197A-10-3, Battle Memorial Institute, 1967.

Bass, F. G., "Boundary Conditions for the Mean Electromagnetic Field on a Surface with Random Irregularities and Fluctuations of Impedance," Izv. Vyssh. Zav. Radiofiz., vol. 3, 1960, pp. 72-78.

Bass, F. G., "On the Theory of Combinational Scattering of Waves by a Rough Surface," Izv. Vyssh. Zav. Radiofiz., vol. 4, 1961, pp. 58-66.

Bass, F. G. and V. G. Bocharov, "On the Theory of Electromagnetic Waves from a Statistically Uneven Surface," Radio Engineering and Electronics (Translation of Radioteckhnika i electronika), vol. 3, 1958, pp. 251-258.

Beckmann, P. and A. Spizzichino, The Scattering of Electromagnetic Waves from Rough Surfaces, The MacMillan Co., New York, 1963.

Bendat, J. S., Principles and Applications of Random Noise Theory, John Wiley and Sons, Inc., New York 1958.

Bennet, H.E., "Specular Reflectance of Aluminized Ground Glass and the Height Distribution of Surface Irregularities," J. Opt. Soc. Am., vol. 53, no. 12, Dec. 1963.

Bhattacharyya, B.K., "Electromagnetic Induction in a Two-Layer Earth," J. Geophys. Res., vol. 60, no. 3, 1955, pp. 279-288.

Biot, M. A., "Reflection on a Rough Surface from an Acoustic Point Source," J. Acoust. Soc. Am., vol. 29, 1957, pp. 1193-1200.

Biot, M.A., "Some New Aspects of the Reflection of Electromagnetic Waves on a Rough Surface," J. Appl. Phys., vol. 28. 1957, pp. 1455-1483.

Biot, M.A., "On the Reflection of Electromagnetic Waves on a Rough Surface," J. Appl. Phys., vol. 29, 1958, p. 998.

Blackman, R. B. and J. W. Tukey, The Measurement of Power Spectra, Dover Publications, Inc., New York 1958.

Blacksmith, P., R. E. Hiatt and R. B. Mack, "Introduction to Radar Cross-Section Measurements," Proc. IEEE, Aug. 1965.

Blevis, B. C. and J. H. Chapman, "Characteristics of 488 Mc/s Radio Signal Reflected from the Moon," J. Res. NBS, vol. 64, 1960, pp. 331-334.

Branely, E. N., "The Diffraction of Waves by an Irregular Refracting Medium," Proc. Roy. Soc., vol. A225, 1954, p. 515.

Braude, S. Ya., "The Fresnel Coefficients for a Rough Surface," Izv. Vyssh. Zav. Radiofiz., vol. 2, 1959, pp. 691-696.

Brekhovskikh, L. M. "Diffraction of Waves on a Rough Surface," Zh. Eksper. Theor. Fiz., vol. 23, 1952, pp. 275-288. (Translation by R.N. Goss, Naval Electronics Laboratory, San Diego, Calif.)

Brekhovskikh, L. M., Waves in Layered Media, Academic Press, 1960.

Brown, W. E., "A Lunar and Planetary Echo Theory," J. Geophys. Res., vol. 65, 1960, p. 3087.

Browne, I.C., J. V. Evans, J. K. Hargreaves, and W.A.S. Murray, "Radio Echoes from the Moon," Proc. Phys. Soc. London, vol. 69, 1956, pp. 901-920.

Bullington, K., "Reflection Coefficients of Irregular Terrain," Proc. IRE, vol. 42, 1954, pp. 1258-1262.

Bullington, K., "Radio Propagation at Frequencies above 30 Mc/s," Proc. IRE, vol. 35, 1947, p. 1122.

Burman, R., "Some Approximate Formulas Concerning the Reflection of Electromagnetic Waves from a Stratified Semi-Infinite Medium," Radio Science, vol. 68D, no. 11, 1964, pp. 1215-1218.

Burrows, C. R. and S. S. Atwood, Radio Wave Propagation, Academic Press, 1949, New York.

Campbell, J.P., "Backscattering Characteristics of Land and Sea at X-Band," Proc. of National Conf. on Aero Elect., May 1958.

Campbell, J.P., "Backscattering Characteristics of Land and Sea at X-Band," Trans. of the 1959 Symposium on Radar Return, Univ. of New Mexico, NOTS TP 23338, May 1959.

Carlson, J.F. and A.E. Heins, "The Reflection of an Electromagnetic Plane Wave by an Infinite Set of Plates," Quart. Appl. Math., vol. 4, 1946, pp. 313-329.

Carlson, J.F. and A. E. Heins, "The Reflection of an Electromagnetic Plane Wave by an Infinite Set of Plates," Quart. Appl. Math., vol. 5, 1947, pp. 82-88.

Chu, C. M. and S. W. Churchill, "Multiple Scattering by Randomly Distributed Obstacles -- Method of Solution," Trans. IRE, vol. AP-4, 1956, p. 142.

Clarke, R. H., "Theoretical Characteristics of Radiation Reflected Obliquely from a Rough Conducting Surface," Proc. IEE, vol. 110, 1963, p. 91.

Clarke, R. H., "Measurements on Radiation Reflected Obliquely from a Rough Surface," Proc. IEE, vol. 110, 1963, p. 1921.

Clapp, R. E., "A Theoretical and Experimental Study of Ground Return," MIT Rad. Lab. Report No. 1024, April, 1946.

Constant, F. W., Theoretical Physics, Addison-Wesley Publishing Co., Cambridge, Mass., 1954.

Cosgriff, R. L., W. H. Peake and R. C. Taylor, "Electromagnetic Reflectesa Properties of Natural Surfaces with Application to Design and Other Scenes," Ohio State University Antenna Lab, Feb. 1, 1959.

Cosgriff, R. F., W. H. Peake and R. C. Taylor, "Terrain Scattering Properties for Sensor System Design, Terrain Handbook II," Engr. Exp. Sta., Ohio State Univ., May 1960.

Cowan, E. W., "X-Band Sea Return Measurements," MIT Research Laboratory Report No. 870, 1946.

Crawford, A. B. and W. C. Jakes, "Selective Fadings of Microwaves," Bell Syst. Tech. Jour., vol. 31, 1952, p. 68.

Daniels, F. B., "Radar Determination of the Scattering Properties of the Moon," Nature (6B), vol. 187, no. 4735, July 1960, p. 399.

Daniels, F. B., "A Theory of Radar Reflection from the Moon and Planets," J. Geophys. Res., vol. 66, 1961, p. 1787.

Daniels, F. B., "Radar Reflections from a Rough Moon Described by a Composite Correlation Function," J. Geophys. Res., vol. 68, 1963, p. 6251.

Davenport, W. B. and W. L. Root, An Introduction to the Theory of Random Signals and Noise, McGraw-Hill Book Co., Inc., 1958.

Davies, H., "The Reflection of Electromagnetic Waves from a Rough Surface," Proc. IEEE, Part IV, vol. 101, 1954, pp. 209-214.

Davies, H., "The Reflection of Electromagnetic Waves from a Rough Surface," J. Elec. Eng. London, Part 4, vol. 101, 1954, pp. 209-215.

Davies, H., "The Reflection of Electromagnetic Waves from a Rough Surface," Proc. IEEE, Part III, vol. 102, 1955, p. 148.

De, A. C. "Reflection of Microwaves from Earth's Surface," Indian J. of Meteorol. Geophys., vol. II, 1960, pp. 45-49.

Dye, J.E., "Ground and Sea Return Signal Characteristics of Microwave Pulse Altimeters," Trans. of Symp. on Radar Return, Univ. of New Mexico, NOTS TP 2333B, 1959.

Eckart, C., "The Scattering of Sound from the Sea Surface," J. Acoust. Soc. Am., vol. 25, 1953, pp. 566-570.

Edison, A. R., "An Acoustic Simulator for Modeling Backscatter of Electromagnetic Waves," Univ. of New Mexico Engr. Exp. Sta. Tech. Report No. EE-62, 1961.

Edison, A. R., D. Bliss, and G. Policky, "Acoustic Wave Propagation in a Random Medium," Fall Meeting International Scientific Radio Union, 1963.

Edison, A. R., R. K. Moore and B.D. Warner, "Radar Terrain Return Measured at Near-Vertical Incidence," Trans. IRE, vol. AP-8, 1960, pp. 246-254.

Ergin, K., "Energy Ratio of the Seismic Waves Reflected and Refracted at a Rock-Water Boundary," Bull. Seism. Soc. Amer., vol. 42, 1952, pp. 349-372.

Evans, J. V., "The Scattering of Radio Waves by the Moon," Proc. Phys. Soc. London, vol. 70, 1957, pp. 1105-1112.

Evans, J. V., "Radio-Echo Observations of the Moon at 3.6 cm Wavelength," Lincoln Lab., MIT, TR-256, 1962.

Evans, J. V., "Radio Echo Observations of the Moon at 68 cm Wavelength," Lincoln Lab., MIT, TR-272, 1962.

Evans, J. V., "Radar Methods of Studying Distant Planetary Surfaces," Proc. of the Conf. on Physics of the Solar System and Re-Entry Dynamics, Va. Poly. Inst., Blacksbury, pp. 237-259.

Evans, J. V., S. Evans, and J. H. Thompson, "The Rapid Fading of the Moon Echoes at 100 Mc/s," Paris Symp. on Radio Astronomy, Stanford Univ. Press, 1959.

Evans, J. V. and G. H. Pettengill, "The Scattering Behavior of the Moon at Wavelengths of 3.6, 68, and 784 Centimeters," J. Geophys. Res., vol. 68, 1963, p. 423.

Evans, J. V. and G. H. Pettengill, "The Radar Cross-Section of the Moon," J. Geophys. Res., vol. 68, no. 17, Sept. 1963, pp. 5098-5099.

Evans, J. V. and G. H. Pettengill, "The Scattering Properties of the Lunar Surface at Radio Wave Lengths," Chapter 5 of The Moon, Meteorites and Comets, edited by Middlehurst and Kuiper, University of Chicago Press, 1963, pp. 129-164.

Evans, J. V. and G. H. Pettengill, "The Scattering Behavior of the Moon at Wavelengths of 3.6, 68 and 784 centimeters," J. Geophys. Res., vol. 68, no. 2, 1963, pp. 423-447.

Ewing, W. M., W. S. Jardetsky and F. Press, Elastic Waves in Layered Media, McGraw-Hill Book Company, Inc., New York, 19[illegible]

Feinberg, Ye. L., "The Propagation of Radio Waves Along the Surface of the Earth," Izd. Akad. Nauk SSSR, Moscow, 1961.

Franceschetto, G., "Scattering from Plane Layered Media," IEEE Trans. on A & P, vol. AP-12, 1964, pp. 754-763.

Frederick, J. R., Ultrasonic Engineering, John Wiley and Sons, Inc., New York, 1965.

Fricker, F. J., R. P. Ingalls, W. C. Mason, and M. L. Stone, "UHF Moon Reflections," Spring Meeting International Scientific Radio Union, 1958.

Friedlander, F. G., Sound Pulses, Cambridge University Press, Cambridge, 1958.

Fung, A. K., "Theory of Radar Scatter from Rough Surfaces, Bistatic and Monostatic, with Application to Lunar Radar Return," J. Geophys. Res., vol. 69, no. 6, March 1964, pp. 1063-1073.

Fung, A. K. and R. K. Moore, "Effects of Structure Size on Moon and Earth Radar Returns at Various Angles," J. Geophys. Res., vol. 69, no. 6, 1964, pp. 1075-1081.

Fung, A. K., R. K. Moore, and B. E. Parkins, "Notes on Backscattering and Depolarization by Gently Undulating Surfaces," J. Geophys. Res., March 1965, pp. 1559-1562.

Fung, A. K., "Scattering and Depolarization of Electromagnetic Waves from a Rough Surface," Proc. IEEE (Communications), vol. 54, March 1966, pp. 395-396.

Fung, A. K., "Character of Wave Depolarization by a Perfectly Conducting Rough Surface and its Application to Earth and Moon Experiments," Planet, Space Sci., vol. 15, 1967, pp. 1337-1347.

Goldman, R., Ultrasonic Technology, Reinhold Publ. Corp., New York, 1962.

Gourt, C. W., "Determination of Reflection Coefficient of the Sea," Proc. IEE, Part B, vol. 102, 1955, pp. 827-830.

Grant, C. R. and B. S. Yapplee, "Backscattering from Water and Land at Centimeter and Millimeter Wavelengths," Proc. IRE, vol. 45, 1957, pp. 976-982.

Grasyuk, D. S., "Scattering of Sound Waves by the Uneven Surface of an Elastic Body," Soviet Physics-Acoustics, vol. 6, 1960, pp. 26-29.

Gulin, E. P., "Amplitude and Phase Fluctuations of a Sound Wave Reflected from a Statistically Uneven Surface," Soviet Physics-Acoustics, vol. 8, 1963, pp. 335-339.

Gulin, E. P., "Amplitude and Phase Fluctuations of a Sound Wave Reflected from a Sinusoidal Surface," Soviet Physics-Acoustics, vol. 8, 1963, pp. 223-227.

Gulin, E. P., "The Correlation of Amplitude and Phase Fluctuations in Sound Waves Reflected from a Statistically Rough Surface," Soviet Physics-Acoustics, vol. 8, 1963, pp. 335-339.

Gulin, E. P. and K. I. Malyshev, "Statistical Characteristics of Sound Signals Reflected from the Undulating Sea Surface," Soviet Physics-Acoustics, vol. 8, 1963, pp. 226-234.

Gupta, R. N., "Reflection of Sound Waves from Transition Layers," J. Acoust. Soc. Am., vol. 39, no. 3, 1966, pp. 255-260.

Hagfors, T., "Some Properties of Radio Waves Reflected from the Moon and Their Relation to the Lunar Surface," J. Geophys. Res., vol. 66, no. 3, March 1961, p. 777.

Hagfors, T., "Backscatter from an Undulating Surface with Applications to Radar Returns from the Moon," J. Geophys. Res., vol. 69, 1964, pp. 3779-3784.

Hargreaves, J. K., "Radio Observations of the Lunar Surface," Proc. Phys. Soc., vol. 73, 1959, pp. 536-537.

Hayre, H. S. "Radar Scattering Cross-Section Applied to Moon Return," Proc. IRE, vol. 49, 1961, p. 1433.

Hayre, H. S., "Lunar Backscatter Theories," Ph.D. Thesis, University of New Mexico, 1962.

Hayre, H. S. and R. K. Moore, "Theoretical Scattering Coefficient for Near Vertical Incidence from Contour Maps," J. Res. NBS D. Radio Propagation, vol. 65-D, 1961, pp. 427-432.

Hoffman, W. C., "Scattering of Electromagnetic Waves from a Random Surface," Quar. Appl. Math, vol. 13, no. 3, 1955, pp. 291-304.

Hueter, T. F. and R. H. Bolt, Sonics, John Wiley and Sons, Inc., New York, 1955.

Hughes, D. S., W. L. Pondrom, and R. L. Mims, "Transmission of Elastic Pulses in Metal Rods," Physical Rev., vol. 75, no. 10, 1949, pp. 1552-1556.

Hughes, V. A., "Roughness of the Moon as a Radar Reflector," Nature, vol. 186, no. 4728, 1960, pp. 873-874.

Hughes, V. A., "Radio Wave Scattering from the Lunar Surface," Proc. Phys. Soc., vol. 78, 1961, pp. 988-997.

Isakovich, M. A., "The Scattering of Waves from a Statistically Rough Surface," Zhurn. Eksp. Teor. Fix., vol. 23, 1952, pp. 305-314.

Jones, J. L., C. B. Leslie, and L. E. Barton, "Acoustic Characteristics of Underwater Bottoms," J. Acoust. Soc. Am., vol. 36, 1964, pp. 154-163.

Jordan, E. C., "Acoustic Models of Radio Antennas," Ohio State Univ. Engr. Exp. Station Bull. #108, 1941.

Karhunen, K., "Über Lineare Methoden in der Wahrscheinlichkeitsrechnung," Ann. Acad. Scient. Fenincae (A), vol. 37, 1947, pp. 1-79.

Katsenelenbaum, B. A., "On the Problem of Normal Incidence of a Plane Electromagnetic Wave Onto a Periodic Boundary Between Two Dielectrics," Radiotekhn. i. Elektr., vol. 5, 1960, pp. 1929-1932.

Katz, I. and L. M. Spetner, "Polarization and Depression Angle Dependence of Radar Terrain Return," J. Res. NBS, vol. 64-D, 1960, pp. 483-486.

Kaufman, D. E. and D. H. Lenhert, "The Scattering of Electromagnetic Waves from a Rough Surface of Arbitrary Dielectric Constant," Kansas State University Tech. Report EE-TR-6, 1967.

Kay, I. and R. A. Silverman, "Multiple Scattering by a Random Stack of Dielectric Slabs," Nuovo Cimento, vol. 9, 1958, pp. 626-645.

Kelvin, Baltimore Lectures, London, 1904.

Kerr, D. E., Propagation of Short Radio Waves, McGraw-Hill Book Co., Inc., New York, 1951.

Kerr, F. J., "Radio Echoes from Sun, Moon and Planets," Encycl. of Phys., vol. 52, 1959, pp. 449-464.

Koepsel, W. W. and N. Ahmed, "Radar Cross Section of a Geometric Shape Using Acoustic Simulation," University of New Mexico Engr. Exp. Sta. Tech. Report EE-80, 1962.

Kolsky, H., Stress Waves in Solids, Clarendon Press, London, 1953.

Kovalev, A. A., and S. I. Posdnyak, "The Scattering of Electromagnetic Waves by Statistically Rough Surfaces with Finite Conductivity," Radiotekhn., vol. 16, 1961, pp. 31-36.

Kraus, J. D., Antennas, McGraw-Hill, New York, 1950.

Krishen, K., W. W. Koepsel, and S. H. Durrani, "Cross-Polarization Measurements and Their Relation to Target Surface Properties," IEEE Trans. A & P, vol. AP-14, September 1966.

Krishen, K. and W. W. Koepsel, "Reflection from Rough Layers," Kansas State Univ. Dept. of Electr. Engr. Tech. Report EE-TR-11, 1968.

Kumar, V. R., S. H. Durrani, and W. W. Koepsel, "Backscatter of Electromagnetic Waves from a Rough Layer," Tech. Report EE-TR-3, Kansas State Univ. Dept. of Electr. Engr., also Proc. IEEE, vol. 54, no. 9, 1966, pp. 1191-1192.

Lapin, A. D., "Sound Scattering at a Rough Solid Surface," Soviet Physics-Acoustics, vol. 10, no. 1, July 1964, p. 58.

Leadabrand, R. L. et al. "Radio Scattering from the Surface of the Moon," Proc. IRE, vol. 48, 1960, pp. 932-933.

Lundien, J. R., "Terrain Analysis by Electromagnetic Means," U.S. Army Engineer Waterways Experiment Station Technical Report No. 3-693, September 1966.

Lynch, P. J., "Backscatter from Inhomogeneous Media," Physical Review, vol. 130, no. 3, 1963, pp. 1235-1243.

Lynn, V. L., M. D. Sohigian and E. A. Crocker, "Radar Observations of the Moon at a Wavelength of 8.6 Millimeters," J. Geophys. Res., 1964.

MacDonald, H. C., P. A. Brennan and L. F. Dellwig, "Geologic Evaluation by Radar of NASA Sedimentary Test Site," IEEE Trans. Geosci. Electr., vol. GE-5, no. 3, December 1967, pp. 72-78.

Mackenzie, K. V., "Bottom Reverberation for 530 and 1030 cps Sound in Deep Water," J. Acoust. Soc. Am., vol. 33, 1961, pp. 1498-1504.

Maestri, A., "Hydroacoustic Simulation of Antenna Radiation Characteristics," Melpar, Inc., Falls Church, Va., Tech. Report No. TP-1-26, 1961.

Magnus, W., "On the Scattering Effect of a Rough Plane Surface," Research Report EM-40, Inst. Math. Sc., New York University, 1952.

Marsh, H. W., "Nonspecular Scattering of Underwater Sound by the Sea Surface," Underwater Acoustics, 1962, pp. 193-197.

Marsh, H. W., M. Schulkin and S. G. Kneale, "Scattering or Underwater Sound by the Sea Surface," J. Acoust. Soc. Am., vol. 33, no. 3, March 1961, pp. 334-340.

McGavin, R. E. and L. J. Maloney, "Study at 1.046 Mc/s of the Reflection Coefficient of Irregular Terrain at Grazing Angles," J. Res. NBS, vol. 63D, 1959, pp. 235-248.

McKinney, C. M. and C. D. Anderson, "Measurements of Backscattering of Sound from the Ocean Bottom," J. Acoust. Soc. Am., vol. 36, 1964, pp. 158-163.

McPetre, J. S., "The Reflection Coefficient of the Earth's Surface for Radio Waves," J. IEEE, vol. 82, 1938, p. 214.

Mellen, R. H., "Doppler Shift of Sonar Backscatter from the Sea Surface," J. Acoust. Soc. Am., vol. 36, 1964, pp. 1395-1396.

Meyer, E., "Experiments on CM Waves with Acoustic Techniques Made in Gottingen," J. Acoust. Soc. Am., vol. 30, 1958, pp. 624-632.

Middleton, D., An Introduction to Statistical Communication Theory, McGraw-Hill Book Company, Inc., New York, 1960.

Miles, J. W., "On Nonspecular Reflection at a Rough Surface," J. Acoust. Soc. Am., vol. 26, 1954, pp. 191-199.

Millman, G. H. and F. L. Rose, "Radar Reflections from the Moon at 425 Mc/s," J. Res. NBS, vol. 67D, 1963, p. 107.

Millington, G., "The Reflection Coefficient of a Linearly Graded Layer," Marconi Rev., vol. 12, 1949, p. 140.

Mitzner, K. M., "Theory of the Scattering of Electromagnetic Waves by Irregular Interfaces," Antenna Laboratory, Calif. Inst. Tech., Tech. Report No. 30, Jan. 1964.

Mofensen, J., "Radar Echoes from the Moon," Electronics, vol. 19, 1946, pp. 92-98.

Moore, R. K., "Acoustic Simulation of Radar Return," Microwaves, vol. 1, 1962, pp. 20-25.

Moore, R. K., "Resolution of Vertical Incidence Radar Return into Random and Specular Components," Univ. of New Mexico, Engr. Exp. Sta. Tech. Report EE-6, July 1957.

Moore, R. K. and C. S. Williams, "Radar Terrain Return at Near Vertical Incidence," Proc. IRE, vol. 45, 1957, pp. 228-238.

Moore, R. K., "Radar as a Remote Sensor," CRES Tech. Report 61-7, University of Kansas, January 1966.

Moore, R. K., "Radar Scatterometry -- An Active Remote Sensing Tool," Proc. of the Fourth Symp. on Remote Sensing of the Environment, Univ. of Mich., April 11-14, 1966, Ann Arbor, Mich.

Moore, R. K. and B. E. Parkins, "Omnidirectional Scattering of Acoustic Waves from Rough Surfaces of Known Statistics," J. Acoust. Soc. Am., no. 1, July 1966, pp. 170-175.

Moore, R. K., "Radar Return from the Ground," Engr. Bull. No. 59, Univ. of Kansas, 1969.

Morse, P. M., Vibration and Sound, McGraw-Hill Book Company, Inc. New York 1948.

Morse, P. M. and H. Feshbach, Methods of Theoretical Physics, McGraw-Hill Book Company, Inc. 1953.

Muhleman, D. O., "Radar Scattering from Venus and the Moon," Astro. J., Feb. 1964.

Navier, C.L.M.H., Mem. Acad. Sci. Paris, t.7, 1827.

Nolle, A. W., W. A. Hoyer, J. F. Mifsud, W. R. Runyan, and M. B. Ward, "Acoustical Properties of Water-Filled Sands," J. Acoust. Soc. Am., vol. 35, 1963, pp. 1394-1408.

Ohio State University, "Theoretical and Experimental Analysis of the Electromagnetic Scattering and Radiative Properties of Terrain, with Emphasis on Lunar-Like Surfaces," Antenna Laboratory Report No. 1388-12, 1963.

Oxehufwud, A., "Tests Conducted over Highly Reflective Terrain at 4,000, 6,000, and 11,000 Mc.," Trans. Amer. IEE, vol. I, no. 78, 1959, pp. 265-270.

Parker, J. G., "Reflection of Plane Sound Waves from an Irregular Surface," J. Acoust. Soc. Am., vol. 28, 1956, pp. 672-680.

Parkins, B. E., "The Omnidirectional Scattering of Acoustic Waves from Rough Surfaces with Application to Electromagnetic Scattering," (Ph.D. Thesis), CRES Report 48-4, University of Kansas, July 1960.

Patterson, R. B., "Backscatter of Sound from a Rough Boundary, J. Acoust. Soc. Am., vol. 35, no. 12, Dec. 1963, p. 2010.

Peake, W. H., "Interaction of Electromagnetic Radiation with Some Natural Surfaces," Ohio State Univ. Report No. 898-2, May 30, 1958.

Peake, W. H., "Theory of Radar Return from Terrain," IRE National Convention Record, Pt. 1, on Antennas and Propagation, 1959.

Pettengill, G. H., "Measurement of Lunar Reflectivity Using the Millstone Radar," Proc. IRE, vol. 48, 1960, pp. 933-934.

Poisson, S. D., Men Acad. Sci. Paris, t.8, 1829.

Price, R., P. E. Green, J. J. Goblick, R. H. Kingston, L. T. Kraft, G. H. Pettengill, R. Silver, and W. B. Smith, "Radar Echoes from Venus," Science, vol. 129, March 1959, pp. 751-753.

Proud, J. M., R. T. Beyer, and P. Tamarkin, "Reflection of Sound from Randomly Rough Surfaces," J. Appl. Phys., vol. 31, 1960, pp. 543-553.

Rayleigh, Lord, The Theory of Sound, 3rd ed. MacMillan, London, 1896.

Rea, D. G., N. Hetherington, and R. Mifflin, "The Analysis of Radar Echoes from the Moon," J. Geophys. Res., vol. 69, no. 24, Dec. 1964, pp. 5217-5223.

Redheffer, R., "The Dependence of Reflection on the Incidence Angle," Trans. IRE, vol. MIT-7, 1959, pp. 423-429.

Rice, S. O., "Reflection of Electromagnetic Wave from Slightly Rough Surfaces," Comm. Pure Appl. Math, vol. 4, 1951, pp. 351-378.

Rice, S. O., "Reflection of Electromagnetic Waves by Slightly Rough Surfaces," The Theory of Electromagnetic Waves (A Symposium), Interscience Publ. Co., 1951.

Rouse, J. W., Jr., W. P. Waite, and R. L. Walters, "Use of Orbital Radars for Geoscience Investigations," Proc. of the Third Space Congress, March 7-9, 1966, Cocoa Beach, Fla.

Senior, T.B.A., "Radar Reflection Characteristics of the Moon," Paris Symposium on Radioastronomy, Stanford Univ. Press, 1959.

Senior, T.B.A. and K. M. Siegel, "A Theory of Radar Scattering by the Moon," J. Res. NBS, vol. 64D, 1960, pp. 217-229.

Sherwood, E. M., "S-Band Measurements of Reflection Coefficients for Various Types of Earth," Sperry Gyroscope Co., Report No. 5220-129, Oct. 1943.

Sherwood, E. M., "Reflection Coefficients of Irregular Terrain at 10 cm," Proc. IRE, vol. 43, 1955, pp. 877-878.

Shulman, L. A., "The Reflection of Electromagnetic Waves from a Semi-Infinite Periodic Layer Structure," Uch. Zap. Tadzh. Univ., vol. 10, 1957, pp. 103-109.

Shung, W. S., W. W. Koepsel and S. H. Durrani, "Backscatter of Ultrasonic Waves from a Rough Layer," Tech. Report EE-TR-4, Dept. of EE, Kansas State University, May 1966.

Silver, S., Microwave Antenna Theory and Design, McGraw-Hill, New York, 1941

Simonett, D. S., "Future and Present Needs of Remote Sensing in Geography," Proc. Fourth Symp. on Remote Sensing of the Environment, Univ. of Mich., April 1966, Ann Arbor, Mich.

Skolnik, M. I. Introduction to Radar Systems, McGraw-Hill, New York, 1962.

Spetner, L. M., "Further Analysis of Radar Terrain Return," Johns Hopkins University AD-654 355, Nov. 10, 1959, Processed for Defense Documentation Center, Defense Supply Agency.

Spetner, L. M., "A Statistical Model for Forward Scattering of Waves of a Rough Surface," Trans. IRE AP-6, 1958, pp. 88-94.

Spetner, L. M., "Radar Terrain Return: A Theoretical Approach," Johns Hopkins University Report No. AD 654 408, May 20, 1959, Processed for Defense Documentation Center, Defense Supply Agency.

Spetner, L. M., "A Statistical Model for Radar Terrain Return," Trans. IRE, vol. AP-8, 1960, pp. 242-246.

Stokes, G. G., Phil. Mag, vol. 32, 1848, p. 343.

Straiton, A., "Reflection of Centimeter Water Waves from Ground and Water," Trans. IRE, vol. AP-4, Aug. 1955.

Straiton, A. W., J. P. Gerhardt, A. H. LaGrone, and C. W. Tolbert, "Reflection of Centimeter and Millimeter Radio Waves from the Surface of a Small Lake," Elec. Engr. Res. Lab., Univ. of Texas, Report No. 63, May 1952.

Stratton, J. A., Electromagnetic Theory, McGraw-Hill, New York, 1941.

Taylor, R. C., "Terrain Return Measurements at X, K_u, and K_a Band," IRE Convention Record Part I, vol. 7, 1959.

Taylor, R. C., "The Terrain Scattering Problem," Radar Reflectivity Measurements Symposium, Space Surveillance and Instrumentation Branch, Rome Air Development Center Research and Tech. Division, Air Force Systems Command, Griffiss Air Force Base, New York, Tech. Report RADC-TDR-64-24, April 1964.

Trexler, J. H., "Lunar Radio Echoes," Proc. IRE, vol. 46, 1958, pp. 286-292.

Twersky, V., "On the Non-Specular Reflection of Plane Waves of Sound," J. Acoust. Soc. Am., vol. 22, 1950, pp. 539-546.

Twersky, V., "Reflection Coefficients for Certain Rough Surfaces," J. Appl. Phys., vol. 24, 1953, pp. 569-660.

Twersky, V., "Certain Transmission and Reflection Theorems," J. Appl. Phys., vol. 25, 1954, pp. 859-862.

Twersky, V., "Acoustic Bulk Parameters of Random Volume Distribution of Small Scatters," J. Acoust. Soc. Am., vol. 36, no. 7, 1964, pp. 1314-1329.

Urick, R. J., "The Backscattering of Sound from a Harbor Bottom," J. Acoust. Soc. Am., vol. 26, 1954, pp. 231-235.

Urick, R. J., "The Processes of Sound Scattering at the Ocean Surface and Bottom," J. Marine Research, vol. 15, 1957, pp. 134-148.

Urick, R. J. and R. M. Hoover, "Backscattering of Sound from the Sea Surface: Its Measurement, Causes, and Application to the Prediction of Reverberation Levels," J. Acoust. Soc. Am., vol. 28, 1957, p. 1038.

Urusovskii, I. A., "Sound Scattering by a Sinusoidally Uneven Surface Characterized by Normal Acoustical Conductivity," Soviet Physics-Acoustics, vol. 5, 1960, pp. 362-369.

Urosovskii, I.A., "Diffraction of Sound on a Periodically Uneven and Inhomogeneous Surface," Soviet Physics-Doklady, vol. 5, 1960, pp. 345-348.

Urusovskii, I.A., "Diffraction by a Periodic Surface," Soviet Physics-Acoustics, Jan. 1965, p. 287.

Valenzuela, Gaspar R., "Depolarization of Electromagnetic Waves by Slightly Rough Surfaces," IEEE Trans. on Ant. and Prop., vol. AP-15, no. 4, July 1967.

Van de Pol, B., "Some Observation on Rayleigh Fading," Tijdschr. Ned. Radiogenoot., vol. 19, Sept. 1954, pp. 223-229.

Victor, W. K., R. Stevens and S. W. Golomb, "Radar Exploration of Venus," Goldstone Observatory Report for March-May 1961. Jet Propulsion Laboratory, Calif. Inst. Tech., Pasadena, Calif. Tech. Report No. 32-132, Aug. 1961.

Wait, J. R., Electromagnetic Waves in Stratified Media, Pergamon Press, MacMillan Co., New York, 1962.

Ward, R. B., "Some Considerations in the Design of a Satellite Radar Altimeter/Sea-Surface Sensing Device," Tech. Rept. L-86-67-3, Electronic Science Lab, Lockheed Palo Alto Research Lab., July, 1967.

Warner, B. D., R. K. Moore, and A. R. Edison, "Acoustic Simulation of Radar Altimeter Signals from Cities," University of New Mexico Engr. Exp. Sta. Tech. Report EE-77, 1962.

Wilf, H. S., Mathematics for the Physical Sciences, John Wiley and Sons, New York 1962.

Williams, W. E., "Reflection and Refraction of Electromagnetic Waves at Plane Interfaces," J. Math. & Phys., vol. 36, 1957, pp. 26-35.

Wiltse, I. C., S. P. Schlesinger, and C. M. Johnson, "Backscattering Characteristics of the Sea in the Region from 10 to 50 kMc," Proc. IRE, vol. 45, 1957, pp. 220-228, pp. 244-246.

Winter, D. F., "A Theory of Radar Reflection from a Rough Moon," J. Res. NBS, vol. 66D, 1962, p. 215.

Yapplee, B. S., R. H. Bruton, K. J. Craig, and N. G. Roman, "Radar Echoes from the Moon at the Wavelength of 10 cm," Proc. IRE, vol. 46, 1958, pp. 293-297.

Yapplee, B. S., N. G. Roman, K. J. Craig, and T. F. Scanlan, "A Lunar Radar Study at 10 cm Wavelength," Paris Symposium on Radio Astronomy, Stanford Univ. Press, 1959.

APPENDIX A

SOUND PROPAGATION IN AN EXTENDED ELASTIC MEDIUM

SOUND PROPAGATION IN AN EXTENDED ELASTIC MEDIUM

A-1. Stress and Strain on an Element

The analysis of this appendix follows that of Kolsky (1953) with part of the notations changed to be more consistant with the usage currently being employed in acoustic simulation.

The stress on a surface element in a solid body has components both normal and tangential to the plane. Using three mutually orthogonal axes, O_x, O_y, O_z, nine components of stress act on three planes normal to these axes and passing through a point P. These will be denoted by σ_{xy}, σ_{yy}, σ_{zz}, σ_{xz}, σ_{xy}, σ_{yz}, etc. The first letter in the subscript denotes the direction of the stress and the second letter defines the plane in which it acts. By considering an infinitesimal rectangular parallelopiped around P with its faces normal to the axes, as shown in Figure 1, and taking moments, it is seen that for static equilibrium $\sigma_{xy} = \sigma_{yx}$, $\sigma_{xz} = \sigma_{zx}$, $\sigma_{yz} = \sigma_{zy}$, so that only six independent components of stress remain. The stresses acting on any other plane through P can be resolved into these six stress components.

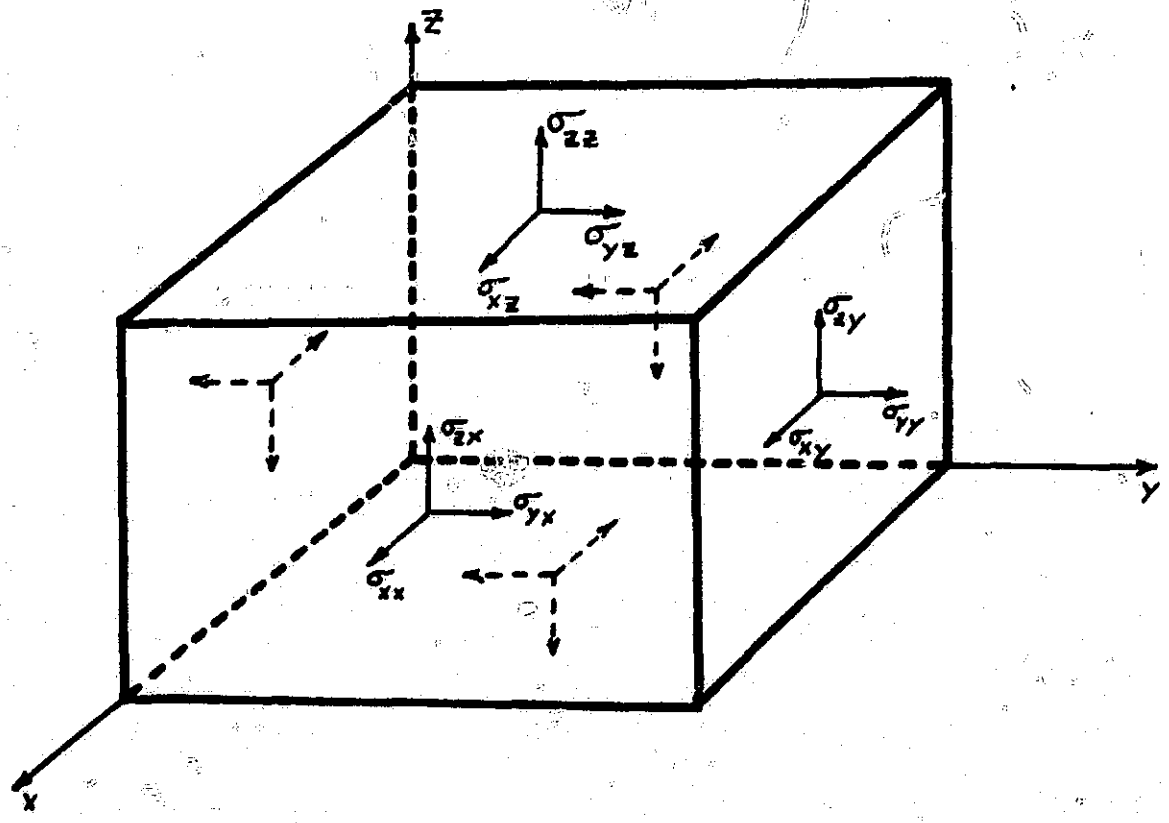

Figure 1. Stress components on parallelopiped

The <u>displacement</u> of any point P in the body may be resolved into components u, v, and w along the x, y, and z axes such that if the original coordinates of P were (x, y, z) they would become (x + u, y + v, z + w). The <u>strain</u> at the point is defined by considering how its position relative to adjacent points has changed. Consider a point very close to P, with undisturbed coordinates ($x + \delta x$, $y + \delta y$, $z + \delta z$) and let the displacement it has undergone by ($u + \delta u$, $v + \delta v$, $w + \delta w$). These can be expanded by a Taylor expansion of the form:

$$\delta u = u + \frac{\partial u}{\partial x}\delta x + \frac{\partial u}{\partial y}\delta y + \frac{\partial u}{\partial z}\delta z + \cdots \qquad \text{(A.1a)}$$

$$v + \delta v = v + \frac{\partial v}{\partial x}\delta x + \frac{\partial v}{\partial y}\delta y + \frac{\partial v}{\partial z}\delta z + \cdots \qquad \text{(A.1b)}$$

$$w + \delta w = w + \frac{\partial w}{\partial x}\delta x + \frac{\partial w}{\partial y}\delta y + \frac{\partial w}{\partial z}\delta z + \cdots \qquad \text{(A.1c)}$$

For sufficiently small δx, δy, and δz only the first order terms are significant and these become:

$$\delta u = \frac{\partial u}{\partial x}\delta x + \frac{\partial u}{\partial y}\delta y + \frac{\partial u}{\partial z}\delta z \qquad \text{(A.2a)}$$

$$\delta v = \frac{\partial v}{\partial x}\delta x + \frac{\partial v}{\partial y}\delta y + \frac{\partial v}{\partial z}\delta z \qquad \text{(A.2b)}$$

$$\delta w = \frac{\partial w}{\partial x}\delta x + \frac{\partial w}{\partial y}\delta y + \frac{\partial w}{\partial z}\delta z \qquad \text{(A.2c)}$$

Thus if the nine partial derivatives in (A.2) are known at the point, the relative displacement of all surrounding points may be found. These nine quantities may be regrouped and defined as:

$$\varepsilon_{xx} = \frac{\partial u}{\partial x} \qquad \varepsilon_{yy} = \frac{\partial v}{\partial y} \qquad \varepsilon_{zz} = \frac{\partial w}{\partial z}$$

$$\varepsilon_{yz} = \frac{\partial w}{\partial y} + \frac{\partial v}{\partial z} \qquad \varepsilon_{zx} = \frac{\partial u}{\partial z} + \frac{\partial w}{\partial x} \qquad \varepsilon_{xy} = \frac{\partial v}{\partial x} + \frac{\partial u}{\partial y}$$

$$2\omega_x = \frac{\partial w}{\partial y} - \frac{\partial v}{\partial z} \qquad 2\omega_y = \frac{\partial u}{\partial z} - \frac{\partial w}{\partial x} \qquad 2\omega_z = \frac{\partial v}{\partial x} - \frac{\partial u}{\partial y}. \qquad \text{(A.3)}$$

The first three quantities ε_{xx}, ε_{yy}, ε_{zz} are seen to correspond to the fractional expansions and contractions of line elements passing through P parallel, respectively, to the x, y, and z axes. The second three ε_{yz}, ε_{zx}, and ε_{xy} correspond to components of sheer strain in the planes denoted by their subscripts. The last three ω_x, ω_y, and ω_z do not correspond to a deformation of the element but are the components of its rotation as a rigid body. Note that if $\hat{x}$, $\hat{y}$, and $\hat{z}$ are unit vectors in the respective directions

$$\text{curl } \vec{s} \equiv \left(\frac{\partial w}{\partial y} - \frac{\partial v}{\partial z}\right)\hat{x} + \left(\frac{\partial u}{\partial z} - \frac{\partial w}{\partial x}\right)\hat{y} + \left(\frac{\partial v}{\partial x} - \frac{\partial u}{\partial y}\right)\hat{z}$$

so that if the displacement of the element is regarded as a vector, $\vec{s}$, the components of $\frac{1}{2}$ curl $\vec{s}$ are ω_x, ω_y, and ω_z.

The first six quantities in (A.3) are called the components of strain. When the last three are zero, curl $\vec{s} = 0$, the deformation is irrotational and described as pure strain.

A-2. Generalized Hooke's Law

Within the elastic range of the material each of the six components of stress at any point is a linear function of the six components of strain. This may be expressed as:

$$\sigma_{xx} = c_{11}\varepsilon_{xx} + c_{12}\varepsilon_{yy} + c_{13}\varepsilon_{zz} + c_{14}\varepsilon_{yz} + c_{15}\varepsilon_{zx} + c_{16}\varepsilon_{xy}$$

$$\sigma_{yy} = c_{21}\varepsilon_{xx}$$

$$\sigma_{zz} = c_{31}\varepsilon_{xx}$$

$$\sigma_{yz} = c_{41}\varepsilon_{xx}$$

$$\sigma_{zx} = c_{51}\varepsilon_{xx}$$

$$\sigma_{xy} = c_{61}\varepsilon_{xx} \quad - - - - - - - - - \quad c_{66}\varepsilon_{xy} \qquad (A.4)$$

where the coefficients are the elastic constants of the material.

In order for the elastic energy to be a univalued function of the strain any coefficient c_{rs} must be equal to c_{sr} (Love, 1927). This reduces the number of independent coefficients from 36 to 21. In an isotropic solid the values of the coefficients must be independent of the choice of axes. This reduces the independent constants to two, namely λ_m and μ_m. Then

$$c_{12} = c_{13} = c_{21} = c_{31} = c_{23} = c_{32} = \lambda_m$$

$$c_{44} = c_{55} = c_{66} = \mu_m$$

$$c_{11} = c_{22} = c_{33} = \lambda_m + 2\mu_m$$

and the other 24 coefficients become zero. Equation (A.4) may thus be written as:

$$\sigma_{xx} = \lambda_m \Delta + 2\mu_m \varepsilon_{xx} \qquad \sigma_{yz} = \mu_m \varepsilon_{yz}$$

$$\sigma_{yy} = \lambda_m \Delta + 2\mu_m \varepsilon_{yy} \qquad \sigma_{zx} = \mu_m \varepsilon_{zx}$$

$$\sigma_{zz} = \lambda_m \Delta + 2\mu_m \varepsilon_{zz} \qquad \sigma_{xy} = \mu_m \varepsilon_{xy} \qquad (A.5)$$

where

$$\Delta = \varepsilon_{xx} + \varepsilon_{yy} + \varepsilon_{zz} = \frac{\partial u}{\partial x} + \frac{\partial v}{\partial y} + \frac{\partial w}{\partial z} = div\ \vec{s}.$$

The change in volume of a unit cube represented by Δ is known as the cubic dilatation.

The two elastic constants, λ_m and μ_m, are known as Lame's constants and completely define the elastic behavior of an isotropic solid. Four other elastic constants are commonly used. These are Young's modulus, E, Poisson's ratio, ν, the bulk modulus, k, and the rigidity modulus which is identical with μ_m. Using (A.5), E, ν, and k may be expressed in terms of λ_m and μ_m. E is defined as the ratio between the uniformly applied plane stress and elongation with the lateral surface free from constraint. Consider the case of σ_{xx} applied and all other stresses being zero. The first three equations then become:

$$\sigma_{xx} = (\lambda_m + 2\mu_m)\varepsilon_{xx} + \lambda_m(\varepsilon_{yy} + \varepsilon_{zz})$$

$$0 = (\lambda_m + 2\mu_m)\varepsilon_{yy} + \lambda_m(\varepsilon_{xx} + \varepsilon_{zz})$$

$$0 = (\lambda_m + 2\mu_m)\varepsilon_{zz} + \lambda_m(\varepsilon_{xx} + \varepsilon_{yy}).$$

Solving for ε_{xx}, ε_{yy}, and ε_{zz} it is seen that

$$\varepsilon_{xx} = \frac{\lambda_m + \mu_m}{\mu_m(3\lambda_m + 2\mu_m)}\sigma_{xx}, \quad \varepsilon_{yy} = \varepsilon_{zz} = \frac{-\lambda_m}{2\mu_m(3\lambda_m + 2\mu_m)}\sigma_{xx}. \qquad (A.6)$$

Young's modulus, E, is given by $\sigma_{xx}/\varepsilon_{xx}$ so:

$$E = \frac{\mu_m(3\lambda_m + 2\mu_m)}{\lambda_m + \mu_m}. \qquad (A.7)$$

Poisson's ratio, ν , is defined as the ratio between the lateral contraction and the longitudinal extension, i.e. $-\varepsilon_{yy}/\varepsilon_{xx}$. Hence

$$\nu = \frac{\lambda_m}{2(\lambda_m+\mu_m)} \quad . \tag{A.8}$$

The bulk modulus, k, is defined as the ratio between applied pressure and the fractional change in volume when the specimen is subjected to hydrostatic pressure. Under these conditions $\sigma_{xx} = \sigma_{yy} = \sigma_{zz} = P$ and $\sigma_{yz} = \sigma_{xz} = \sigma_{xy} = 0$ so that from (A.5)

$$\varepsilon_{xx} = \varepsilon_{yy} = \varepsilon_{zz} = \frac{-P}{3\lambda_m + 2\mu_m} \tag{A.9}$$

and the fractional change in volume is

$$-(\varepsilon_{xx} + \varepsilon_{yy} + \varepsilon_{zz}) = -\Delta \tag{A.10}$$

so that

$$k = \frac{P}{\Delta} = \lambda_m + \frac{2\mu_m}{3} \quad . \tag{A.11}$$

A-3. Equations of Motion

In order to obtain the equations of motion for an elastic medium consider the variation in stress across a small parallelopipedon with the sides parallel to the set of rectangular axes, Figure 2. The components of stress will vary linearly across the faces so to obtain the force acting on each face the value of the stress at the center of each face is multiplied by the area of that face.

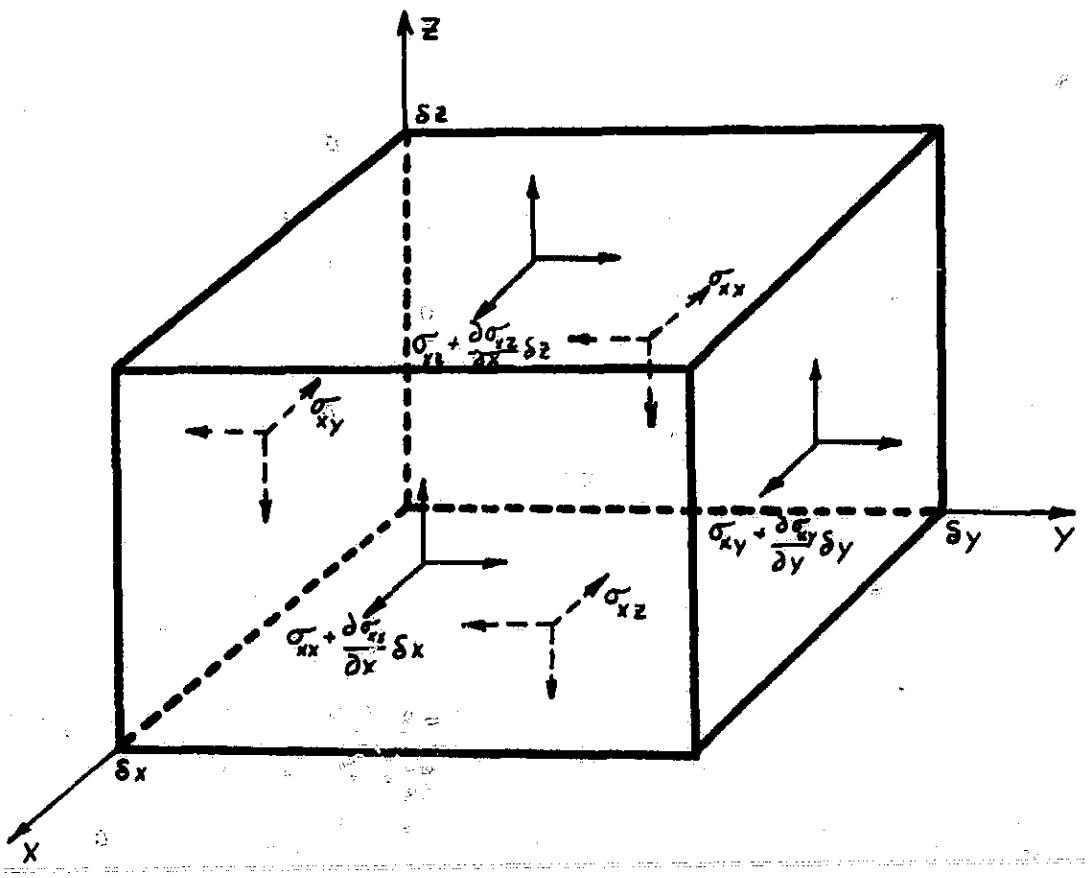

Figure 2. Stresses on Parallelopiped

As seen from the figure, six separate forces will be acting parallel to each axis. If the resultant force in the x-direction is considered it becomes:

$$\left[\left(\sigma_{xx} + \frac{\partial \sigma_{xx}}{\partial x}\delta x\right) - \sigma_{xx}\right]\delta y \delta z + \left[\left(\sigma_{xy} + \frac{\partial \sigma_{xy}}{\partial y}\delta y\right) - \sigma_{xy}\right]\delta x \delta z + \left[\left(\sigma_{xz} + \frac{\partial \sigma_{xz}}{\partial z}\delta z\right) - \sigma_{xz}\right]\delta x \delta y \quad (A.12)$$

which simplifies to

$$\left(\frac{\partial \sigma_{xx}}{\partial x} + \frac{\partial \sigma_{xy}}{\partial y} + \frac{\partial \sigma_{xz}}{\partial z}\right)\delta x \delta y \delta z. \quad (A.13)$$

If the body forces such as gravity are neglected the application of Newton's second law of motion shows that this must equal

$$\rho \delta x \delta y \delta z \frac{\partial^2 u}{\partial t^2} \quad (A.14)$$

where ρ is the density of the element and u is the displacement in the x-direction as before. This gives

$$\rho \frac{\partial^2 u}{\partial t^2} = \frac{\partial \sigma_{xx}}{\partial x} + \frac{\partial \sigma_{xy}}{\partial y} + \frac{\partial \sigma_{xz}}{\partial z} \qquad \text{(A.15a)}$$

and similarly for v and w.

$$\rho \frac{\partial^2 v}{\partial t^2} = \frac{\partial \sigma_{yx}}{\partial x} + \frac{\partial \sigma_{yy}}{\partial y} + \frac{\partial \sigma_{yz}}{\partial z} \qquad \text{(A.15b)}$$

$$\rho \frac{\partial^2 w}{\partial t^2} = \frac{\partial \sigma_{zx}}{\partial x} + \frac{\partial \sigma_{zy}}{\partial y} + \frac{\partial \sigma_{zz}}{\partial z}. \qquad \text{(A.15c)}$$

These equations of motion hold no matter what the elastic constants of the medium are but in order to solve them for a specific case the elastic relations must be used. For an isotropic medium these are given by (A.5), and substituting from these for the stress components in (A.15a) gives

$$\rho \frac{\partial^2 u}{\partial t^2} = \frac{\partial}{\partial x}(\lambda_m \Delta + 2\mu_m \varepsilon_{xx}) + \frac{\partial}{\partial y}(\mu_m \varepsilon_{xy}) + \frac{\partial}{\partial z}(\mu_m \varepsilon_{xz}). \qquad \text{(A.16)}$$

Now from the definitions of (A.3)

$$\varepsilon_{xx} = \frac{\partial u}{\partial x}, \quad \varepsilon_{xz} = \frac{\partial w}{\partial x} + \frac{\partial u}{\partial z}, \quad \varepsilon_{xy} = \frac{\partial v}{\partial x} + \frac{\partial u}{\partial y}. \qquad \text{(A.17)}$$

Thus (A.16) becomes

$$\rho \frac{\partial^2 u}{\partial t^2} = \lambda_m \frac{\partial \Delta}{\partial x} + 2\mu_m \frac{\partial^2 u}{\partial x^2} + \mu_m \left(\frac{\partial^2 v}{\partial x \partial y} + \frac{\partial^2 u}{\partial y^2} + \frac{\partial^2 w}{\partial x \partial z} + \frac{\partial^2 u}{\partial z^2} \right). \qquad \text{(A.18)}$$

Rearranging terms and using the relation, $\nabla^2 = \left(\frac{\partial^2}{\partial x^2} + \frac{\partial^2}{\partial y^2} + \frac{\partial^2}{\partial z^2} \right)$

$$\rho \frac{\partial^2 u}{\partial t^2} = (\lambda_m + \mu_m) \frac{\partial \Delta}{\partial x} + \mu_m \nabla^2 u. \qquad \text{(A.19)}$$

Similarly

$$\rho \frac{\partial^2 v}{\partial t^2} = (\lambda_m + \mu_m) \frac{\partial \Delta}{\partial y} + \mu_m \nabla^2 v \qquad \text{(A.20)}$$

$$\rho \frac{\partial^2 w}{\partial t^2} = (\lambda_m + \mu_m) \frac{\partial \Delta}{\partial z} + \mu_m \nabla^2 w. \qquad \text{(A.21)}$$

Differentiating (A.19) with respect to x gives

$$\rho \frac{\partial^3 u}{\partial x \, \partial t^2} = (\lambda_m + \mu_m) \frac{\partial^2 \Delta}{\partial x^2} + \mu_m \nabla^2 \frac{\partial u}{\partial x}.$$

Repeating for (A.20) and (A.13)

$$\rho \frac{\partial^3 v}{\partial y \, \partial t^2} = (\lambda_m + \mu_m) \frac{\partial^2 \Delta}{\partial y^2} + \mu_m \nabla^2 \frac{\partial v}{\partial y} \qquad \text{(A.22)}$$

$$\rho \frac{\partial^3 w}{\partial z \, \partial t^2} = (\lambda_m + \mu_m) \frac{\partial^2 \Delta}{\partial z^2} + \mu_m \nabla^2 \frac{\partial w}{\partial z} \qquad \text{(A.23)}$$

adding these become:

$$\rho \frac{\partial^2 \Delta}{\partial t^2} = (\lambda_m + 2\mu_m) \nabla^2 \Delta. \qquad \text{(A.24)}$$

This is a wave equation and shows that the dilatation, Δ, is propagated through the medium with a velocity of $[(\lambda_m + 2\mu_m)/\rho]^{1/2}$.

As another choice eliminate Δ between (A.20) and (A.21).

$$\rho \frac{\partial^2}{\partial t^2} \frac{\partial v}{\partial z} = (\lambda_m + \mu_m) \frac{\partial^2 \Delta}{\partial y \partial z} + \mu_m \nabla^2 \frac{\partial v}{\partial z} \qquad \text{(A.25)}$$

$$\rho \frac{\partial^2}{\partial t^2} \frac{\partial w}{\partial y} = (\lambda_m + \mu_m) \frac{\partial^2 \Delta}{\partial y \partial z} + \mu_m \nabla^2 \frac{\partial w}{\partial y}. \qquad \text{(A.26)}$$

Subtracting

$$\rho \frac{\partial^2}{\partial t^2}\left(\frac{\partial w}{\partial v} - \frac{\partial v}{\partial z}\right) = \mu_m \nabla^2\left(\frac{\partial w}{\partial y} - \frac{\partial v}{\partial z}\right). \qquad \text{(A.27)}$$

But $\frac{\partial w}{\partial y} - \frac{\partial v}{\partial z} = 2\omega_x$ by (A.3) so this can be written as

$$\rho \frac{\partial^2 \omega_x}{\partial t^2} = \mu_m \nabla^2 \omega_x. \qquad \text{(A.28)}$$

Similar equations may be obtained for ω_y and ω_z. Thus the rotation is propagated with velocity $\sqrt{\mu_m/\rho}$.

If the dilation is zero (A.15), (A.16), and (A.19) become

$$\rho \frac{\partial^2 u}{\partial t^2} = \mu_m \nabla^2 u \qquad \text{(A.29a)}$$

$$\rho \frac{\partial^2 v}{\partial t^2} = \mu_m \nabla^2 v \qquad \text{(A.29b)}$$

$$\rho \frac{\partial^2 w}{\partial t^2} = \mu_m \nabla^2 w. \qquad \text{(A.29c)}$$

The condition that the rotations ω_x, ω_y, and ω_z all vanish is satisfied if u, v, and w satisfy the conditions

$$u = \frac{\partial \phi}{\partial x}, \quad v = \frac{\partial \phi}{\partial y}, \quad \text{and} \quad w = \frac{\partial \phi}{\partial z}.$$

where ϕ is a potential function. Then

$$\Delta = \nabla^2 \phi \qquad \text{and} \qquad \frac{\partial \Delta}{\partial x} = \nabla^2 u.$$

Substituting these into (A.15):

$$\rho \frac{\partial^2 u}{\partial t^2} = (\lambda_m + 2\mu_m)\nabla^2 u \qquad \text{(A.30)}$$

and similarly for v and w.

Thus it is shown that in the interior of an elastic solid waves may be propagated with one of two different velocities. Waves involving no rotation travel with velocity $c_1 = \sqrt{(\lambda_m + 2\mu_m)/\rho}$ while waves involving no dilatation travel at $c_2 = \sqrt{\mu_m/\rho}$. Strictly speaking these waves should be called <u>irrotational</u> and <u>equivoluminal</u> respectively. The irrotational waves are more commonly called dilatational, longitudinal, compressional, or P-waves while the equivoluminal waves are known as transverse, lateral, or shear waves. In keeping with most of the literature of sound propagation the remainder of this writing will refer to them as the longitudinal and shear waves.

It can be shown that any plane wave propagated through an isotropic elastic medium must travel with one or the other of these velocities, c_1 or c_2. Since the medium is considered isotropic there is no loss of generality if a plane wave propagating parallel to the x-axis is considered. Let its velocity of propagation be c; then the displacements u, v, and w will be functions of a single parameter $\psi = x - ct$.

Then:

$$\frac{\partial^2 u}{\partial t^2} = c^2 \frac{\partial^2 u}{\partial \psi^2} \qquad \frac{\partial^2 v}{\partial t^2} = c^2 \frac{\partial^2 v}{\partial \psi^2} \qquad \frac{\partial^2 w}{\partial t^2} = c^2 \frac{\partial^2 w}{\partial \psi^2}$$

$$\frac{\partial^2 u}{\partial x^2} = \frac{\partial^2 u}{\partial \psi^2} \qquad \frac{\partial^2 v}{\partial x^2} = \frac{\partial^2 v}{\partial \psi^2} \qquad \frac{\partial^2 w}{\partial x^2} = \frac{\partial^2 w}{\partial \psi^2} \tag{A.31}$$

and the partials with respect to y and z are all zero. Substituting these into the first equation of motion (A.19) gives:

$$\rho c^2 \frac{\partial^2 u}{\partial \psi^2} = (\lambda_m + \mu_m) \frac{\partial^2 u}{\partial \psi^2}. \tag{A.32}$$

Similarly from (A.20)and (A.21)

$$\rho c^2 \frac{\partial^2 v}{\partial \psi^2} = \mu_m \frac{\partial^2 v}{\partial \psi^2} \tag{A.33}$$

$$\rho c^2 \frac{\partial^2 w}{\partial \psi^2} = \mu_m \frac{\partial^2 w}{\partial \psi^2}. \qquad (A.34)$$

Equations (A.32), (A.33), and (A.34) can be satisfied in one of two ways: either $c^2=(\lambda_m+2\mu_m)/\rho$ and $\frac{\partial^2 v}{\partial \psi^2} = \frac{\partial^2 w}{\partial \psi^2} = 0$, or $c^2=\mu_m/\rho$ and $\frac{\partial^2 u}{\partial \psi^2} = 0$. The first case corresponds to longitudinal waves, in which the motion is along the direction of propagation and in the second case the motion is transverse and parallel to the wave front.

The theory of transverse elastic body waves was first investigated by Navier (1827) and, a little later, more rigorously by Poisson (1829). These treatments appeared about the same time as Fresnel's theory of the transverse nature of light vibrations. Since prior to this the concept of transverse vibrations propagated through a medium had not been considered, subsequent developments in the theory of elastic waves tended to become associated with discussions on the propagation of light. (See for example Stokes [1848] and Kelvin [1904].)

The velocity of the shear waves depends only on the density and the shear modulus of the medium and it might appear intuitively that the velocity of the longitudinal waves should depend only on the density and the bulk modulus, k, but $k = \lambda_m + \frac{3}{2}\mu_m$ from (A.8) and the shear modulus is also involved. The physical reason for this is that in the propagation of longitudinal waves the medium is not subjected to a simple compression but to a combination of compression and shear. To see this consider a small cube of material in the path of such a plane wave traveling in the x-direction; its cross-sectional area normal to the x-axis will not alter during the passage of the wave but its x-dimension will be altered. Thus there is a change in shape of the element as well as a change in volume and the resistance of the medium to shear comes into play.

Equations (A.24), (A.28), and (A.29) are all of the form:

$$\frac{\partial^2 \alpha}{\partial t^2} = c^2 \nabla^2 \alpha \qquad (A.35)$$

and when the deformation is a function of only one coordinate, for example x, the equation becomes:

$$\frac{\partial^2 \alpha}{\partial t^2} = c^2 \frac{\partial^2 \alpha}{\partial x^2}. \qquad \text{(A.30)}$$

The general solution for this equation is:

$$\alpha = f(x-ct) + F(x+ct) \qquad \text{(A.37)}$$

where f and F are arbitrary functions depending on the initial conditions. F corresponds to a plane wave traveling along the negative x-axis and f to one along the positive x-axis. For each wave it may be seen that, if at any time t_1, α is a given function of x at a later time, t_2, it will have the same shape displaced along the x-axis a distance $c(t_2 - t_1)$

If the disturbance is spreading from a point, the deformation will depend only on the value of the radius vector from the point, $\vec{r}$. Since $r^2 = x^2 + y^2 + z^2$ we have:

$$\frac{\partial^2 \alpha}{\partial x^2} = \frac{x^2}{r^2} \frac{\partial^2 \alpha}{\partial r^2} + \frac{1}{r}\left(\frac{r^2 - x^2}{r^2}\right) \frac{\partial x}{\partial r}. \qquad \text{(A.38)}$$

With similar equations for $\frac{\partial^2 \alpha}{\partial y^2}$ and $\frac{\partial^2 \alpha}{\partial z^2}$ so (A.36) becomes:

$$\frac{\partial^2 \alpha}{\partial t^2} = c^2\left(\frac{\partial^2 \alpha}{\partial r^2} + \frac{2}{r}\frac{\partial \alpha}{\partial r}\right) \text{ or } \frac{\partial^2 (r\alpha)}{\partial t^2} = c^2 \frac{\partial^2 (r\alpha)}{\partial r^2}. \qquad \text{(A.39)}$$

This is of the same form as (A.36) and its solution is:

$$r\alpha = f(r-ct) + F(r+ct). \qquad \text{(A.40)}$$

Now f and F represent spherical waves, f is diverging from the origin and F is converging. The amplitude is inversely proportional to the distance r in both cases.

APPENDIX B

THE REFLECTION OF SOUND FROM A PLANE INTERFACE

THE REFLECTION OF SOUND FROM A PLANE INTERFACE

B-1. Reflection and transmission at a fluid-fluid interface

Although no fluid-fluid interface exists in the system to be considered in this report, this is the case which has both a reflected wave and a single transmitted wave generated at the interface. By not having to deal with the generation of shear waves the problem is simplified considerably for a better intuitive understanding. The case of fluid-solid will then be covered to complete the system. The method used for both of these cases follows basically that of Brekhovskikh (1960) with some of the notations changed to be more consistant with the rest of this report.

The sound field will be characterized by the acoustic potential ϕ. The particle velocity and the acoustic pressure in a harmonic wave (the time dependence is $e^{+i\omega t}$) will be expressed through ϕ by the equations

$$\vec{v} = -\operatorname{grad}\phi \quad , \quad p = +i\omega\rho\phi \tag{B.1}$$

Consider the problem of the reflection of a plane sound wave at a plane boundary separating two media. The density of the medium in which the wave is incident, the upper medium, is denoted by ρ, and the acoustic velocity by c. The corresponding quantities in the lower medium are denoted by ρ_1 and c_1. The angle of incidence is denoted by θ and the angle of refraction by θ_1. The normal to the wave front lies in the plane of the diagram (Fig. B-1).

Using these notations and suppressing the time factor, $e^{+i\omega t}$, the incident wave can be written as

$$\phi_{inc} = A \exp\,[ik(-x \sin\theta + z \cos\theta)] \tag{B.2}$$

where A is the amplitude of the wave. The reflected wave can be written as

$$\phi_{ref} = RA\exp[ik(-x \sin\theta - z \cos\theta)] \tag{B.3}$$

where R is the reflection coefficient. Assuming a linear system the total potential in the upper medium will be

$$\phi = \phi_{inc} + \phi_{ref} = A\exp[ik(-x\sin\Theta + z\cos\Theta)] + RA\exp[ik(-x\sin\Theta + z\cos\Theta)]$$

$$= A\exp(-ikx\sin\Theta)[\exp(+ikz\cos\Theta) + R\exp(-ikz\cos\Theta)] \quad (B.4)$$

The refracted wave can be written in the form

$$\phi_1 = TA\exp[ik_1(-x\sin\Theta_1 + z\cos\Theta_1)] \quad (B.5)$$

where T is the transmission coefficient and $k_1 = \omega/c_1$ is the wave number in the lower medium.

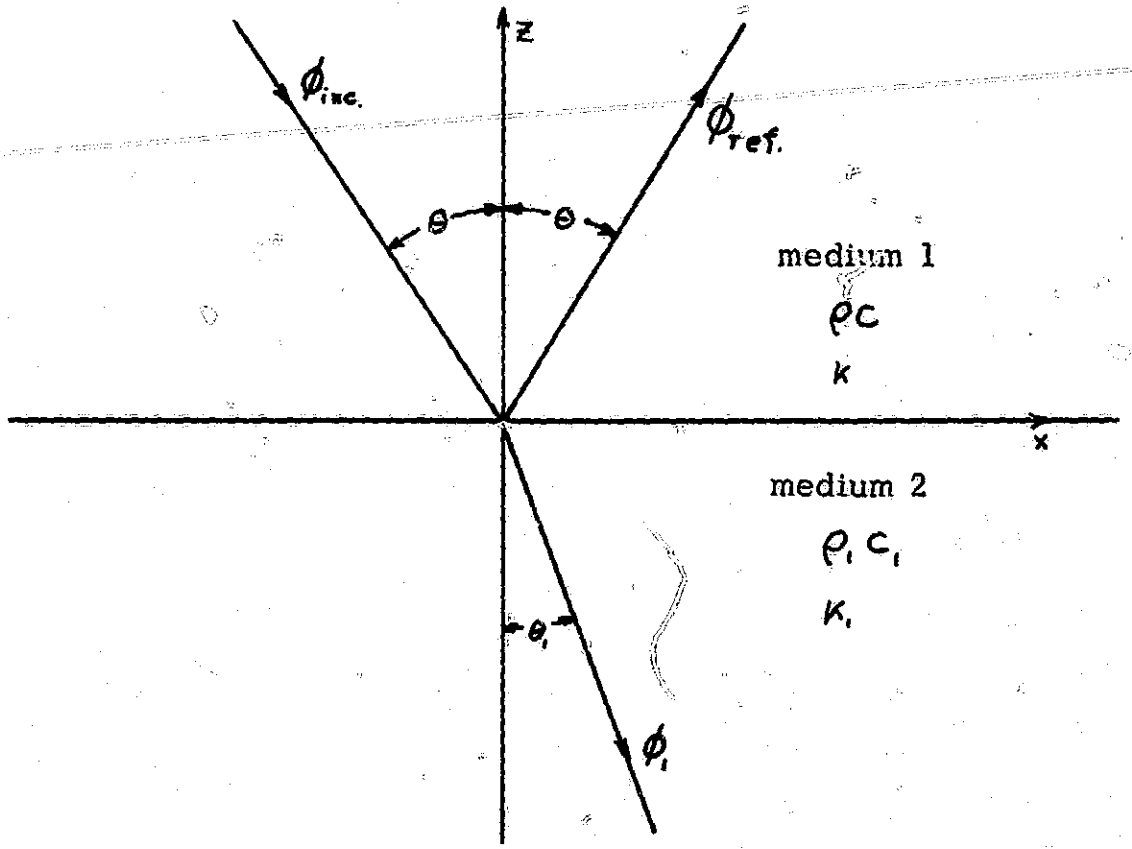

Figure B-1. The Reflection and Refraction of a Plane Sound Wave

The boundary conditions for this system are that the acoustic pressure and the normal component of the particle velocity must be continuous across the interface at $z = 0$. Using (B.1) these conditions can be written as

$$\rho \phi|_{z=0} = \rho_1 \phi_1|_{z=0} \tag{B.6}$$

$$\frac{\partial \phi}{\partial z}\bigg|_{z=0} = \frac{\partial \phi_1}{\partial z}\bigg|_{z=0} \tag{B.7}$$

from which the two unknown coefficients R and T, as well as the angle of refraction θ_1, can be found.

Substituting (B.4) and (B.5) into (B.6) gives

$$\rho(1+R) = \rho_1 T \exp\left[-i(k_1 \sin\theta_1 - k \sin\theta)x\right] \tag{B.8}$$

Since the left hand side is independent of x, the right hand side must also be independent of x for the equality to hold for all x. This yields the well known refraction law since the only way to satisfy the condition is for

$$k \sin\theta = k_1 \sin\theta_1 \tag{B.9}$$

This relation expresses the equality of the phase velocities of waves in both media propagating along the interface. It can also be written as

$$\frac{\sin\theta}{\sin\theta_1} = n \qquad \text{where} \quad n = \frac{k_1}{k} = \frac{c}{c_1} \tag{B.10}$$

Applying this to (B.8) yields

$$T = m(1+R) \qquad \text{where} \quad m = \frac{\rho_1}{\rho} \tag{B.11}$$

Moreover, substituting (B.4) and (B.5) into (B.7) gives

$$\cos\theta\,(1-R) = n T \cos\theta_1 \tag{B.12}$$

From (B.11) and (B.12) comes

$$R = \frac{m\cos\theta - n\cos\theta_1}{m\cos\theta + n\cos\theta_1} . \qquad (B.13)$$

Which can also be written as

$$R = \frac{m\cos\theta - \sqrt{n^2 - \sin^2\theta}}{m\cos\theta + \sqrt{n^2 - \sin^2\theta}} . \qquad (B.14)$$

Thus the unknown quantities in (B.3) and (B.5) can be determined from the boundary conditions and the problem can be considered solved. Before progressing to another interface however, we shall consider some of the implications of these results.

At normal incidence ($\theta = \theta_1 = 0^\circ$), (B.3) gives

$$R = \frac{m - n}{m + n} = \frac{\rho_1 c_1 - \rho c}{\rho_1 c_1 + \rho c} . \qquad (B.15)$$

The quantity $z = \rho c$ is called the characteristic impedance of the medium. Using impedance the reflection coefficient can also be written as

$$R = \frac{z_1 - z}{z_1 + z} . \qquad (B.16)$$

If the normal impedances Z_1 and Z are defined as

$$Z_1 = \frac{\rho_1 c_1}{\cos\theta_1} , \quad Z = \frac{\rho c}{\cos\theta}$$

the reflection coefficient for any incident angle becomes

$$R = \frac{Z_1 - Z}{Z_1 + Z} . \qquad (B.17)$$

As follows from (B.14) the reflection coefficient will become zero at an angle θ satisfying

$$m\cos\theta = \sqrt{n^2 - \sin^2\theta} = 0. \qquad (B.18)$$

In this case there is no reflected wave and the boundary is completely transparent. Solving (B.18) for this angle, θ_b, gives

$$\sin\theta_b = \sqrt{\frac{m^2 - n^2}{m^2 - 1}} . \qquad (B.19)$$

This angle is analogous to Brewster's angle for electromagnetic waves. Note that Θ_b need not be a real angle and complete transmission will not necessarily be observed in any particular case. Rather it is seen that the condition

$$0 \leq \frac{m^2 - n^2}{m^2 - 1} \leq 1$$

must be satisfied. Hence, when $m > 1$, n must be such that $1 < n < m$, and $m < 1$ required $1 > n > m$.

When $n < 1$ and the angle of incidence satisfied the condition $\sin\Theta > n$, total reflection will occur. In this case (B.14) becomes

$$R = \frac{m\cos\Theta - i\sqrt{\sin^2\Theta - n^2}}{m\cos\Theta + i\sqrt{\sin^2\Theta - n^2}}, \qquad \text{(B.20)}$$

B-2. Reflection and Transmission at a Fluid-Solid Interface

Now we shall generalize the problem considered above to include the case where one of the bounding media is a solid.

The particle velocity at any point of a solid medium can be expressed through a scalar and a vector potential, using the equation (See Appendix A).

$$\vec{v} = -\,\mathrm{grad}\,\phi + \mathrm{curl}\,\psi. \qquad \text{(B.21)}$$

In the special case of a plane problem oriented such that all quantities depend only on the coordinates x and z, and that the particle trajectories also lie in the xz-plane, the potential ψ can be chosen such that only its y-component, which will be denoted by ψ, differs from zero. Then, according to (B.21), $\vec{v}$ will be a vector with components

$$v_x = -\frac{\partial\phi}{\partial x} - \frac{\partial\psi}{\partial z}, \quad v_y = 0, \text{ and } v_z = -\frac{\partial\phi}{\partial z} + \frac{\partial\psi}{\partial x} \qquad \text{(B.22)}$$

ϕ and ψ are the potentials of the longitudinal and shear waves, respectively. In Appendix A these potentials were shown to satisfy the wave equations

$$\nabla^2\phi = \frac{1}{c_1^2}\frac{\partial^2\phi}{\partial t^2} \quad , \quad \nabla^2\psi = \frac{1}{c_2^2}\frac{\partial^2\psi}{\partial t^2} \tag{B.23}$$

where

$$c_1 = \sqrt{(\lambda_m + 2\mu_m)/\rho} \tag{B.24a}$$

$$c_2 = \sqrt{\mu_m/\rho} \tag{B.24b}$$

are the velocities of propagation of the longitudinal and shear waves as before.

The normal components of the stress and displacement must be continuous across the boundary between the solid and the liquid. The tangential component of stress must also be continuous, but since the tangential stress cannot exist in the fluid this condition reduces to the requirement that the tangential stress at the boundary of the solid be zero.

In the case of the plane problem the following stress components are of interest (A.7)

$$\sigma_{zz} = \lambda_m\left(\frac{\partial u}{\partial x} + \frac{\partial w}{\partial z}\right) + 2\mu_m\frac{\partial w}{\partial z} \tag{B.25a}$$

$$\sigma_{zx} = \mu_m\left(\frac{\partial u}{\partial z} + \frac{\partial w}{\partial x}\right) \tag{B.25b}$$

$$\sigma_{yz} = 0 \tag{B.25c}$$

where u and w are displacements along the x- and z-axes, respectively, as before. The z-axis is taken as normal to the interface. It is useful to express the displacement and the stress in terms of the potentials ψ

and ϕ. To do this use (B.22) and take into account that the displacement components u and w are obtained from the velocity components v_x and v_z by dividing by $+i\omega$. Quantities referring to the solid will be denoted by the subscript 1, and the quantities referring to the liquid will have no subscripts. The elasticity of the liquid will be characterized by λ_m, the acoustic velocity c, and the density ρ using (B.24a), with μ set equal to zero.

The sound field in the liquid is characterized by the potential ϕ. Obviously, all the relations obtained for the solid medium can be extended to the liquid by setting $\psi = 0$ and $\mu = 0$. In particular, from (B.21) the connection between $\vec{v}$ and ϕ will be of the form

$$\vec{v} = -\text{grad}\,\phi \tag{B.26}$$

Then from (B.1) the acoustic pressure will be

$$p = i\omega\rho\phi \tag{B.27}$$

The boundary conditions at $z = 0$ can be written:

continuity of σ_{zz}

$$\lambda_m \nabla^2\phi = \lambda_{m_1}\nabla^2\phi_1 + 2\mu_{m_1}\left(\frac{\partial^2\phi_1}{\partial z^2} + \frac{\partial^2\psi_1}{\partial z\,\partial x}\right); \tag{B.28}$$

σ_{yz} equal to zero

$$2\frac{\partial^2\psi}{\partial x\,\partial z} + \frac{\partial^2\psi}{\partial x^2} - \frac{\partial^2\psi_1}{\partial z^2} = 0; \tag{B.29}$$

continuity of u

$$\frac{\partial\phi}{\partial z} = \frac{\partial\phi_1}{\partial z} + \frac{\partial\psi_1}{\partial x}. \tag{B.30}$$

Using these boundary conditions the influence of the fluid-solid interface on wave propagation can now be determined. Let the sound wave be incident on the interface from the liquid and let the wave be prescribed by the potential

$$\phi_{inc} = A\exp\left[ik\left(-x\sin\Theta + z\cos\Theta\right)\right] \tag{B.31}$$

where, again, A is the wave amplitude and θ is the incident angle.

The reflected wave may be written in the form

$$\phi_{ref} = A R \exp\left[-ik(x \sin\theta + z\cos\theta)\right]. \tag{B.32}$$

Thus, the total sound field in the liquid will be

$$\phi = A\left[\exp(ikz\cos\theta) + R\exp(-ikz\cos\theta)\right]\exp(-ikx\sin\theta) \tag{B.33}$$

A longitudinal and a shear wave will be present in the solid. These waves can be written as

$$\phi_1 = A T \exp\left[-ik_1(x\sin\theta_1 - z\cos\theta_1)\right] \tag{B.34}$$

$$\psi_1 = A P \exp\left[-ik_1(x\sin\gamma_1 - z\cos\gamma_1)\right] \tag{B.35}$$

where k, k_1, and k_1 are wave numbers

$$k = \frac{\omega}{c}, \quad k_1 = \frac{\omega}{c_1}, \quad \text{and } k_1 = \frac{\omega}{c_2} \tag{B.36}$$

and θ_1 and γ_1 are the angles between the z-axis and the normals to the wave fronts of the longitudinal and shear waves in the solid. These angles are defined in Figure B-2.

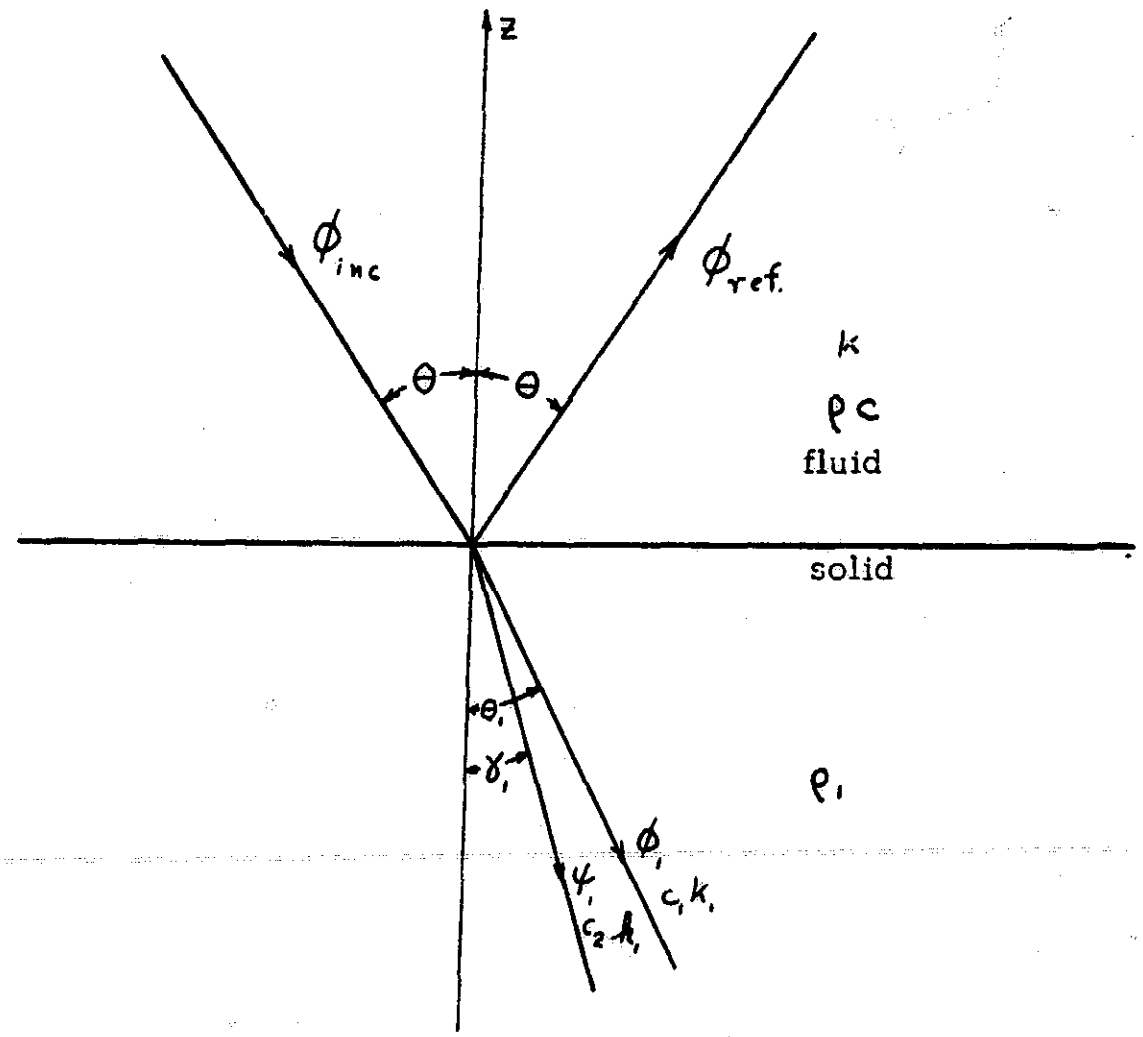

Figure B-2. Geometry of the Fluid-Solid Interface

The problem can be considered solved when R, T, P, θ_1 and γ_1 are all known. Substituting (B.33), (B.34) and (B.35) into (B.28), (B.29) and (B.30) with z = 0 yields three equations from which these quantities may be found. For example (B.30) gives

$$k\cos\theta(R-1) = -k_1\cos\theta_1 T\exp\left[-i(k_1\sin\theta_1 - k\sin\theta)x\right] + k_1\sin\gamma_1 P\exp\left[-i(k_1\sin\gamma_1 - k\sin\theta)x\right]. \qquad (B.37)$$

Since the left hand side of this equation is independent of x, the right hand side must also be independent of x. This can be true only if the equation

$$k \sin\theta = k_1 \sin\theta_1 = k_1 \sin\gamma_1 \qquad \text{(B.38)}$$

is satisfied, whence the directions of the waves in the solid are determined.

Now (B.37) can be written

$$k \cos\theta (R-1) = -k_1 \cos\theta_1 T + k_1 \sin\gamma_1 P. \qquad \text{(B.39)}$$

Similarly

$$k_1^2 T \sin 2\theta_1 + k_1^2 P \cos 2\gamma_1 = 0 \qquad \text{(B.40)}$$

from (B.29). Adding and subtracting $2\mu_{m_1} \frac{\partial^2 \phi_1}{\partial x^2}$ on the right hand side of (B-28) and using

$$\nabla^2 \phi_1 \equiv \frac{\partial^2 \phi_1}{\partial x^2} + \frac{\partial^2 \phi_1}{\partial z^2}$$

this equation can be rewritten as

$$\lambda_m \nabla^2 \phi = (\lambda_{m_1} + 2\mu_{m_1}) \nabla^2 \phi_1 + 2\mu_{m_1} \left(\frac{\partial^2 \phi_1}{\partial x \partial z} - \frac{\partial^2 \phi_1}{\partial x^2} \right) \quad \text{at } z = 0. \qquad \text{(B.41)}$$

Remembering that

$$\lambda_m = \rho c^2 = \rho \frac{\omega^2}{k^2}, \quad \lambda_{m_1} + 2\mu_{m_1} = \rho_1 \frac{\omega^2}{k_1^2}, \quad \mu_{m_1} = \rho_1 \frac{\omega^2}{k_1^2}$$

and the wave equation

$$\nabla^2 \phi = -k^2 \phi \qquad \nabla^2 \phi_1 = -k^2 \phi_1$$

(B.41) can be simplified to

$$\frac{1}{m} \phi = \phi_1 - \frac{2}{k_1^2} \left(\frac{\partial^2 \psi_1}{\partial x \partial z} - \frac{\partial^2 \phi_1}{\partial x^2} \right) \quad \text{at } z = 0 \qquad \text{(B.42)}$$

where

$$m = \frac{\rho_1}{\rho} \tag{B.43}$$

Substituting the values of ϕ, ϕ_1, and ψ_1 into (B.42) yields a third equation for the determination of the coefficients R, T and P,

$$\frac{1}{m}(1+R) = \left(1 - 2\frac{k_1^2}{k_1^2}\sin^2\theta\right)T - \sin 2\gamma_1 P \tag{B.44}$$

Solving the system of equations (B.39), (B.40) and (B.44), and making some transformations using (B.38) gives

$$R = \frac{Z_1\cos^2 2\gamma_1 + Z_s \sin^2 2\gamma_1 - Z}{Z_1\cos^2 2\gamma_1 + Z_s \sin^2 2\gamma_1 + Z}$$

$$= \frac{Z_1 - \frac{c_2^2}{c^2}\sin^2\theta[4Z_s - 5Z_1] - \frac{c_2^4}{c^4}\sin^4\theta[Z_1 + 4Z_s] - Z}{Z_1 - \frac{c_2^2}{c^2}\sin^2\theta[4Z_s - 5Z_1] - \frac{c_2^4}{c^4}\sin^4\theta[Z_1 + 4Z_s] + Z} \tag{B.45}$$

where Z, Z_1, and Z_s denote, respectively, the impedances for sound waves in the liquid and longitudinal and shear waves in the solid

$$Z = \frac{\rho c}{\cos\theta}, \quad Z_1 = \frac{\rho_1 c_1}{\cos\theta_1} \quad \text{and} \quad Z_s = \frac{\rho_1 c_2}{\cos\gamma_1} \tag{B.46}$$

Also

$$T = \frac{1}{m}\frac{2Z_1\cos 2\gamma_1}{Z_1\cos^2 2\gamma_1 + Z_s\sin^2 2\gamma_1 + Z}$$

$$= \frac{1}{m}\frac{2Z_1\left(1 - 2\frac{c_2^2}{c^2}\sin^2\theta\right)}{Z_1 - \frac{c_2^2}{c^2}\sin^2\theta[4Z_s - 5Z_1] - \frac{c_2^4}{c^4}\sin^4\theta[Z_1 + 4Z_s] + Z} \tag{B.47}$$

$$P = -\frac{1}{m}\frac{2Z_s\sin 2\gamma_1}{Z_1\cos^2 2\gamma_1 + Z_s\sin^2 2\gamma_1 + Z}$$

$$= -\frac{1}{m}\frac{4Z_s\frac{c_2}{c^2}\sin\theta\sqrt{c^2 - c_2^2\sin^2\theta}}{Z_1 - \frac{c_2^2}{c^2}\sin^2\theta[4Z_s - 5Z_1] - \frac{c_2^4}{c^4}\sin^4\theta[Z_1 + 4Z_s] + Z} \tag{B.48}$$

Now, let us consider some implications of these results. At normal incidence ($\theta = \theta_1 = \gamma_1 = 0$) we have,

$$R = \frac{Z_1 - Z}{Z_1 + Z}, \quad T = \frac{1}{m}\frac{2Z_1}{Z_1 + Z}, \text{ and } P = 0 \tag{B.49}$$

which corresponds to the fluid-fluid case since no shear wave is generated. On the contrary setting T = 0 means

$$1 - 2\frac{c_2^2}{c^2}\sin^2\theta = 0$$

or

$$\theta = \sin^{-1}\left(\frac{c}{\sqrt{2}\, c_2}\right)$$

which gives $\gamma_1 = 45^\circ$ since

$$\gamma_1 = \sin^{-1}\left(\frac{c_2}{c}\sin\theta\right) = \sin^{-1}\left(\frac{c_2}{c}\frac{c}{c_2\sqrt{2}}\right)$$

from (B.28) we have

$$R = \frac{Z_s - Z}{Z_s + Z}, \quad T = 0, \text{ and } P = -\frac{1}{m}\frac{2Z_s}{Z_s + Z} \tag{B.50}$$

implying that shear waves but no longitudinal waves will be generated in the solid.

Now consider the case in which a longitudinal wave of amplitude A is incident from the solid onto the solid-fluid interface. This wave will excite the following system of three waves at the boundary:

(1) a reflected longitudinal wave (amplitude B_1)
(2) a reflected shear wave (amplitude B_s)
(3) a sound wave in the liquid (amplitude D).

The entire system of waves may be written in the form

$$\phi = D \exp\left[-ik(x \sin\theta + z\cos\theta)\right] \tag{B.51}$$

for the sound wave in the liquid

$$\phi_1 = A \exp\left[-ik(x \sin\theta_1 + z \cos\theta_1)\right] + B_1 \exp\left[-ik(x \sin\theta_1 - z\cos\theta_1)\right] \tag{B.52}$$

for the incident and reflected longitudinal waves and

$$\psi_1 = B_s \exp\left[-ik_1(x \sin\gamma_1 - z\cos\gamma_1)\right] \tag{B.53}$$

for the reflected shear wave.

Using the boundary conditions (B.28), (B.29) and (B.30) as before gives

$$R' = \frac{Z + Z_s \sin^2 2\gamma_1 - Z_1 \cos^2 2\gamma_1}{Z + Z_s \sin^2 2\gamma_1 + Z_1 \cos^2 2\gamma_1}$$

$$= \frac{Z + \frac{c_2^2}{c_1^2}\sin^2\theta_1(4Z_s + 5Z_1) - 4\frac{c_2^4}{c_1^4}\sin^4\theta_1(Z_s + Z_1) - Z_1}{Z + \frac{c_2^2}{c_1^2}\sin^2\theta_1(4Z_s - 5Z_1) - 4\frac{c_2^4}{c_1^4}\sin^4\theta_1(Z_s - Z_1) + Z_1} \tag{B.54}$$

$$T' = (1-R')\frac{c\cos\theta_1}{c_1\cos\theta\cos^2 2\gamma_1}$$

$$= (1-R')\frac{c\cos\theta_1}{\sqrt{c_1^2 - c^2\sin^2\theta_1}\left[1 - 5\frac{c_2^2}{c^2}\sin^2\theta_1 + 4\frac{c_2^4}{c_1^4}\sin^4\theta_1\right]} \tag{B.55}$$

$$P' = (1 - R')\left(\frac{c_2}{c_1}\right)^2 \frac{\sin 2\theta_1}{\cos 2\gamma_1}$$

$$= (1 - R') \frac{c_2^2 \sin 2\theta_1}{c_1^2 - 2c_2^2 \sin^2 \theta_1} .$$

(B.56)

Similarly when a shear wave (of amplitude A_s) with particle motion in the xz-plane is incident on the boundary from the solid the system of waves can be written in the form

$$\phi = D \exp\left[-ik(x \sin\theta + z \cos\theta)\right] \qquad \text{(B.57)}$$

for the sound wave in the liquid

$$\phi_1 = B_1 \exp\left[-ik_1(x \sin\theta_1 - z \cos\theta_1)\right] \qquad \text{(B.58)}$$

for the reflected longitudinal wave in the solid; and

$$\psi_1 = A_s \exp\left[-ik_1(x \sin\gamma_1 + z \cos\gamma_1)\right]$$

$$+ B_s \exp\left[-ik_1(x \sin\gamma_1 - z \cos\gamma_1)\right] \qquad \text{(B.59)}$$

for the incident and reflected shear waves.

Again using the boundary conditions yields

$$R'' = -\frac{Z + Z_1 \cos^2 2\gamma_1 - Z_s \sin^2 2\gamma_1}{Z + Z_1 \cos^2 2\gamma_1 + Z_s \sin^2 2\gamma_1}$$

(B.60)

$$T'' = (1+R'')\ \frac{t\ n\Theta}{2\sin^2\gamma_1}$$

$$= (1+R'')\ \frac{c}{2\sin\gamma_1\sqrt{c_2^2 - c^2\sin^2\gamma_1}}$$

(B.61)

$$P'' = -\left(\frac{c_1}{c_2}\right)^2 (1+R'')\ \frac{\cos 2\gamma_1}{\sin 2\theta_1}$$

$$= -(1+R'')\ \frac{c_1^2\cos 2\gamma_1}{2\sin\gamma_1\sqrt{c_2^2 - c^2\sin^2\gamma_1}}$$

(B.62)

The only case remaining to be investigated is a shear wave with particle motion parallel to the interface. A wave of this type creates neither normal displacements nor normal stresses at the interface. This means it will not excite a sound wave in the liquid or a longitudinal wave in the solid. The one boundary condition left is satisfied by a reflected shear wave of the same amplitude.

Thus all waves incident on a fluid-solid interface have been considered since, in an isotropic, linear solid, a plane wave of arbitrary polarization can be considered as a superposition of waves of the polarizations investigated.

APPENDIX C

EXPERIMENTAL DETERMINATION OF THE MATERIAL CONSTANTS

EXPERIMENTAL DETERMINATION OF THE MATERIAL CONSTANTS

C-1. Wax Floating on the Water

The piece of wax used was cast with both sides flat and parallel. The thickness was then measured and found to be 37 mm. The transducers were aimed at the surface of the water from below and carefully adjusted for maximum signal reflected from the smooth water to determine normal incidence. This signal was taken as coming from a perfect reflector and recorded for comparison with that reflected from the wax. The wax was then floated across the illuminated area and the return observed. Two distinct pulses were found and the amplitudes and relative timing were recorded. With this information it should be possible to obtain an estimate of the reflection coefficient, the attenuation constant, and the velocity of propagation for the wax.

The measured values were:

Return	Attenuation	Voltage	Time Delay
Calibration	70 dB	3 vpp	2031 μs
First pulse	46 dB	2.4 vpp	1994 μs
Second pulse	46 dB	2.2 vpp	2032 μs

"Attenuation" refers to the value of attenuation inserted ahead of the receiver to avoid saturation and the difference corresponds to the change of system gain. Using these values, (B.49) and (B.55) the desired quantities were calculated as follows:

$$v = \frac{x}{\Delta t} = \frac{2(3.7 \times 10^{-2})}{38 \times 10^{-6}} = 1900 \text{ m/sec} \qquad \text{(C.1)}$$

$$R = \frac{V_{1st}}{V_{cal}} \qquad \text{(C.2)}$$

where V_{cal} is the signal received from a perfect reflector and V_{1st} is the amplitude of the first pulse from the wax. Since the system gain was different for the two voltages as measured this must be taken into account. This gain change was 24 dB which corresponds to a voltage ratio of 1/16, yielding:

$$R = \frac{2.4}{3(16)} = .05. \qquad (C.3)$$

From (B.49) $R = \frac{Z_1 - Z}{Z_1 + Z}$ which for $Z_1 > Z$ gives a positive reflection coefficient. Since $Z = \rho c$ and $Z_1 = \rho_1 c_1$ this value can be calculated as a check by

$$Z = 1.5 \times 10^6 \qquad Z_1 = (.9)(1900) \times 10^3 = 1.7 \times 10^6$$

$$R = \frac{.2}{3.2} = 0.062 \qquad (C.4)$$

which is in good agreement with the measured value.

The attenuation constant, α_ℓ, was determined by using the relation

$$V_{2nd} = V_{cal.}\, T\, T'\, e^{-\alpha x} \qquad (C.5)$$

where $T = \frac{\rho}{\rho_1}(1-R)$ is the transmission coefficient from the water to the wax,

$T' = \frac{c}{c_1}(1-R')$ is the transmission coefficient from the wax to the water,

x is the total distance traveled through the wax, and

V_{2nd} is the amplitude of the second pulse.

This is the equation for transmission through a section of material but since the wax/air interface has a reflection coefficient of unity it also applies to this case. Solving for α_ℓ and substituting the experimentally determined values yields

$$\alpha_l = \frac{1}{x} \ln \frac{T T' V_{cal.}}{V_{2nd}}$$

$$= \frac{1}{7.4} \ln \frac{(1.006)(.83)(3)(16)}{2.2} = \frac{1}{7.4} \ln 19.1 = .39 \text{ nep/cm} \quad \text{(C.6)}$$

These results were such that it was thought the wax was worthy of further testing.

C-2. Longitudinal Waves Through a Section of Wax

For a more accurate determination of v_l and α_l a rod of wax was cast with a diameter of 50 mm and a final length of 128 mm after the ends were cut square. This is thick enough that the velocity of propagation is very close to that of an infinite piece.

The transducers used were first placed in direct contact with each other, with a small amount of wax applied as a couplant to insure tight coupling, and the received voltage was recorded. They were then applied to the ends of the rod and the time delay and attenuation introduced by the rod were measured to give

$$\Delta t = 68 \mu s$$

$$V_o/V_i = 1/312$$

These data were used to calculate the following constants

$$v_l = 128/68 = 1870 \text{ m/sec} \quad \text{(C.7)}$$

$$\alpha_l = \frac{1}{12.8} \ln 312 = \frac{5.75}{12.8} = .45 \text{ nep/cm} \quad \text{(C.8)}$$

which agree very well with the preliminary results.

C-3. Wax Prism

To measure the shear wave velocity a prism was constructed of the wax. By illuminating one face of the prism at an angle other than normal incidence a shear wave as well as a longitudinal wave was generated in the wax. At the other side mode conversion would also occur, generating a longitudinal wave in the water at an angle determined by the refractive index between the velocity of propagation in the water and in the wax.

The prism was cast with an included angle of 45°. The available molding facilities would only allow the prism to be 20 cm from apex to base, which restricted the angles that could be used without having a corner interfere. The faces of the finished prism were not as flat as desired due to the shrinking of the wax on cooling but the curvature was determined to be small enough that a fair estimate of the velocities could be made.

This prism was submerged in the water with one transducer aimed at the center of the front face at 22.5° from normal incidence (perpendicular to the center line of the prism). The second transducer was then scanned in an arc behind the prism and the signal received was recorded as a function of angle. Two distinct peaks were found as expected. The longitudinal wave gave a large peak at 12° and the shear wave produced a much smaller peak at -38°.

Referring to Figure C-1 the equations for this prism are

$$n = \frac{v}{v_1} \tag{C.9a}$$

$$\sin \Theta_1 = n \sin \phi_1 \tag{C.9b}$$

$$\sin \Theta_2 \quad n \sin \phi_2 \tag{C.9c}$$

$$\phi_2 = 45^{\circ} - \phi_1 \tag{C.9d}$$

$$\Theta_2 = 22.5^{\circ} - \phi_m \tag{C.9e}$$

where n is the desired result and the angles Θ_1 and ϕ_m are known.

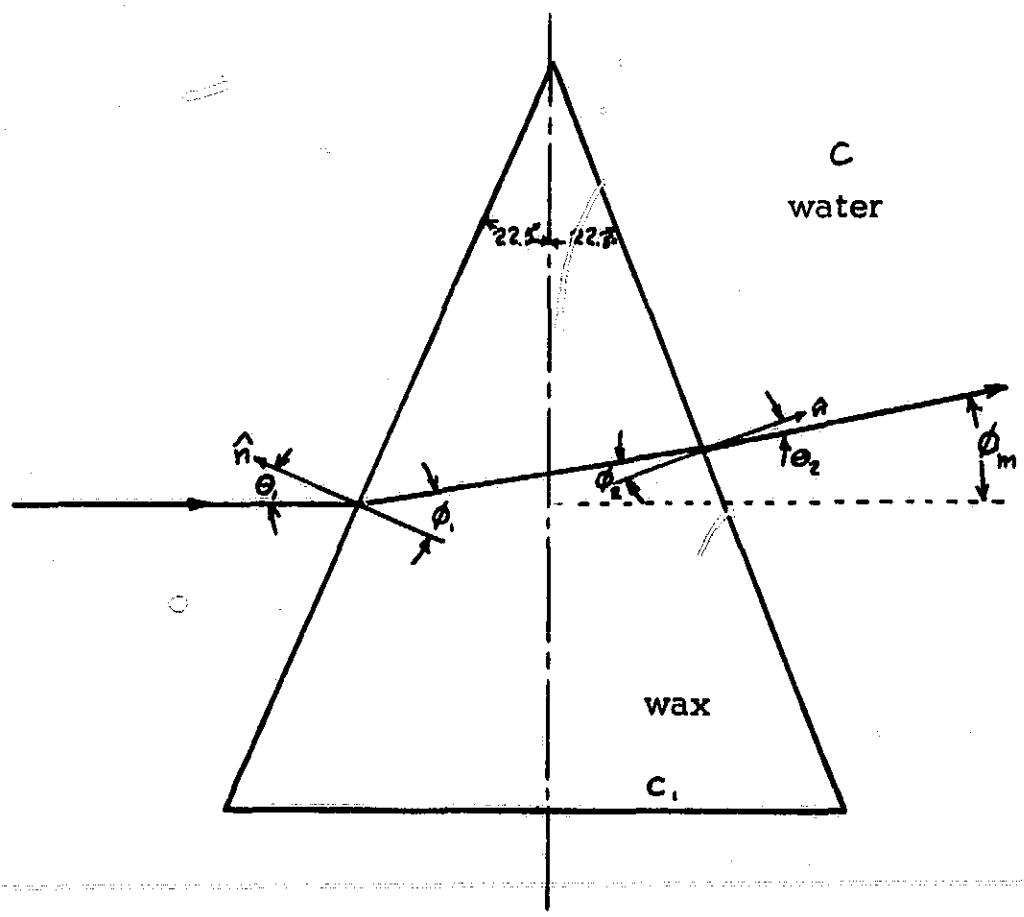

Figure C-1. Definition of Angles for Derivation of Prism Equations.

These equations can be used to find n directly but the expression is very complicated so an intermediate step of solving for ϕ_2 was used. Start by substituting (C.9d) into (C.9c) which gives

$$\sin\theta_1 = n \sin(45^\circ - \phi_2)$$

$$= n(\sin 45^\circ \cos\phi_2 - \cos 45^\circ \sin\phi_2)$$

$$= \frac{n}{\sqrt{2}}(\cos\phi_2 - \sin\phi_2) \qquad (C.10)$$

since $\sin 45^\circ = \cos 45^\circ = (2)^{-\frac{1}{2}}$. Dividing both sides by $\sin\theta_2$ yields

$$\frac{\sin\theta_1}{\sin\theta_2} = \frac{n}{\sqrt{2}}\left(\frac{\cos\phi_2 - \sin\phi_2}{\sin\theta_2}\right) \tag{C.11}$$

but using (C.9c) this can be written as

$$\frac{\sin\theta_1}{\sin\theta_2} = \frac{1}{\sqrt{2}}\left(\frac{\cos\phi_2 - \sin\phi_2}{\sin\phi_2}\right) \tag{C.12}$$

$$= \frac{1}{\sqrt{2}}\left(\cot\phi_2 - 1\right)$$

or

$$\cot\phi_2 = \sqrt{2}\,\frac{\sin\theta_1}{\sin\theta_2} + 1 \tag{C.13}$$

which can be used to find ϕ_2 since θ_1 and θ_2 were determined experimentally. Once ϕ_2 is known (C.9c) is used again to find n by

$$n = \frac{\sin\theta_2}{\sin\phi_2}\,. \tag{C.14}$$

Applying this to the experimental results of the longitudinal wave we get

$$\theta_2 = 22.5^\circ - 12^\circ = 10.5^\circ$$

$$\cot\phi_2 = \sqrt{2}\,\frac{\sin 22.5^\circ}{\sin 10.5^\circ} + 1$$

$$= 1.414\,\frac{.383}{.182} + 1 = 3.98, \tag{C.15}$$

Which means

$$\phi_2 = \cot^{-1} 3.98 = 14.1^\circ \tag{C.16}$$

giving

$$n = \frac{.182}{.244} = .745 \tag{C.17}$$

and

$$c_1 = \frac{c}{n} = \frac{1500}{.745} = 2010 \text{ m/sec.} \tag{C.18}$$

Similarly for the shear wave

$$\theta_2 = 22.5° - (-38°) = 60.5° \tag{C.19}$$

$$\cot \phi_2 = \sqrt{2}\ \frac{\sin 22.5°}{\sin 60.5°} + 1$$

$$= 1.414\ \frac{.383}{.870} + 1 = 1.633$$

(C.20)

$$\phi_2 = \cot^{-1} 1.633 = 31.3° \tag{C.21}$$

$$n = \frac{.870}{.522} = 1.66 \tag{C.22}$$

$$c_2 = \frac{1500}{1.66} = 900 \text{ m/sec} \tag{C.23}$$

Thus an estimate of the velocities was made. The longitudinal wave velocity found was higher than that previously determined but was of the same order of magnitude, with the error being attributed to the curvature of the prism sides. This error should also be present in the measurement of the shear velocity which would imply an actual velocity somewhat less than the 900 m/s determined here.

C-4. Method of Hughes

The method of Hughes (1949) consists of driving one end of a right circular cylinder with a pulse-modulated carrier of longitudinal waves and detecting longitudinal waves at the other end. The detected signal consists of a series of pulses with the delay times the important parameter. The delay from the start of the transmitted burst to the leading edge of the pulse string, T, corresponds to the time for the longitudinal wave to traverse the material under test. The time between the first and second pulse, Δt, is the sum of infinitely many waves that have traversed a path such as ABCD shown in Figure C-2. These arise because the transmitted longitudinal wave is not strictly parallel to the surface and mode conversion takes place at the reflection. The path AB is traveled as a longitudinal wave, BC is traversed as a shear wave, and CD is again a longitudinal wave. All these waves suffer the same delay for crossing the rod one time in shear so the result is a second pulse at the detector end. Also present are following pulses generated by paths such as ABCEF.

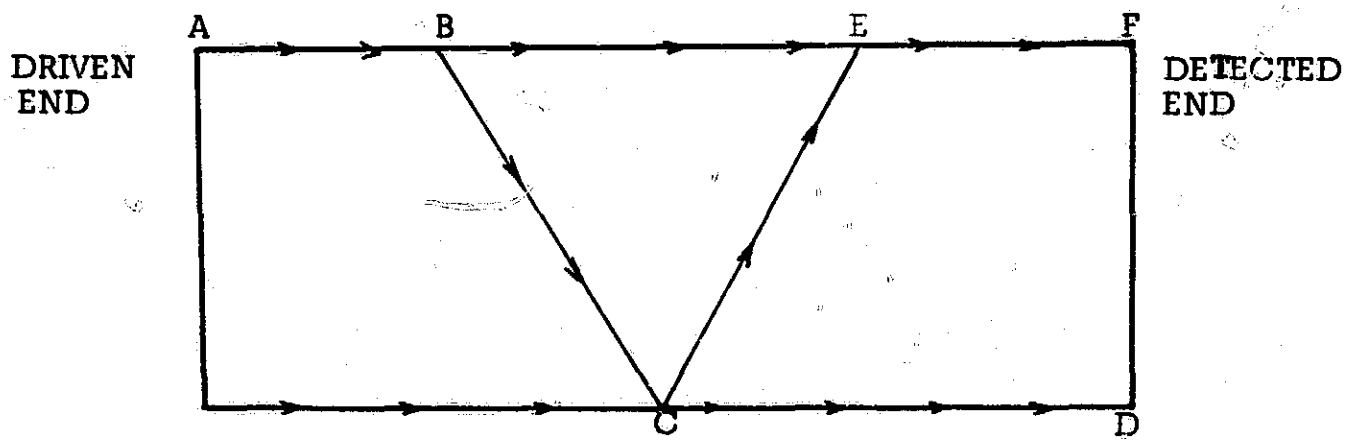

Figure C-2. Two Possible Paths for Sound Waves in a Solid Cylinder

As shown by Hughes the time between pulses is

$$\Delta t = D\left[\left(c_1^2 - c_2^2\right)^{1/2} / c_1 c_2\right]. \qquad (C.24)$$

This equation can be solved for c_2 since the diameter of the rod, D, and c_1 are known quantities and Δ t is measured experimentally. This gives

$$c_2 = c_1 \sqrt{\frac{D}{c_1^2 \Delta t^2 + D}} \qquad \text{(C.25)}$$

This method was implemented by casting a circular cylinder of the wax then mounting a transducer on each end of it. This first attempt did not produce the distinct pulses as expected but only an extended trailing edge of the main pulse. The cylinder was then cut open to determine the cause of the discrepancy. It was found to have large cracks at the center caused by the stresses produced by contraction of the wax as it cooled in the mold.

To eliminate these cracks it was decided to extrude a cylinder for the test. A mold was prepared with one end slightly smaller than the main section. This was filled with molten wax then slowly cooled while a reservoir of molten wax was maintained on top to reduce the formation of stress cracks. After being thoroughly cooled the cylinder was forced out the smaller end to form the final test piece. The ends of this were then sectioned and determined to be of a homogeneous nature. The transducers were then mounted and one was driven with bursts of 350 KHz with pulse length of 60 μs. The signal received at the other end was then observed and the pertinent times recorded. Photographs of the received signal are shown in Figure C-3.

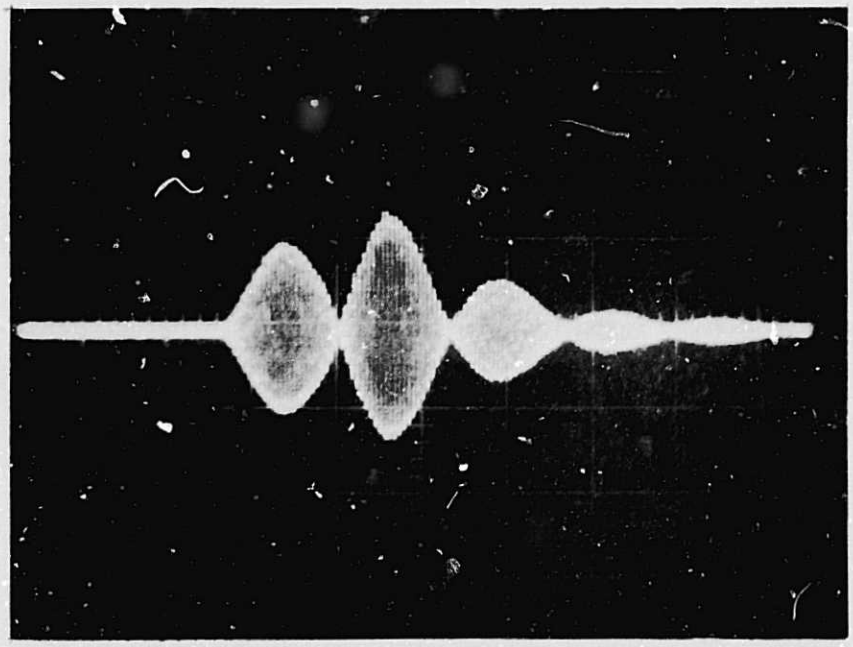

(a) Start of Trace Corresponds to Start of Transmitted Pulse. Time Scale = 50 μs/cm

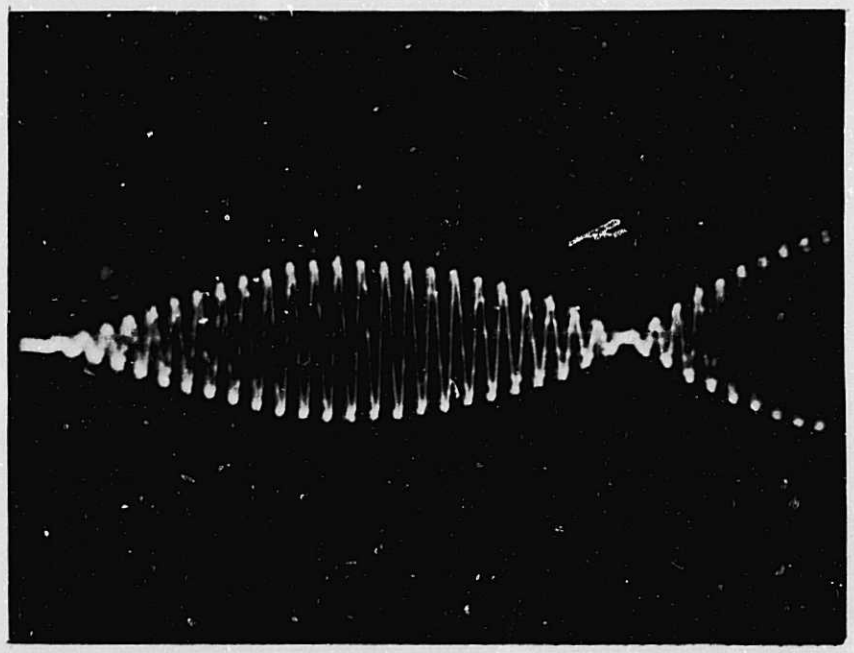

(b) Expanded Sweep Showing Δt More Clearly. Time scale = 10 μs/cm.

Figure C-3. Photographs of Signal Received at Detector End of Rod Number One.

A second rod with a different diameter and length was then constructed by the same technique to serve as a check of the experimental method. The different dimensions would eliminate any possibility of a spurious spatial resonance effect which could have caused erroneous results. The dimensions and experimental results for both rods are tabulated below:

Parameter	Rod #1	Rod #2
Length	22.5 cm	13.0 cm
Diameter	3.9 cm	4.4 cm
Frequency	350 KHz	350 KHz
T	125 μs	73 μs
Δt	68 μs	76 μs
c_1	1800 m/sec	1782 m/sec
c_2	550 m/sec	552 m/sec

The good agreement between the two independent experiments should not be considered as an indication of true accuracy but it does give more confidence in the results obtained.

C-5. Shear Attenuation

To measure the shear attenuation it was necessary to excite a shear wave through a section of the material and determine the loss per unit distance. This would have been easy if shear mode transducers had been available. Such was not the case, however. Shear waves are also generated by mode conversion when an interface is illuminated at other than normal incidence, as shown in Appendix B. To eliminate errors due to inaccurate knowledge of the material parameters, it was decided to use a difference method by comparing the change of attenuation between two different thicknesses of the material. To reduce the effect of the longitudinal wave, the interface should be illuminated at an angle beyond the critical angle for these waves. The critical angle can be determined by

setting the angle of refraction equal to 90° and using Snell's law to solve for the incident angle. This gives

$$\theta_c = \sin^{-1}\left(\frac{c}{c_1}\sin\theta_1\right)$$

$$\text{for } \theta_1 = 90°$$

$$\theta_c = \sin^{-1}\left(\frac{c}{c_1}\right) = \sin^{-1}\left(\frac{1500}{1800}\right) = 56.5°. \qquad \text{(C.26)}$$

Using an incident angle of 66° should thus give no longitudinal waves in the material.

Two slabs of wax were prepared with thicknesses of 1.4 cm and 4.3 cm. These were mounted end-to-end such that the transducers could be moved from one to the other without changing anything except the thickness of wax. The difference between the two thicknesses was 53 dB attenuation as measured experimentally.

The path length of the shear wave through the wax can be determined from the incident angle, θ, Snell's law, and the thickness, T, by

$$\gamma_1 = \sin^{-1}\left(\frac{c_s}{c}\sin\theta\right) \qquad \text{(C.27)}$$

$$L = \frac{T}{\cos\gamma_1} = \frac{T}{\sqrt{1-\left(\frac{c_s}{c}\sin\theta\right)^2}} = \frac{T}{.947}. \qquad \text{(C.28)}$$

For the thinner piece

$$L = \frac{1.4}{.947} = 1.48 \text{ cm} \qquad \text{(C.29)}$$

and the thick section

$$L = \frac{4.3}{.947} = 4.54 \text{ cm}, \qquad \text{(C.30)}$$

Thus $\Delta L = 4.54 - 1.48 = 3.06$ cm

and the attenuation per centimeter is

$$\frac{Attn.}{cm} = \frac{Attn.}{\Delta L} = \frac{53}{3.06} = 17.25 \text{ dB/cm} \qquad \text{(C.31)}$$

for the shear wave in wax. This corresponds to

$$\alpha = 2.75 \text{ nep/cm}. \qquad \text{(C.32)}$$

C-6. Material Constants

With the values of c_1, c_2 and ρ determined by the preceding methods the results derived in Appendix A can be used to determine the mechanical constants for the material. Lame's constant μ_m was calculated by using the relation

$$c_2 = \sqrt{\frac{\mu_m}{\rho}}$$

which means

$$\mu_m = \rho c_2^2 = (9.37)(5.50)^2 \times 10^6$$

$$= 2.83 \times 10^8 \text{ newton/m}^2. \qquad \text{(C.33)}$$

Similarly λ_m can be found from μ_m, ρ and c_1 by

$$c_1 = \sqrt{\frac{\lambda_m + 2\mu_m}{\rho}}$$

Solving for λ_m gives

$$\lambda_m = \rho c_1^2 - 2\mu_m$$

$$= [(9.37)(1.8)^2 - 2(2.83)]10^8 = 2.47 \times 10^9 \text{ newton/m}^2 \qquad \text{(C.34)}$$

Once Lame's constants have been determined any of the other commonly used elastic constants can be calculated from (A.6) to (A.8). Young's modulus, E is found by (A.6) to be

$$E = \frac{\mu_m (3\lambda_m + 2\mu_m)}{\lambda_m + \mu_m} = 8.21 \text{ newton/m}^2. \qquad \text{(C.34)}$$

Poisson's ratio is

$$\nu = \frac{\lambda_m}{2(\lambda_m + \mu_m)} = .449 \qquad \text{(C.35)}$$

from (A.7). Finally from (A.8) the bulk modulus k_m is

$$k_m = \lambda_m + \frac{2\mu_m}{3} = 2.65 \times 10^9 \text{ newtons/m}^2 \qquad \text{(C.36)}$$

C-7 Wax-Water Interface

The equations of Appendix B were programmed to allow the computation of reflection and transmission coefficients for the three possible cases, i.e. longitudinal wave in water hitting the wax, longitudinal wave coming out of the wax, and a shear wave striking the water from the wax. Also computed were the magnitudes of the two-way transmission through the wax. This program computed these quantities for each case with the angle of incidence changed in increments of 5°. The only ones found to be significant were the longitudinal waves. This program is reproduced in Figure C-4. The coefficients of interest appear in Chapter III as Figures 3-11--3-16.

```
      ARSIN(X)=ATAN(X)/SQRT(1.0-X*X)
      C=1500
      C1=1800
      C2=550
      RHO=1000
      RHO1=937
      FM=RHO1/RHO
      RC=RHO*C
      R1C1=RHO1*C1
      R1C2=RHO1*C2
      C1C=C1/C
      C2C=C2/C
      C1C2=C1/C2
      C1C22=C1C2*C1C2
      WRITE(6,5)
5     FORMAT(3X,5HTHETA,8X,1HR,10X,1HT,10X,1HP,9X,2HR1,9X,2H
     1T1,9X,2HP1,9X,2HR2,9X,2HT2,9X,2HP2,8X,4HT*T1,7X,4HP*T2)
      DO 20 I 2,11
      THETA=(I-1)*5
      TH=THETA*0.01745
      STH=SIN(TH)
      CTH=COS(TH)
      TTH=STH/CTH
      C1CSTH=C1C*STH
      C2CSTH=C2C*STH
      TH1=ARSIN(C1CSTH)
      CTH1=COS(TH1)
      TTH1=2.*TH1
      STTH1=SIN(TTH1)
      GM1=ARSIN(C2CSTH)
      CGM1=COS(GM1)
      TGM1=2.*GM1
      STGM1=SIN(TGM1)
      CTGM1=COS(TGM1)
      STGM12=STGM1*STGM1
      CTGM12=CTGM1*CTGM1
      Z=RC/CTH
      Z1=R1C1/CTH1
      ZS=R1C2/CGM1
      Z1CS=Z1*CTGM1
      Z1CS2=Z1CS*CTGM1
      ZSSN=ZS*STGM1
      ZSSN2=ZSSN*STGM1
      D=Z+Z1CS2+ZSSN2
      R=(-Z+Z1CS2+ZSSN2)/D
      FMD=FM*D
      T=2.*Z1CS/FMD
      P=-2.*ZSSN/FMD
      R1=(Z-Z1CS2+ZSSN2)/D
      T1=CTH1*(1.-R1)/(C1C*CTH*CTGM12)
      P1=STTH1*(1.-R1)/(C1C22*CTGM1)
      R2=(-Z-Z1CS2+ZSSN2)/D
      T2=TTH*(1.+R2)/(2.*STGM12)
```

```
      P2=-(C1C22*CTGM1*(1.+R2))/STTH1
      TT1=T*T1
      PT2=P*T2
      WRITE(6,10) THETA,R,T,P,R1,T1,P1,R2,T2,P2,TT1,PT2
10    FORMAT(12(1X,1PE10.2))
20    CONTINUE
      STOP
      END
```

Figure C-4. Program to Determine Reflection and Transmission Coefficients for Wax-Water Interface.